SIGGRAPH ’95 Course Notes

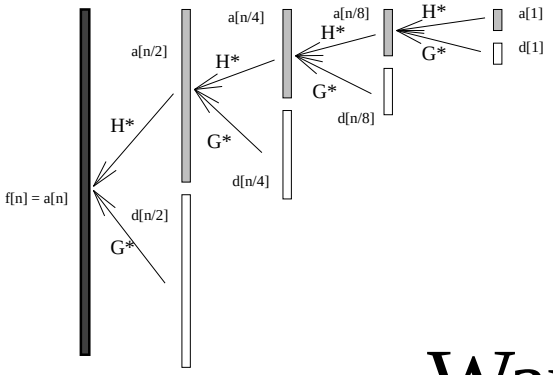

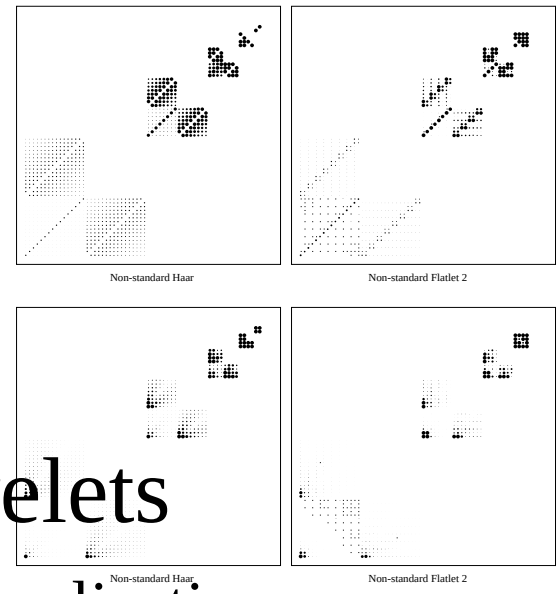

Wavelets
and their Applications in Computer Graphics

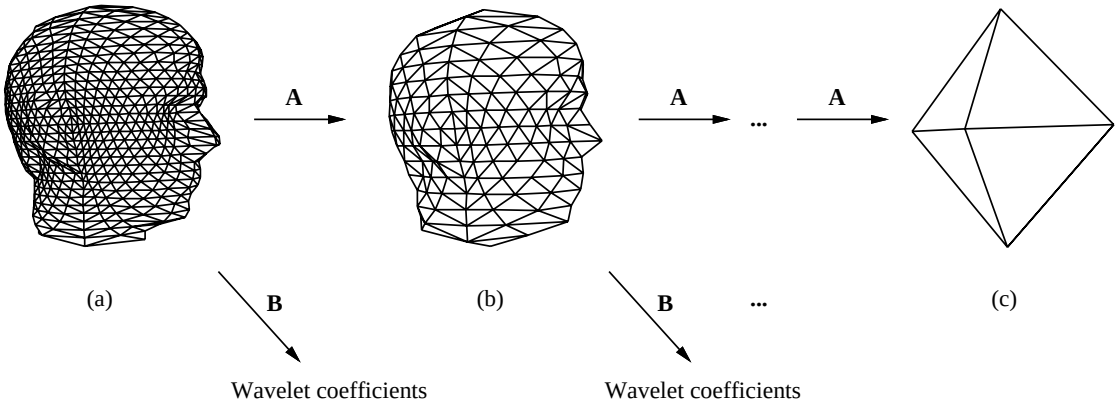

Organizer:
Alain Fournier
University of British Columbia

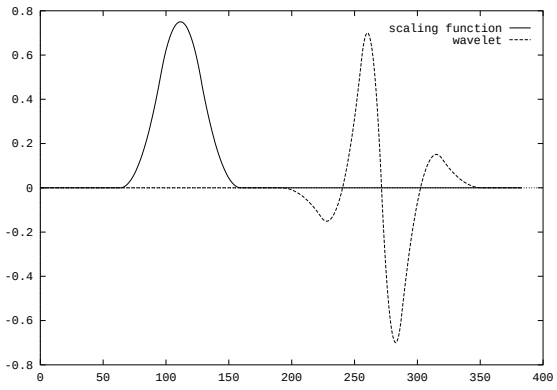

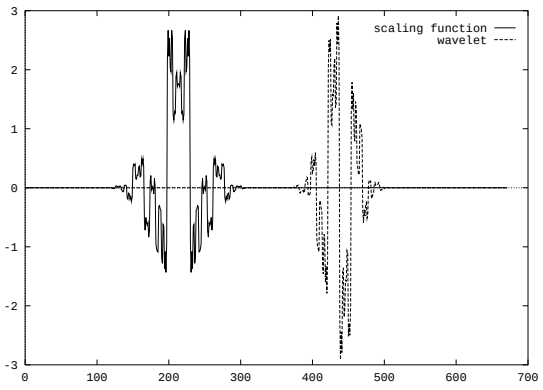

Nothing to do with sea or anything else.
Over and over it vanishes with the wave.

– Shinkichi Takahashi

Lecturers

Michael F. Cohen
Microsoft Research
One Microsoft Way
Redmond, WA 98052
mcohen@microsoft.com

Tony D. DeRose
Department of Computer Science and Engineering FR-35
University of Washington
Seattle, Washington 98195
derose@cs.washington.edu

Alain Fournier
Department of Computer Science
University of British Columbia
2366 Main Mall
Vancouver, British Columbia V6T 1Z4
fournier@cs.ubc.ca

Michael Lounsbery
Alias Research
219 S. Washington St.
P.O. Box 4561
Seattle, WA 98104
louns@ag.alias.com

Leena-Maija Reissell
Department of Computer Science
University of British Columbia
2366 Main Mall
Vancouver, British Columbia V6T 1Z4
reissell@cs.ubc.ca

Peter Schröder
Department of Computer Science
Le Conte 209F
University of South Carolina
Columbia, SC 29208
ps@math.scarolina.edu

Wim Sweldens
Department of Mathematics
University of South Carolina
Columbia, SC 29208
sweldens@math.scarolina.edu

Table of Contents

N : Preamble

1 Prolegomenon

These are the notes for the Course #26, **Wavelets and their Applications in Computer Graphics** given at the Siggraph '95 Conference. They are an longer and we hope improved version of the notes for a similar course given at Siggraph '94 (in Orlando). The lecturers and authors of the notes are (in alphabetical order) Michael Cohen, Tony DeRose, Alain Fournier, Michael Lounsbery, Leena-Maija Reissell, Peter Schröder and Wim Sweldens.

Michael Cohen is on the research staff at Microsoft Research in Redmond, Washington. Until recently, he was on the faculty at Princeton University. He is one of the originators of the radiosity method for image synthesis. More recently, he has been developing wavelet methods to create efficient algorithms for geometric design and hierarchical spacetime control for linked figure animation.

Tony DeRose is Associate Professor at the Department of Computer Science at the University of Washington. His main research interests are computer aided design of curves and surfaces, and he has applied wavelet techniques in particular to multiresolution representation of surfaces.

Alain Fournier is a Professor in the Department of Computer Science at the University of British Columbia. His research interests include modelling of natural phenomena, filtering and illumination models. His interest in wavelets derived from their use to represent light flux and to compute local illumination within a global illumination algorithm he is currently developing.

Michael Lounsbery is currently at Alias Research in Seattle (or the company formerly known as such). He obtained his PhD from the University of Washington with a thesis on multi-resolution analysis with wavelet bases.

Leena Reissell is a Research Associate in Computer Science at UBC. She has developed wavelet methods for curves and surfaces, as well as wavelet based motion planning algorithms. Her current research interests include wavelet applications in geometric modeling, robotics, and motion extraction.

Peter Schröder received his PhD in Computer Science from Princeton University where his research focused on wavelet methods for illumination computations. He continued his work with wavelets as a Postdoctoral Fellow at the University of South Carolina where he has pursued generalizations of wavelet constructions. Other research activities of his have included dynamic modelling for computer animation, massively parallel graphics algorithms, and scientific visualization.

Wim Sweldens is a Research Assistant of the Belgian National Science Foundation at the Department of

Computer Science of the Katholieke Universiteit Leuven, and a Research Fellow at the Department of Mathematics of the University of South Carolina. He just joined the applied mathematics group at ATT Bell Laboratories. His research interests include the construction of non-algebraic wavelets and their applications in numerical analysis and image processing. He is one of the most regular editors of the Wavelet Digest.

In the past few years *wavelets* have been developed both as a new analytic tool in mathematics and as a powerful source of practical tools for many applications from differential equations to image processing. Wavelets and wavelet transforms are important to researchers and practitioners in computer graphics because they are a natural step from classic Fourier techniques in image processing, filtering and reconstruction, but also because they hold promises in shape and light modelling as well. It is clear that wavelets and wavelet transforms can become as important and ubiquitous in computer graphics as spline-based technique are now.

This course, in its second instantiation, is intented to give the necessary mathematical background on wavelets, and explore the main applications, both current and potential, to computer graphics. The emphasis is put on the connection between wavelets and the tools and concepts which should be familiar to any skilled computer graphics person: Fourier techniques, pyramidal schemes, spline representations. We also tried to give a representative sample of recent research results, most of them presented by their authors.

The main objective of the course (through the lectures and through these notes) is to provide enough background on wavelets so that a researcher or skilled practitioner in computer graphics can understand the nature and properties of wavelets, and assess their suitability to solve specific problems in computer graphics. Our goal is that after the course and/or the study of these notes one should be able to access the basic mathematical literature on wavelets, understand and review critically the current computer graphics literature using them, and have some intuition about the pluses and minuses of wavelets and wavelet transform for a specific application.

We have tried to make these notes quite uniform in presentation and level, and give them a common list of references, pagination and style. At the same time we hope you still hear distinct voices. We have not tried to eradicate redundancy, because we believe that it is part and parcel of human communication and learning. We tried to keep the notation consistent as well but we left variations representative of what is normally found in the literature. It should be noted that the references are by no mean exhaustive. The literature of wavelets is by now huge. The entries are almost exclusively references made in the text, but see Chapter VIII for more pointers to the literature.

The CD-ROM version includes an animation (720 frames) made by compressing (see Chapter IV) and reconstructing 6 different images (the portraits of the lecturers) with six different wavelet bases. The text includes at the beginning of the first 6 chapters four frames (at 256×256 resolution originally) of each sequence. This gives an idea (of course limited by the resolution and quality of the display you see them on) of the characteristics and artefacts associated with the various transforms. In order of appearance, the sequences are Alain Fournier with Adelson bases, Leena-Maija Reissell with pseudo-coiflets, Michael Lounsbery with Daubechies 4, Wim Sweldens with Daubechies 8, Tony DeRose with Battle-Lemarié, Peter Schröder with Haar and Michael Cohen with coiflets 4. All of these (with the exception of Adelson) are described in the text. Michael Lounsbery version does not appear in the CD-ROM due to lack of time.

Besides the authors/lecturers, many people have helped put these notes together. Research collaborators are identified in the relevant sections, some of them as co-authors. The latex/postscript version of these notes have been produced at the Department of Computer Science at the University of British Columbia. Last year Chris Romanzin has been instrumental in bringing them into existence. Without him they would

be a disparate collection of individual sections, and Alain Fournier's notes would be in troff. This year Christian Vinther picked up the torch, and thanks to Latex amazing memory, problems we had licked last year reappeared immediately. That gave him a few fun nights removing most of them. Bob Lewis, also at UBC, has contributed greatly to the content of the first section, mostly through code and general understanding of the issues. The images heading the chapters, and the animation found on the CD-ROM were all computed with his code (also to be found on the disc -see Chapter VIII). Parag Jain implemented an interactive program which was useful to explore various wavelet image compressions. Finally we want to thank Stephan R. Keith (even more so than last year) the production editor of the CD-ROM, who was most helpful, patient and efficient as he had to deal with dozens of helpless, impatient and scattered note writers.

Alain Fournier

I: Introduction

Alain FOURNIER

University of British Columbia

1 Scale

1.1 Image pyramids

Analyzing, manipulating and generating data at various scales should be a familiar concept to anybody involved in Computer Graphics. We will start with "image" pyramids[1].

In pyramids such as a *MIP map* used for filtering, successive averages are built from the initial signal. Figure I.1 shows a schematic representation of the operations and the results.

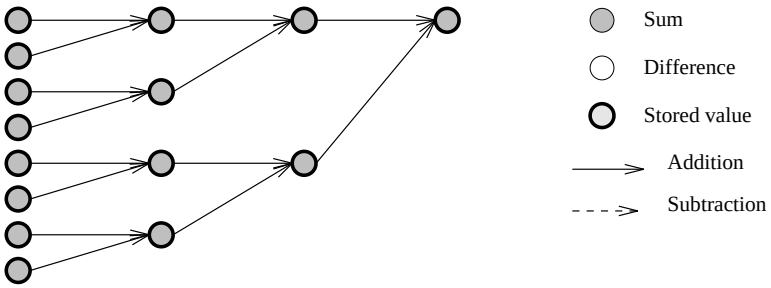

Figure I.1: Mean pyramid

It is clear that it can be seen as the result of applying box filters scaled and translated over the signal. For n initial values we have $\log_2(n)$ stages, and $2n - 1$ terms in the result. Moreover because of the order we have

[1]We will use the word "image" even though our examples in this section are for 1D signals.

chosen for the operations we only had to compute $n-1$ additions (and shifts if means are stored instead of sums).

This is not a good scheme for reconstruction, since all we need is the last row of values to reconstruct the signal (of course they are sufficient since they are the initial values, but they are also necessary since only a sum of adjacent values is available from the levels above). We can observe, though, that there is some redundancy in the data. Calling $s_{i,j}$ the jth element of level i (0 being the top of the pyramid, $k = \log_2(n)$ being the bottom level) we have:

$$s_{i,j} = \frac{(s_{i+1,2j} + s_{i+1,2j+1})}{2}$$

We can instead store $s_{0,0}$ as before, but at the level below we store:

$$s'_{1,0} = \frac{(s_{1,0} - s_{1,1})}{2}$$

It is clear that by adding $s_{0,0}$ and $s'_{1,0}$ we retrieve $s_{1,0}$ and by subtracting $s_{0,0}$ and $s'_{1,0}$ we retrieve $s_{1,1}$. We therefore have the same information with one less element. The same modification applied recursively through the pyramid results in $n-1$ values being stored in $k-1$ levels. Since we need the top value as well ($s_{0,0}$), and the sums as intermediary results, the computational scheme becomes as shown in Figure I.2. The price we have to pay is that now to effect a reconstruction we have to start at the top of the pyramid and stop at the level desired. The computational scheme for the reconstruction is given in Figure I.3.

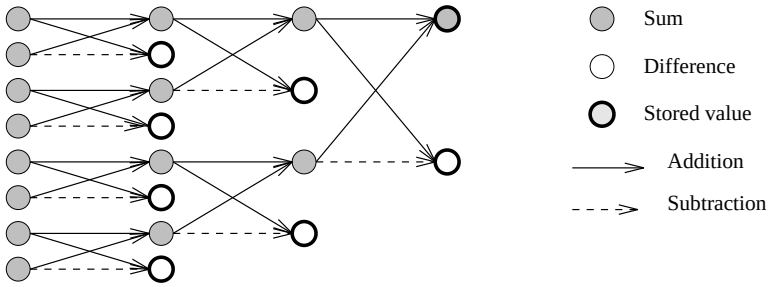

Figure I.2: Building the pyramid with differences

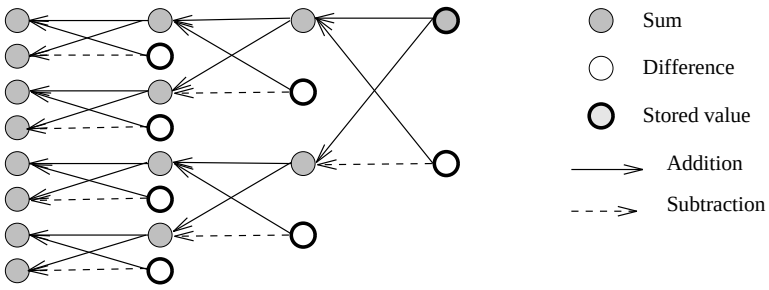

Figure I.3: Reconstructing the signal from difference pyramid

If we look at the operations as applying a filter to the signal, we can see easily that the successive filters in the difference pyramid are (1/2, 1/2) and (1/2, -1/2), their scales and translates. We will see that they are characteristics of the Haar transform. Notice also that this scheme computes the pyramid in $O(n)$ operations.

2 Frequency

The standard Fourier transform is especially useful for *stationary* signals, that is for signals whose properties do not change much (stationarity can be defined more precisely for stochastic processes, but a vague concept is sufficient here) with time (or through space for images). For signals such as images with sharp edges and other discontinuities, however, one problem with Fourier transform and Fourier synthesis is that in order to accommodate a discontinuity high frequency terms appear and they are not localized, but are added everywhere. In the following examples we will use for simplicity and clarity *piece-wise constant* signals and piece-wise constant basis functions to show the characteristics of several transforms and encoding schemes. Two sample 1-D signals will be used, one with a single step, the other with a (small) range of scales in constant spans. The signals are shown in Figure I.4 and Figure I.5.

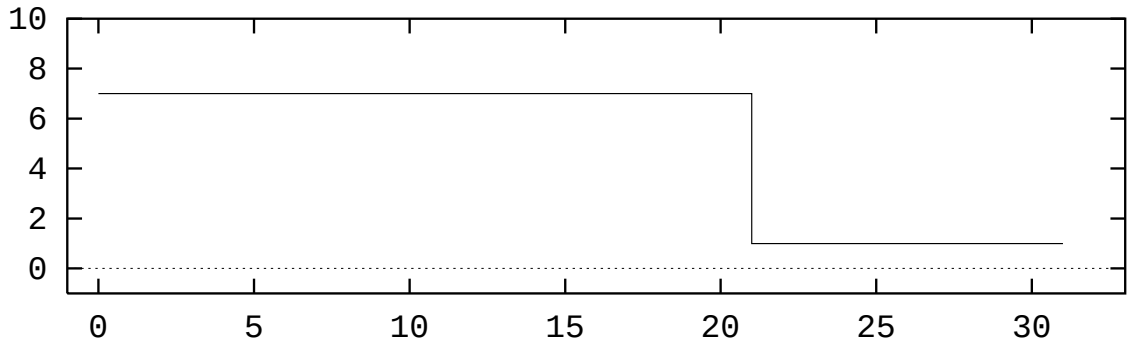

Figure I.4: Piece-wise constant 1-D signal (signal 1)

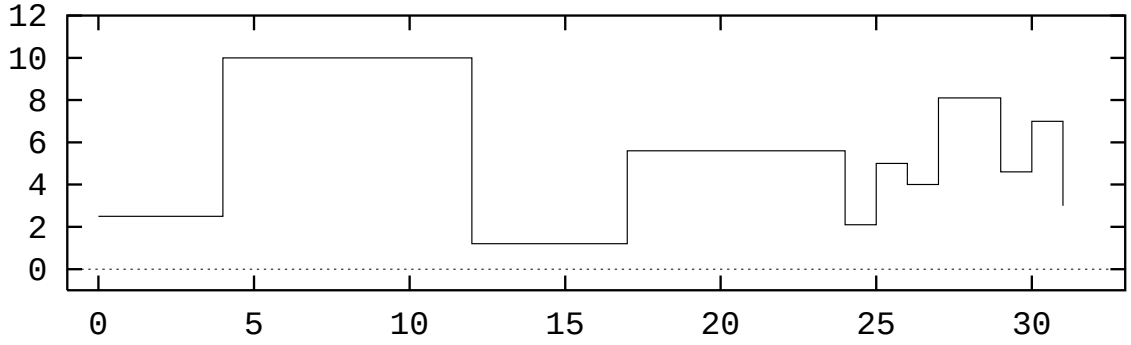

Figure I.5: Piece-wise constant 1-D signal (signal 2)

3 The Walsh transform

A transform similar in properties to the Fourier transform, but with piece-wise constant bases is the *Walsh transform*. The first 8 basis functions of the Walsh transform $W_i(t)$ are as shown in Figure I.6. The Walsh

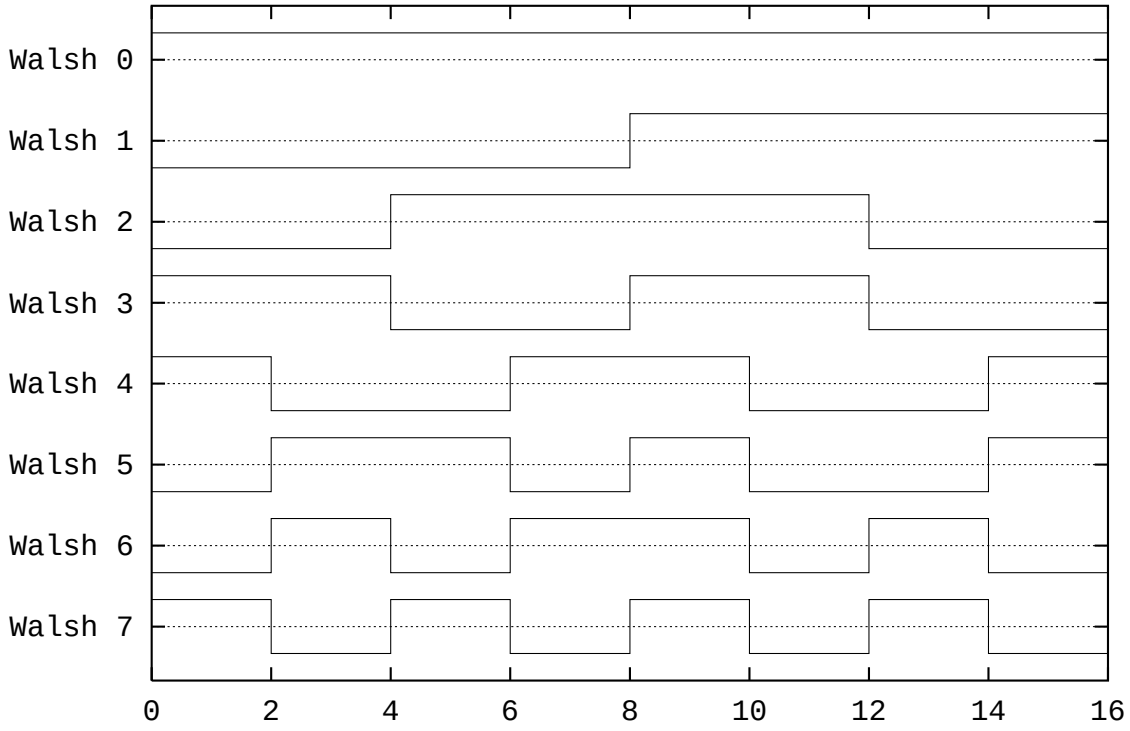

Figure I.6: First 8 Walsh bases

functions are normally defined for $-\frac{1}{2} \leq t \leq \frac{1}{2}$, and are always 0 outside of this interval (so what is plotted in the preceding figure is actually $W_i(\frac{t}{16} - \frac{1}{2})$). They have various ordering for their index i, so always make sure you know which ordering is used when dealing with $W_i(t)$. The most common, used here, is where i is equal to the number of zero crossings of the function (the so-called *sequency* order). They are various definitions for them (see [14]). A simple recursive one is:

$$W_{2j+q}(t) = (-1)^{\frac{j}{2}+q} \times [\, W_j\,(2t + \frac{1}{2}) + (-1)^{(j+q)}\, W_j\,(2t - \frac{1}{2})\,]$$

with $W_0(t) = 1$. Where j ranges from 0 to ∞ and $q = 0$ *or* 1. The Walsh transform is a series of coefficients given by:

$$w_i = \int_{-\frac{1}{2}}^{\frac{1}{2}} f(t)\, W_i(t)\, dt$$

and the function can be reconstructed as:

$$f(t) = \sum_{i=0}^{\infty} w_i \, W_i(t)$$

Figures I.7 and I.8 show the coefficients of the Walsh basis for both of the above signals.

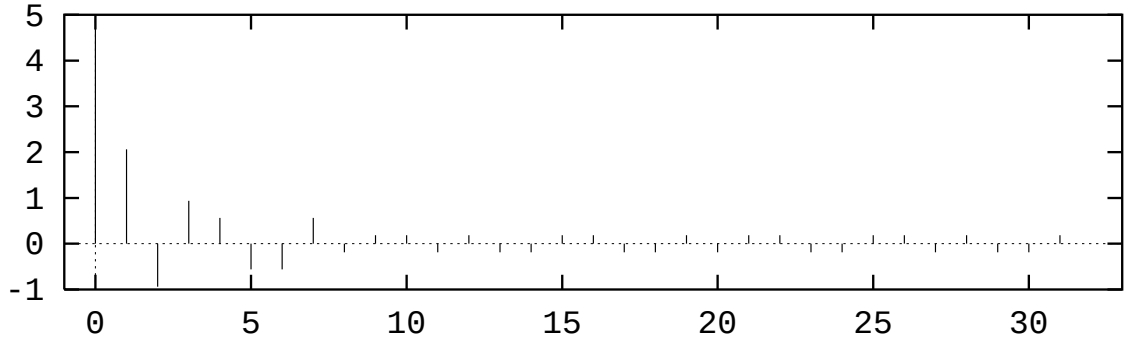

Figure I.7: Walsh coefficients for signal 1.

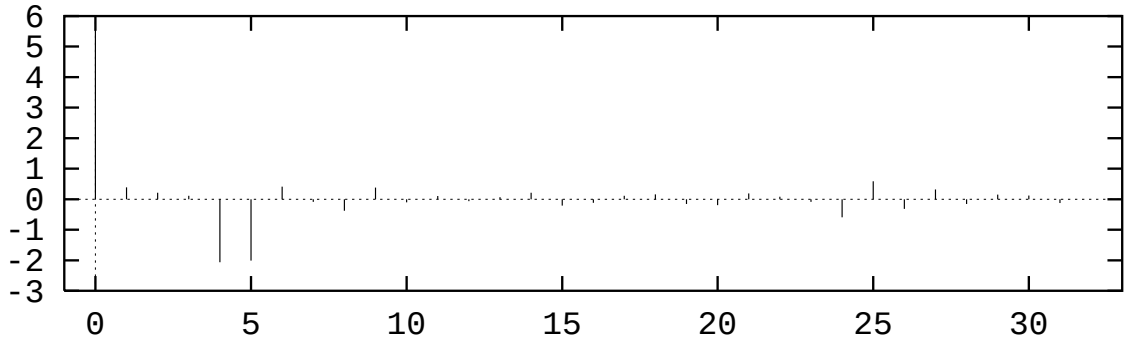

Figure I.8: Walsh coefficients for signal 2.

Note that since the original signals have discontinuities only at integral values, the signals are exactly represented by the first 32 Walsh bases at most. But we should also note that in this example, as well as would be the case for a Fourier transform, the presence of a single discontinuity at 21 for signal 1 introduces the highest "frequency" basis, and it has to be added globally for all t. In general cases the coefficients for each basis function decrease rapidly as the order increases, and that usually allows for a simplification (or *compression*) of the representation of the original signal by dropping the basis functions whose coefficients are small (obviously with loss of information if the coefficients are not 0).

4 Windowed Fourier transforms

One way to localize the high frequencies while preserving the linearity of the operator is to use a *windowed Fourier transform* (*WFT*) also known as a *short-time Fourier transform* (*STFT*). Given a window function $w(t)$ (we require that the function has a finite integral and is non-zero over a finite interval) we define the windowed Fourier transform of the signal $f(t)$ as:

$$F_W(\tau, f) = \int_{-\infty}^{\infty} f(t)\, w^*(t-\tau)\, e^{-2i\pi ft}\, dt$$

In words, the transform is the Fourier transform of the signal with the filter applied. Of course we got a two-variable function as an answer, with τ, the position at which the filter is applied, being the additional variable. This was first presented by Gabor [87]. It is clear that the filter function $w(t)$ allows us a window on the frequency spectrum of $f(t)$ around τ. An alternate view is to see the filter impulse response modulated to the frequency being applied to the Fourier transform of the signal $f(t)$ "for all times" (this is known in signal processing as a *modulated filter bank*).

We have acquired the ability to localize the frequencies, but we have also acquired some new problems. One, inherent to the technique, is the fact we have one more variable. Another is that it is not possible to get high accuracy in both the position (in time) and frequency of a contributing discontinuity. The *bandwidth*, or spread in frequency, of the window $w(t)$, with $W(f)$ its Fourier transform, can be defined as:

$$\Delta f^2 = \frac{\int f^2\, |W(f)|^2\, df}{\int |W(f)|^2\, df}$$

The spread in time is given by:

$$\Delta t^2 = \frac{\int t^2\, |w(t)|^2\, dt}{\int |w(t)|^2\, dt}$$

By Parseval's theorem both denominators are equal, and equal to the energy of $w(t)$. In both cases these values represent the root mean square average (other kinds of averages could be considered).

Exercise 1: Compute Δf and Δt for the box filter as a function of A and T_0. □

If we have a signal consisting of two δ pulses in time, they cannot be discriminated by a WFT using this $w(t)$ if they are Δt apart or less. Similarly two pure sine waves (δ pulses in frequency) cannot be discriminated if they are Δf apart or less. We can improve the frequency discrimination by choosing a $w(t)$ with a smaller Δf, and similarly for time, but unfortunately they are not independent. In fact there is an equality, the

Heisenberg inequality that bounds their product:

$$\Delta t \times \Delta f \geq \frac{1}{4\pi}$$

The lower bound is achieved by the Gaussian [87]. The other aspect of this problem is that once the window is chosen, the resolution limit is the same over all times and frequencies. This means that there is no *adaptability* of the analysis, and if we want good time resolution of the short bursts, we have to sacrifice good frequency description of the long smooth sections.

To illustrate with a piece-wise constant transform, we can use the Walsh transform again, and use a *box* as the window. The box is defined as:

$$w(t) = \begin{cases} 1 & \text{if } -2 \leq t < 2 \\ 0 & \text{otherwise} \end{cases}$$

This box has a width of 4. It is important to note the the Δf for this window is infinite in the measure given above. We will position the windows 1 unit apart. This will result in redundancy in the results, since the windows overlap considerably, but we will address this issue later. Figure I.9 and I.10 show the result for the two signals. In these figures the 32 rows correspond to the 32 positions of the window, while the 32 columns correspond to the coefficients of the Walsh transform. The area of the circles is proportional to the magnitude of the coefficients, and they are filled in black for a positive value and lighter grey for a negative value.

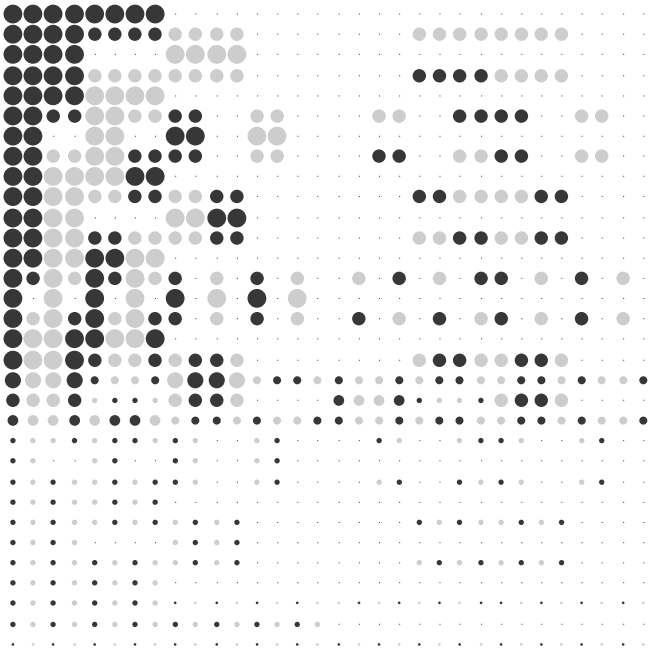

Figure I.9: Signal 1 analysed with windowed Walsh transform

5 Relative Frequency Analysis

One obvious "fix" to this problem is to let the window, and therefore the Δf vary as a function of the frequency. A simple relation is to require $\frac{\Delta f}{f} = c$, c being a constant. This approach is been used in signal processing, where it is known as *constant-Q* analysis. Figure I.11 illustrates the difference in frequency space between a constant bandwidth window and a constant relative bandwidth window (there $c = 2$).

The goal is to increase the resolution in time (space) for sharp discontinuities while keeping a good frequency resolution at high frequencies. Of course if the signal is composed of high frequencies of long duration (as in a very noisy signal), this strategy does not pay off, but if the signal is composed of relatively long smooth areas separated by well-localized sharp discontinuities (as in many real or computer-generated images and scenes) then this approach will be effective.

6 Continuous Wavelet Transform

We can choose any set of windows to achieve the constant relative bandwidth, but a simple version is if all the windows are scaled version of each other. To simplify notation, let us define $h(t)$ as:

$$h(t) = w(t)\, e^{-2i\pi f_0 t}$$

and scaled versions of $h(t)$:

$$h_a(t) = \frac{1}{\sqrt{|a|}}\, h(\frac{t}{a})$$

where a is the scale factor (that is $f = \frac{f_0}{a}$), and the constant $\frac{1}{\sqrt{|a|}}$ is for energy normalization. The WFT now becomes:

$$WF(\tau, a) = \frac{1}{\sqrt{|a|}} \int f(t)\, h^*(\frac{t-\tau}{a})\, dt$$

This is known as a *wavelet transform*, and $h(t)$ is the *basic wavelet*. It is clear from the above formula that the basic wavelet is scaled, translated and convolved with the signal to compute the transform. The translation corresponds to moving the window over the time signal, and the scaling, which is often called *dilation* in the context of wavelets, corresponds to the filter frequency bandwidth scaling.

We have used the particular form of $h(t)$ related to the window $w(t)$, but the transform $WF()$ can be defined with any function $h(t)$ satisfying the requirements for a bandpass function, that is it is sufficiently *regular* (see [162] for a definition of regular) its square integral is finite (in the $\mathbf{L}^2$ sense) and its integral $\int h(t)\, dt = 0$.

We can rewrite the basic wavelet as:

$$h_{a,\tau} = \frac{1}{\sqrt{a}}\, h(\frac{t-\tau}{a})$$

to emphasize that we use a set of "basis" functions. The transform is then written as:

$$WF(\tau, a) = \int f(t)\, h^*_{a,\tau}(t)\, dt$$

We can reconstruct the signal as:

$$f(t) = c \int WF(\tau, a)\, h_{a,\tau}(t)\, \frac{da\ dt}{a^2}$$

where c is a constant depending on $h(t)$. The reconstruction looks like a sum of coefficients of orthogonal bases, but the $h_{a,\tau}(t)$ are in fact highly redundant, since they are defined for every point in the a, τ space. Nevertheless the formula above is correct if $\int h^2(t)\ dt$ is finite and $\int h(t)\ dt = 0$ (well, almost).

7 From Continuous to Discrete and Back

Since there is a lot of redundancy in the continuous application of the basic wavelet, a natural question if whether we can discretize a and τ in such a way that we obtain a true orthonormal basis. Following Daubechies [49] one can notice that if we consider two scales $a_0 < a_1$, the coefficients at scale a_1 can be sampled at a lower rate than for a_0 since they correspond to a lower frequency. In fact the sampling rate can be proportional to $\frac{a_0}{a_1}$. Generally, if:

$$a = a_0^i \qquad \tau = j\ a_0^i\ T$$

(i and j integers, T a period) the wavelets are:

$$h_{ij}(t) = a_0^{-\frac{i}{2}}\ h(a_0^{-i}\ t - jT)$$

and the discretized wavelets coefficients are:

$$c_{ij} = \int f(t)\, h_{ij}^*(t)\ dt$$

We hope that with a suitable choice of $h(t)$, a_0 and T we can then reconstruct $f(t)$ as:

$$f(t)\ \simeq\ c \sum_i \sum_j c_{ij}\, h_{ij}(t)$$

It is clear that for a_0 close to 1 and T small, we are close to the continuous case, and the conditions on $h(t)$ will be mild, but as a_0 increases only very special $h(t)$ will work.

7.1 Haar Transform

We can try again the example of the windowed Walsh transform with the box window. Choosing $a_0 = 2$ for the dilation factor, the widths of the boxes will be 32, 16, 8, 4 and 2. We will limit the spacings so that there is no overlap between the windows of the same width[2]. In this case this means spacings of 1×32, 2×16, 4×8, 8×4 and 16×2, for a total of 31 transforms. The coefficients and reconstructed signal are given in Figure I.12 in "circle" form and in Figure I.13 in bar graph form.

It is clear that there is a lot of redundancy in the transforms, as seen by the many coefficients of equal magnitude. We can see the windows as applying to the signal or equivalently as applying to the basis functions. If we consider the Walsh functions and apply the box window properly scaled and translated, we can observe that we get a lot of duplicates in the new "basis" functions, and if we remove them we get

[2]If there are gaps between the windows, obviously some of the samples will be missed altogether. If there are overlaps, the "children" of the boxes will overlap too, and parts of the signal will be over-represented (infinitely so at the limit).

a new set of basis functions (of course it remains to be proved that they are really basis functions). These happen to be the Haar functions, defined by Haar [99] and well known today as the bases for piece-wise constant wavelets (see Figure I.14).

Figures I.15 and I.16 show the coefficients of the Haar basis for both of our exemplar signals. Figure I.17 shows the Haar coefficients for signal 2 with circles for easier comparisons with the windowed Walsh transform.

One can prove that the same information is contained in these 32 values that was in the 31×32 values of the windowed Walsh transforms. It is also clear from the plots that there are many zero coefficients, and in particular for signal 1 the magnitude of the Haar coefficients localize the discontinuities in the signal.

7.2 Image Pyramids Revisited

We can now generalize the concept of image pyramids to what is known in filtering as a *subband coding scheme*. We have applied recursively two operators to the signal to subsample it by 2. The first one is the box, and is a *smoothing*, or a *low-pass* filter, and the other is the basic Haar wavelet, or a *detail* or a *high-pass* filter. In our specific example the detail filter picks out exactly what is necessary to reconstruct the signal later. In general, if we have a low-pass filter $h(n)$, a high-pass filter $g(n)$, and a signal $f(n)$ [3], we can compute the subsampled smooth version:

$$a(k) = \sum_i f(i)\, h(-i + 2k)$$

and the subsampled detail version:

$$d(k) = \sum_i f(i)\, g(-i + 2k)$$

If the smoothing filter is orthogonal to its translates, then the two filters are related as:

$$g(L - 1 - i) = (-1)^i\, h(i)$$

(where L is the length of the filter, which is assumed finite and even). The reconstruction is then exact, and computed as:

$$f(i) = \sum_k [\, a(k)\, h(-i + 2k) + d(k)\, g(-i + 2k)\,]$$

We can apply this scheme recursively to the new smoothed signal $a()$, which is half the size of $f()$, until we have two vectors $a()$ and $d()$ of length 1 after $\log_2(n)$ applications. It is clear that as in the Haar transform this scheme has only $O(n)$ cost. The computational scheme is shown in Figure I.18. The computational scheme for the reconstruction is given in Figure I.19. H is the application (sum over i) of the smoothing filter, G the application of the detail filter, and H^* and G* denote the sum over k of the smoothing and detail filters, respectively.

[3] It would be better to call $l()$ the low pass filter and $h()$ the high pass filter, and some do, but we will use here the usual symbols.

7.3 Dyadic Wavelet Transforms

We have sort of "stumbled" upon the Haar wavelet, from two different directions (from the windowed Walsh transform and from the difference pyramid). We need better methods than that to construct new wavelets and express their basic properties. This is exactly what most of the recent work on wavelets is about [50].

We reproduce the following development from Mallat & Zhong [133]. Consider a wavelet function $\psi(t)$. All we ask is that its average $\int \psi(t)\, dt = 0$. Let us write $\psi_i(t)$ its dilation by a factor of 2^i:

$$\psi_i \;=\; \frac{1}{2^i}\,\psi(\frac{t}{2^i})$$

The wavelet transform of $f(t)$ at scale 2^i is given by:

$$WF_i(t) \;=\; f * \psi_i(t) \;=\; \int_{-\infty}^{\infty} f(\tau)\,\psi_i(t-\tau)\,d\tau$$

The dyadic wavelet transform is the sequence of functions

$$\mathbf{WF}[f()] \;=\; [WF_i(t)] \;\; i \in \mathbf{Z}$$

We want to see how well $\mathbf{WF}$ represents $f(t)$ and how to reconstruct it from its transform. Looking at the Fourier transform (we use $F(f)$ or $\mathbf{F}[f(t)]$ as notation for the Fourier transform of $f(t)$):

$$\mathbf{F}[WF_i(t)] \;=\; F(f)\,\mathbf{\Psi}(2^i f) \tag{1}$$

If we impose that there exists two strictly positive constants A and B such that:

$$\forall f,\; A \;\leq\; \sum_{i=-\infty}^{\infty} |\mathbf{\Psi}(2^i f)|^2 \;\leq\; B \tag{2}$$

we guarantee that everywhere on the frequency axis the sum of the dilations of $\psi()$ have a finite norm. If this is true, then $F(f)$, and therefore $f(t)$ can be recovered from its dyadic wavelet transform. The reconstructing wavelet $\chi(t)$ is any function such that its Fourier transform $X(f)$ satisfies:

$$\sum_{i=-\infty}^{\infty} \mathbf{\Psi}(2^i f)\, X(2^i f) = 1 \tag{3}$$

An infinity of $\chi()$ satisfies (3) if (2) is valid. We can then reconstruct $f(t)$ using:

$$f(t) \;=\; \sum_{i=-\infty}^{\infty} WF_i(t)\,\chi_i(t) \tag{4}$$

Exercise 2: Prove equation (4) by taking its Fourier transform, and inserting (1) and (3). □

Using Parseval's theorem and equations (2) and (4), we can deduce a relation between the norms of $f(t)$ and of its wavelet transform:

$$A \parallel f() \parallel^2 \ \leq \ \sum_{i=-\infty}^{\infty} \parallel WF_i(t) \parallel^2 \ \leq \ B \parallel f() \parallel^2 \tag{5}$$

This proves that the wavelet transform is also *stable*, and can be made close in the $\mathbf{L}^2$ norm by having $\frac{A}{B}$ close to 1.

It is important to note that the wavelet transform may be redundant, in the sense that the some of the information in W_i can be contained in others W_j subspaces. For a more precise statement see [133]

7.4 Discrete Wavelet Transform

To obtain a discrete transform, we have to realize that the scales have a lower limit for a discrete signal. Let us say that $i = 0$ correspond to the limit. We introduce a new *smoothing function* $\phi()$ such that its Fourier transform is:

$$| \Phi(f) |^2 = \sum_{i=1}^{\infty} \Psi(2^i f) \, X(2^i f) \tag{6}$$

From (3) one can prove that $\int \phi(t) \, dt = 1$, and therefore is really a smoothing function (a filter). We can now define the operator:

$$SF_i(t) = \int f(\tau) \, \phi_i(t - \tau) \, d\tau$$

with $\phi_i(t) = \frac{1}{2^i} \, \phi(\frac{t}{2^i})$. So $SF_i(t)$ is a smoothing of $f(t)$ at scale 2^i. From equation (6) we can write:

$$| \Phi(f) |^2 - | \Phi(2^j) |^2 = \sum_{i=1}^{j} \Psi(2^i f) \, X(2^i f)$$

This shows that the high frequencies of $f(t)$ removed by the smoothing operation at scale 2^j can be recovered by the dyadic wavelet transform $WF_i(t)$, $1 \ \leq \ i \ \leq \ j$.

Now we can handle a discrete signal f_n by assuming that there exists a function $f(t)$ such that:

$$SF_1(n) \ = \ f_n$$

This function is not necessarily unique. We can then apply the dyadic wavelet transforms of $f(t)$ at the larger scales, which need only the values of $f(n + w)$, where w are integer shifts depending on $\psi()$ and the scale. Then the sequence of $SF_i(n)$ and $WF_i(n)$ is the discrete dyadic wavelet transform of f_n. This is of course the same scheme used in the generalized multiresolution pyramid. This again tells us that there is a $O(n)$ scheme to compute this transform.

7.5 Multiresolution Analysis

A theoretical framework for wavelet decomposition [130] can be summarized as follows. Given functions in $\mathbf{L}^2$ (this applies as well to vectors) assume a sequence of nested subspaces V_i such that:

$$\cdots V_{-2} \subset V_{-1} \subset V_0 \subset V_1 \subset V_2 \cdots$$

If a function $f(t) \in V_i$ then all translates by multiples of 2^{-i} also belongs ($f(t - 2^{-i}k) \in V_i$). We also want that $f(2t) \in V_{i+1}$. If we call W_i the *orthogonal complement* of V_i with respect to V_{i+1}. We write it:

$$V_{i+1} = W_i \oplus V_i$$

In words, W_i has the details missing from V_i to go to V_{i+1}. By iteration, any space can be reached by:

$$V_i = W_i \oplus W_{i-1} \oplus W_{i-2} \oplus W_{i-3} \cdots \tag{7}$$

Therefore every function in $\mathbf{L}^2$ can be expressed as the sum of the spaces W_i. If V_0 admits an orthonormal basis $\phi_j(t - j)$ and its integer translates ($2^0 = 1$), then V_i has $\phi_{ij} = c_j\phi(2^i - j)$ as bases. There will exist a wavelet $\psi_0()$ which spans the space W_0 with its translates, and its dilations $\psi_{ij}()$ will span W_i. Because of (7), therefore, every function in $\mathbf{L}^2$ can be expressed as a sum of $\psi_{ij}()$, a *wavelet basis*. We then see that a function can be expressed as a sum of wavelets, each representing details of the function at finer and finer scales.

A simple example of a function ϕ is a box of width 1. If we take as V_0 the space of all functions constant within each integer interval $[\, j, j + 1\,)$, it is clear that the integer translates of the box spans that space.

Exercise 3: Show that boxes of width 2^i span the spaces V_i. Should there be a scaling factor when going from width 2^i to 2^{i-1}. Show that the Haar wavelets are the basis for W_i corresponding to the box for V_i. □

7.6 Constructing Wavelets

7.6.1 Smoothing Functions

To develop new dyadic wavelets, we need to find smoothing functions $\phi()$ which obey the basic dilation equation:

$$\phi(t) = \sum_k c_k \, \phi(2t - k)$$

This way, each ϕ_i can be expressed as a linear combination of its scaled version, and if it cover the subspace V_0 with its translates, its dyadic scales will cover the other V_i subspace. Recalling that $\int \phi(t)\, dt = 1$, and integrating both sides of the above equation, we get:

$$\int \phi(t)\, dt = \sum_k c_k \int \phi(2t - k)\, dt$$

and since $d(2t - k) = 2dt$, then $\sum_k c_k = 2$. One can see that when $c_0 = c_1 = 1$, for instance, we obtain the box function, which is the Haar smoothing function.

Three construction methods have been used to produce new $\phi(t)$ (see Strang [177] for details).

1. Iterate the recursive relation starting with the box function and some c values. This will give the splines family (box, hat , quadratic, cubic, etc..) with the initial values [1,1], [$\frac{1}{2}, 1, \frac{1}{2}$], [$\frac{1}{4}, \frac{3}{4}, \frac{3}{4}, \frac{1}{4}$], [$\frac{1}{8}, \frac{4}{8}, \frac{6}{8}, \frac{4}{8}, \frac{1}{8}$]. One of Daubechies' wavelets, noted D_4, is obtained by this method with [$\frac{1+\sqrt{3}}{4}, \frac{3+\sqrt{3}}{4}, \frac{3-\sqrt{3}}{4}, \frac{1-\sqrt{3}}{4}$].
2. Work from the Fourier transform of $\phi()$ (equation (6)). Imposing particular forms on it and the Fourier transform of $\psi()$ and $\chi()$ can lead to a choice of suitable functions. See for instance in Mallat & Zhong [133] how they obtain a wavelet which is the derivative of a cubic spline filter function.
3. Work directly with the recursion. If $\phi()$ is known at the integers, applying the recursion gives the values at all points of values $\frac{i}{2^j}$.

7.6.2 Approximation and Orthogonality

The basic properties for approximation accuracy and orthogonality are given, for instance, in Strang [177]. The essential statement is that a number p characterize the smoothing function $\phi()$ such that:

- polynomials of degree $p - 1$ are linear combinations of $\phi()$ and its translates
- smooth functions are approximated with error $\mathbf{O}(h^p)$ at scale $h = 2^{-j}$
- the first p moments of $\psi()$ are 0:

$$\int t^n\, \psi(t)\, dt = 0, \;\; n = 0, \ldots, p - 1$$

Those are known as the *vanishing moments*. For Haar, $p = 1$, for D_4 $p = 2$.

The function $\psi()$ is defined as $\phi()$, but using the differences:

$$\psi(t) = \sum (-1)^k\, c_{1-k}\, \phi(2t - k)$$

The function so defined is orthogonal to $\phi()$ and its translates. If the coefficients c_i are such that

$$\sum c_k c_{k-2m} = 2\delta_{0m}$$

and $\phi_0()$ is orthogonal to its translates, then so are all the $\phi_i()$ at any scale, and the $\psi_i()$ at any scale. If they are constructed from the box function as in method 1, then the orthogonality is achieved.

7.7 Matrix Notation

A compact and easy to manipulate notation to compute the transformations is using matrices (infinite in principle). Assuming that $c_i, i = 0 \ldots L-1$ are the coefficients of the dilation equation then the matrix $[H]$ is defined such that $H_{ij} = \frac{1}{2}\, c_{2i-j}$. The matrix $[G]$ is defined by $G_{ij} = \frac{1}{2}\,(-1)^{j+1}\, c_{j+1-2i}$. The factor $\frac{1}{2}$ could be replaced by $\frac{1}{\sqrt{2}}$ for energy normalization (note that sometimes this factor is already folded into the c_i, be sure you take this into account for coding). The matrix $[H]$ is the smoothing filter (*the restriction operator* in multigrid language), and $[G]$ the detail filter (the *interpolation operator*).

The low-pass filtering operation is now applying the $[H]$ matrix to the vector of values f. The size of the submatrix applied is $\frac{n}{2} \times n$ if n is the original size of the vector $2^J = n$. The length of the result is half the length of the original vector. For the high pass filter the matrix $[G]$ is applied similarly. The process is repeated J times until only one value each of a and d is obtained.

The reconstruction matrices in the orthogonal cases are merely the transpose of $[H^*] = [H]^T$ and $[G^*] = [G]^T$ (with factor of 1 if $\frac{1}{2}$ is used, $\frac{1}{\sqrt{2}}$ otherwise). The reconstruction operation is then:

$$a^j = [H^*]\, a^{j-1} + [G^*]\, d^{j-1}$$

with $j = 1, \ldots, J$. as shown in Figure I.19.

As an example we can now compute the wavelet itself, by inputing a unit vector and applying the inverse wavelet transform. For example, the fifth basis from D_4 is given in Figure I.20.

Of course by construction all the other bases are translated and scaled versions of this one.

7.8 Multiscale Edge Detection

There is an important connection between wavelets and edge detection, since wavelets transforms are well adapted to "react" locally to rapid changes in values of the signal. This is made more precise by Mallat and Zhong [133]. Given a smoothing function $\theta()$ (related to $\phi()$, but not the same), such that $\int \theta(t)\, dt = 1$ and it converges to 0 at infinity, if its first and second derivative exist, they are wavelets:

$$\psi^1(t) = \frac{d\theta(t)}{dt} \text{ and } \psi^2(t) = \frac{d^2\theta(t)}{dt^2}$$

If we use these wavelets to compute the wavelet transform of some function $f(t)$, noting $\psi_a(t) = \frac{1}{a}\, \psi(\frac{t}{a})$:

$$WF^1{}_a(t) = f * \psi^1{}_a(t) = f * (a\frac{d\theta_a}{dt})(t) = a\frac{d}{dt}(f * \theta_a)(t)$$

$$WF^2{}_a(t) = f * \psi^2{}_a(t) = f * (a^2\frac{d^2\theta_a}{dt^2})(t) = a^2\frac{d^2}{dt^2}(f * \theta_a)(t)$$

So the wavelet transforms are the first and second derivative of the signal smoothed at scale a. The local extrema of $WF^1{}_a(t)$ are zero-crossings of $WF^2{}_a(t)$ and inflection points of $f * \theta_a(t)$. If $\theta(t)$ is a Gaussian, then zero-crossing detection is equivalent to the Marr-Hildreth [139] edge detector, and extrema detection equivalent to Canny [17] edge detection.

8 Multi-dimensional Wavelets

For many applications, in particular for image processing and image compression, we need to generalize wavelets transforms to two dimensions. First, we will consider how to perform a wavelet transform of the pixel values in a two-dimensional image. Then the scaling functions and wavelets that form a two-dimensional wavelet basis. We will use the Haar basis as a simple example, but it will apply to other bases as well[4]. There are two ways we can generalize the one-dimensional wavelet transform to two dimensions, *standard* and *non-standard* decomposition (since a multi-dimensional wavelet transform is frequently referred to in the literature as a *wavelet decomposition*, we will use that term in this section).

8.1 Standard Decomposition

To obtain the *standard decomposition* [15] of an image, we first apply the one-dimensional wavelet transform to each row of pixel values. This operation gives us an average value along with detail coefficients for each row. Next, we treat these transformed rows as if they were themselves an image, and apply the one-dimensional transform to each column. The resulting values are all detail coefficients except for a single overall average coefficient. We illustrate each step of the standard decomposition in Figure I.21.

The standard decomposition of an image gives coefficients for a basis formed by the *standard construction* [15] of a two-dimensional basis. Similarly, the non-standard decomposition gives coefficients for the *non-standard construction* of basis functions.

The standard construction of a two-dimensional wavelet basis consists of all possible tensor products of one-dimensional basis functions. For example, when we start with the one-dimensional Haar basis for V^2, we get the two-dimensional basis for V^2 that is shown in Figure I.22. In general we define the new functions from the 1D smooth and wavelet functions:

$$\phi(u) \times \phi(v) \quad \phi(u) \times \psi(v) \quad \psi(u) \times \phi(v) \quad \psi(u) \times \psi(v)$$

These are orthogonal if the 1-D version are, and the first is a smoothing function, the other three are wavelets.

8.2 Non-Standard Decomposition

The second type of two-dimensional wavelet transform, called the *non-standard decomposition*, alternates between operations on rows and columns. First, we perform one step of horizontal pairwise averaging and differencing on the pixel values in each row of the image. Next, we apply vertical pairwise averaging and differencing to each column of the result. To complete the transformation, we repeat this process recursively on the quadrant containing averages in both directions. Figure I.23 shows all the steps involved in the non-standard decomposition of an image.

The *non-standard construction* of a two-dimensional basis proceeds by first defining a two-dimensional scaling function,

$$\phi\phi(x, y) \quad := \quad \phi(x)\,\phi(y),$$

[4]This section is largely copied, with kind permission, from a University of Washington Technical Report (94-09-11) by Eric Stollnitz, Tony DeRose and David Salesin.

and three wavelet functions,

$$\begin{aligned} \phi\psi(x,y) &:= \phi(x)\,\psi(y) \\ \psi\phi(x,y) &:= \psi(x)\,\phi(y) \\ \psi\psi(x,y) &:= \psi(x)\,\psi(y). \end{aligned}$$

The basis consists of a single coarse scaling function along with all possible scales and translates of the three wavelet functions. This construction results in the basis for V^2 shown in Figure I.24.

We have presented both the standard and non-standard approaches to wavelet transforms and basis functions because they each have advantages. The standard decomposition of an image is appealing because it can be accomplished simply by performing one-dimensional transforms on all the rows and then on all the columns. On the other hand, it is slightly more efficient to compute the non-standard decomposition of an image. Each step of the non-standard decomposition computes one quarter of the coefficients that the previous step did, as opposed to one half in the standard case.

Another consideration is the *support* of each basis function, meaning the portion of each function's domain where that function is non-zero. All of the non-standard basis functions have square supports, while some of the standard basis functions have non-square supports. Depending upon the application, one of these choices may be more favorable than another.

8.3 Quincunx Scheme

One can define a sublattice in $\mathbf{Z}^2$ by selecting only points (i, j) which satisfies:

$$\begin{pmatrix} i \\ j \end{pmatrix} = \begin{pmatrix} 1 & 1 \\ 1 & -1 \end{pmatrix} \begin{pmatrix} m \\ n \end{pmatrix}$$

for all $m, n \in \mathbf{Z}$. One can construct non-separable smoothing and detail functions based on this sampling matrix, with a subsampling factor of 2 (as opposed to 4 in the separable case). The iteration scheme is then identical to the one for the 1-D case [50].

9 Applications of Wavelets in Graphics

Except for the illustration of signal compression in 1D, this is only a brief overview. The following sections cover most of these topics in useful details.

9.1 Signal Compression

A transform can be used for signal compression, either by keeping all the coefficients, and hoping that there will be enough 0 coefficients to save space in storage (and transmission). This will be a *loss-less* compression, and clearly the compression ratio will depend on the signal. Transforms for our test signals indicate that there are indeed many 0 coefficients for simple signals. If we are willing to lose some information on the signal, we can *clamp* the coefficients, that is set to 0 all the coefficients whose absolute values are less than some threshold (user-defined). One can then reconstruct an approximation (a "simplified" version) of the original signal. There is an abundant literature on the topic, and this is one of the biggest applications of

wavelets so far. Chapter IV covers this topic.

To illustrate some of the results with wavelets *vs* we can test the transforms on signals more realistic than our previous examples (albeit still 1D).

The following figure (Figure I.25) shows a signal (signal 3) which is made of 256 samples of the red signal off a digitized video frame of a real scene (a corner of a typical lab). Figure I.26 shows the coefficients of the Walsh transform for this signal. If we apply the Haar transform to our exemplar signal, we obtain the following coefficients (Figure I.27). We can now reconstruct that signal, but first we remove all the coefficients whose absolute value is not greater than 1 (which leaves 28 non-zero coefficients). The result is shown in Figure I.28. For another example we use one of Daubechies' wavelets, noted D_4. It is a compact wavelet, but not smooth. We obtain the following coefficients (Figure I.29).

We can now reconstruct that signal, this time clamping the coefficients at 7 (warning: this is sensitive to the constants used in the transform). This leaves 35 non-zero coefficients. The result is shown in Figure I.30.

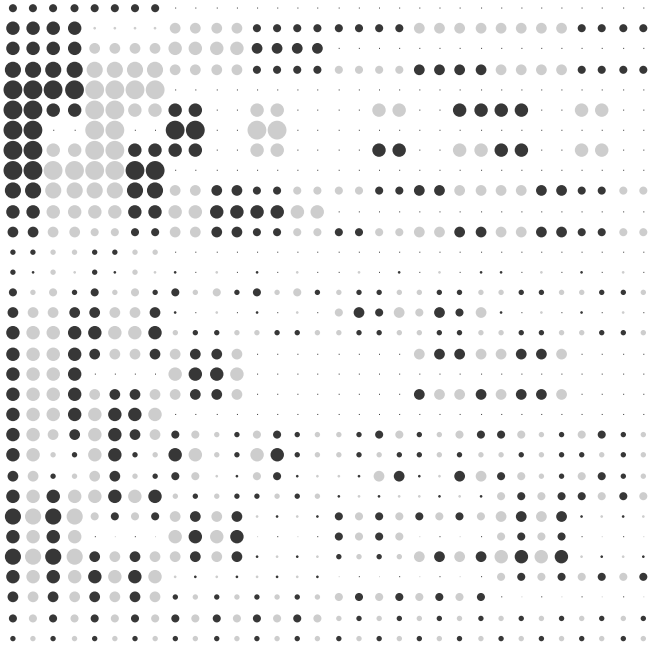

Figure I.10: Signal 2 analysed with windowed Walsh transform

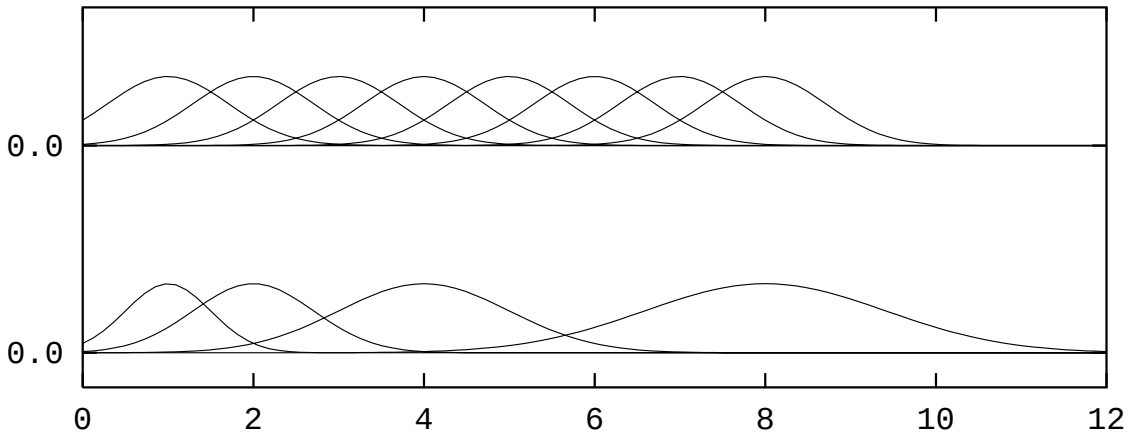

Figure I.11: Constant bandwidth vs constant relative bandwidth window

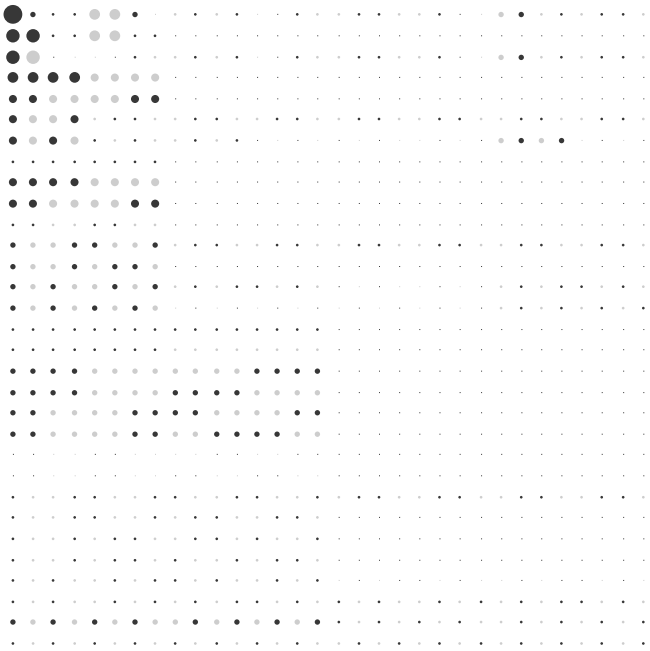

Figure I.12: Signal 2 analysed with scaled windowed Walsh transform

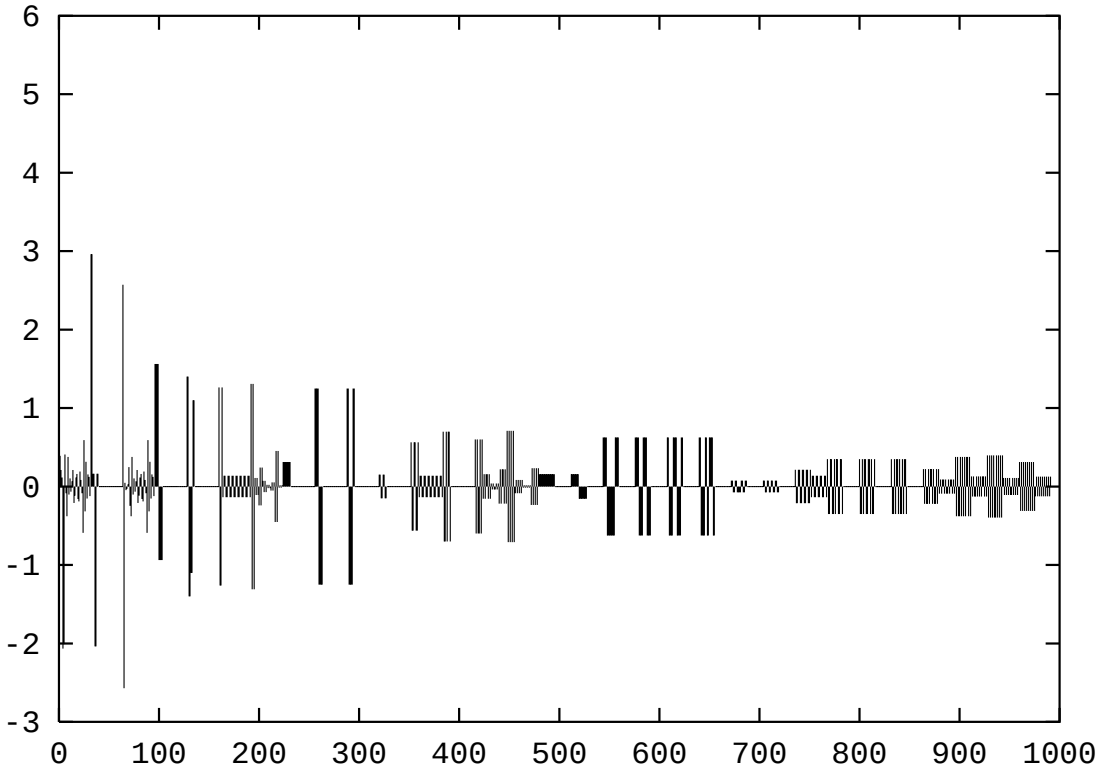

Figure I.13: Signal 2 analysed with scaled windowed Walsh transform (bar graph)

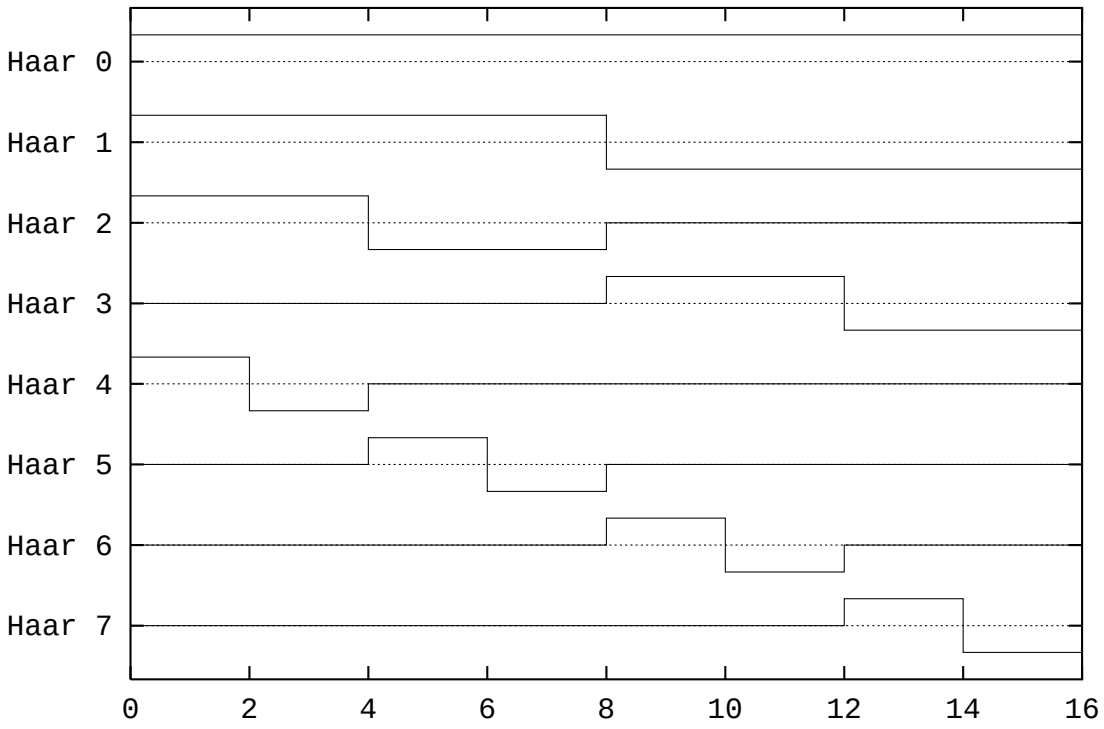

Figure I.14: First 8 Haar bases

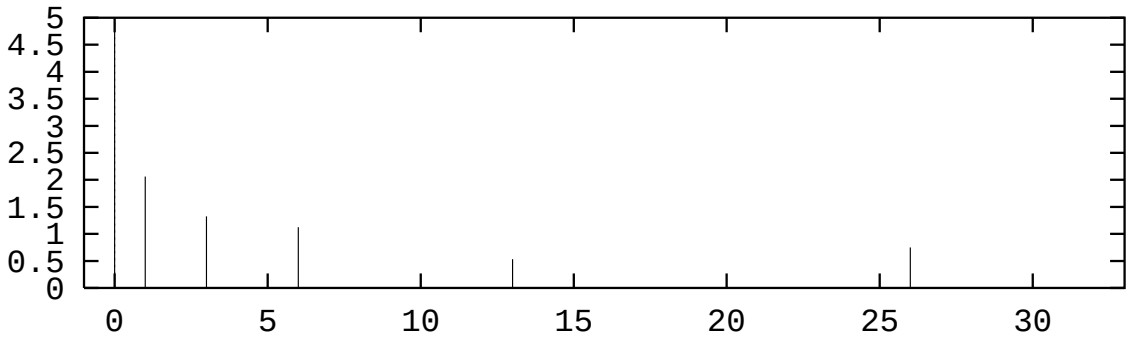

Figure I.15: Haar coefficients for signal 1.

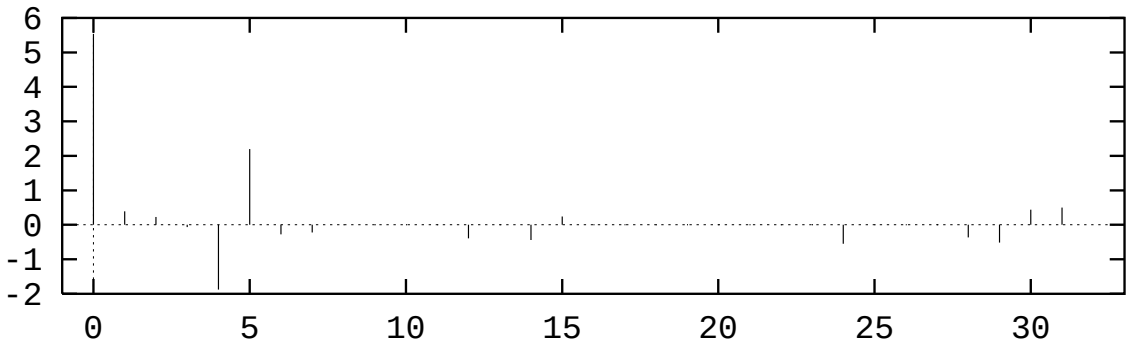

Figure I.16: Haar coefficients for signal 2.

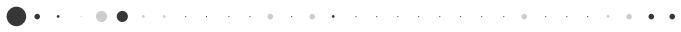

Figure I.17: Haar coefficients for signal 2 (circle plot).

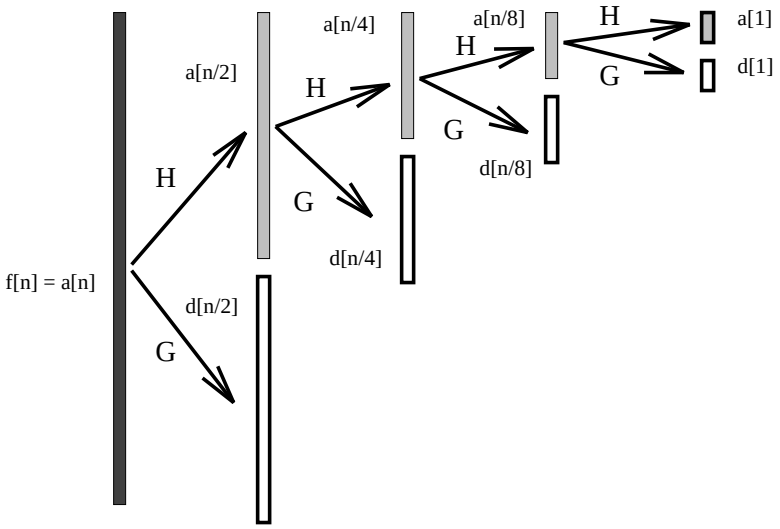

Figure I.18: Discrete wavelet transform as a pyramid

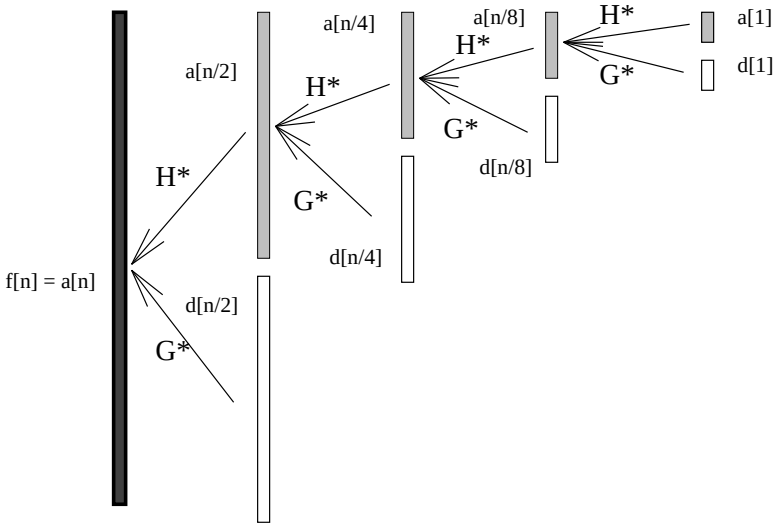

Figure I.19: Reconstructing the signal from wavelet pyramid

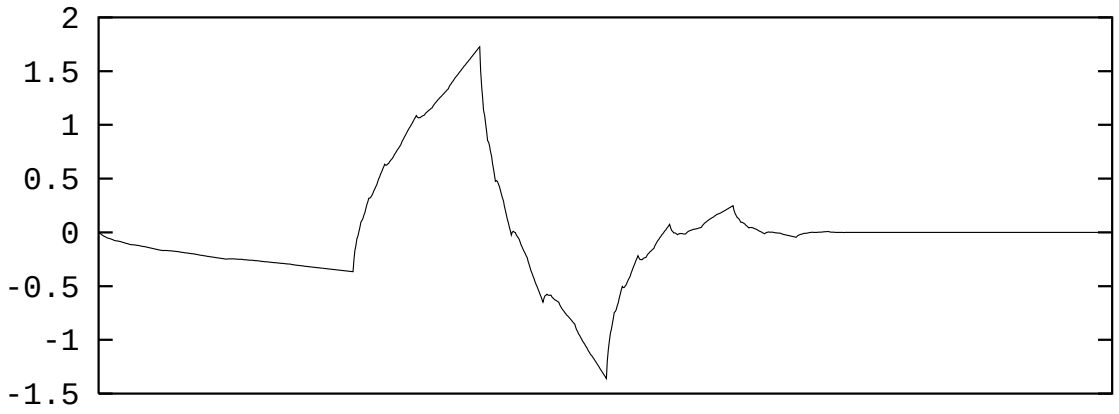

Figure I.20: Wavelet basis function (from D_4)

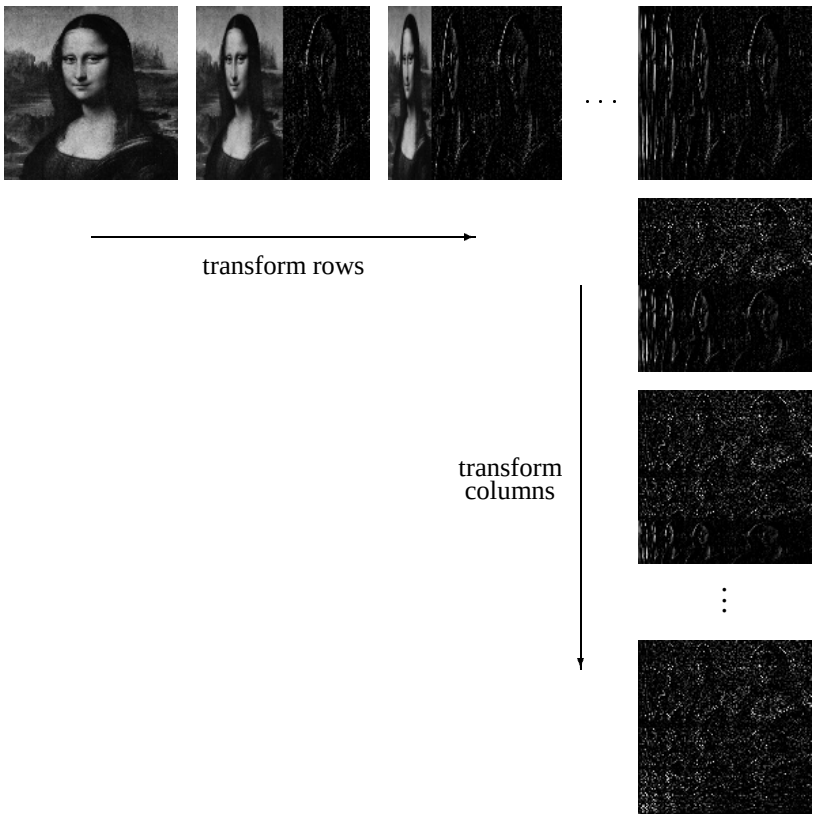

Figure I.21: Standard decomposition of an image.

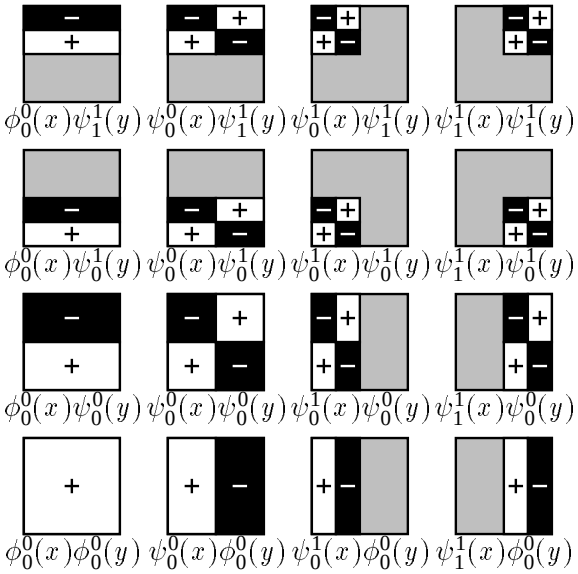

Figure I.22: The standard construction of a two-dimensional Haar wavelet basis for V^2. In the unnormalized case, functions are $+1$ where plus signs appear, -1 where minus signs appear, and 0 in gray regions.

Figure I.23: Non-standard decomposition of an image.

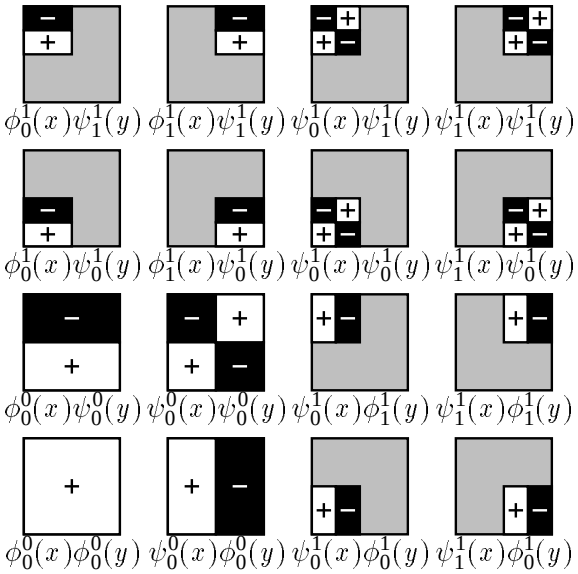

Figure I.24: The non-standard construction of a two-dimensional Haar wavelet basis for V^2.

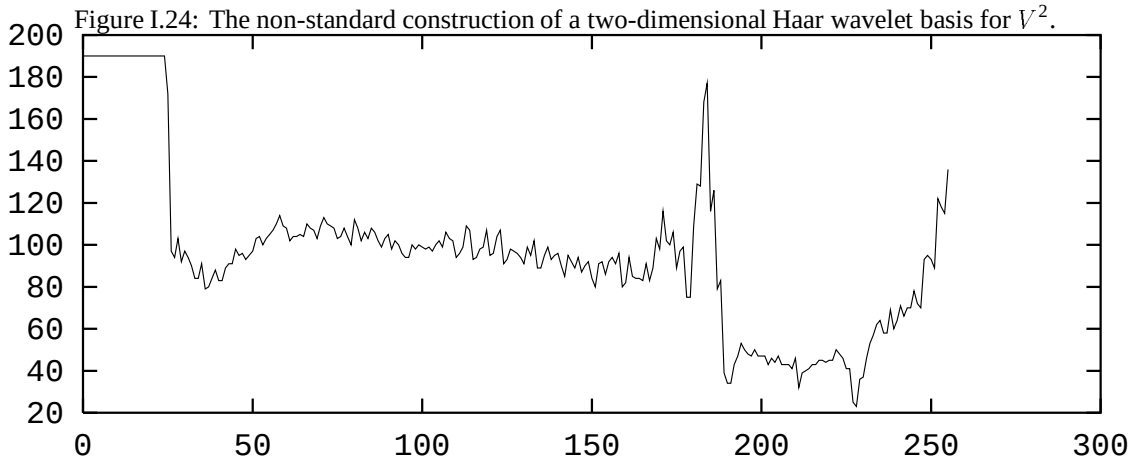

Figure I.25: 1D section of digitized video (signal 3)

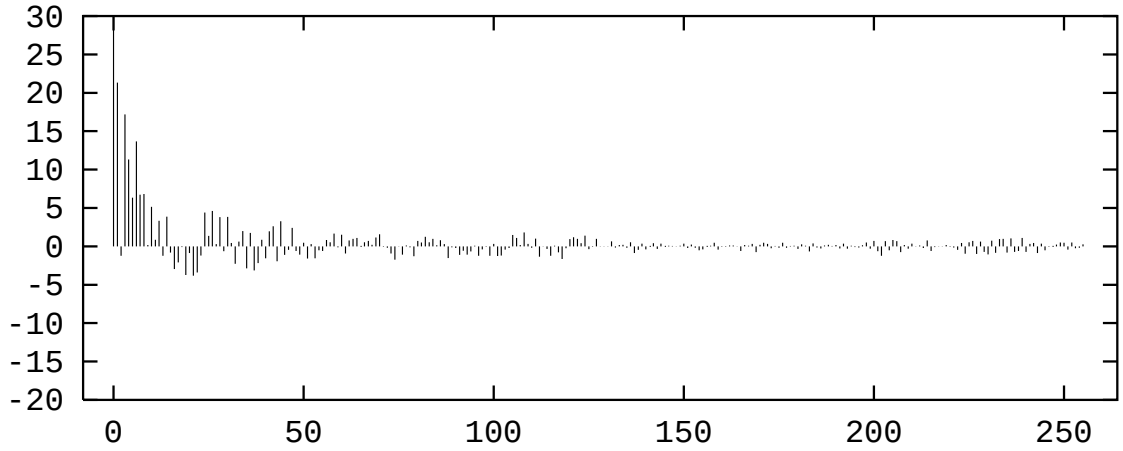

Figure I.26: Walsh transform of signal 3

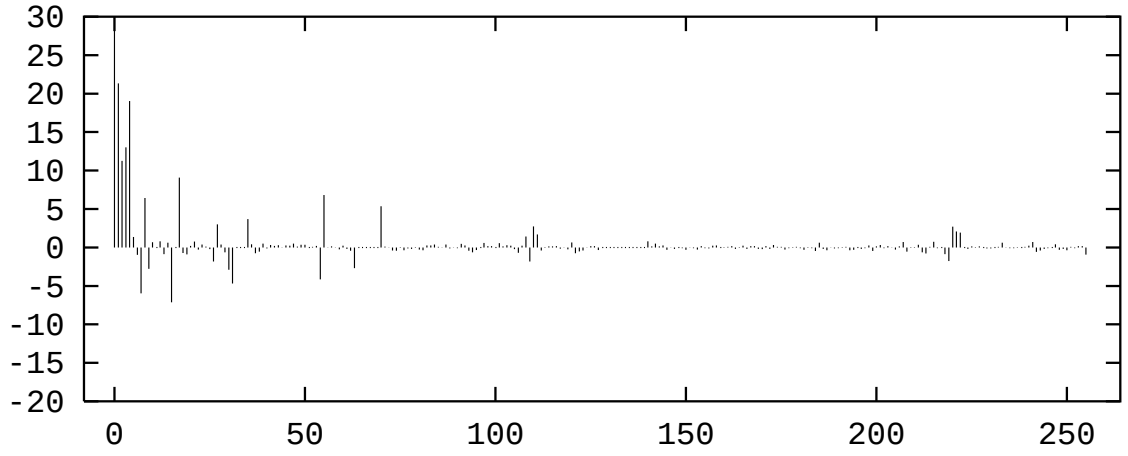

Figure I.27: Haar transform of signal 3

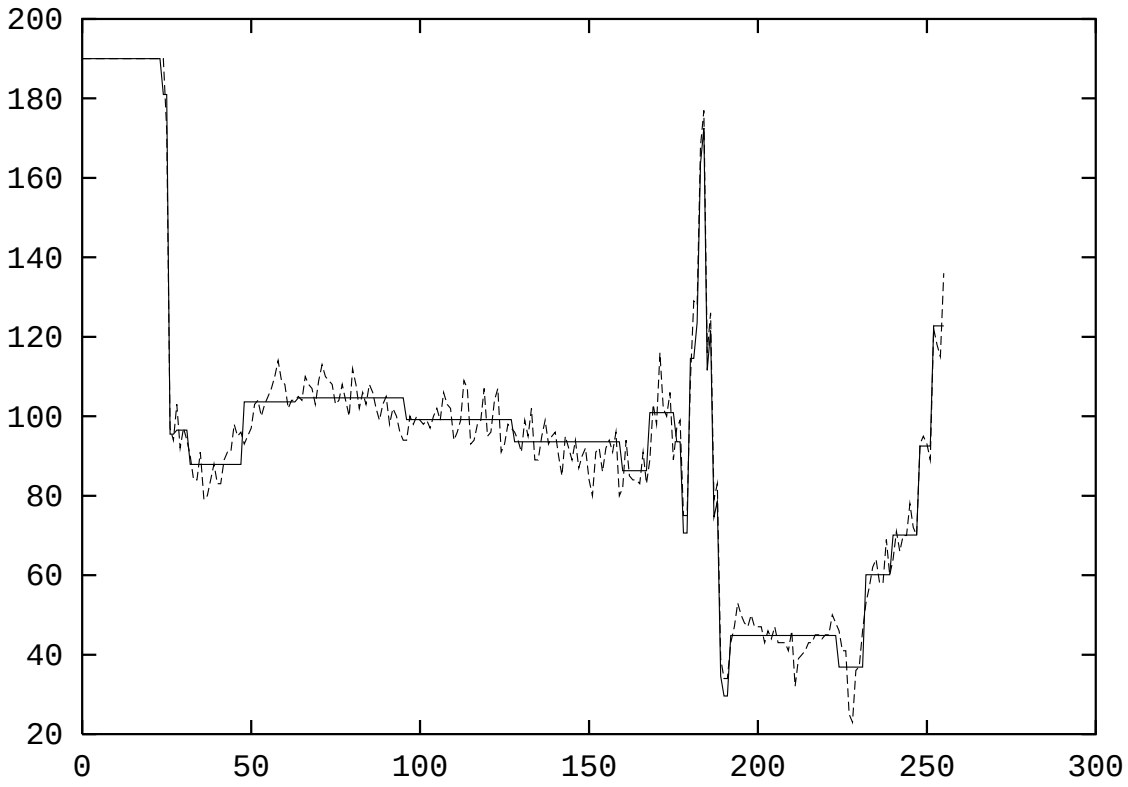

Figure I.28: Reconstructed signal 3 with 28 Haar coefficients

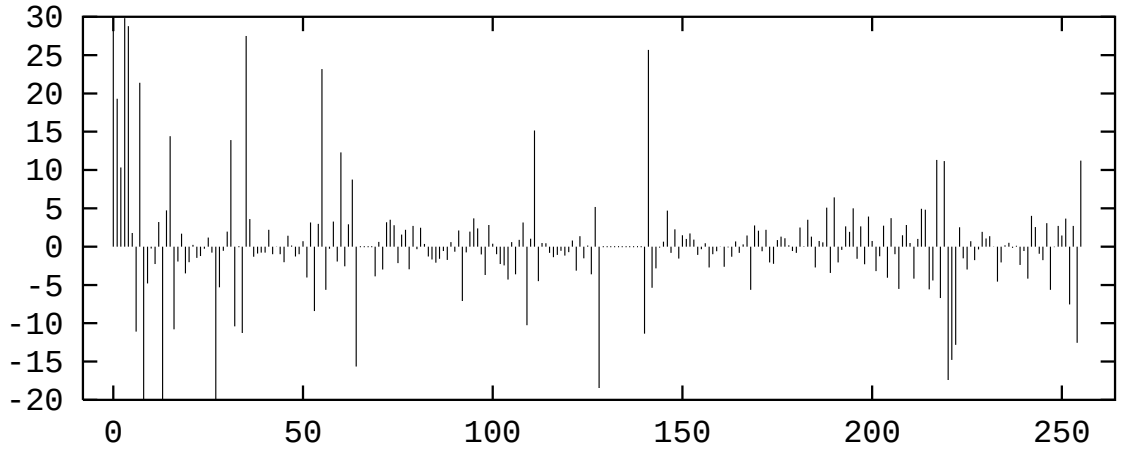

Figure I.29: D_4 transform of signal 3

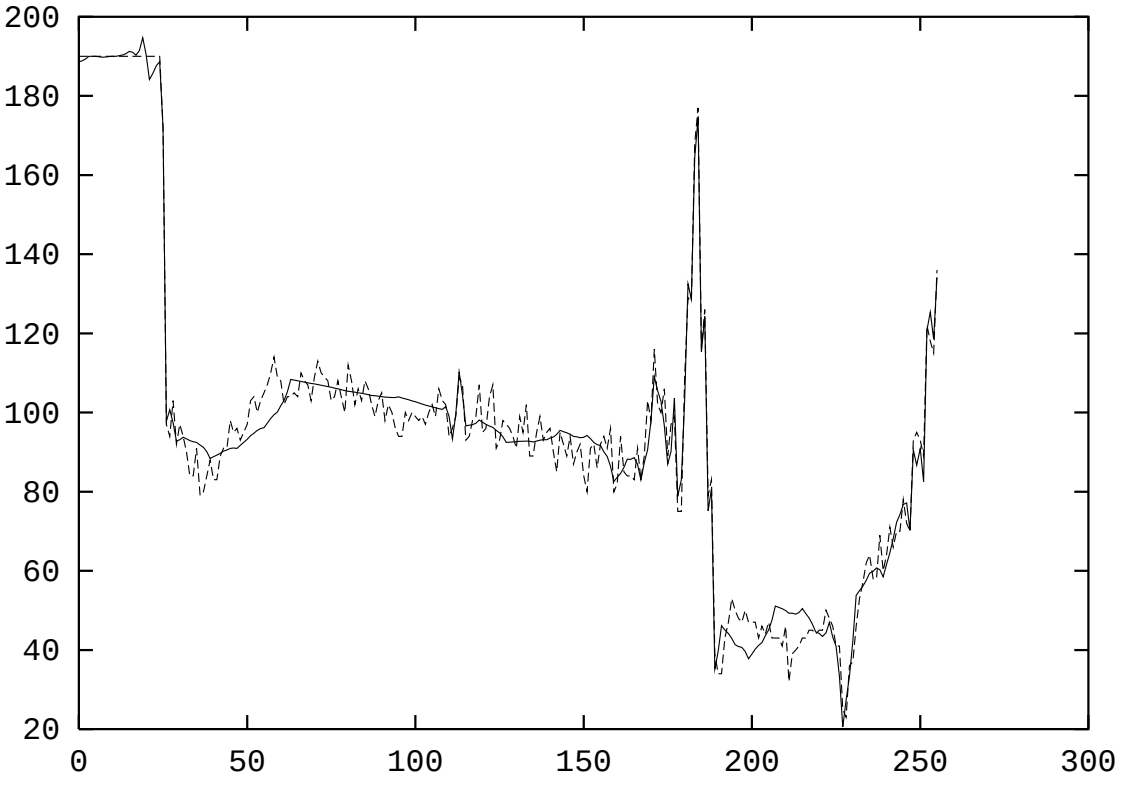

Figure I.30: Reconstructed signal 3 with 35 D_4 coefficients

We now go through the same series with a signal (signal 4) sampled across a computer generated image (Figure I.31). Figure I.32 shows the coefficients of the Walsh transform for this signal. If we apply the Haar transform to this signal, we obtain the following coefficients (Figure I.33). We can now again reconstruct the signal, but first we remove all the coefficients whose absolute value is not greater than 1 (which leaves 47 non-zero coefficients). The result is shown in Figure I.34. Now with D_4. We obtain the following coefficients (Figure I.35). Again we clamp the coefficients at 7. This leaves 70 non-zero coefficients. The result is shown in Figure I.36.

Chapter IV will cover the topic in its practical context, image processing.

9.2 Modelling of Curves and Surfaces

This application is also only beginning, even though the concept of multi-resolution modelling has been around, both in graphics [83] and in vision [145]. Chapter V will describe several applications in this area.

9.3 Radiosity Computations

To compute global illumination in a scene, the current favourite approach is using "radiosity" [39]. This approach leads to a system of integral equations, which can be solved by restricting the solutions to a subspace spanned by a finite basis. We then can choose wavelets basis to span that subspace, hoping that the resulting matrix necessary to solve the system will be sparse. Chapter VI will elaborate on this topic.

10 Other Applications

There are many more applications of wavelets relevant to computer graphics. As a sample, Chapter VII will survey applications to spacetime control, variational modeling, solutions of integral and differential equations, light flux representations and computation of fractal processes.

An interesting area of application of wavelet techniques not covered here is in paint systems. A paper at this conference (by D. F. Berman. J. T. Bartell and D. H. Salesin) describes a system based on the Haar basis to implement *multiresolution painting*. The inherent hierarchy of the wavelet transform allows the user to paint using common painting operations such as *over* and *erase* at any level of detail needed. Another implementation of the same concept is from Luis Velho and Ken Perlin. They use a biorthogonal spline basis for smoothness (remember that in the straightforward case the wavelet smoothing filter serves as a reconstruction filter when the user zooms into the "empty spaces"). A price is paid in performance (more non-zero elements in the filters), but the parameters of the trade-off are of course changing rapidly.

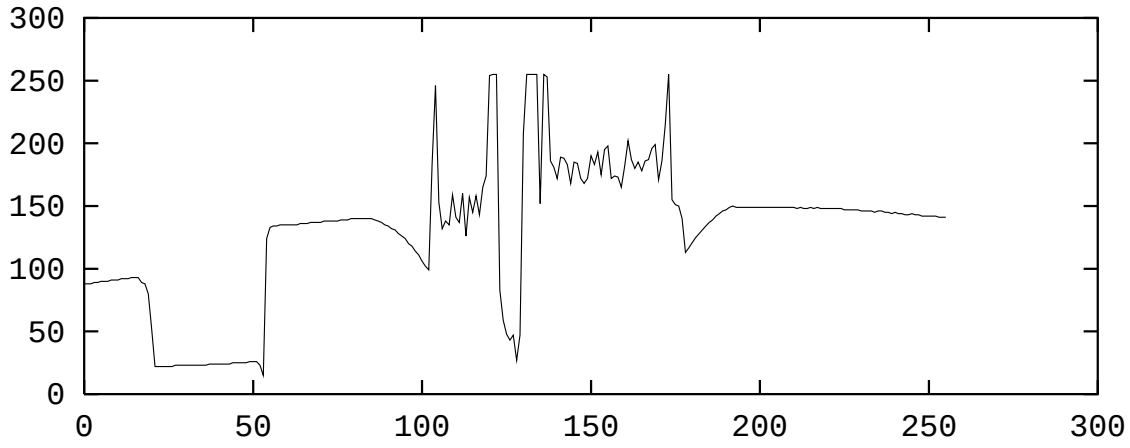

Figure I.31: 1D section of computer generated image (signal 4)

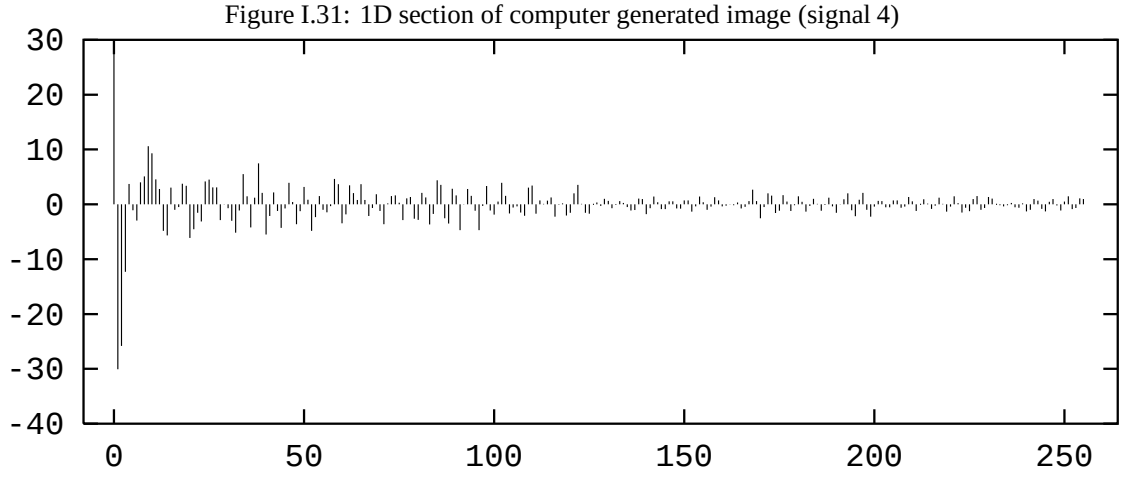

Figure I.32: Walsh transform of signal 4

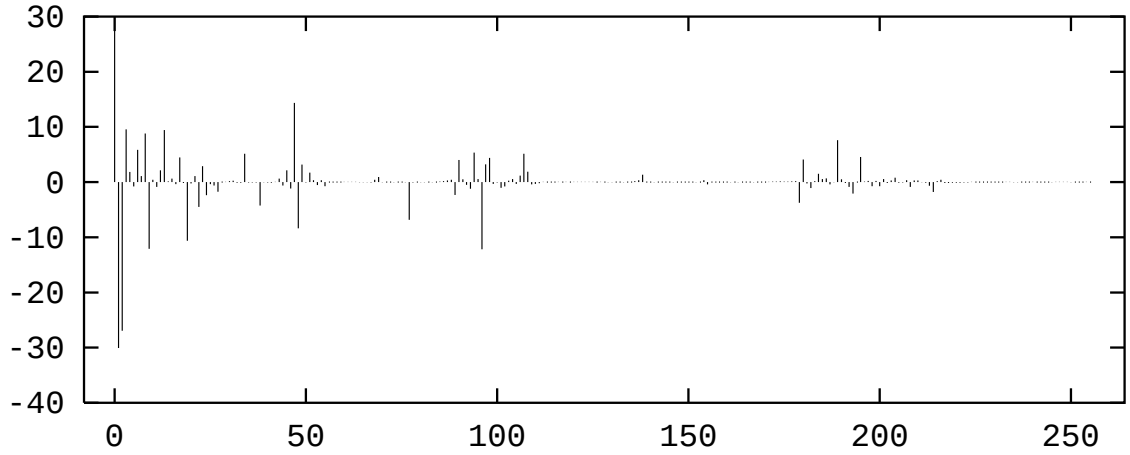

Figure I.33: Haar transform of signal 4

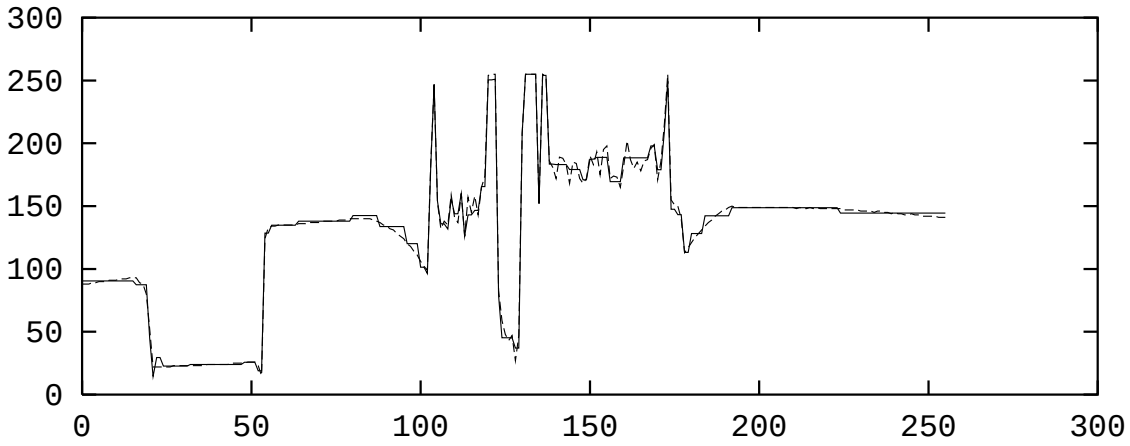

Figure I.34: Reconstructed signal with 47 Haar coefficients

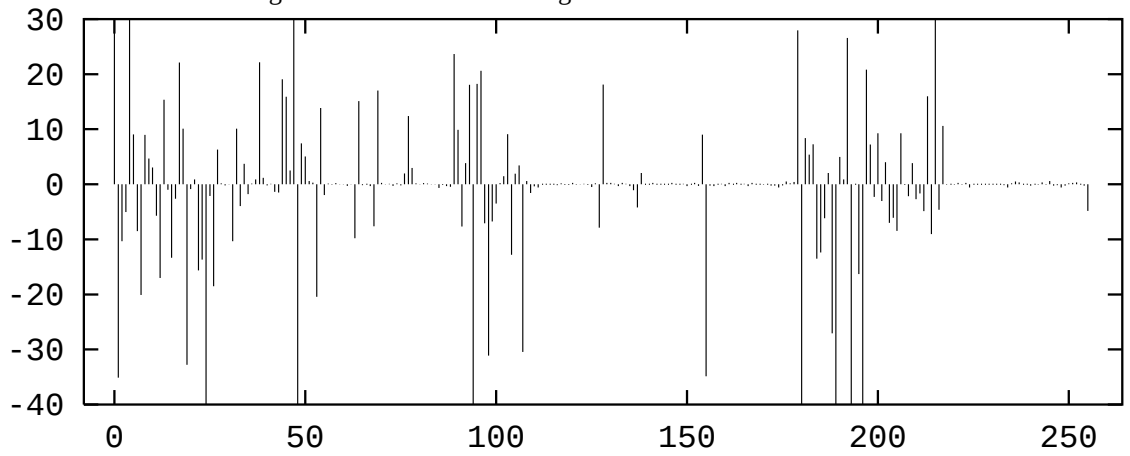

Figure I.35: D_4 transform of signal 4

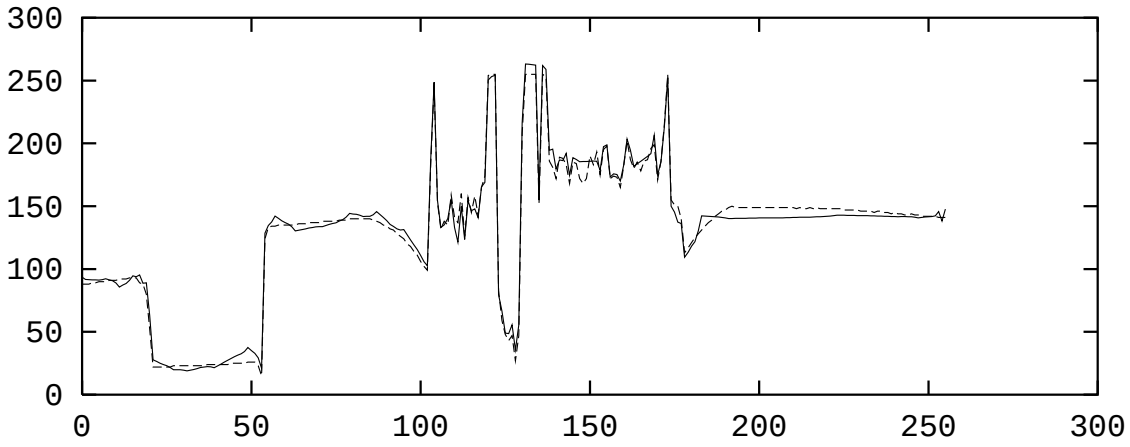

Figure I.36: Reconstructed signal 4 with 70 D_4 coefficients

II: Multiresolution and Wavelets

Leena-Maija REISSELL
University of British Columbia

1 Introduction

This section discusses the properties of the basic discrete wavelet transform. The concentration is on orthonormal multiresolution wavelets, but we also briefly review common extensions, such as biorthogonal wavelets. The fundamental ideas in the development of orthonormal multiresolution wavelet bases generalize to many other wavelet constructions.

The *orthonormal wavelet decomposition* of discrete data is obtained by a pyramid filtering algorithm which also allows exact reconstruction of the original data from the new coefficients. Finding this wavelet decomposition is easy, and we start by giving a quick recipe for doing this. However, it is surprisingly difficult to find suitable, preferably finite, filters for the algorithm. One objective in this chapter is to find and characterize such filters. The other is to understand what the wavelet decomposition says about the data, and to briefly justify its use in common applications.

In order to study the properties of the wavelet decomposition and construct suitable filters, we change our viewpoint from pyramid filtering to spaces of functions. A discrete data sequence represents a function in a given basis. Similarly, the wavelet decomposition of data is the representation of the function in a *wavelet basis*, which is formed by the discrete dilations and translations of a suitable basic wavelet. This is analx ogous to the control point representation of a function using underlying cardinal B-spline functions.

For simplicity, we will restrict the discussion to the 1-d case. There will be some justification of selected results, but no formal proofs. More details can be found in the texts [50] and [26] and the review paper [113]. A brief overview is also given in [177].

1.1 A recipe for finding wavelet coefficients

The wavelet decomposition of data is derived from 2-channel subband filtering with two filter sequences (h_k), the *smoothing* or *scaling filter*, and (g_k), the *detail*, or *wavelet, filter*. These filters should have the following special properties:

Filter conditions:

- $\sum_k h_k = \sqrt{2}$
- $g_j = (-1)^j h_{1-j}$
- $\sum_k g_k = 0$
- $\sum_k h_k h_{k+2m} = \delta_{0m}$, for all m

At first glance, these conditions may look slightly strange, but they in fact contain the requirements for exact reconstruction. The wavelet filter (h_k) is sometimes called the *mirror* filter of the filter (h_k), since it is given by the elements of the scaling filter but in backwards order, and with every other element negated. For simplicity, we only consider filters which are finite and real.

The two-element filter $(1, 1)$, normalized suitably, is a simple example – this filter yields the Haar pyramid scheme. Another example which satisfies these conditions is the 4-element filter

$$D_4: \quad \frac{1+\sqrt{3}}{4\sqrt{2}}, \ \frac{3+\sqrt{3}}{4\sqrt{2}}, \ \frac{3-\sqrt{3}}{4\sqrt{2}}, \ \frac{1-\sqrt{3}}{4\sqrt{2}} \ ,$$

constructed by Daubechies.

We now look more closely at where these conditions come from. Two-channel filtering of the data sequence $\mathbf{x} = (x_i)$ by a filter (h_k) means filtering which yields two new sequences:

$$y_i = \sum_k h_k x_{2i+k} \ = \ \sum_k h_{k-2i} x_k, \quad z_i = \sum_k g_k x_{2i+k} \ = \ \sum_k g_{k-2i} x_k. \tag{1}$$

In matrix form, this filtering can be expressed as follows:

$$\mathbf{y} = \mathbf{H}\mathbf{x}, \quad \mathbf{z} = \mathbf{G}\mathbf{x}.$$

Here the matrix $\mathbf{H} = (h_{k-2i})_{ik}$ is a convolution matrix, with every other row dropped:

$$\begin{pmatrix} \dots & 0 & h_0 & h_1 & h_2 & h_3 & 0 & 0 & 0 & \dots & \dots \\ \dots & \dots & \dots & 0 & h_0 & h_1 & h_2 & h_3 & 0 & 0 & \dots \\ \dots & \dots & \dots & \dots & \dots & 0 & h_0 & h_1 & h_2 & h_3 & 0 \\ \dots & & & & & & & & & & \end{pmatrix}$$

The matrix $\mathbf{G}$ is defined similarly using the detail filter (g_k). The 2-channel filtering process "downsamples" (by dropping alternate rows from the convolution matrix) and produces a sequence half the length of the

original. The normalization conditions for the filters imply that the filter (h_i) constitutes a lowpass filter which smooths data and the filter (g_i) a highpass filter which picks out the detail; this difference in filter roles can also be seen in the examples in the previous section.

Reconstruction is performed in the opposite direction using the adjoint filtering operation:

$$x_i = \sum_k h_{i-2k} y_k + g_{i-2k} z_k . \tag{2}$$

In matrix form: $\mathbf{x} = \mathbf{H^T y} + \mathbf{G^T z}$, where $\mathbf{H^T}$ is the transpose of $\mathbf{H}$:

$$\begin{pmatrix} h_0 & \dots & \dots \\ h_1 & 0 & 0 \\ h_2 & h_0 & 0 \\ h_3 & h_1 & 0 \\ 0 & h_2 & h_0 \\ 0 & h_3 & h_1 \\ 0 & 0 & h_2 \\ \dots & & \end{pmatrix}$$

The reconstruction step filters and upsamples: the upsampling produces a sequence twice as long as the sequences started with.

Note: Some of the filter requirements often show up in slightly different forms in the literature. For instance, the normalization to $\sqrt{2}$ is a convention stemming from the derivation of the filters, but it is also common to normalize the sum of the filter elements to equal 1. Similarly, the wavelet filter definition can appear with different indices: the filter elements can for instance be shifted by an even number of steps. The differences due to these changes are minor.

Similarly, decomposition filtering is often defined using the following convention:

$$y'_i = \sum_k h_{2i-k} x_k , \quad z'_i = \sum_k g_{2i-k} x_k . \tag{3}$$

The only difference is that the filter is applied "backwards" in the scheme (3), conforming to the usual convolution notation, and forwards in (1). Again, there is no real difference between the definitions. We choose the "forward" one only because it agrees notationally with the standard definition of wavelets via dilations and translations. If decomposition is performed as in (3), the reconstruction operation (2) should be replaced by:

$$x_i = \sum_k h_k y'_{\frac{i+k}{2}} + g_k z'_{\frac{i+k}{2}} . \tag{4}$$

1.2 Wavelet decomposition

We should theoretically deal with data of infinite length in this setup. But in practice, let's assume the data has length 2^N. The full wavelet decomposition is found via the *pyramid*, or *tree*, algorithm:

$$\begin{array}{ccccccc} & \mathbf{H} & & \mathbf{H} & & \mathbf{H} & \\ \mathbf{s} & \longrightarrow & \mathbf{s}_1 & \longrightarrow & \mathbf{s}_2 & \longrightarrow & \ldots \\ & \mathbf{G} & & \mathbf{G} & & \mathbf{G} & \\ & \searrow & & \searrow & & \searrow & \\ & & \mathbf{w}_1 & & \mathbf{w}_2 & & \ldots \end{array} \tag{5}$$

The pyramid filtering is performed for N steps, and each step gives sequences half the size of the sequences in the previous step. The intermediate sequences obtained by filtering by $\mathbf{H}$ are called the *scaling coefficients*. The *wavelet coefficients* of the data then consist of all the sequences $\mathbf{w}_l$. In reality, the decomposition is truncated after a given number of steps and data length does not have to be a full power of 2.

The original data can now be reconstructed from the wavelet coefficients and the one final scaling coefficient sequence by using the reconstruction pyramid: this is the decomposition pyramid with the arrows reversed, and using the filters $\mathbf{H^T}$ and $\mathbf{G^T}$.

The filter conditions above can also be expressed in matrix form:

$$\mathbf{H^T H} + \mathbf{G^T G} = \mathbf{I}, \quad \mathbf{GH^T} = \mathbf{HG^T} = \mathbf{0}, \quad \mathbf{GG^T} = \mathbf{HH^T} = \mathbf{I}.$$

Note: In real applications, we have to account for the fact that the data is not infinite. Otherwise, exact reconstruction will fail near the edges of the data for all but the Haar filter. There are many ways of dealing with this; one is to extend the data sufficiently beyond the segment of interest, so that we do have exact reconstruction on the part we care about. Another method, which does not involve adding more elements, is to assume the data is periodic. Incorporated into the filter matrices **H** and **G**, this will produce "wrap-around" effect: for example,

$$\begin{pmatrix} h_0 & h_1 & h_2 & h_3 & 0 & 0 & 0 & 0 \\ 0 & 0 & h_0 & h_1 & h_2 & h_3 & 0 & 0 \\ 0 & 0 & 0 & 0 & h_0 & h_1 & h_2 & h_3 \\ h_2 & h_3 & 0 & 0 & 0 & 0 & h_0 & h_1 \end{pmatrix}$$

There are other methods for dealing with finite data, and they also involve modifying the filters near the edges of the data. We briefly discuss these at the end of this chapter.

How is all this connected to the wavelet transform discussed earlier? The discrete data in a subband coding scheme can also be interpreted as the coefficients of a given set of basis functions – this is analogous to defining splines using control points. In this way the data represents a function, and its wavelet transform in a suitably defined basis consists of exactly the discrete wavelet decomposition of this function.

1.3 Example of wavelet decomposition

The following figure shows a data sequence together with the first few steps of its wavelet decomposition. The filter used is the Daubechies filter D_4 given above. The wavelet coefficients are shown in Figure II.1 for levels 1–3, together with the level 4 scaling coefficients. (The wavelet coefficients are displayed so that finer resolution levels are at the top of the figure and coarser levels are on the bottom.) The scaling coefficients give a sketchy outline of the original data, and the wavelet coefficients indicate where detail has been lost between the successive simplifications of the data in the pyramid algorithm: the larger the coefficient size, the larger the error.

(For clarity, the 0-axis for each wavelet coefficient level has been moved vertically in this picture, but the coefficients have not been scaled. The scaling coefficients have been scaled to be the same size as the original data.)

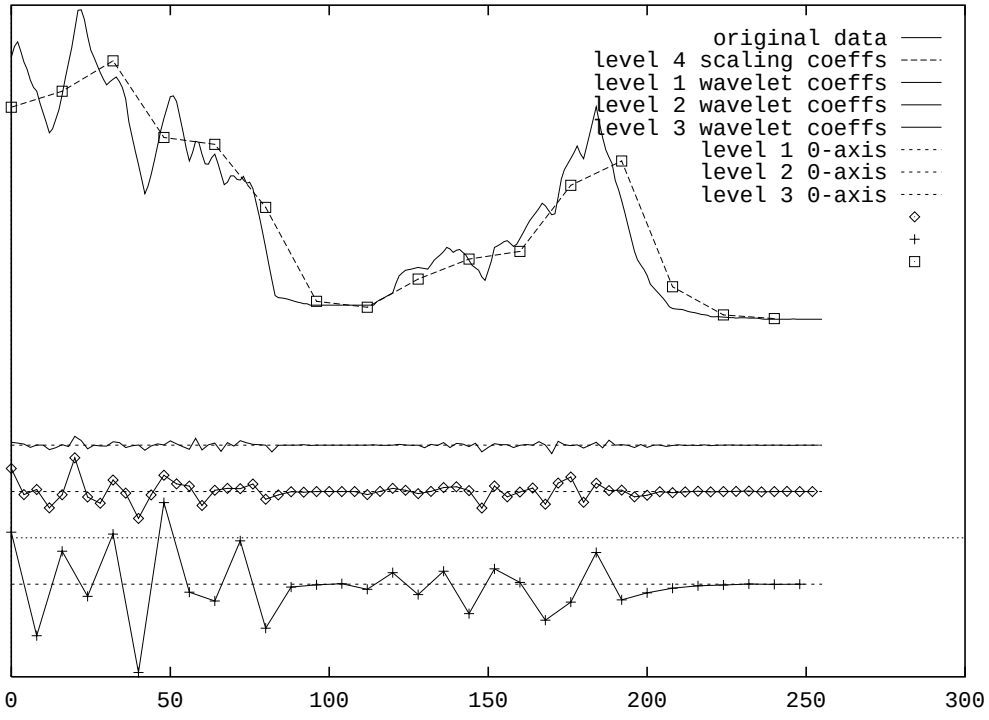

Figure II.1: Wavelet coefficients

1.4 From the continuous wavelet transform to more compact representations

We now shift our viewpoint from discrete data to functions and their representations in given bases, and briefly discuss the relation of the wavelet decomposition to other forms of the wavelet transform.

The continuous wavelet transform for a given basic wavelet ψ was defined as the function taking the scaling and translation parameters a, b to the inner product with the scaled and translated wavelet $\psi_{a,b}$:

$$W(f)(a,b) = w_f(a,b) = \langle f, \psi_{a,b} \rangle = \int f \overline{\psi_{a,b}} dx .$$

The wavelet transform is a map from the space of square integrable functions, L^2, into the space of square integrable functions of two real variables, $L^2(R^2)$. Typically, this map takes functions into a *proper subset* of $L^2(R^2)$. This means that not all reasonable functions $w_f : (a,b) \mapsto w_f(a,b)$ are wavelet transforms of any function and there are heavy constraints on such w_f. This fact can be illustrated by using the Gaussian e^{-x^2} as a basic "wavelet". (The Gaussian is not really an admissible wavelet in our context since its integral is not 0, but it is a good example of the properties of the transform obtained using inner products.) In this case, the wavelet transform $w_f(a,b)$ of any function f satisfies the heat equation

$$\frac{\partial^2 w_f}{\partial^2 b} - \frac{\partial w_f}{\partial a} = 0.$$

So, since most functions $w(a,b)$ do not satisfy the heat equation, they are not the wavelet transform of *any* square integrable f. – In practice, this means for instance that attempts to "edit" a function by moving its wavelet coefficients are questionable, since there is no guarantee that the new coefficients represent anything reasonable in terms of the chosen wavelet transform.

The continuous wavelet transform $w_f(a,b)$ is also redundant: the function f can be recovered from only a subset of the values $w_f(a,b)$.

Most discretizations of the continuous wavelet transform have similar properties. They are redundant representations with restrictions on the allowable transforms. Redundancy, for instance, can be useful in many areas; however, some applications, such as data compression, benefit from more compact representations.

Nonredundancy and a full correspondence between functions and sequences representing potential wavelet transforms can be achieved by using a discretized wavelet family which forms an *orthonormal basis* for the space of square integrable functions L^2. We will look for orthonormal bases which arise from the simplest special case of the discrete wavelet transform: the one with integer dilation and translation steps of 2 and 1, respectively. The wavelet family then consists of the functions:

$$\psi_{m,n}(x) = \sqrt{2^m}\, \psi(2^m x - n).$$

The functions are normalized here to have L^2 norm $\|\psi\| = (\int |\psi|^2)^{1/2} = 1$.

In this case, the wavelet transform $w_f(a,b)$ is now a sequence of reals $w_{m,n}$. For some choices of ψ, these wavelets form an orthonormal basis. There is a 1-1, onto correspondence between square integrable

functions and square summable sequences using the orthonormal wavelet transform. One example of an orthonormal wavelet was the Haar wavelet, which was also connected with a pyramid filtering scheme. We will next discuss a more general method of finding such wavelet bases, multiresolution analysis, and its connection with 2-channel subband filtering.

Note: It is possible to consider multiresolution schemes with more general dilations as well, but we will deal here with the dyadic case only.

2 Multiresolution: definition and basic consequences

The first goal is to construct orthonormal bases of wavelets and to show how these are related to pyramid schemes. For simplicity, we will limit the description here to the 1-dimensional case.

Multiresolution is a general method for constructing orthonormal bases, developed by Mallat and Meyer [134], [142]. We should note that even though most orthonormal wavelet bases come from multiresolution, not all do. However, most "nice" ones do: for instance, all orthonormal bases with a compactly supported ψ (that is, ψ which vanishes outside a finite interval) are known to come from multiresolution [118].

Intuitively, multiresolution slices the space L^2 into a nested sequence of subspaces V_i, where each V_i corresponds to a different scale. The multiresolution is completely determined by the choice of a special function, called the *scaling function*. (This function in fact corresponds to the scaling filter of the pyramid scheme.) More formally:

Multiresolution definition

An *orthonormal multiresolution analysis* for L^2 generated by the *scaling function* ϕ is a sequence of closed subspaces[1]

$$\ldots \subset V_{-1} \subset V_0 \subset V_1 \subset \ldots$$

which satisfy:

- $\overline{\cup V_n} = L^2$

  This condition states that all functions in the space are arbitrarily close to functions in the multiresolution spaces.

- $\cap V_n = \{0\}$

- $f \in V_0 \longleftrightarrow f(2^i \cdot) \in V_i$

  This is the multiresolution condition. As i increases, the spaces V_i correspond to "finer resolution": if the function f is in the basic multiresolution space V_0, then the narrower, finer resolution function $f(2^i \cdot) : \; x \mapsto f(2^i x)$ is in the space indexed by i.

[1] Daubechies [50] indexes the subspaces in the opposite direction.

– $f \in V_i \longleftrightarrow f(\cdot - j) \in V_i$

This condition means that the spaces are shift invariant: integer translates of any function in the space must still be in the space.

– The translates $\phi_{i,j}$, where

$$\phi_{ij}(x) = \sqrt{2^i}\phi(2^i x - j)$$

form an orthonormal basis for V_i.

The orthonormality condition can be relaxed – we will go into this and other generalizations in more detail later. We will however allow general (non-orthonormal) multiresolutions to be built with a scaling function which satisfies the following:

– independence: the translates $\phi_{i,j}$ must be linearly independent

– stability: the translates ϕ_{0j} on level 0 must satisfy:

There are positive constants A and B s.t. for all f generated by the ϕ_{0j}, $f = \sum_j c_j \phi_{0j}$, with (c_j) in l^2,

$$A\,(\sum_j |c_j|^2)^{1/2} \;\leq\; \|f\| \;\leq\; B\,(\sum_j |c_j|^2)^{1/2}. \tag{6}$$

This condition guarantees that each function has a unique representation in terms of the translates of ϕ, and that this representation effectively behaves like the representation in an orthonormal basis: the L^2 norm of a function is equivalent to the l^2 norm $\|(c_j)\| = (\sum_j |c_j|^2)^{1/2}$ of its coefficient sequence.

2.1 Wavelet spaces

As a consequence of the definition, we can approximate a given function f by functions from the multiresolution subspaces: for instance, if $P_i(f)$ denotes the orthonormal projection of f into the subspace V_i, we get:

$$f = \lim_{i \to \infty} P_i(f).$$

Now, define the *scaling coefficients* of the function f as the components of the projection P_i. Because of the orthonormality, these are given by the inner products

$$s_{ij}(f) = \langle f, \phi_{ij} \rangle \ .$$

We want to also represent the error in each approximation; the error between the successive approximations at each step i is an object in a complement space $V_{i+1} - V_i$. Since we are working towards obtaining

orthonormal bases, we will choose the orthogonal complement to represent the approximation error. The *wavelet spaces* W_i are defined as the orthogonal complements of V_i in the larger space V_{i+1},

$$W_i = V_{i+1} \ominus V_i, \quad W_i \perp V_i.$$

Since we are also looking for a situation analogous to the continuous wavelet transform, we need a single function ψ which generates all the wavelet spaces:

Wavelet property

Each W_i is generated by the translates $\psi_{i,j}$ of the function ψ, where

$$\psi_{i,j}(x) = \sqrt{2^i}\psi(2^i x - j).$$

If this extra property is satisfied, as an immediate consequence, we have

- multiresolution for W_i's: $f \in W_0 \longleftrightarrow f(2^i \cdot) \in W_i$
- shift invariance for W_i's: $f \in W_i \longleftrightarrow f(\cdot - j) \in W_i$
- orthonormality between wavelet spaces: $W_i \perp W_k, i \neq k$.
- all L^2 functions can be obtained uniquely as a sum of all the error components, or:

$$L^2 = \bigoplus W_i.$$

From this, orthonormal multiresolution will now immediately yield an orthonormal basis consisting of translations and dilations of the wavelet ψ. The *wavelet coefficients* of f are the coefficients of f with respect to this basis:

$$w_{ij}(f) = \langle f, \psi_{ij} \rangle ,$$

and the L^2-norm of a function f can now be expressed in terms of the wavelet coefficients:

$$\|f\| = (\sum_{ij} |w_{ij}|^2)^{1/2} = \|(w_{ij})\|.$$

The wavelet property in fact holds under the most general multiresolution assumptions we consider, even if the multiresolution is not orthonormal.

Under practical conditions, the ϕ generating the multiresolution is a smoothing function, that is, its integral does not vanish:

$$\int \phi \, dx \neq 0.$$

We will make this a requirement when finding scaling functions. Similarly, for orthonormal bases, ψ will satisfy the basic condition on wavelets: $\int \psi \, dx = 0$. We will not require this property explicitly, since it will turn out to be satisfied in practical situations automatically from the definitions.

We also want to require ϕ and its Fourier transform $\hat{\phi}$ to have reasonable decay, to guarantee localization both in the usual space and in frequency space. The space localization part is often taken care of by the use of compactly supported scaling functions and wavelets, that is, wavelets which vanish outside a finite interval.

2.2 The refinement equation

We will now continue to look for conditions the scaling function ϕ has to satisfy for (orthonormal) multiresolution, and how the definition is related to subband filtering.

In the multiresolution situation, we have two subspaces $V_0 \subset V_1$, generated respectively by integer translates of $\phi(x)$ and $\phi(2x)$. The subspace relation implies that $\phi(x)$ must be generated by the finer scale functions $\phi(2x - j)$:

$$\phi(x) = \sqrt{2} \sum_j h_j \phi(2x - j), \tag{7}$$

with $\sum_j |h_j|^2 < \infty$. This equation, known as the *dilation* or *refinement equation* is the principal relation determining the multiresolution. It will hold for any two successive levels in the multiresolution hierarchy.

It is easy to check that the solution of the dilation equation must be unique, once the normalization of the function ϕ is fixed. This means that the coefficients of the equation, (h_i) can be used to determine the scaling function, and the multiresolution. Further, the scaling function will be compactly supported exactly when the filter sequence is finite.

Since $W_0 \subset V_1$, we also know that the wavelet must satisfy a similar equation:

$$\psi(x) = \sqrt{2} \sum_j g_j \phi(2x - j). \tag{8}$$

The similarity of the coefficients in these equations to the filter coefficients in the introduction is not coincidental! The next section looks at the connection of multiresolution to subband filtering.

2.3 Connection to filtering

In general, finding inner products with the translates of a single function is connected to convolution. This can be seen for instance by looking at the following function, obtained by taking inner products with

$\psi_a : \psi_a(t) = \psi(x - a)$:

$$u_f(a) = \langle f, \psi_a \rangle = \int f(x)\psi(x - a)dx = f * \psi^*,$$

where ψ^* is obtained from ψ by reflection.

In the multiresolution situation, the scaling and wavelet coefficients are found by filtering from the scaling coefficients on a finer level, without having to calculate the inner products explicitly. This can be seen directly from the refinement and wavelet equations in the following way. The refinement equation on level i, rewritten in terms of the functions $\phi_{i+1,j}$ is:

$$\phi_{i0}(x) = \sum_j h_j \phi_{i+1,j}(x).$$

More generally, expressing ϕ_{ik} in terms of the finer level functions, using the refinement equation:

$$\phi_{ik}(x) = \sum_j h_j \phi_{i+1,2k+j}(x) = \sum_j h_{j-2k} \phi_{i+1,j}(x).$$

The scaling coefficients $\mathbf{s}_i$ on level i are then

$$\mathbf{s}_{ik} = \langle f, \phi_{ik} \rangle = \sum_j h_{j-2k} \langle f, \phi_{i+1,j} \rangle = (\mathbf{H}\mathbf{s}_{i+1})_k.$$

Here $\mathbf{H} = (h_{j-2k})_{kj}$ is the modified convolution matrix with respect to the filter (h_j), with every other row dropped, exactly as in Section 1.1.

For wavelet coefficients we have similarly:

$$\mathbf{w}_i = \mathbf{G}\mathbf{s}_{\mathbf{i+1}},$$

where $\mathbf{G} = (g_{j-2k})$ is the convolution and downsampling matrix with respect to the filter (g_j).

This of course means that the wavelet and scaling coefficients can now computed by a pyramid filtering scheme with exact reconstruction, as in Section 1.1, once we know the scaling coefficients on one level.

2.4 Obtaining scaling functions by iterated filtering

What do scaling functions and wavelets look like? The multiresolution conditions have another consequence for the scaling function: the function is obtained by a sequence of iterated filtering.

2.4.1 Computing ϕ using the cascade algorithm

The function ϕ can be approximated by iteration essentially by applying the reconstruction algorithm to a scaling coefficient sequence

$$\mathbf{x}_0 = (\ldots\ 0,\ 0,\ 0,\ 0,\ 1,\ 0,\ 0,\ 0,\ 0,\ \ldots),$$

with all wavelet coefficients set to 0. This corresponds to a single scaling function at the position indicated by the 1.

In this case we reconstruct and scale (the normalization will otherwise shrink each reconstruction by $1/\sqrt{2}$). This means applying the filter $\sqrt{2}\,\mathbf{H}^T$ repeatedly:

$$\mathbf{x}_{i+1} = \sqrt{2}\,\mathbf{H}^T\mathbf{x}_i.$$

Each sequence refines the previous one and the process can be shown to approach ϕ at the limit. This is sometimes called the *cascade algorithm*, and it constitutes the simplest way to draw pictures of a scaling function. Because the filters are finite, the algorithm can be easily modified to approximate portions of the scaling function more efficiently, without drawing the whole function.

The wavelet can be drawn in the same way by applying the filter $\sqrt{2}\,\mathbf{G}^T$ once to the sequence of zeros and a single 1:

$$\mathbf{x}_0 = (\ldots\ 0,\ 0,\ 0,\ 0,\ 1,\ 0,\ 0,\ 0,\ 0,\ \ldots)\,, \quad \mathbf{x}_1 = \sqrt{2}\,\mathbf{G}^T\mathbf{x}_0,$$

and then performing the above iteration with $\mathbf{H}^T$ on the result:

$$\mathbf{x}_{i+1} = \sqrt{2}\,\mathbf{H}^T\mathbf{x}_i,\ \ i \geq 2.$$

Figure II.2 depicts the results of applying the cascade algorithm to the Daubechies filter D_4: $\frac{1+\sqrt{3}}{4\sqrt{2}}, \frac{3+\sqrt{3}}{4\sqrt{2}}, \frac{3-\sqrt{3}}{4\sqrt{2}}, \frac{1-\sqrt{3}}{4\sqrt{2}}$.

2.4.2 Computing ϕ at dyadic values

If finding an approximation to ϕ is not enough, but precise values are needed, these can be calculated using the same cascade algorithm, as follows. Suppose the values of the ϕ at integers are known. Then the values of ϕ at all points $2^{-n}k$, where $n > 0$ and k are integers, can be computed from the refinement equation

$$\phi(x) = \sqrt{2}\ \sum_j h_j \phi(2x - j).$$

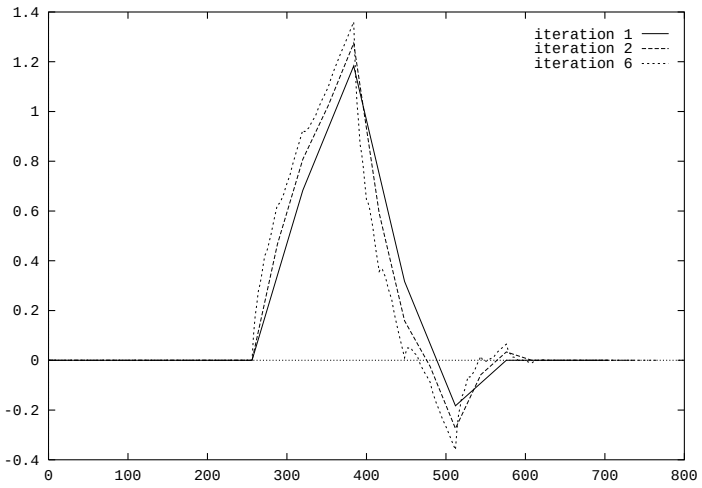

Figure II.2: Cascade algorithm applied to the Daubechies filter

In other words, begin with the vector $\mathbf{x}_0$ consisting of the integer values of ϕ, and iterate:

$$\mathbf{x}_{i+1} = \sqrt{2}\,\mathbf{H}^T\mathbf{x}_i.$$

If the filter length is N, the integer values $\phi(0), \phi(1), \ldots$ can be found as the eigenvector corresponding to the eigenvalue 1 of the $N-1 \times N-1$ matrix $(\sqrt{(2)}h_{j-2i} : i, j = 1, \ldots, N-1)$, obtained by truncation from **H** and normalized by $\sqrt{2}$. This can be seen easily by substituting integers $0, 1, \ldots$ for x into the refinement equation.

2.4.3 The Fourier transform of ϕ

The cascade algorithm converges to ϕ , if the scaling function solution ϕ of a refinement equation exists. If we begin with a given refinement equation, we don't necessarily know that the cascade algorithm converges, and that there is any solution at all. The proofs of the existence of scaling functions usually look at the corresponding algorithm in Fourier space and show that the Fourier transform of ϕ is a well defined L^2 function.

Suppose we begin with the refinement equation (7). As mentioned, the solution ϕ , if one exists, is unique once the normalization for $\int \phi \neq 0$ is fixed. This condition is equivalent to the Fourier transform condition $\hat{\phi}(0) \neq 0$. We set $\int \phi = 1$, or $\hat{\phi}(0) = 1/\sqrt{2\pi}$.

The Fourier transform of ϕ is now obtained from the refinement equation as before, by iteration. The FT form of the refinement equation is

$$\hat{\phi}(\omega) = 1/\sqrt{2}\,(\sum_k h_k e^{-ik\omega/2})\hat{\phi}(\omega/2).$$

(Translation in Fourier transform becomes a phase shift, and scaling is inverted.) The key function here is the following 2π- periodic function corresponding to the filter:

$$m_0(\omega) = 1/\sqrt{2}\,(\sum_k h_k e^{-ik\omega}), \tag{9}$$

and so the refinement equation is

$$\hat{\phi}(\omega) = m_0(\omega/2)\hat{\phi}(\omega/2). \tag{10}$$

For this to make sense, we must have $m_0(0) = 1$. Iterating this FT refinement equation we get

$$\hat{\phi}(\omega) = m_0(\omega/2)\hat{\phi}(\omega/2) = m_0(\omega/2)m_0(\omega/4)\hat{\phi}(\omega/4) = \ldots.$$

This suggests that the choice for the Fourier transform of the function ϕ is the infinite product

$$\mathbf{\Phi}_\infty(\omega) \;=\; C \;\prod_1^\infty m_0(\frac{\omega}{2^k}).$$

Our normalization condition $\hat{\phi}(0) = 1/\sqrt{2\pi}$ implies that the constant C is $1/\sqrt{2\pi}$, since $m_0(0) = 1$. If this product converges pointwise almost everywhere, it in fact defines an L^2 function (which is then the Fourier transform of the required L^2 function ϕ) ([134]).

2.4.4 Examples

Scaling functions can also have closed forms; one such function is the box function. More generally, B-splines are examples of functions which satisfy a refinement equation. (Their translates are not orthonormal, however.) There are $n + 2$ many refinement equation coefficients for the degree n cardinal B-spline, and they are given by

$$\frac{1}{2^n}\begin{pmatrix} n+1 \\ k \end{pmatrix}$$

multiplied by a normalization factor $\sqrt{2}$. For instance, a quadratic spline has the coefficients $\sqrt{2}\,(1/8, 3/8, 3/8, 1/8)$.

The fact that B-splines satisfy a refinement equation can also be seen from their definition as convolutions: the degree 0 (order 1) B-spline N_1 is the box function, and degree $n-1$, order n, splines N_n for higher n are obtained recursively by

$$N_{n+1} = N_n * N_1.$$

The Fourier transform of N_n is

$$(\frac{1-e^{-i\omega}}{i\omega})^n.$$

The following Figure II.3 shows a quadratic B-spline and the components of the refinement equation.

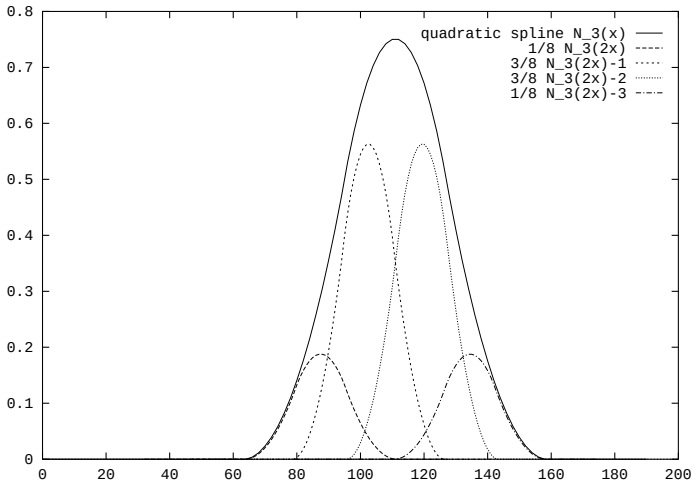

Figure II.3: B-spline and its refinement equation

How do we obtain other scaling functions, and, especially, how do we obtain scaling functions for orthonormal multiresolution? The general method is to begin with a filter (h_i) and iterate using the above procedures. If the iteration starts with an arbitrary filter, we can only hope that the process ends in something reasonable! In the next sections we will give conditions on the filter which guarantee that the scaling function built this way does in fact give a valid L^2 function and a valid orthonormal multiresolution. Further conditions are required to allow scaling functions with a given degree of differentiability and guarantee other properties. (Conditions can also be obtained for the existence of a scaling function defined by a refinement scheme, without orthonormality requirements. These refinement schemes, and their special cases, functions obtained by subdivision, have also been explored independently of wavelets: see [71], [20].)

The necessary conditions on the filter turn out to be the exact reconstruction conditions given in the introductory "recipe". These are combined with some further requirements which guarantee that the corresponding wavelets form a suitable basis. Although the necessary conditions are simple to state, they are in fact difficult to satisfy. Given the matrix $\mathbf{H}$, it's not hard to guess what the elements of the convolution matrix $\mathbf{G}$ have to be in order to satisfy the orthogonality condition $\mathbf{G}\mathbf{H}^T = 0$. However, it is not at all easy to build longer filters $\mathbf{H}$ so that the remaining exact reconstruction properties are satisfied. Expressing these conditions in an alternative form will eventually lead to Daubechies' general method for constructing

finite filters for this. (We should note that the generalization to biorthogonal wavelets allows easier filter constructions. But this construction is usually also carried out in Fourier space, and much of the analysis remains the same as here.)

3 Requirements on filters for multiresolution

We can start from the filters (h_i) and (g_i) and try to pin down the requirements needed for these to generate a valid orthonormal multiresolution and wavelet. It's convenient to look at these in Fourier transform form. If we take F.T.'s of both sides of the refinement and wavelet equations (7) and (8), we get, as before,

$$\hat{\phi}(\omega) = 1/\sqrt{2}\,(\sum_k h_k e^{-ik\omega/2})\hat{\phi}(\omega/2) \tag{11}$$

$$\hat{\psi}(\omega) = 1/\sqrt{2}\,(\sum_k g_k e^{-ik\omega/2})\hat{\phi}(\omega/2) \tag{12}$$

The filters correspond to the $2\pi-$ periodic filter functions

$$m_0(x) = 1/\sqrt{2}\,(\sum_k h_k e^{-ikx}) \tag{13}$$

$$m_1(x) = 1/\sqrt{2}\,(\sum_k g_k e^{-ikx}) \tag{14}$$

and the refinement equation and wavelet equation become

$$\hat{\phi}(\omega) = m_0(\omega/2)\hat{\phi}(\omega/2), \quad \hat{\psi}(\omega) = m_1(\omega/2)\hat{\phi}(\omega/2).$$

These identities just express the fact that one function is obtained using translates of another, scaled function.

3.1 Basic requirements for the scaling function

We will first look at the basic consequences of the multiresolution definition. The scaling function must be such that

$$\overline{\cup V_n} = L^2.$$

For functions with reasonable Fourier transforms[2], and which satisfy the minimal stability conditions, this property holds when

[2] $\hat{\phi}$ bounded and continuous near 0 . . .

$$\int \phi \neq 0.$$

This integral condition is also necessary in most cases. The integral condition implies all of the following:

- $\hat{\phi}(0) \neq 0$
  We fix $\hat{\phi}(0) = 1/\sqrt{2\pi}$, as discussed before.
- $m_0(0) = 1$
- $\sum_k \phi(x-k) = 1$
- $\sum h_k = \sqrt{2}$

For instance, the normalization condition $\sum h_k = \sqrt{2}$ can essentially be obtained from the refinement equation by integrating both sides and using the fact that the integral of ϕ does not vanish. Condition $\hat{\phi}(0) \neq 0$ is a restatement of the integral condition, and the requirement on m_0 follows from the FT form of the refinement equation

$$\hat{\phi}(\omega) = m_0(\omega/2)\hat{\phi}(\omega/2).$$

The normalization conditions were already mentioned in Section 2.4.3. These conditions constitute a "smoothing property" for the filter (h_k), and they allow the approximation of functions from the multiresolution spaces.

3.2 Wavelet definition

We want to find a wavelet ψ which generates the orthogonal complement of V_0 in V_1. The wavelet ψ is a combination of the translates of finer resolution ϕ's:

$$\psi(x) = \sqrt{2} \sum_j g_j \phi(2x-j),$$

for the filter (g_j), and the corresponding filter function is m_1. Can this filter be chosen so that ψ is orthogonal to the translates of ϕ (and generates the space of all such functions in V_1)? The orthogonality of ψ to the translates of ψ can be expressed in FT form as:

$$0 = \langle \hat{\phi}_{0n}, \hat{\psi} \rangle = 2 \int m_0(\omega/2)\overline{m_1}(\omega/2)|\hat{\phi}(\omega/2)|^2 e^{in\omega} d\omega =$$

$$\int_0^{2\pi} e^{in\omega} \sum_k m_0(\omega/2+\pi k)\overline{m_1}(\omega/2+\pi k)|\hat{\phi}(\omega/2+\pi k)|^2 d\omega.$$

The last formulation is obtained by splitting the integral over the whole frequency axis into slices of length 2π. The fact that this integral vanishes implies that, almost everywhere, the sum term must vanish also:

$$\sum_k m_0(\omega/2 + \pi k)\overline{m_1}(\omega/2 + \pi k)|\hat{\phi}(\omega + \pi k)|^2 = 0. \tag{15}$$

With some manipulation (splitting the sum into parts for even and odd k to use periodicity), this leads to the condition

$$m_1(\omega)\overline{m_0(\omega)} + m_1(\omega + \pi)\overline{m_0(\omega + \pi)} = 0. \tag{16}$$

This in turn is satisfied for instance by the function

$$m_1(\omega) = -e^{-i\omega}\overline{m_0(\omega + \pi)}.$$

(This can be seen by substituting into the equation and noting that $e^{-i\omega} + e^{-i(\omega+\pi)} = 0$.)

By writing out the definition of the filter function m_1, it is also easy to see that this corresponds to the mirror filter definition given earlier: $g_j = (-1)^j\overline{h_{1-j}}$.

It is possible to show, by repeating a similar argument for an arbitrary function f in W_0, that the wavelet chosen will in fact span the complement wavelet spaces. This argument will also give the possible choices for ψ (there are infinitely many of them). The general form for the filter function m_1 is

$$m_1(\omega) = \nu(\omega)\overline{m_0(\omega + \pi)},$$

where ν is 2π-periodic and satisfies $\nu(\omega + \pi) + \nu(\omega) = 0$. In addition, for deducing orthonormality of the translates of ψ from the same property for ϕ , we also need $|\nu| = 1$. Above we chose the ν to be simply $-e^{-i\omega}$, but other choices are possible: any shift of this filter by an even number elements (that is, multiplication of ν by $e^{-2ni\omega}$) would still give a suitable wavelet.

This definition works irrespective of the orthonormality of the multiresolution, provided the stability condition holds. If the multiresolution is not orthonormal, the corresponding wavelet is often called a *prewavelet*, or a *semiorthogonal* wavelet ([26]).

Again, it can be seen from the wavelet equation (8), that the wavelet filter must satisfy $(g_k) = 0$ for $\int \psi = 0$ to hold. This is also equivalent to saying that m_0 has a zero at π. This condition follows from the previous normalization condition $m_0(0) = 1$ assuming minimal continuity requirements.

3.3 Orthonormality

Inner products of the translates of ϕ can be expressed in Fourier transform form:

$$\langle \phi_{00}, \phi_{0n} \rangle \;=\; \int |\hat{\phi}|^2 e^{in\omega} d\omega = \int_0^{2\pi} e^{in\omega} \sum_k |\hat{\phi}(\omega + 2\pi k)|^2 d\omega.$$

The last equation is again obtained by splitting the original integral over the whole frequency axis into slices of length 2π. From this, we get the following conditions:

Orthonormality:

$$\sum_k |\hat{\phi}(\omega + 2\pi k)|^2 = 1/2\pi \quad \text{almost everywhere}. \tag{17}$$

The less restrictive stability condition requires that this quantity is between some positive numbers.

Stability:

$$0 < \alpha \leq \sum_k |\hat{\phi}(\omega + 2\pi k)|^2 \leq \beta \quad \text{almost everywhere}.$$

The above sum is a 2π-periodic function which is generally important in multiresolution, since it governs the stability and orthonormality of the translates of ϕ , that is, whether the choice of ϕ makes sense as a basic scaling function.

A necessary orthonormality condition is now found by the same procedures as before from the condition (17): substitute the refinement equation into (17) for $\hat{\phi}$, and use periodicity:

$$|m_0(\omega)|^2 + |m_0(\omega + \pi)|^2 = 1. \tag{18}$$

The wavelet and orthonormality conditions (16) and (18) can also be expressed more simply by stating that the following matrix is unitary (that is, its columns are orthonormal):

$$\begin{pmatrix} m_0(\omega) & m_1(\omega) \\ m_0(\omega + \pi) & m_1(\omega + \pi) \end{pmatrix}.$$

3.4 Summary of necessary conditions for orthonormal multiresolution

The following conditions are necessary[3] to define an orthonormal multiresolution and the accompanying orthonormal wavelet bases:

Conditions for filter coefficients in Fourier transform form

[3] under some minimally restrictive conditions

- $m_0(0) = 1, \quad m_0(\pi) = 0$
- $|m_0(\omega)|^2 + |m_0(\omega + \pi)|^2 = 1$
- $m_1(\omega) = \nu(\omega)\overline{m_0(\omega + \pi)}$,
  with ν 2π-periodic, $|\nu| = 1$, and $\nu(\omega + \pi) + \nu(\omega) = 0$. A standard choice for m_1 is

$$m_1(\omega) = -e^{-i\omega}\overline{m_0(\omega + \pi)}. \tag{19}$$

These conditions can also be expressed in directly in terms of the original filters. Using the standard choice (19) for the wavelet filter:

Corresponding conditions for filter coefficients

- normalization conditions for smoothing and wavelet filter: $\sum_k h_k = \sqrt{2}; \quad \sum_k g_k = 0;$
- orthonormality: $\sum_k h_k \overline{h_{k+2m}} = \delta_{0m}$, for all m
- wavelet: $g_j = (-1)^j \overline{h_{1-j}}$

The equivalence of the filter coefficient conditions to the previous ones can be seen relatively easily by rewriting the Fourier transform conditions. The filter conditions are the same as the exact reconstruction conditions given in the introductory section 1.1.

3.5 Sufficiency of conditions

While the above conditions are necessary for the generation of an orthonormal multiresolution analysis and the appropriate scaling function, these conditions don't always guarantee that we actually get an orthonormal basis, or even that the key stability condition (6) holds. Nor do they guarantee that a scaling function ϕ satisfying these conditions can be found. Various authors ([134], [48], [32], ...) have developed sufficient conditions for this – necessary and sufficient conditions are found in [32], [117]. We briefly review some of these sufficient conditions.

3.5.1 Sufficient conditions

Suppose that the following conditions by Mallat are added to the necessary conditions above:

- filter decay condition: $|h_k| = O(\frac{1}{1+k^2})$
- $m_0(\omega) \neq 0$ for $\omega \in [-\pi/2, \pi/2]$.

Then the product

$$\frac{1}{\sqrt{2\pi}} \prod_{1}^{\infty} m_0(\frac{\omega}{2^k})$$

converges to an L^2 function $\hat{\phi}_\infty(\xi)$, and the function ϕ generates a multiresolution analysis.

Daubechies [48] gives a different condition on the filter tranfer function m_0, which, when added to the necessary conditions above, is sufficient:

- $m_0(\omega) = ((1 + e^{i\omega})/2)^N m(\omega)$, where $\sup_\omega |m(\omega)| \leq 2^{N-1/2}$.

3.5.2 Necessary and sufficient conditions for compactly supported orthonormal multiresolution

Finally, there are conditions which are necessary and sufficient for a *compactly supported* scaling function to define a multiresolution analysis. Cohen ([32]) gave such conditions using the above necessary conditions and an extra condition involving the zeros of $m_0(\omega)$. This extra requirement is equivalent to the following condition, which uses the eigenvectors of a matrix [117]:

Assume the filter (h_i) is finite, with indices from 0 to N, such that the corresponding filter function

$$m_0(\omega) = 1/\sqrt{2} \sum h_k e^{-ik\omega}$$

satisfies $m_0(0) = 1$ and the necessary orthonormality condition (18). Define

$$A_{lk} = \sum_{0}^{N} h_n \overline{h_{k-2l-n}}$$

with $|l|, |k| \leq N - 1$.

Then the following is a necessary and sufficient condition for the corresponding scaling function to exist and generate an orthonormal multiresolution analysis:

> The eigenvalue 1 of the matrix A is nondegenerate.

3.5.3 Example

The following example from [50] shows that the exact reconstruction conditions alone are not enough to guarantee that the resulting wavelets are orthonormal. The following scaling filter satisfies the necessary orthonormality condition but does not actually give an orthonormal basis:

$$m_0(\omega) = \frac{1}{2}(1 + e^{-3i\omega}).$$

The filter leads to a ϕ whose translates are not orthonormal: using the iterated product definition of $\hat{\phi}$, we find that

$$\hat{\phi} = \frac{1}{\sqrt{2\pi}} e^{-3i\omega/2} \text{sinc}(3\omega/2).$$

Then ϕ, the inverse transform of this, equals the dilated box function, which is $1/3$ between 0 and 3, and 0 elsewhere. It's immediately seen that the integer translates of this ϕ are not orthonormal.

3.6 Construction of compactly supported orthonormal wavelets

The first orthonormal wavelet bases were functions supported on the whole real line. Examples of these are Meyer's wavelets, and the Battle-Lemarié wavelets (see [50]). Although the Battle-Lemarié wavelets produce good results, the filters for these functions are infinite, a drawback in many applications. The only known orthonormal wavelets corresponding to finite filters were the Haar wavelets. This situation changed when Daubechies used the filter conditions above to directly construct families of compactly supported wavelets [48].

We will briefly outline the Daubechies construction here. For more details, see for instance [50]. (The development in this section is not necessary for following the rest of the material.)

By the results above, we require the filter function $m_0(\omega)$,

$$m_0(\omega) = 1/\sqrt{2}\ (\sum_k h_k e^{-ik\omega}),$$

to satisfy the orthonormality condition

$$|m_0(\omega)|^2 + |m_0(\omega + \pi)|^2 = 1.$$

We also want the following new condition:

$$m_0(\omega) = (1/2(1 + e^{i\omega}))^N Q(e^{i\omega}).$$

This allows the resulting function to have certain regularity and approximation properties – for future reference, N is the number of *vanishing moments* of the wavelet, discussed in more detail in a later section. We also assume that $m_0(\omega)$ consists of a finite sum of the powers e^{-ikx}, that is, $m_0(\omega)$ is a trigonometric polynomial.

One of the main steps of the construction is finding the trigonometric polynomial $P = |m_0(\omega)|^2$. This is first rewritten by taking out the $(1 + e^{i\omega})^N$ factor:

$$|m_0(\omega)|^2 = (\cos^2(\omega/2))^N \left| Q(1 - \cos^2(\omega/2)) \right|^2$$

and we let $y = 1 - \cos^2(\omega/2)$. Then the orthonormality condition becomes an equation for finding the polynomial $Q(y)$:

$$y^N Q(1-y) + (1-y)^N Q(y) = 1$$

This condition can be solved explicitly. The following constitutes the unique form of the solutions:

$$Q(y) = \sum_0^{N-1} \left(\begin{array}{c} N-1+k \\ k \end{array} \right) y^k \; + \; y^N F(1/2 - y), \tag{20}$$

where F is any odd polynomial such that $Q(y) \geq 0$ for $y \in [0, 1]$.

Finally, we need to obtain m_0 from $|m_0|^2$. In fact, $|m_0|^2$ can be factored *explicitly* into its complex factors using a result by Riesz – this technique is called spectral factorization in signal processing. For positive even trigonometric polynomials A, Riesz's lemma implies the existence of a "square root" polynomial B s.t. $A = |B|^2$. This polynomial is not unique. By making certain choices in the square root we arrive at the Daubechies scaling functions ϕ_{2N}^D. The standard wavelet condition then yields the wavelets ψ_{2N}^D. (Other choices in the factorization lead to different orthonormal wavelets.)

The wavelets are compactly supported: the supports of ϕ_{2N}^D and ψ_{2N}^D are $[0, 2N-1]$ and $[1-N, N]$. The Daubechies wavelets have regularity which increases linearly with the number N, and so the wavelets can be chosen to be arbitrary smooth at the price of increasing their support length. For most N, this construction cannot be given in a closed form, and there is no nice analytical formula for describing the resulting wavelets.

3.6.1 Examples

For $N = 1$ the Daubechies wavelets are the Haar wavelets.

For $N = 2$ we have the wavelet ψ_4^D which has made previous appearances here. The filter function m_0 is

$$m_0(\omega) = [1/2(1 + e^{i\omega})]^2 \; 1/2[(1 + \sqrt{3}) + (1 - \sqrt{3})e^{i\omega}].$$

(It is easy to verify that this satisfies the orthonormality equation above.) The scaling filter (h_i) is obtained by writing out m_0 as the full trigonometric polynomial :

$$\frac{1+\sqrt{3}}{4\sqrt{2}}, \; \frac{3+\sqrt{3}}{4\sqrt{2}}, \; \frac{3-\sqrt{3}}{4\sqrt{2}}, \; \frac{1-\sqrt{3}}{4\sqrt{2}} \quad .$$

The following figures show the Daubechies scaling functions and wavelets for $N = 2, 4$:

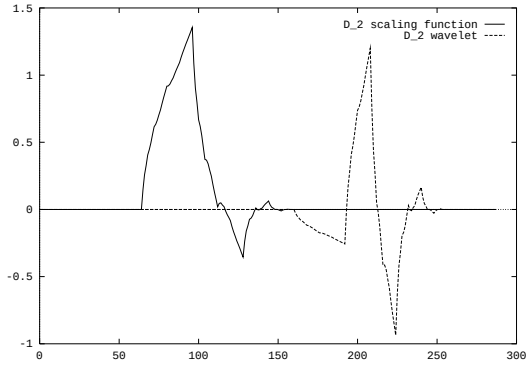

Figure II.4: D_4

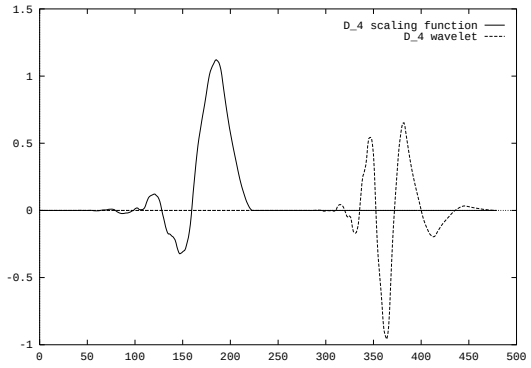

Figure II.5: D_8

3.7 Some shortcomings of compactly supported orthonormal bases

There are tradeoffs to using compactly supported orthonormal bases. The bases are convenient and simple to use. However, no symmetry or antisymmetry is possible for these wavelets (apart from the Haar wavelet), and "nice" compactly supported functions (e.g. splines) cannot be used. The Daubechies scaling functions and wavelets have in general no closed analytical expression although they can be computed to arbitrary precision with a rapidly converging algorithm.

Some of these shortcomings can be remedied by using biorthogonal and semiorthogonal wavelet constructions (Section 5.2).

4 Approximation properties

In this section we will look at some of the properties of the wavelet decomposition and sketch the reason why wavelets are useful in application such as compression. The wavelet decomposition is a complete description of the underlying function, and so the behavior of wavelet coefficients can be used to get information about the original data. This coefficient behavior in turn is closely tied to the approximation properties of the chosen wavelets.

4.1 Approximation from multiresolution spaces

A key condition for understanding the behavior of orthonormal wavelets and their generalizations in function approximation is the vanishing moment condition, defined below.

The integral of a wavelet is 0 in our context. Extending this to higher orders gives the vanishing moment condition, which has the following equivalent forms. The m^{th} moment of a function f is defined as

$$\int x^m \psi(x) dx.$$

Vanishing moment conditions

- The first N moments of ψ vanish: for $m = 0, \ldots, N-1$

$$\int x^m \psi(x) dx = 0$$

- $m_0(\omega) = \frac{1}{\sqrt{2}} \sum h_k e^{ik\xi}$ has a zero of order N-1 at $\omega = \pi$

  (That is, the m^{th} derivatives of m_0, for $m = 0, \ldots, N-1$, all vanish at π.)
- $m_0(\omega)$ can be factored as $m_0(\omega) = (1 + e^{i\omega})^N f(\omega)$
- $\sum k^m g_k = \sum (-1)^k k^m h_k = 0 \quad$ for $m = 0, ..., N$.

The last condition is based on expressing the m^{th} moment of the wavelet in terms of the wavelet filter coefficients (g_i). These conditions guarantee that polynomials up to degree $N-1$ are (locally) in the multiresolution spaces. important for deducing the approximation properties of the multiresolution spaces. Vanishing moments also form a necessary condition for ψ to be C^N, or N times continuously differentiable.

> If the compactly supported orthonormal basis wavelet ψ is in C^N, with bounded derivatives,[4] then the first N moments of ψ must vanish.

There are orthonormal wavelets with arbitrarily large vanishing moments: the Daubechies wavelets are a family indexed by the number of vanishing moments $2N$.

The following result on the approximation properties of the wavelet decomposition is a direct consequence of results on approximation from translation invariant spaces ([178]).

Approximation from multiresolution spaces

Suppose (V_i) is a multiresolution with a wavelet ψ. If ψ has N vanishing moments, the error of approximating a function f with at least N derivatives from the multiresolution space V_i is:

$$\| f - P_i f \| \;\leq\; C\; 2^{-iN} \;\| \; f \; \|_{W^N} \; .$$

(The norm of the function is the Sobolev space norm obtained from the derivative norms $\| \; f \; \|^2_{W^N} = \sum_n \| f^{(n)} \|^2$.)

Using the fact that the L^2-norm of a function f is $(\sum_{ij} |w_{ij}|^2)^{1/2}$, where the w_{ij} are the wavelet coefficients of f, the above also implies that the wavelet coefficients of a sufficiently smooth function decay by levels at least as a power of 2^N, provided ψ has N vanishing moments:

$$\max_j |w_{ij}| \leq C\; 2^{-iN}.$$

The rate of decay is governed by the number of vanishing moments of the wavelet used. As an example, Haar wavelets have only one vanishing moment (the minimum allowed here), which means that they don't approximate functions very rapidly. Similarly, the Haar coefficients do not tend to zero fast at finer levels, so Haar wavelets will not produce as marked a contrast in coefficient size between smooth and non-smooth sections of data as wavelets with more vanishing moments.

The approximation result above also leads to a characterization of certain "smoothness" spaces, Sobolev spaces, in terms of wavelet coefficient behavior [142]. Many other spaces can be characterized by wavelet coefficients ([142]) – these include the L^pspaces, $1 < p < \infty$, Hölder spaces, and Besov spaces. The wavelet decomposition can even be modified to apply to L^p, $p \leq 1$ ([60]).

[4] This also holds for wavelets with sufficiently rapid decay.

4.1.1 Examples

The following figures show the wavelet coefficients for data with varying differentiability using two wavelets: the Haar wavelet with one vanishing moment, and the Daubechies wavelet D_8 with 4 vanishing moments. The wavelet coefficients are given with the finest level at the top.[5] Due to the difference in vanishing moments, the coefficients for D_8 are smaller and decay faster in the smoother data sections (i.e., the data sections with more differentiability).

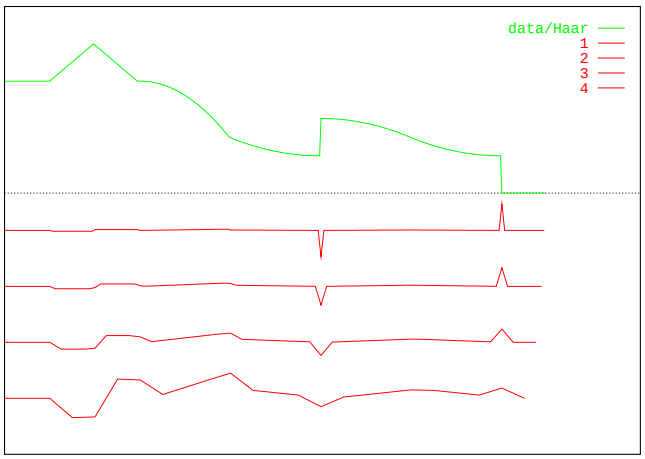

Figure II.6: Haar wavelet

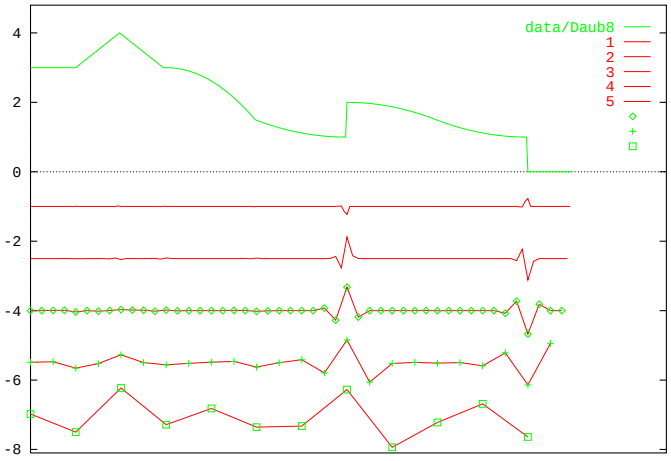

Figure II.7: D_8 wavelet

[5]The wavelet coefficients have again been moved vertically for display but not scaled. For clarity, the 0-axes for the coefficients have not been shown explicitly.

4.2 Approximation using the largest wavelet coefficients

Wavelet applications also use other types of approximation. This is typical in compression: in these situations approximation occurs from spaces Σ_n consisting of functions with n nonzero wavelet coefficients. Unlike the multiresolution spaces, these are not linear spaces, since they are not closed under addition. If the same number of points n is used in both methods, the resulting approximation error from the space Σ_n is smaller than the the approximation error using the corresponding multiresolution space.

In the underlying space L^2, approximation from Σ_n is based on the following. Suppose that f is the function to be approximated. If A is the set of coefficients (i, j) chosen to be in the approximating function f_A, the L^2 norm of the error is

$$\|f - f_A\| \;=\; (\sum_{(i,j)\notin A} |w_{ij}|^2\ )^{1/2}.$$

This means that the L^2-error is smallest when the n largest wavelet coefficients are chosen for the approximation. This corresponds to simple threshold compression of the wavelet coefficient information. From the above results it is clear that for smooth data, compression rates improve as the number of vanishing moments of the wavelet increases.

It is possible to extend the method of choosing the largest wavelet coefficients to approximating within spaces L^p, $p \neq 2$, and to link functions with certain global smoothness properties with the asymptotic properties of this approximation ([60]). These results do also have practical consequences, for instance in analyzing the compression rates of images coded by wavelet coefficient thresholding – see [58].

4.3 Local regularity

We have mentioned above that global differentiability, or regularity, can be characterized by the behavior of the wavelet coefficients across scales. What about the local existence of derivatives, or local regularity? Local regularity at a point a can be studied for instance by using the notion of Lipschitz continuity: a function f is said to be α-Lipschitz at a, $0 < \alpha < 1$, if

$$|f(x) - f(a)| \;\leq\; C\ |x - a|^{\alpha}.$$

As an example, a step discontinuity has Lipschitz exponent 0. Extensions of this concept to $\alpha > 1$ are made by requiring the highest derivative to satisfy the above equation.

The following result by Jaffard [107] characterizes the local behavior of wavelet coefficients near an α-Lipschitz point:

– If f is α-Lipschitz at a, $\alpha < N$, and the wavelet ψ is C^N and has at least N vanishing moments, then

$$\max_{(i,j)\in A}|w_{ij}| \;\leq\; C\ 2^{-i(1/2+\alpha)}$$

where A contains those index pairs (i, j) for which $a \in$ support(ψ_{ij}).

The converse holds with some modifications. The theorem requires the wavelet itself to have a certain amount of differentiability. (The relative smoothness, or regularity, of a given wavelet can be determined using various methods [53], [73] – for an outline of some of these, see for instance [50].)

Figure 4.3 illustrates this behavior near a step discontinuity, where $\alpha = 0$. The coefficients decay as $O((\frac{1}{\sqrt{2}})^i)$.

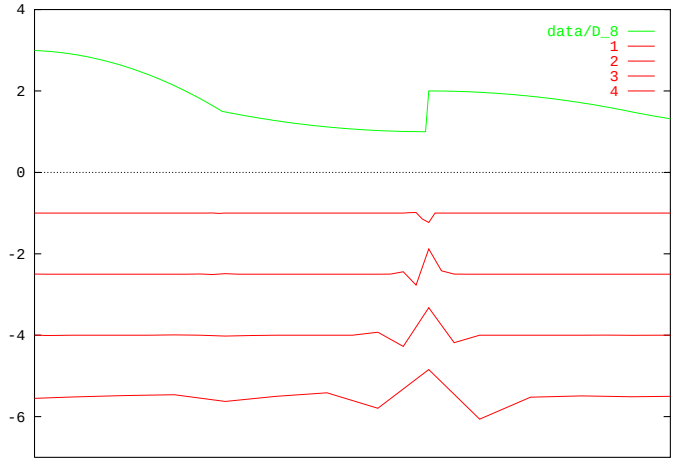

Figure II.8: Decay of wavelet coefficients at a step discontinuity.

Local variations in the decay rate of wavelet coefficients can also be seen from the examples in Figures II.6 and II.7.

Thees properties mean that orthonormal wavelets can in theory be used in discontinuity and edge detection. However, in practice, orthonormal wavelet bases are not best suited for finding estimates of the Lipschitz constants. Similar results as the one above hold for the continuous wavelet transform, but without any restrictions on the smoothness of the wavelet, and edge detection has been performed with success with these methods. The "discrete dyadic wavelets" of Mallat are also used in edge detection [131], [132] (as well as in compression to improve the coding of image discontinuities). The method isolates as key elements the local maxima of the redundant wavelet transform.

5 Extensions of orthonormal wavelet bases

Orthonormality is a very restrictive condition, and orthonormal wavelet constructions become relatively complicated. We want to expand the allowable range of functions: we keep "as much orthogonality" as necessary or desirable, while allowing more general scaling functions, which still satisfy the refinement equation. Such scaling functions include "nice" functions, for instance splines. (Splines define a multiresolution, although not an orthonormal one.) There are several ways to obtain wavelets in this situation.

We assume throughout that we start with a function ϕ defining a stable (6), but not necessarily orthonormal multiresolution analysis (V_i).

5.1 Orthogonalization

Orthogonalization procedures can be used to form a new scaling function ϕ^* whose dilations and translates generate the multiresolution spaces, and provide an orthonormal basis for each V_i. One way of doing this is the following (Meyer): let

$$\hat{\phi^*} = \phi / \sqrt{2\pi \sum_k \hat{\phi}(\omega + 2\pi k)^2}.$$

This sum in the denominator is connected to the inner product of two translates of ϕ and can be explicitly computed for some functions, for instance B-splines.

One drawback of this orthogonalization, and related orthogonalization procedures, is that the resulting new scaling functions are usually not compactly supported and so the wavelets are not compactly supported either.

5.1.1 Example: Battle-Lemarié wavelets

Battle-Lemarié wavelets can be obtained this way from B-spline multiresolution – this means that the multiresolution spaces spanned by the new scaling functions are exactly the spline multiresolution spaces. The new scaling functions and the corresponding wavelets have infinite support, but decay exponentially fast. The scaling function is depicted in Figure II.9.

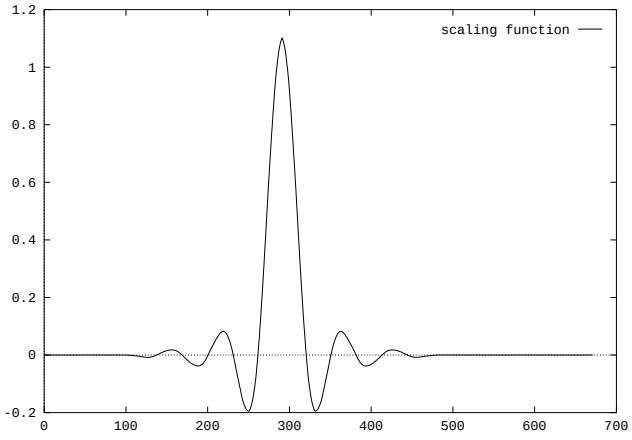

Figure II.9: Battle-Lemarié scaling function

5.2 Biorthogonal wavelets

Biorthogonal wavelets were introduced in [33]. In this construction, orthonormal wavelets are generalized by using two sets of functions, $\phi_{ij}, \psi_{ij}, \tilde{\phi}_{ij}, \tilde{\psi}_{ij}$. The wavelets $(\psi_{ij}), (\tilde{\psi}_{ij})$ do not form orthogonal bases, but they are required to form dual bases for L^2:

$$\langle \psi_{ij}, \tilde{\psi}_{i'j'} \rangle \quad = \delta_{ii'} \delta_{jj'},$$

and the following "analyzing" and "reconstructing" relations hold:

$$f = \sum_{ij} \langle f, \psi_{i,j} \rangle \;\; \tilde{\psi}^i_j = \sum_{ij} \langle f, \tilde{\psi}^i_j \rangle \;\; \psi_{i,j}.$$

An analogue for this situation is common for the continuous wavelet transform.

In this case have two dual multiresolutions V_i, $\tilde{V}_i$, and the complement wavelet spaces W_i, $\tilde{W}_i$. We do not necessarily get orthogonality between W_i and V_i, but have instead $W_i \perp \tilde{V}_i$ and $V_i \perp \tilde{W}_i$. The two multiresolutions may also coincide.

We also have two sets of filters: the usual filter matrices H and G and the dual filter matrices $\tilde{H}$ and $\tilde{G}$. For orthonormal wavelets, $\tilde{H} = H$ and $\tilde{G} = G$. The advantage of the added generality here is that all filters can be chosen to be finite *and* to have other required properties, such as symmetry. It is also much easier to construct biorthogonal filters than orthonormal ones.

In an application, one of the filter pairs is selected as the "analyzing" pair, and the other one the "reconstructing" pair. Here we choose the primal filters for the reconstruction and the dual ones for obtaining the coefficients. Otherwise, reverse the roles of primal and dual in the diagram below. (We think of the primal scaling filter here as the "nicer" filter of the two. This filter is the one usually used in reconstruction.) The decomposition into wavelet coefficients and the corresponding reconstruction is now obtained by almost the same pyramidal algorithm as before:

Decomposition and reconstruction:

$$\begin{array}{ccccc} & & \tilde{\mathbf{H}} & & \\ \mathbf{s} & \longrightarrow & & \mathbf{s}_1 & \\ & & \tilde{\mathbf{G}} & & \\ & & \searrow & & \\ & & & \mathbf{w}_1 & \end{array} \qquad \begin{array}{ccccc} & & \mathbf{H}^T & & \\ \mathbf{s} & \longleftarrow & & \mathbf{s}_1 & \\ & & \mathbf{G}^T & & \\ & & \nwarrow & & \\ & & & \mathbf{w}_1 & \end{array} \tag{21}$$

Note: the definition of the wavelet filter G is connected to the *dual* scaling filter $\tilde{H}$, and similarly for the dual wavelet filter. This means that the previous results in Section 4.1 have to be adjusted accordingly: for instance, the conditions on vanishing moments for approximation are now on the dual wavelet (assuming the convention that the primal functions are used for reconstruction).

5.2.1 Formal conditions for biorthogonality

Suppose we have $m_0, m_1, \tilde{m_0}, \tilde{m_1}$ corresponding to the filters $(g_i), (h_i)$ and the dual filters $(\tilde{g}_i), (\tilde{h}_i)$ as before. We also require the normalization condition $m_0(0) = 1$ and its dual $\tilde{m}_0(0) = 1$. (The first condition could be relaxed [113].)

We can obtain the dual wavelets from the primal scaling functions and vice versa by the usual definitions:

$$m_1(\omega) = -e^{-i\omega}\overline{\tilde{m}_0(\omega + \pi)}, \quad \tilde{m}_1(\omega) = -e^{-i\omega}\overline{m_0(\omega + \pi)}. \tag{22}$$

This choice has the advantage of allowing all four filters to be finite. With the choice of wavelets fixed as above, the necessary condition for biorthogonality of the wavelets, or the exact reconstruction property, can be expressed as

$$m_0(\omega)\overline{\tilde{m}_0(\omega)} + m_0(\omega+\pi)\overline{\tilde{m}_0(\omega+\pi)} = 1. \tag{23}$$

This replaces the necessary orthonormality condition we had before. Necessary and sufficient conditions similar to those for orthonormal wavelets are given in [33].

When allowing a more general choice of wavelet than the one in (22), the necessary conditions are the following:

$$m_0(\omega)\overline{\tilde{m}_0(\omega)} + m_1(\omega)\overline{\tilde{m}_1(\omega)} = 0 \tag{24}$$

$$m_0(\omega+\pi)\overline{\tilde{m}_0(\omega)} - m_1(\omega+\pi)\overline{\tilde{m}_1(\omega)} = 0. \tag{25}$$

For details and examples of the construction of spline-based biorthogonal wavelets, see [33]. Additional theoretical material is covered in [26], [30], [113], and [190].

5.3 Examples

The following figures II.10 and II.11 depict biorthogonal wavelets based on the quadratic B-spline. The number of vanishing moments for both wavelets is 3, and the dual scaling filter length is 8. The dual scaling function does not have very much regularity. It is possible to get smoother functions by increasing the number of vanishing moments; this will quickly result in long filters. (However, in many applications high regularity for both sets of functions is of less importance than fast filtering, and in these cases the shorter filters are adequate.)

Other examples of biorthogonal wavelets, connected to interpolating scaling functions, are constructed in [165], [161].

5.4 Semiorthogonal wavelets

Semiorthogonal wavelets ([30], [26]) are biorthogonal wavelets for which the two multiresolutions coincide, and the wavelet spaces are obtained as orthogonal complements. Semiorthogonal wavelets are not generally fully orthonormal, but they do possess this property between levels:

$$W_i \perp W_k, \quad i \neq k.$$

The dual scaling $\tilde{\phi}$ function can be obtained as

$$\hat{\tilde{\phi}} = \hat{\tilde{\phi}}/(\sum_k \hat{\phi}(\omega + 2\pi k)^2).$$

The dual will generate the same spaces as ϕ; however, it is generally not a compactly supported function, even if ϕ is. The denominator can be computed explicitly for some functions, for instance B-splines [30]. The wavelets are computed using the general biorthogonality conditions (24) and (25). Chui and Wang [31] choose (the unique) wavelets with minimal support length; dual wavelets are computed from the biorthogonality conditions. We will not get into the general construction here but refer to their paper and [26], [30].

If ϕ is a cardinal B-spline of order n, the corresponding minimal support semiorthogonal wavelet is also a B-spline function of order n, with support in $[0, 2n]$. The underlying multiresolution spaces for this construction are the same as the ones for the orthonormal Battle-Lemarié wavelets. The dual functions are not compactly supported – this means that if the spline is used as a reconstructing function, the analyzing filters are not finite.

5.5 Other extensions of wavelets

There are many other ways to extend the scope of wavelets. Even within the "standard" framework here, examples of more general constructions include p-adic wavelets (wavelets corresponding to dilation by an integer p, or even a rational), and wavelet packets. Wavelet packets extend the 2-channel filtering by the filters H and G to all previous filtering results, including the original wavelet coefficients. This gives a full binary decomposition tree. Depending on which members of this tree are selected, the original space is split into different orthonormal bases. Applications, such as image and audio compression, can then choose among these bases to obtain optimal results. For more on these and other extensions see for instance [50], [41].

5.6 Wavelets on intervals

The original definition of wavelets uses functions defined on the whole real line. In practical cases we want to find the wavelet decomposition of a finite sequence, or of a function defined only on an interval. It is possible to extend the data over the endpoints for instance by making it cyclic, by padding with zeros, by reflection, or by fitting a polynomial to the ends of the discrete data set. This is expensive and, for many of these methods, the discontinuities at the ends will produce artificial edge effects.

To avoid these drawbacks, it is also possible to define special wavelets on an interval: these consist of the usual wavelets, when their supports are completely inside the interval, and special modified edge wavelets. Examples of interval wavelets can be found in [143], [35]. These constructions can be carried out so that the edge wavelets have the required approximation properties, and they apply to biorthogonal as well as orthonormal wavelets.

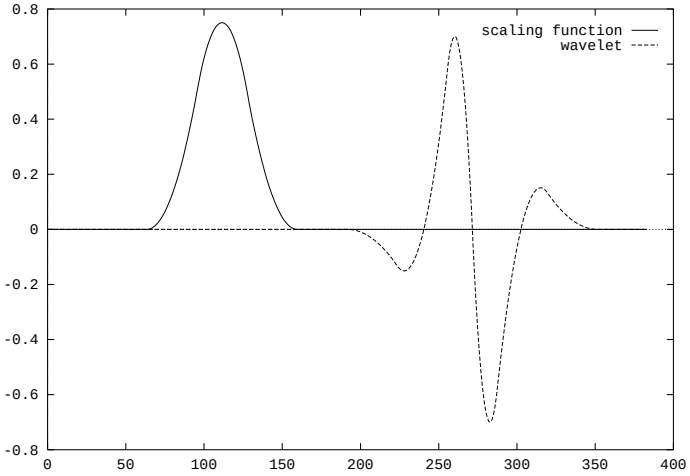

Figure II.10: Quadratic spline functions

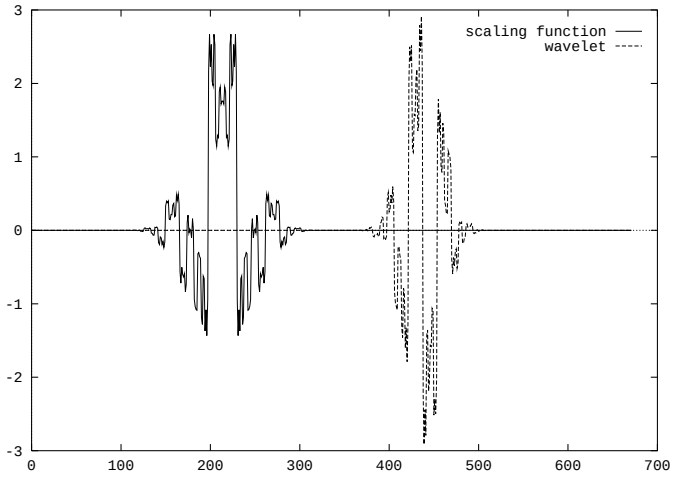

Figure II.11: Dual scaling function and wavelet

III: Building Your Own Wavelets at Home




Wim SWELDENS
University of South Carolina

Peter SCHRÖDER
Princeton University

1 Introduction

In earlier chapters we have seen classical constructions of wavelets on the infinite real line. The filter sequences for scaling functions and wavelets are typically derived through the use of Fourier techniques and the consideration of certain trigonometric polynomials and their properties [51]. From a user's point of view though, the constructions are not always suitable for straightforward implementation or specialization to particular cases, such as boundaries.

The purpose of this chapter is to show that very simple techniques exist which allow the construction of versatile families of scaling functions and wavelets under very general circumstances. Some of these constructions will lead to well studied classical cases, others to wavelets custom-designed to certain applications. None of the techniques, interpolating subdivision [56], average interpolation [62], and lifting [179, 181], are new, but taken together they result in a straightforward and easy to implement toolkit.

To make the treatment as accessible as possible we will take a very "nuts and bolts", algorithmic approach. In particular we will initially ignore many of the mathematical details and introduce the basic techniques with a sequence of examples. Other sections will be devoted to more formal and rigorous mathematical descriptions of the underlying principles. On first reading one can skip these sections which are marked with an asterisk.

All the algorithms can be derived via simple arguments involving nothing more than polynomial interpolation. In fact constraints such as specialization to intervals, boundary conditions, biorthogonality with respect to a weighted inner product, and irregular samples, are easily incorporated.

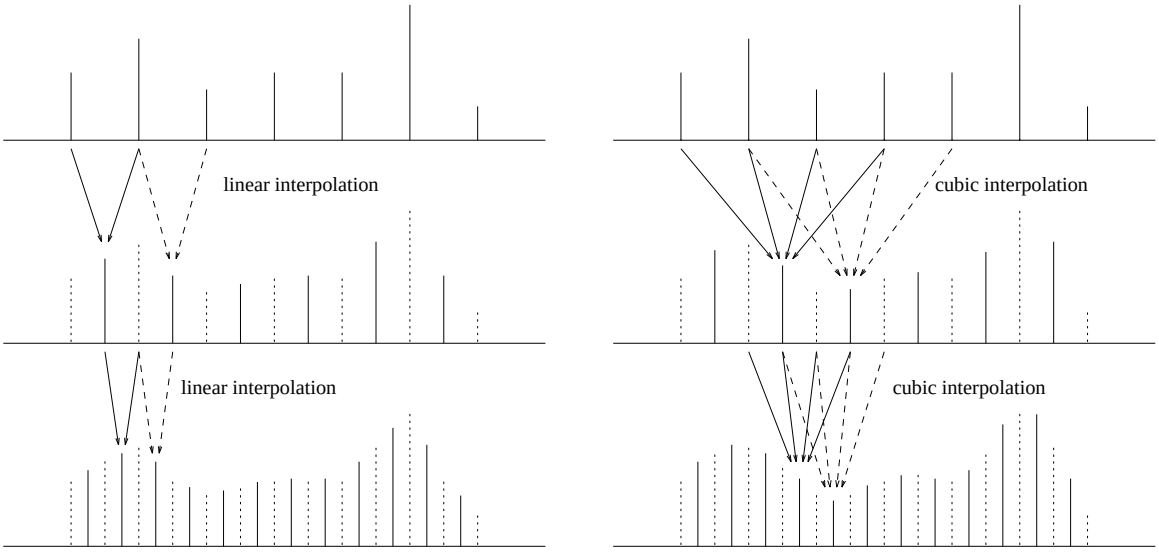

Figure III.1: Examples of interpolating subdivision. On the left a diagram showing the filling in of "in between" samples by linear interpolation between neighboring samples. On the right the same idea is applied to higher order interpolation using two neighbors to either side and the unique cubic polynomial which interpolates these. This process is repeated an infinitum to define the limit function.

We begin with the construction of scaling functions by interpolating subdivision, and average-interpolation. Later we show how this fits into a general framework and how the lifting scheme can be used to construct "second generation wavelets." Finally we demonstrate some of these generalizations with concrete examples and conclude with a discussion of the properties of these constructions (as far as they are known) and point out the questions which require further research.

2 Interpolating Subdivision

2.1 Algorithm

To motivate the construction of interpolating scaling functions we begin by considering the problem of interpolating a sequence of data values. To be concrete, suppose we have the samples $\{\lambda_{0,k} \mid k \in \mathbf{Z}\}$ of some unknown function given at the integers $\{x_{0,k} = k\}$. How can we define an extension of these values to a function defined on the whole real line? Obviously there are many possible approaches. Deslauriers and Dubuc attacked this problem by defining a recursive procedure for finding the value of an interpolating function at all dyadic points [56, 57]. We will refer to this as *interpolating subdivision*. For our purposes this is a particularly well suited approach since we are interested in constructions which obey refinement relations. As we will see later these will lead to a particular set of wavelets.

Perhaps the simplest way to set up such an interpolating subdivision scheme is the following. Let $\{\lambda_{0,k}\}$ be the original sample values. Now define a refined sequence of sample values recursively as

$$\begin{aligned} \lambda_{j+1,2k} &= \lambda_{j,k} \\ \lambda_{j+1,2k+1} &= 1/2\,(\lambda_{j,k} + \lambda_{j,k+1}), \end{aligned}$$

and place the $\lambda_{j,k}$ at locations $x_{j,k} = k\,2^{-j}$. Or in words, new values are inserted halfway between old

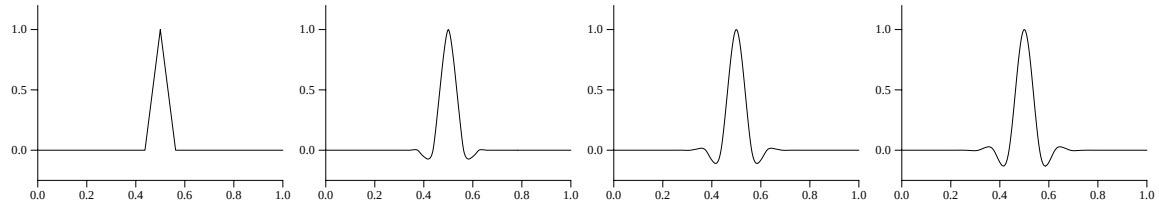

Figure III.2: Scaling functions which result from interpolating subdivision Going from left to right the order N of the subdivision is 2, 4, 6, and 8.

values by linearly interpolating the two neighboring old values (see the left side of Figure III.1). It is not difficult to see that in the limit this will result in a piecewise linear interpolation of the original sample values. Suppose the initial sample values given to us were actually samples of a linear polynomial. In that case our subdivision scheme will exactly reproduce that polynomial.

Let us consider fancier interpolation schemes. For example, instead of defining the new value at the midpoint between two old values as a linear interpolation of the neighboring values we can use two neighboring values on either side and define the (unique) cubic polynomial $p(x)$ which interpolates those four values

$$\begin{aligned} \lambda_{j,k-1} &= p(x_{j,k-1}) \\ \lambda_{j,k} &= p(x_{j,k}) \\ \lambda_{j,k+1} &= p(x_{j,k+1}) \\ \lambda_{j,k+2} &= p(x_{j,k+2}). \end{aligned}$$

The new sample value (odd index) will then be the value that this cubic polynomial takes on at the midpoint, while all old samples (even index) are preserved

$$\begin{aligned} \lambda_{j+1,2k} &= \lambda_{j,k} \\ \lambda_{j+1,2k+1} &= p(x_{j+1,2k+1}). \end{aligned}$$

Figure III.1 (right side) shows this process in a diagram.

Even though each step in the subdivision involves cubic polynomials the limit function will not be a polynomial anymore. While we don't have a sense yet as to what the limit function looks like it is easy to see that it can reproduce cubic polynomials. Assume that the original sequence of sample values came from some given cubic polynomial. In that case the interpolating polynomial over each set of 4 neighboring sample values will be the same polynomial and all newly generated samples will be on the original cubic polynomial, in the limit reproducing it. In general we use N (N even) samples and build a polynomials of degree $N-1$. We then say that the *order* of the subdivision scheme is N.

Next we define a function, which Deslauriers and Dubuc refer to as the *fundamental solution*, but which we will refer to as the *scaling function*: set all $\lambda_{0,k}$ equal to zero except for $\lambda_{0,0}$ which is set to 1. Now run the interpolating subdivision ad infinitum. The resulting function is $\varphi(x)$, the scaling function. Figure III.2 shows the scaling functions which result from the interpolating subdivision of order 2, 4, 6, and 8 (left to right).

What makes interpolating subdivision so attractive from an implementation point of view is that we only need a routine which can construct an interpolating polynomial given some number of sample values and

locations. The new sample value is then simply given by the evaluation of this polynomial at the new, refined location. A particularly efficient (and stable) procedure for this is Neville's algorithm [175, 156]. Notice also that nothing in the definition of this procedure requires the original samples to be located at integers. Later we will use this feature to define scaling functions over irregular subdivisions. Interval boundaries for finite sequences are also easily accommodated. E.g., for the cubic construction described above we can take 1 sample on the left and 3 on the right at the left boundary of an interval. We will come back to this in Section 4.

First we turn to a more formal definition of the interpolating subdivision in the regular case ($x_{j,k} = k\,2^{-j}$) and discuss some of the properties of the scaling functions.

2.2 Formal Description*

The interpolating subdivision scheme can formally be defined as follows. For each group of $N = 2D$ coefficients $\{\lambda_{j,k-D+1}, \ldots, \lambda_{j,k}, \ldots, \lambda_{j,k+D}\}$, it involves two steps:

1. Construct a polynomial p of degree $N - 1$ so that

$$p(x_{j,k+l}) \;=\; \lambda_{j,k+l} \;\text{ for }\; -D+1 \leqslant l \leqslant D.$$

2. Calculate one coefficient on the next finer level as the value of this polynomial at $x_{j+1,2k+1}$

$$\lambda_{j+1,2k+1} \;=\; p(x_{j+1,2k+1}).$$

The properties of the resulting scaling function $\varphi(x)$ are given in the following table.

1. **Compact support:** $\varphi(x)$ is exactly zero outside the interval $[-N, N]$. This easily follows from the locality of the subdivision scheme.

2. **Interpolation:** $\varphi(x)$ is interpolating in the sense that $\varphi(0) = 1$ and $\varphi(k) = 0$ for $k \neq 0$. This immediately follows from the definition.

3. **Symmetry:** $\varphi(x)$ is symmetric. This follows from the symmetry of the construction.

4. **Polynomial reproduction:** The scaling functions and its translates reproduces polynomials up to degree $N - 1$. In other words

$$\sum_k k^p \, \varphi(x - k) \;=\; x^p \;\text{ for }\; 0 \leqslant p < N.$$

   This can be seen by starting the subdivision scheme with the sequence k^p and using the fact that the subdivision definition insures the reproduction of polynomials up to degree $N - 1$.

5. **Smoothness:** Typically $\varphi \in C^\alpha$ where $\alpha = \alpha(N)$. We know that $\alpha(4) < 2$ and $\alpha(6) < 2.830$ (strict bounds). Also, the smoothness increases linearly with N. This fact is much less trivial than the previous ones. We refer to [56, 57].

6. **Refinability:** This means it satisfies a *refinement relation* of the form

$$\varphi(x) \;=\; \sum_{l=-N}^{N} h_l \, \varphi(2x - l).$$

   This can be seen as follows. Do one step in the subdivision starting from $\lambda_{0,k} = \delta_{k,0}$. Call the result $h_l \;=\; \lambda_{1,l}$. It is easy to see that only $2N + 1$ coefficients h_l are non-zero. Now, start the subdivision scheme from level 1 with these values $\lambda_{1,l}$. The refinement relation follows from the fact that this should give the same result as starting from level 0 with the values $\lambda_{0,k}$. Also because of interpolation, it follows that $h_{2l} = \delta_{l,0}$. We refer to the h_l as *filter coefficients*.

We next define the scaling function $\varphi_{j,k}(x)$ as the limit function of the subdivision scheme started on level j with $\lambda_{j,k} = \delta_{k,0}$. A moment's thought reveals that $\varphi_{j,k}(x) = \varphi(2^j x - k)$. With a change of variables in the refinement relation we get

$$\varphi_{j,k} \;=\; \sum_l h_{l-2k} \, \varphi_{j+1,l}.$$

With these facts in hand consider some original sequence of sample values $\lambda_{j,k}$ at level j. Simply using linear superposition and starting the subdivision scheme at level j, yields a limit function $f(x)$ of the form

$$f(x) \;=\; \sum_k \lambda_{j,k} \, \varphi_{j,k}(x).$$

The same limit function $f(x)$ can also be written as

$$f(x) \;=\; \sum_l \lambda_{j+1,l} \, \varphi_{j+1,l}(x).$$

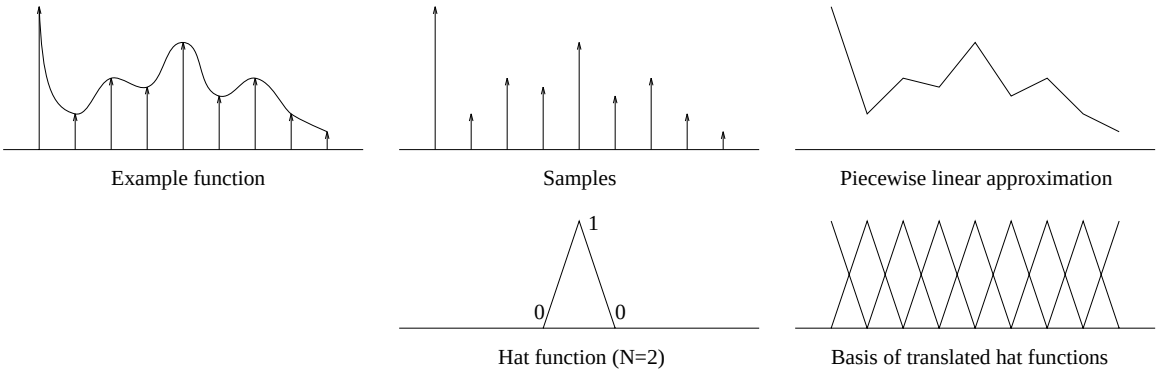

Figure III.3: An example function is sampled at a number of locations. The values at these sample points are used as coefficients in the interpolating scheme of $N = 2$. The scaling function of $N = 2$ is the familiar hat function and the basis for the approximation is a set of translated hat functions $\varphi_{j,k}(x) = \varphi(2^j x - k)$.

Equating these two ways of writing f and using the refinement relation to replace $\varphi_{j,k}$ with a linear combination of $\varphi_{j+1,l}$ we get

$$\sum_l \lambda_{j+1,l}\, \varphi_{j+1,l}(x) = \sum_k \lambda_{j,k} \sum_l h_{l-2k}\, \varphi_{j+1,l}\,.$$

Evaluating both sides at $x_{j+1,k}$ we finally arrive at

$$\lambda_{j+1,l} \;=\; \sum_k h_{l-2k}\, \lambda_{j,k}\,.$$

This equation has the same structure as the usual inverse wavelet transform (synthesis) in case all wavelet coefficients are set to zero.

In the case of linear subdivision, the filter coefficients are $h_l = \{1/2, 1, 1/2\}$. The associated scaling function is the familiar linear B-spline "hat" function, see Figure III.3. The cubic case leads to filters $h_l = \{-1/16, 0, 9/16, 1, 9/16, 0, -1/16\}$. The general expression is

$$h_{2k+1} = (-1)^{D+k}\, \frac{\prod_{i=0}^{2D-1}(i - D + 1/2)}{(k + 1/2)(D + k)!(D - k - 1)!},$$

for odd numbered coefficients. The even numbered ones are $h_{2k} = \delta_{k,0}$.

3 Average-Interpolating Subdivision

3.1 Algorithm

In contrast to the interpolating subdivision scheme of Deslauriers-Dubuc we now consider average-interpolation as introduced by Donoho [62]. The starting point of interpolating subdivision was a set of samples of some function. Suppose that instead of samples we are given averages of some unknown function over intervals

$$\lambda_{0,k} = \int_k^{k+1} f(x)\, dx\,.$$

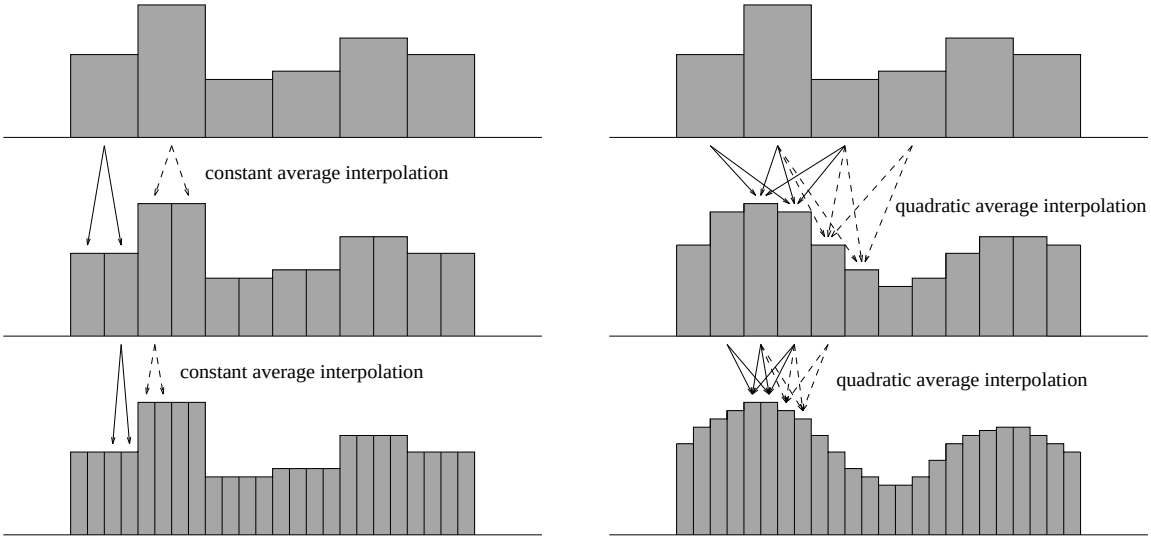

Figure III.4: Examples of average-interpolation. On the left a diagram showing the constant average-interpolation scheme. Each subinterval gets the average of a constant function defined by the parent interval. On the right the same idea is applied to higher order average-interpolation using a neighboring interval on either side. The unique quadratic polynomial which has the correct averages over one such triple is used to compute the averages over the subintervals of the middle interval. This process is repeated an infinitum to define the limit function.

Such values might arise from a physical device which does not perform point sampling but integration as is done, for example, by a CCD cell (to a first approximation). How can we use such values to define a function whose averages are exactly the measurement values given to us? One obvious answer is to use these values to define a piecewise constant function which takes on the value $\lambda_{0,k}$ for $x \in [k, k+1]$. This corresponds to the following constant average-interpolation scheme

$$\begin{aligned} \lambda_{j+1,2k} &= \lambda_{j,k} \\ \lambda_{j+1,2k+1} &= \lambda_{j,k}\,. \end{aligned}$$

In words, we assign averages to each subinterval (left and right) by setting them to be the same value as the average for the parent interval. Cascading this procedure ad infinitum we get a function which is defined everywhere and is piecewise constant. Furthermore its averages over intervals $[k, k+1]$ match the observed averages. The disadvantage of this simple scheme is that the limit function is not smooth. In order to understand how to increase the smoothness of such a reconstruction we again define a general *average*-interpolating procedure.

One way to think about the previous scheme is to describe it as follows. We assume that the (unknown) function we are dealing with is a *constant polynomial* over the interval $[k\,2^{-j}, (k+1)2^{-j}]$. The values of $\lambda_{j+1,2k}$ and $\lambda_{j+1,2k+1}$ then follow as the averages of this polynomial over the respective subintervals. The diagram on the left side of Figure III.4 illustrates this scheme.

Just as before we can extend this idea to higher order polynomials. The next natural choice is quadratic. For a given interval consider the intervals to its left and right. Define the (unique) quadratic polynomial $p(x)$

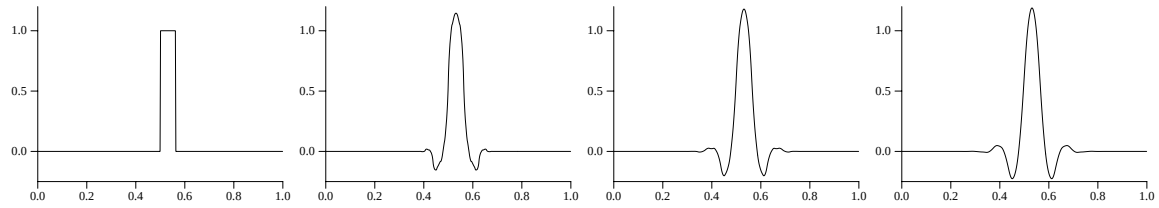

Figure III.5: Scaling functions which result from average interpolation. Going from left to right orders of the respective subdivision schemes were 1, 3, 5, and 7.

such that

$$\begin{aligned}
\lambda_{j,k-1} &= \int_{(k-1)\,2^{-j}}^{k\,2^{-j}} p(x)\,dx \\
\lambda_{j,k} &= \int_{k\,2^{-j}}^{(k+1)\,2^{-j}} p(x)\,dx \\
\lambda_{j,k+1} &= \int_{(k+1)\,2^{-j}}^{(k+2)\,2^{-j}} p(x)\,dx.
\end{aligned}$$

Now compute $\lambda_{j+1,2k}$ and $\lambda_{j+1,2k+1}$ as the average of this polynomial over the subintervals of $[k\,2^{-j}, (k+1)2^{-j}]$

$$\begin{aligned}
\lambda_{j+1,2k} &= 2\int_{k\,2^{-j}}^{(2k+1)\,2^{-j-1}} p(x)\,dx \\
\lambda_{j+1,2k+1} &= 2\int_{(2k+1)\,2^{-j-1}}^{(k+1)\,2^{-j}} p(x)\,dx.
\end{aligned}$$

Figure III.4 (right side) shows this procedure.

It is not immediately clear what the limit function of this process will look like, but it easy to see that the procedure will reproduce quadratic polynomials. Assume that the initial averages $\{\lambda_{0,k}\}$ were averages of a given quadratic polynomial. In that case the unique polynomial $p(x)$ which has the prescribed averages over each triple of intervals will always be that same polynomial which gave rise to the initial set of averages. Since the interval sizes go to zero and the averages over the intervals approach the value of the underlying function in the limit the original quadratic polynomial will be reproduced.

We can now define the scaling function exactly the same way as in the interpolating subdivision case. In general we use N intervals (N odd) to construct a polynomial of degree $N-1$. Again N is the order of the subdivision scheme. Figure III.5 shows the scaling functions of order 1, 3, 5, and 7 (left to right).

Just as the earlier interpolating subdivision process this scheme also has the virtue that it is very easy to implement. The conditions on the integrals of the polynomial result in an easily solvable linear system relating the coefficients of p to the $\lambda_{j,k}$. In its simplest form (we will see more general versions later on) we can streamline this computation even further by taking advantage of the fact that the integral of a polynomial is itself another polynomial. This leads to another interpolation problem

$$\begin{aligned}
0 &= P(x_{j,k-1}) \\
\lambda_{j,k} &= P(x_{j,k})
\end{aligned}$$

$$\begin{aligned} \lambda_{j,k} + \lambda_{j,k+1} &= P(x_{j,k+1}) \\ \lambda_{j,k} + \lambda_{j,k+1} + \lambda_{j,k+2} &= P(x_{j,k+2}). \end{aligned}$$

Given such a polynomial P the finer averages become

$$\begin{aligned} \lambda_{j+1,2k} &= 2\,(P(x_{j+1,2k+1}) - \lambda_{j,k}) \\ \lambda_{j+1,2k+1} &= 2\,(\lambda_{j,k+1} - P(x_{j+1,2k+1})). \end{aligned}$$

This computation, just like the earlier interpolating subdivision, can be implemented in a stable and very efficient way with a simple Neville interpolation algorithm.

Notice again how we have not assumed that the $x_{j,k}$ are regular and generalizations to non-even sized intervals are possible without fundamental changes. As in the earlier case boundaries are easily absorbed by taking two intervals to the right at the left boundary, for example. We can also allow weighted averages. All of these generalizations will be discussed in more detail in Section 4.

In the next section we again take a more formal look at these ideas in the regular case.

3.2 Formal Description*

The average-interpolating subdivision scheme of order N can be defined as follows. For each group of $N = 2D + 1$ coefficients $\{\lambda_{j,k-D}, \ldots, \lambda_{j,k}, \ldots, \lambda_{j,k+D}\}$, it involves two steps:

1. Construct a polynomial p of degree $N - 1$ so that

$$\int_{(k+l)\,2^{-j}}^{(k+l+1)\,2^{-j}} p(x)\,dx \;=\; \lambda_{j,k+l} \;\text{ for }\; -D \leqslant l \leqslant D.$$

2. Calculate two coefficients on the next finer level as

$$\lambda_{j+1,2k} = 2\int_{k\,2^{-j}}^{(2k+1)\,2^{-j-1}} p(x)\,dx \;\text{ and }\; \lambda_{j+1,2k+1} = 2\int_{(2k+1)\,2^{-j-1}}^{(k+1)\,2^{-j}} p(x)\,dx\,.$$

The properties of the scaling function are given in the following table, see [62].

1. **Compact support:** $\varphi(x)$ is exactly zero outside the interval $[-N+1, N]$. This easily follows from the locality of the subdivision scheme.

2. **Average-interpolation:** $\varphi(x)$ is average-interpolating in the sense that

$$\int_k^{k+1} \varphi(x)\, dx \;=\; \delta_{k,0}.$$

   This immediately follows from the definition.

3. **Symmetry:** $\varphi(x)$ is symmetric around $x = 1/2$. This follows from the symmetry of the construction.

4. **Polynomial reproduction:** $\varphi(x)$ reproduces polynomials up to degree $N-1$. In other words

$$\sum_k 1/(p+1)\,((k+1)^{p+1} - k^{p+1})\,\varphi(x-k) \;=\; x^p \;\text{ for }\; 0 \leqslant p < N.$$

   This can be seen by starting the scheme with this particular coefficient sequence and using the fact that the subdivision reproduces polynomials up to degree $N-1$.

5. **Smoothness:** $\varphi(x)$ is continuous of order R, with $R = R(N) > 0$. One can show that $R(3) \geqslant .678$, $R(5) \geqslant 1.272$, $R(7) \geqslant 1.826$, $R(9) \geqslant 2.354$, and asymptotically $R(N) \approx .2075N$ [62].

6. **Refinability:** $\varphi(x)$ satisfies a refinement relation of the form

$$\varphi(x) \;=\; \sum_{l=-N+1}^{N} h_l\, \varphi(2x-l).$$

   This follows from similar reasoning as in the interpolating case starting from $\lambda_{k,0} = \delta_{k,0}$. The construction then implies that $h_0 = h_1 = 1$ and $h_{2l} \;=\; -h_{2l+1}$ if $l \neq 0$.

Next consider some original sequence of averages $\lambda_{j,k}$ at level j. Simply using linear superposition and starting the subdivision scheme at level j, yields a limit function $f(x)$ of the form

$$f(x) \;=\; \sum_k \lambda_{j,k}\, \varphi_{j,k}(x).$$

The same limit function $f(x)$ can also be written as

$$f(x) \;=\; \sum_l \lambda_{j+1,l}\, \varphi_{j+1,l}(x).$$

Equating these two ways of writing f and using the refinement relation to replace $\varphi_{j,k}$ with a linear combination of $\varphi_{j+1,l}$ we again get

$$\lambda_{j+1,l} \;=\; \sum_k h_{l-2k}\, \lambda_{j,k}.$$

This equation has the same structure as the usual inverse wavelet transform (synthesis) in case all wavelet coefficients are set to zero.

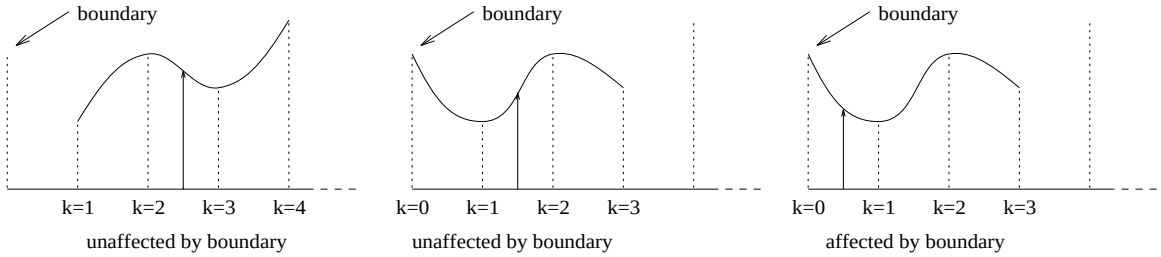

Figure III.6: Behavior of the cubic interpolating subdivision near the boundary. The midpoint samples between $k = 2, 3$ and $k = 1, 2$ are unaffected by the boundary. When attempting to compute the midpoint sample for the interval $k = 0, 1$ we must modify the procedure since there is no neighbor to the left for the cubic interpolation problem. Instead we choose 3 neighbors to the right. Note how this results in the same cubic polynomial as used in the definition of the midpoint value $k = 1, 2$. The procedure clearly preserves the cubic reconstruction property even at the interval boundary and is thus the natural choice for the boundary modification.

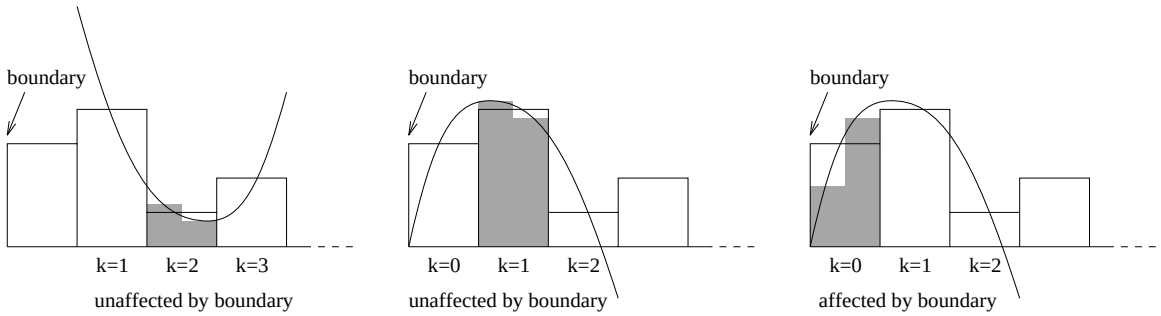

Figure III.7: Behavior of the quadratic average-interpolation process near the boundary. The averages for the subintervals $k = 2$ and $k = 1$ are unaffected. When attempting to compute the finer averages for the left most interval the procedure needs to be modified since no further average to the left of $k = 0$ exists for the average-interpolation problem. Instead we use 2 intervals to the right of $k = 0$, effectively reusing the same average-interpolating polynomial constructed for the subinterval averages on $k = 1$. Once again it is immediately clear that this is the natural modification to the process near the boundary, since it insures that the crucial quadratic reproduction property is preserved.

4 Generalizations

So far we have been discussing scaling functions defined on the real line with sample locations $x_{j,k} = k\,2^{-j}$. This has the nice feature that all scaling functions are translates and dilates of one fixed function. However, the true power of subdivision schemes lies in the fact that they can also be used in much more general settings. In particular we are interested in the following cases:

1. **Interval constructions:** When working with finite data it is desirable to have basis functions adapted to life on an interval. This way no half solutions such as zero padding, periodization, or reflection are needed. We point out that many wavelet constructions on the interval already exist, see [4, 36, 24], but we would like to use the subdivision schemes of the previous sections since they lead to easy implementations.

2. **Weighted inner products:** Often one needs a basis adapted to a weighted inner product instead of the regular L^2 inner product. A weighted inner product of two functions f and g is defined as

$$\langle f, g \rangle = \int w(x)\, f(x)\, g(x)\, dx,$$

where $w(x)$ is some positive function. Weighted wavelets are extremely useful in the solution of boundary value ODEs, see [112, 180]. Also, as we will see later, they are useful in the approximation of functions with singularities.

3. **Irregular samples:** In many practical applications, the samples do not necessarily live on a regular grid. Resampling is awkward. A basis adapted to the irregular grid is desired.

The exciting aspect of subdivision schemes is that they adapt in a straightforward way to these settings. Let us discuss this in more detail.

Both of the subdivision schemes we discussed assemble N coefficients $\lambda_{j,k}$ in each step. These uniquely define a polynomial p of degree $N-1$. This polynomial is then used to generate one (interpolating case) or two (average-interpolation case) new coefficients $\lambda_{j+1,l}$. Each time the new coefficients are located in the middle of the N old coefficients. When working on an interval the same principle can be used as long as we are sufficiently far from the boundary. Close to the boundary we need to adapt this scheme. Consider the case where one wants to generate a new coefficient $\lambda_{j+1,l}$ but is unable to find old samples $\lambda_{j,k}$ equally spaced to the left or right of the new sample, simply because they are not available. The basic idea is then to choose, from the set of available samples $\lambda_{j,k}$, those N which are closest to the new coefficient $\lambda_{j+1,l}$.

To be concrete, take the interval $[0,1]$. In the interpolating case we have 2^j+1 coefficients $\lambda_{j,k}$ at locations $k\,2^{-j}$ for $0 \leqslant k \leqslant 2^j$. In the average-interpolation case we have 2^j coefficients $\lambda_{j,k}$ corresponding to the intervals $[k\,2^{-j}, (k+1)\,2^{-j}]$ for $0 \leqslant k < 2^j$. Now consider the interpolating case as an example. The left most coefficient $\lambda_{j+1,0}$ is simply $\lambda_{j,0}$. The next one, $\lambda_{j+1,1}$ is found by constructing the interpolating polynomial to the points $(x_{j,k}, \lambda_{j,k})$ for $0 \leqslant k < N$ and evaluating it at $x_{j+1,1}$. For $\lambda_{j+1,2}$ we evaluate the same polynomial p at $x_{j+1,2}$. Similar constructions work for the other N boundary coefficients, the right side, and the average-interpolation case. Figures III.6 and III.7 show this idea for a concrete example in the interpolating and average-interpolation case. Figure III.8 shows the scaling functions affected by the boundary for both the interpolating and average-interpolation case.

Next, take the case of a weighted inner product. In the interpolating case, nothing changes. In the average-interpolation case, the only thing we need to do is to replace the integrals with weighted integrals. We now construct a polynomial p of degree $N-1$ so that

$$\int_{x_{j,k+l}}^{x_{j,k+l+1}} w(x)\, p(x)\, dx = |I_{j,k+l}|\, \lambda_{j,k+l} \quad \text{for} \quad -D \leqslant l \leqslant D,$$

where

$$|I_{j,k}| = \int_{x_{j,k}}^{x_{j,k+1}} w(x)\, dx.$$

Then we calculate two coefficients on the next finer level as

$$\lambda_{j+1,2k} = 1/|I_{j+1,2k}| \int_{x_{j,k}}^{x_{j+1,2k+1}} w(x)\, p(x)\, dx \quad \text{and} \quad \lambda_{j+1,2k+1} = 1/|I_{j+1,2k+1}| \int_{x_{j+1,2k+1}}^{x_{j,k+1}} w(x)\, p(x)\, dx.$$

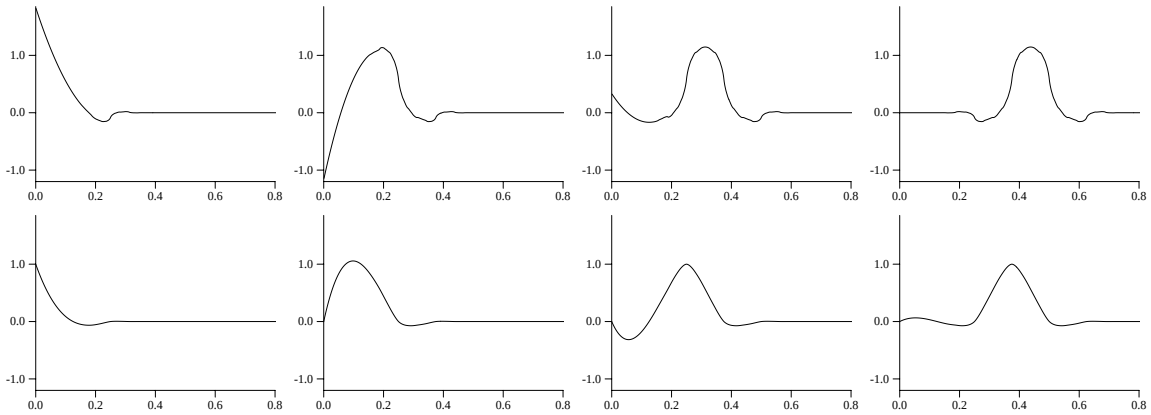

Figure III.8: Examples of scaling functions affected by a boundary. On top the scaling function of quadratic ($N = 3$) average-interpolation at $j = 3$ and $k = 0, 1, 2, 3$. On the bottom the scaling functions of cubic ($N = 4$) interpolation at $j = 3$ and $k = 0, 1, 2, 3$. Note how the boundary scaling functions are still interpolating.

Everything else remains the same, except the fact that the polynomial problem cannot be recast into a Neville algorithm any longer since the integral of a polynomial times the weight function is not necessarily a polynomial. This construction of weighted wavelets using average-interpolation was first done in [180].

The case of irregular samples can also be accommodated by observing that neither of the subdivision schemes requires samples on a regular grid. We can take an arbitrarily spaced set of points $x_{j,k}$ with $x_{j+1,2k} = x_{j,k}$ and $x_{j,k} < x_{j,k+1}$. In the interpolating case a coefficient $\lambda_{j,k}$ lives at $x_{j,k}$, while in the average-interpolation case a coefficient $\lambda_{j,k}$ is associated with the interval $[x_{j,k}, x_{j,k+1}]$. The subdivision schemes can now be applied in a straightforward manner.

Obviously any combinations of these three cases can also be accommodated.

5 Multiresolution Analysis

5.1 Introduction

In the above sections we have discussed two subdivision schemes to generate scaling functions and pointed out how their definitions left plenty of room for generalizations. The resulting modifications to the algorithms are straightforward. We have yet to introduce the wavelets that go with these scaling functions. In order to do so we need a slightly more formal framework in which to embed the above scaling function constructions. In particular we need a framework which allows us to carry over all the generalizations described above. This general framework we refer to as "second generation wavelets." The ambition of second generation wavelets is to generalize the construction of wavelets and scaling functions to intervals, bounded domains, curves and surfaces, weights, irregular samples, etc. In these settings translation and dilation cannot be used any more. Second generation wavelets rely on the fact that translation and dilation are not fundamental to obtain wavelets with desirable properties such as localization in space and frequency and fast transforms.

We begin with a discussion of multiresolution analysis before showing how second generation wavelets can be constructed with the lifting scheme.

5.2 Generalized Refinement Relations

In classical constructions, scaling functions are defined as the dyadic translates and dilates of one fixed scaling function $\varphi(x)$. I.e., the classical scaling functions satisfy a refinement relation of the form

$$\varphi_{j,k} \;=\; \sum_l h_{l-2k}\, \varphi_{j+1,l}.$$

However, in the generalizations discussed in the previous section, the scaling functions constructed through subdivision are not necessarily translates and dilates of one fixed function. However they still satisfy refinement relations which we can find as follows. Start the subdivision on level j with $\lambda_{j,k} = \delta_{0,k}$. We know that the subdivision scheme converges to $\varphi_{j,k}$. Now do only one step of the subdivision scheme. Call the resulting coefficients $h_{j,k,l} = \lambda_{j+1,l}$. Only a finite number are non zero. Since starting the subdivision scheme at level $j+1$ with the $\{h_{j,k,l} \mid l\}$ coefficients also converges to $\varphi_{j,k}$, we have that

$$\varphi_{j,k} \;=\; \sum_l h_{j,k,l}\, \varphi_{j+1,l}.$$

The coefficients of the refinement relation are thus different for each scaling function.

5.3 Formal Description*

Before we begin, let us fix notation. We will always assume the interval $[0,1]$, a weight function $w(x)$, and possibly irregular samples $x_{j,k}$. The coarsest level will be denoted $j = 0$. The index k ranges from 0 to 2^j in the interpolation case and from 0 to $2^j - 1$ in the average-interpolation case. In the refinement relations, $0 \leqslant k < 2^j(+1)$ while $0 \leqslant l < 2^{j+1}(+1)$.

We begin with the definition of multiresolution analysis in this general context. A multiresolution analysis is a set of closed subspaces $V_j \subset \mathrm{L}^2([0,1])$ with $j \in \mathbf{N}$, which are defined as

$$V_j \;=\; \text{span}\,\{\varphi_{j,k} \mid 0 \leqslant k < 2^j(+1)\}.$$

It follows from the refinement relations that the spaces are nested, $V_j \subset V_{j+1}$. We require that every function of finite energy can be approximated arbitrarily close with scaling functions, or

$$\bigcup_{j>0} V_j \text{ is dense in } \mathrm{L}^2.$$

In other words, projection operators $P_j : \mathrm{L}^2(X) \to V_j$ exist, so that for every $f \in \mathrm{L}^2$

$$\lim_{j\to\infty} P_j\, f \;=\; f.$$

The question now is: how do we find these projection operators P_j? In case the $\varphi_{j,k}$ form an orthonormal basis for V_j, the answer would be easy. We let

$$P_j\, f \;=\; \sum_k \langle\, f, \varphi_{j,k} \,\rangle\; \varphi_{j,k},$$

i.e., the coefficients of the projection of f can be found by taking inner products against the basis functions themselves. However, in general, it is very hard to construct orthonormal scaling functions. Instead we consider a more general, biorthogonal setting. In that setting we have a second set of scaling functions, *dual*

scaling functions $\tilde{\varphi}_{j,k}$, so that we can write

$$P_j f \;=\; \sum_k \langle\, f, \tilde{\varphi}_{j,k} \,\rangle\; \varphi_{j,k},$$

i.e., we need a second set of functions such that when we take inner products of f against them, they yield exactly the right coefficients with respect to $\varphi_{j,k}$.

How can we find these dual scaling functions? Their defining property follows from the requirement that P_j be a projection operator, i.e., $P_j\, P_j = P_j$. Using some arbitrary test function f and substituting $P_j f$ into P_j we find that scaling functions and dual scaling functions have to be *biorthogonal* in the sense that

$$\langle\, \varphi_{j,k}, \tilde{\varphi}_{j,k'} \,\rangle \;=\; \delta_{k,k'}.$$

For normalization purposes, we always let

$$\int_0^1 w(x)\, \tilde{\varphi}_{j,k}(x)\, dx \;=\; 1. \tag{1}$$

5.4 Examples

We already encountered dual functions in both of the subdivision schemes. Indeed, average-interpolation subdivision relies on the fact that the $\lambda_{j,k}$ are local averages, i.e., inner products with box functions. If we let $\lambda_{j,k} = \langle\, f, \tilde{\varphi}_{j,k} \,\rangle$, according to (1) the dual functions are (cf. Section 4)

$$\tilde{\varphi}_{j,k} \;=\; \chi_{I_{j,k}} / |I_{j,k}|.$$

Note that in the canonical case with $w(x) = 1$ the dual functions are box functions of height inversely proportional to the width of their support.

In the interpolating case, the $\lambda_{j,k}$ were actual evaluations of the function. This implies that

$$\tilde{\varphi}_{j,k}(x) \;=\; \delta(x - x_{j,k}),$$

since taking inner products with (formal) duals, which are Dirac pulses, amounts to evaluating the function at the location where the pulse is located.

5.5 Polynomial Reproduction

With the above ideas about dual scaling functions in the back of our minds we can now better appreciate the motivation behind the earlier subdivision schemes. It is given by the following: assume that N coefficients $\lambda_{j,k}$ locally are the coefficients of a polynomial of degree $N-1$, then locally generate $\lambda_{j+1,l}$ coefficients so that they are the coefficients of the same polynomial. This implies that if *all* the coefficients $\lambda_{j_0,k}$ on level j_0 are the coefficients of one fixed polynomial of degree less than N, i.e., the function we are trying to synthesize actually *is* a polynomial, then the subdivision scheme will *exactly* reproduce this polynomial. In other words, any polynomial of degree less than N can be reproduced by the scaling functions on each level, or in the language of projection operators

$$P_j\, x^p \;=\; x^p \;\text{ for }\; 0 \leqslant p < N.$$

We then say that the *order* of the multiresolution analysis is N.

Obviously, primal and dual scaling functions are interchangeable and we can define a projection operator with respect to the dual scaling functions by taking inner products with the primal scaling functions

$$\tilde{P}_j = \sum_k \langle\, ., \varphi_{j,k} \,\rangle\, \tilde{\varphi}_{j,k}.$$

This leads to the observation that the dual scaling functions formally also generate a multiresolution analysis. We denote the order of the dual multiresolution analysis by $\tilde{N}$. Any polynomial of degree less than $\tilde{N}$ is reproduced by the dual projection operator. Alternatively we can establish a connection with the primal projection P_j by exploiting the biorthogonality condition which states for f arbitrary

$$\langle\, x^p, P_j f \,\rangle \;=\; \sum_k \langle\, f, \tilde{\varphi}_{j,k} \,\rangle\, \langle\, x^p, \varphi_{j,k} \,\rangle \;=\; \langle\, \tilde{P}_j\, x^p, f \,\rangle \;=\; \langle\, \tilde{P}_{j+1}\, x^p, f \,\rangle \;=\; \langle\, x^p, P_{j+1} f \,\rangle \;\text{ for } 0 \leqslant p < \tilde{N}.$$

Or in other words, the P_j preserve up to $\tilde{N}$ moments. In the interpolating case $\tilde{N} = 0$, i.e., no moments are preserved, while in the average-interpolation case $\tilde{N} = 1$, i.e., the total integral is preserved.

5.6 Subdivision

Let us now reconsider subdivision schemes (both interpolation and average-interpolation). Given the coefficients $\lambda_{j_0,k}$ of a function $f \in V_{j_0}$, with

$$f \;=\; \sum_k \lambda_{j_0,k}\, \varphi_{j_0,k} \;\text{ where }\; \lambda_{j_0,k} \;=\; \langle\, f, \tilde{\varphi}_{j_0,k} \,\rangle\,,$$

a subdivision scheme allows us to synthesize the function f. This is done by rewriting the same f (an element of V_{j_0}), as an element of V_j ($j > j_0$)

$$f \;=\; \sum_k \lambda_{j,k}\, \varphi_{j,k} \;\text{ with }\; \lambda_{j,k} \;=\; \langle\, f, \tilde{\varphi}_{j,k} \,\rangle\,,$$

where we know that

$$\lim_{j \to \infty} \lambda_{j,k\,2^{j-j_0}} \;=\; f(k\,2^{-j_0}).$$

In other words the value of the function f at any point can be found as a limit on the coefficients in the subdivision scheme.

Similar to the regular case, the subdivision scheme can also be written as a filter relation,

$$\lambda_{j+1,l} \;=\; \sum_k h_{j,k,l}\, \lambda_{j,k}.$$

5.7 Coarsening

We have now seen that subdivision uses the primal scaling functions to allow us to go to finer resolutions. How do we go to coarser resolutions? To answer this we need to have a refinement relation for dual scaling functions. As we mentioned earlier, the dual scaling functions also generate a multiresolution analysis and

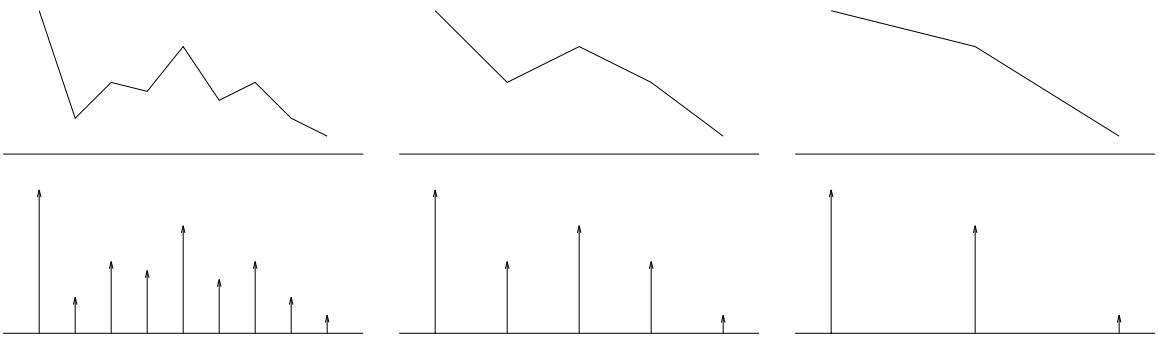

Figure III.9: Successively coarser piecewise linear approximations arrived at by subsampling and interpolating subdivision with $N = 2$.

thus satisfy a dual refinement relation

$$\tilde{\varphi}_{j,k} \;=\; \sum_l \tilde{h}_{j,k,l}\, \tilde{\varphi}_{j+1,l}.$$

Assume now that we are given a projection $P_n f$ and that we want to find the coarser projections $P_j f$ with $j < n$. Recall that the definition of P_j requires inner products with dual functions, $\lambda_{j,k} = \langle f, \tilde{\varphi}_{j,k} \rangle$. Substituting the dual refinement relation in place of $\tilde{\varphi}_{j,k}$ and observing that $\langle f, \tilde{\varphi}_{j+1,l} \rangle = \lambda_{j+1,l}$ we get

$$\lambda_{j,k} \;=\; \sum_l \tilde{h}_{j,k,l}\, \lambda_{j+1,l}. \tag{2}$$

In other words the dual scaling function refinement relation tells us how to filter scaling function coefficients when going from a finer to a coarser level.

5.8 Examples

In the interpolating case it is extremely easy to find the dual scaling function refinement relation. Since the dual scaling functions are Dirac distributions we simply get

$$\lambda_{j,k} \;=\; \lambda_{j+1,2k}.$$

The filter sequence $\tilde{h}_{j,k,l}$ is equal to δ_{l-2k}. An example of coarsening for $N = 2$ is given in Figure III.9.

In the average-interpolation case the dual functions are box functions, normalized so that their (weighted) integral is one. The refinement relation thus is

$$\tilde{\varphi}_{j,k} \;=\; |I_{j+1,2k}|/|I_{j,k}|\, \tilde{\varphi}_{j+1,2k} + |I_{j+1,2k+1}|/|I_{j,k}|\, \tilde{\varphi}_{j+1,2k+1}.$$

It follows that coarser levels are calculated as pairwise weighted averages

$$\lambda_{j,k} \;=\; |I_{j+1,2k}|/|I_{j,k}|\, \lambda_{j+1,2k} + |I_{j+1,2k+1}|/|I_{j,k}|\, \lambda_{j+1,2k+1}.$$

With these relations, we can now build *linear approximation* operators. The idea goes as follows: start with an approximation on level n (the original coefficients), find a coarser approximation P_j with $j < n$, next use P_j to start the cascade algorithm and cascade out to level n again. By doing this for $j = n-1, n-2, n-3, \ldots$,

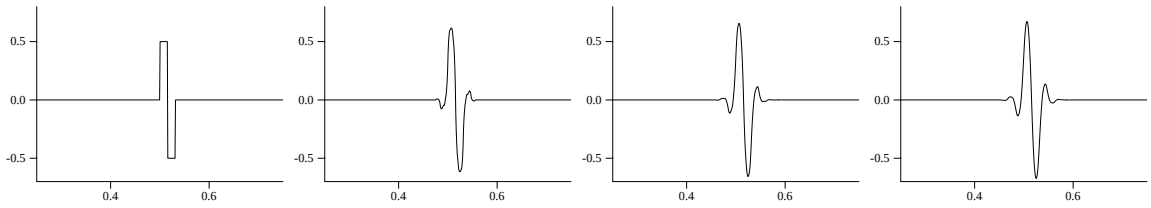

Figure III.10: Wavelets with one vanishing moment associated with average interpolation. Going from left to right are the wavelets which correspond to dual wavelets of 1, 3, 5, and 7 vanishing moments.

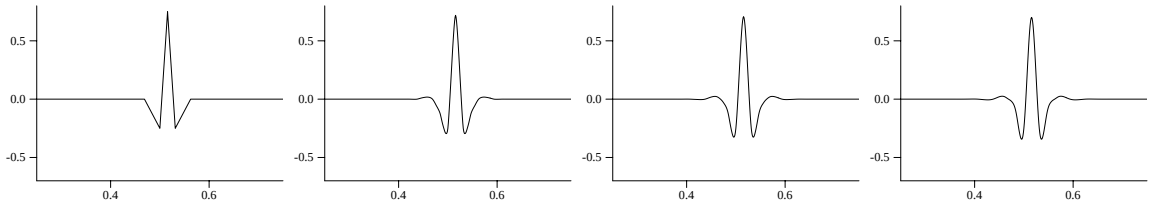

Figure III.11: Wavelets with two vanishing moments associated with interpolating subdivision. Going from left to right are the wavelets which correspond to dual wavelets of 2, 4, 6, and 8 vanishing moments.

we can find smoother and smoother approximations to the original samples. We will come back to this later.

Where are we now? We understand how to do subdivision with both the interpolating and average-interpolating scheme of order N (even and odd respectively). We have also seen the idea of the dual scaling functions, which are Dirac distributions (interpolating), and properly scaled box functions (average-interpolating). These give us the dual scaling function refinement relations. Given these relations we also understand how to go to coarser approximations from a finer approximation. This is the moment when wavelets will finally enter the scene.

6 Second Generation Wavelets

So far the discussion was only concerned with subdivision schemes and how they can be used to build scaling functions. In this section we introduce wavelets. Typically wavelets form a basis for the difference of two consecutive approximations. In the next section we will show how they can be constructed with the *lifting scheme*, a general technique to build biorthogonal wavelets and scaling functions.

6.1 Introducing Wavelets

To hone our intuition some more we begin with wavelets in the classical, i.e., translation and dilation, setting, and consider the interpolating case with linear ("hat") scaling functions.

Assume we are given regular point samples of a function $\{\lambda_{n,k} \mid k\}$ where $\lambda_{n,k} = f(k\,2^{-n})$. By using the linear interpolating scheme ($N = 2$), we can build a piecewise linear approximation to $f(x)$ as seen in Section 2. Let $\varphi(x)$ be the linear Hat function, see Figure III.3. The piecewise linear approximation to $f(x)$ is then

$$P_n f(x) = \sum_{k=0}^{2^n} \lambda_{n,k}\, \varphi(2^n x - k).$$

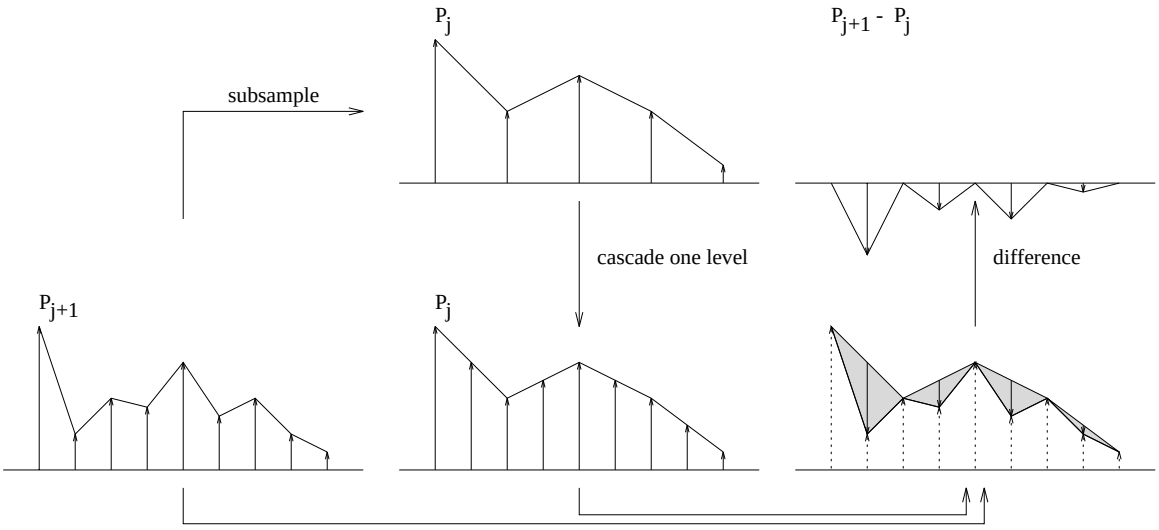

Figure III.12: On the left we begin with the piecewise linear approximation at level $j+1$. After subsampling we arrive at the piecewise linear approximation at level j. Cascading the latter out again to $j+1$ we can take the difference with the original to quantify the detail lost (right side). This detail can itself be written as a linear combination of hat functions at odd indices. These are actually the wavelets.

By definition $P_n f(x)$ interpolates $f(x)$ in points of the form $x = k\,2^{-n}$.

Let us build coarser approximations. Since the dual scaling function is a Dirac distribution ($\tilde{h}_{j,k,l} = \delta_{l-2k}$) this is done by leaving out every other sample, i.e., subsampling the even samples and constructing a new sequence $\lambda_{n-1,k}$ with $0 \leqslant k \leqslant 2^{n-1}$ and $\lambda_{n-1,k} = \lambda_{n,2k}$ (see the discussion in the previous section). By connecting the subsampled sequence again with piecewise linears, we obtain an approximation which interpolates $f(x)$ in points $x = k\,2^{n-1}$ (see Figure III.9). Obviously, we can keep doing this. The coarser approximations can be written as $(j < n)$,

$$P_j\, f(x) \;=\; \sum_{k=0}^{2^j} \lambda_{j,k}\, \varphi(2^j x - k) \;=\; \sum_{k=0}^{2^j} \lambda_{j,k}\, \varphi_{j,k},$$

where $\varphi_{j,k} = \varphi(2^j x - k)$. The function $P_j\, f$ can be constructed trivially since the only operations involved are subsampling and piecewise linear interpolation.

As the approximations become coarser (j becomes smaller) more and more information is lost. We can ask ourselves: is there any way to capture this information? In other words, is there any way to express the difference between two successive approximations P_j and P_{j+1}? This is precisely where wavelets will enter the stage.

Let the coefficients $\gamma_{j,m}$ represent the degrees of freedom of the difference between P_j and P_{j+1} and refer to them as *wavelet coefficients*. Since P_j uses the even subsamples from P_{j+1}, the information lost is essentially contained in the odd samples. The wavelet coefficients can be found as follows. Start from P_{j+1} and subsample to find P_j. By the definition of subsampling and of the scaling function coefficients we know that $\lambda_{j+1,2k} = P_{j+1}\, f(x_{j+1,2k}) = P_j\, f(x_{j,k}) = \lambda_{j,k}$. Now cascade $P_j\, f$ back out one level to find

$P_j f(x_{j+1,2m+1})$ and take the difference between $P_{j+1} f$ and $P_j f$ at $x_{j+1,2m+1}$

$$\gamma_{j,m} \;=\; (P_{j+1} f - P_j f)(x_{j+1,2m+1}) \;=\; \lambda_{j+1,2m+1} - 1/2\,(\lambda_{j,m} + \lambda_{j,m+1}).$$

The wavelet coefficient is thus the difference between $\lambda_{j+1,2m+1}$ and the average of its two neighbors $\lambda_{j,m}$ and $\lambda_{j,m+1}$. In other words, it encodes the amount by which the signal locally *fails to be linear*, see Figure III.12. This is reflected in the computation of the wavelet coefficients from the scaling function coefficients: average two neighboring scaling function coefficients—one step in the subdivision, or the linear "guess"—and subtract from the actual sample value.

The difference between two linear approximation now can be written as

$$P_{j+1} f(x) - P_j f(x) \;=\; \sum_{m=0}^{2^j-1} \gamma_{j,m}\, \varphi_{j+1,2m+1}.$$

Iterating this we find the wavelet series of the original sequence as

$$P_n f(x) \;=\; P_0 f(x) + \sum_{j=0}^{n-1} \sum_{m=0}^{2^j-1} \gamma_{j,m}\, \psi_{j,m}(x), \tag{3}$$

where $\psi_{j,m}(x) = \psi(2^j x - m)$ and $\psi(x) = \varphi(2x-1)$. This wavelet built from interpolating scaling functions was first introduced in [63].

6.2 Formal Description*

In this section, we give the formal definition of wavelets. We immediately do this in the second generation setting, i.e., on an interval, with a weight function and possibly irregular samples.

Since wavelets provide a basis in which to represent the difference between two successive approximations $P_{j+1} f - P_j f$ we define the closed subspaces W_j ($j > 0$) so that

$$V_{j+1} \;=\; V_j \oplus W_j. \tag{4}$$

The difference in dimension between V_{j+1} and V_j is always 2^j, thus the basis of W_j should consist of 2^j wavelets. We denote them as $\psi_{j,m}$ where $0 \leqslant m < 2^j$. Since $W_j \subset V_{j+1}$, a wavelet $\psi_{j,m}$ can be written as a linear combination of scaling functions $\varphi_{j+1,l}$. This leads to the refinement relation

$$\psi_{j,m} \;=\; \sum_l g_{j,m,l}\, \varphi_{j+1,l}. \tag{5}$$

Since

$$V_n \;=\; V_0 \oplus \bigoplus_{j=0}^{n-1} W_j,$$

we can write $P_n f$ as

$$P_n f \;=\; P_0 f + \sum_{j=0}^{n-1} \sum_{m=0}^{2^j-1} \gamma_{j,m}\, \psi_{j,m},$$

and by passing to the limit the wavelet expansion of a function f can be written as

$$f \;=\; P_0\, f + \sum_{j=0}^{\infty} \sum_{m=0}^{2^j-1} \gamma_{j,m}\, \psi_{j,m}. \tag{6}$$

The choice of W_j as a complementary space is not arbitrary, but in fact is determined by the dual scaling functions. Indeed if the wavelets represent the difference $P_{j+1} - P_j$ they depend on how the coarser approximation P_j was calculated from the finer P_{j+1}, which is precisely determined by the dual scaling functions (see Section 5). Since $P_j\, V_{j+1} = V_j$, it follows from (4) that $P_j\, W_j = \{0\}$. In other words, the dual scaling functions and wavelets are orthogonal, or

$$\langle\, \psi_{j,m}, \tilde{\varphi}_{j,k}\, \rangle \;=\; 0.$$

Next question is: how do we find the wavelet coefficients in the expansion (6)? Theoretically these again are defined as inner products with *dual wavelets*,

$$\gamma_{j,m} \;=\; \langle\, f, \tilde{\psi}_{j,m}\, \rangle\,,$$

which requires us to understand the dual wavelets. If the order of the multiresolution analysis is N, and the scaling functions reproduce polynomials up to degree $N-1$, the dual wavelets have N *vanishing moments* since they are required to be orthogonal to the primal scaling functions, which reproduce polynomials of degree $< N$. Similarly the primal wavelet will have $\tilde{N}$ vanishing moments. We saw earlier that that is the same as observing that the projectors P_j preserved $\tilde{N}$ moments. Indeed, if the difference between two projections is encoded by the wavelets and the projectors preserve some number of moments then the wavelets must have exactly that many *vanishing* moments.

7 The Lifting Scheme

So far, we have seen an example of wavelets and have given the definition. In this section we introduce the *lifting scheme*[179, 181] a general technique for constructing biorthogonal second generation wavelets. In fact it is so general, that even the subdivision schemes we studied earlier can be seen as a special case of it.

The wavelets we constructed in the example in the Section 6.1 are not very powerful, and we start out by giving an example which shows how to improve their properties with the help of the lifting scheme.

7.1 Lifting and Interpolation: An Example

The problem with the wavelets of the previous section lies in the fact that the coarser approximations are simply constructed by subsampling the finer approximations. This leads to horrible aliasing effects. Imagine coefficients of $1, 0, 1, 0, \ldots, 1$ at level $j+1$. These would result in the sequence $1, 1, 1, \ldots, 1$ at level j. Or think of what would happen if the original signal were noisy. What we would like is some smoothing before we subsample the signal. Said another way, we want to preserve average properties of the approximation when going from level $j+1$ to level j. Preserving literally the average simply means that the integrals of

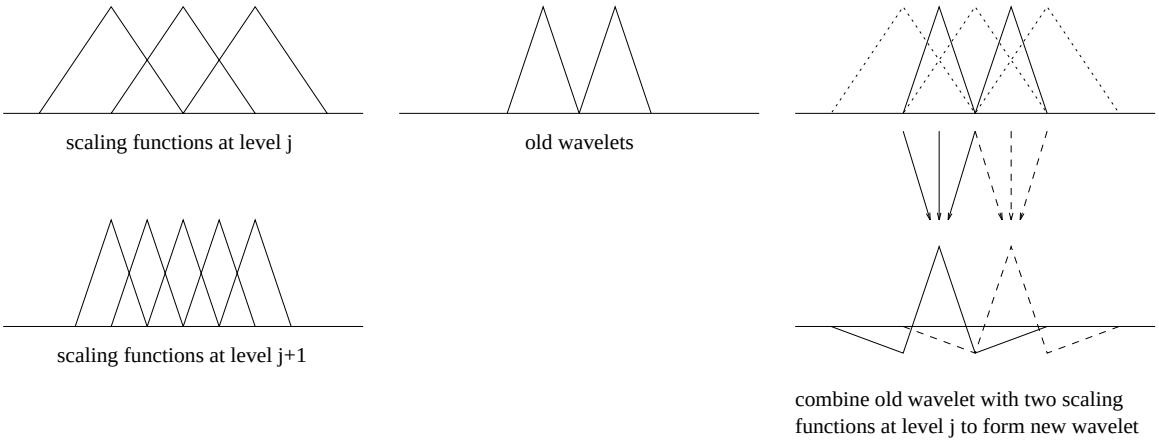

Figure III.13: On the left are some of the hat scaling functions when using pure subsampling. In the middle some of the associated wavelet basis functions, which are simply the odd numbered scaling functions from level $j+1$. Their properties can be improved by lifting. On the right we build a new wavelet from the old one by adding a properly chosen multiple of two neighboring scaling functions from level j to them. The resulting wavelets (two neighboring ones are shown in the lower right) have a vanishing integral.

$P_{j+1}\, f$ and $P_j\, f$ have to be equal, or

$$\int_0^1 P_{j+1}\, f(x)\, dx \;=\; \int_0^1 P_j\, f(x)\, dx\,.$$

Recall that this corresponds to $\tilde{N} = 1$. Conversely, since the wavelets are defined as the difference between two successive levels, they should have a vanishing integral, i.e., $\tilde{N}$ should be at least 1. Consequently we cannot simply omit the odd samples in the coarser approximation, but they must somehow contribute as well.

This can be achieved by first constructing a new wavelet whose integral vanishes. The wavelet we have so far does not have this property, as $\int \psi_{j,m} = \int \varphi_{j+1,2k+1} = 2^{-j-1}$. The basic idea of the lifting scheme is to take an old wavelet and build a new, more performant one by adding in scaling functions of *the same* level, as opposed to writing a wavelet as a linear combination of scaling functions on the *finer* level as in (5). We thus propose a new wavelet of the following form, see Figure III.13,

$$\psi(x) \;=\; \varphi(2x-1) - 1/4\,\varphi(x) - 1/4\,\varphi(x-1).$$

The coefficients are chosen such that the wavelet is symmetric and has a vanishing integral.

As we mentioned before, the wavelet and dual scaling function are orthogonal. If we change the wavelet, also the dual scaling function and thus the computation of coarser approximations must change. We want to formally keep the expansion (3), but with this new definition of ψ and thus a different meaning of P_j. To find the new coarse level coefficients $\lambda_{j,k}$ consider the following equation

$$\sum_{l=0}^{2^{j+1}} \lambda_{j+1,l}\, \varphi_{j+1,l} \;=\; \sum_{k=0}^{2^j} \lambda_{j,k}\, \varphi_{j,k} + \sum_{m=0}^{2^j-1} \gamma_{j,m}\, \psi_{j,m}.$$

By filling in the definition of the new wavelet and evaluating left and right hand side at $x = k\, 2^{-j}$ we find

that

$$\lambda_{j,k} \;=\; \lambda_{j+1,2k} + 1/4\,\gamma_{j,k} + 1/4\,\gamma_{j,k-1}.$$

This corresponds to the definition of the new wavelet. Since the new wavelet is constructed from the old wavelet by adding contributions from neighboring scaling functions of $-1/4$ the properly adjusted scaling function coefficients get contributions of $+1/4$ from neighboring old wavelets.

A coarser approximation is now found as follows: first calculate the $\gamma_{j,m}$ as the failure to be linear, then use these wavelet coefficients to find the coarser $\lambda_{j,k}$. By applying this procedure recursively, we find all $\gamma_{j,m}$ values. This is precisely the *fast wavelet transform*. We are assured that the integral of the approximations is preserved, since the integrals of all the wavelets in the sum do not make any contribution. Alternatively we can interpret this as some amount of smoothing before the subsampling.

Notes:

1. Because of symmetry not only the integral of the wavelet is zero, but also its first moment,

$$\int x\;\psi(x)\,dx = 0.$$

   Thus also the first moment of the approximations is preserved. In fact, as pointed out in [181] the wavelet we just constructed is precisely the $(2,2)$ biorthogonal wavelet of Cohen-Daubechies-Feauveau [33]. If so needed, one can use more neighboring scaling functions in the lifting of the wavelets to assure preservation of higher moments.

2. One advantage of the lifting scheme is that one never has to explicitly form the filters needed to smooth the $\lambda_{j+1,l}$ values before subsampling. Consequently, the wavelet transform can be computed much faster and the whole computation can be done in place. The true power of the lifting scheme, however, lies in the fact that the same construction can also be used in the case of second generation wavelets. We will come back to this in a later section.

3. Actually the easiest choice for the coefficients would have been $\lambda_{j,k} = \lambda_{j+1,2k}$ and $\gamma_{j,m} = \lambda_{j+1,2m+1}$. This choice is called the Lazy wavelet transform [181]. The name Lazy comes from the fact that this transform doesn't really do anything but subsampling the odd samples. We only mention here that any interpolating subdivision scheme can be seen as the result of applying dual lifting to the Lazy wavelet.

4. Another example of the power of lifting is that the inverse transform can be derived immediately. We simply replace all additions (resp. subtractions) in the forward transform by subtractions (resp. additions).

7.2 Lifting: Formal Description*

The subdivision schemes mentioned above yield a set of biorthogonal scaling functions. In a classical (translation and dilation) setting, the wavelets can then easily be found through the connection with quadrature mirror filters. Typically one chooses $g_k = (-1)^k\,h_{1-k}$. In the second generation case, wavelets can not be found this easily. The lifting scheme provides an answer to this question.

The basic idea, which inspired the name, is to start from a simple or trivial multiresolution analysis and build a new, more performant one. This is done by leaving the scaling function untouched. A new wavelet $\psi_{j,m}$ is built by taking the old wavelet $\psi^{\mathcal{O}}_{j,m}$ and adding on linear combinations of scaling functions on the *same* level (and not a *finer* level as in the refinement relation). This results in

$$\psi_{j,m} \;=\; \psi^{\mathcal{O}}_{j,m} - \sum_k s_{j,k,m}\, \varphi_{j,k}.$$

As we already mentioned changing the wavelet affects the dual scaling function. The new dual scaling function is given by

$$\tilde{\varphi}_{j,k} \;=\; \sum_l \tilde{h}^{\mathcal{O}}_{j,k,l}\, \tilde{\varphi}_{j+1,l} + \sum_m s_{j,k,m}\, \tilde{\psi}_{j,m},$$

where $\tilde{h}^{\mathcal{O}}_{j,k,l}$ are the coefficients of the refinement relation of the dual scaling function before lifting. The primal scaling function remains the same after lifting. The dual wavelet changes, but it still obeys its old refinement relation, but now with respect to a new dual scaling function.

A variant of the lifting scheme exists, the *dual lifting scheme*, in which one leaves the dual scaling function untouched, but builds a new dual wavelet and thus a new primal scaling function. The new dual wavelet is given by

$$\tilde{\psi}_{j,m} \;=\; \tilde{\psi}^{\mathcal{O}}_{j,m} - \sum_m \tilde{s}_{j,k,m}\, \tilde{\varphi}_{j,k}.$$

7.3 Lifting and Interpolation: Formal description

In this section we discuss how to use the lifting scheme to construct wavelets in the interpolating case. Let us start out by making the following observation concerning the filters of an interpolating scaling function $\varphi_{j,k}$. By filling in the refinement relation we see that

$$\delta_{k,k'} \;=\; \varphi_{j,k}(x_{j,k'}) \;=\; \sum_l h_{j,k,l}\, \varphi_{j+1,l}\,(x_{j+1,2k'}) \;=\; h_{j,k,2k'}.$$

This implies that we can write the refinement relation as

$$\varphi_{j,k} \;=\; \varphi_{j+1,2k} + \sum_m h_{j,k,2m+1}\, \varphi_{j+1,2m+1}.$$

Next, just as in the classical case, we start with an approximation $P_{j+1}\, f$ and try to build a coarser one $P_j\, f$. First we perform simple subsampling, $\lambda_{j,k} \;=\; \lambda_{j+1,2k}$, which is followed by one step of subdivision of P_j

$$P_j\, f \;=\; \sum_k \lambda_{j,k}\, \varphi_{j,k} \;=\; \sum_k \lambda_{j+1,2k}\, \varphi_{j+1,2k} + \sum_k \sum_m \lambda_{j,k}\, h_{j,k,2m+1}\, \varphi_{j+1,2m+1},$$

using the refinement relation. This expression implies that the difference $P_{j+1} - P_j$ consists only of functions of the form $\varphi_{j+1,2m+1}$. Thus the wavelets are given by

$$\psi_{j,m} \;=\; \varphi_{j+1,2m+1}.$$

The wavelet coefficients can be found by simply identifying components,

$$\gamma_{j,m} \;=\; \lambda_{j+1,2m} - \sum_k h_{j,k,2m+1}\,\lambda_{j,k}.$$

It is not hard to understand that these wavelets form a space complementing V_j in V_{j+1}. They essentially "capture" the odd samples of V_{j+1}, while V_j captures the even samples. To see that the $\psi_{j,m}$ are orthogonal to the $\tilde{\varphi}_{j,k}(x) = \delta(x - x_{j,k})$ is equally easy. It follows from the interpolation properties since $\varphi_{j+1,2m+1}(x_{j,k}) = 0$.

As we mentioned before, this multiresolution analysis suffers from the fact that the integral of the approximations is not preserved which can lead to aliasing. In other words the primal wavelet does not have even one vanishing moment ($\tilde{N} = 0$). Indeed, it is simply a scaling function which has a non zero integral. However a necessary (but not sufficient) condition for the wavelets to form a stable basis, is that $\tilde{N}$ is at least one. The lifting scheme proposes a new wavelet of the form

$$\psi_{j,m} \;=\; \varphi_{j+1,2m+1} - A_{j,m}\,\varphi_{j,m} - B_{j,m}\,\varphi_{j,m+1}.$$

In other words, the new wavelet will be composed of the old wavelet, which itself is just a scaling function, and its immediate scaling function neighbors at level j (see the example in Figure III.13). Here we choose the constants $A_{j,m}$ and $B_{j,m}$ such that

$$\int_0^1 w(x)\,\psi_{j,m}(x)\,dx \;=\; 0 \text{ and } \int_0^1 w(x)\,x\,\psi_{j,m}(x)\,dx \;=\; 0.$$

To find the new $\lambda_{j,k}$ consider the following equation

$$\sum_{l=0}^{2^{j+1}} \lambda_{j+1,l}\,\varphi_{j+1,l} \;=\; \sum_{k=0}^{2^j} \lambda_{j,k}\,\varphi_{j,k} + \sum_{m=0}^{2^j-1} \gamma_{j,m}\,\psi_{j,m}.$$

By filling in the definition of the new, lifted wavelet and evaluating left and right hand side at $x_{j,k}$ we find that

$$\lambda_{j,k} \;=\; \lambda_{j+1,2k} + A_{j,k}\,\gamma_{j,k} + B_{j,k-1}\,\gamma_{j,k-1}.$$

Note: As in the regular case, an interpolating subdivision scheme can be seen as a result of the dual lifting scheme applied to the so-called Lazy wavelet [179].

7.4 Wavelets and Average-Interpolation: An Example

In this section we give an example that shows how the lifting scheme can be used to construct wavelets in the average-interpolation case. Let us first consider the simplest case of average-interpolation, namely piecewise constant approximation ($N = 1$) in the classical translation and dilation case.

We can now write an approximation on level j as

$$P_j\,f(x) \;=\; \sum_{k=0}^{2^j-1} \lambda_{j,k}\,\varphi_{j,k}(x),$$

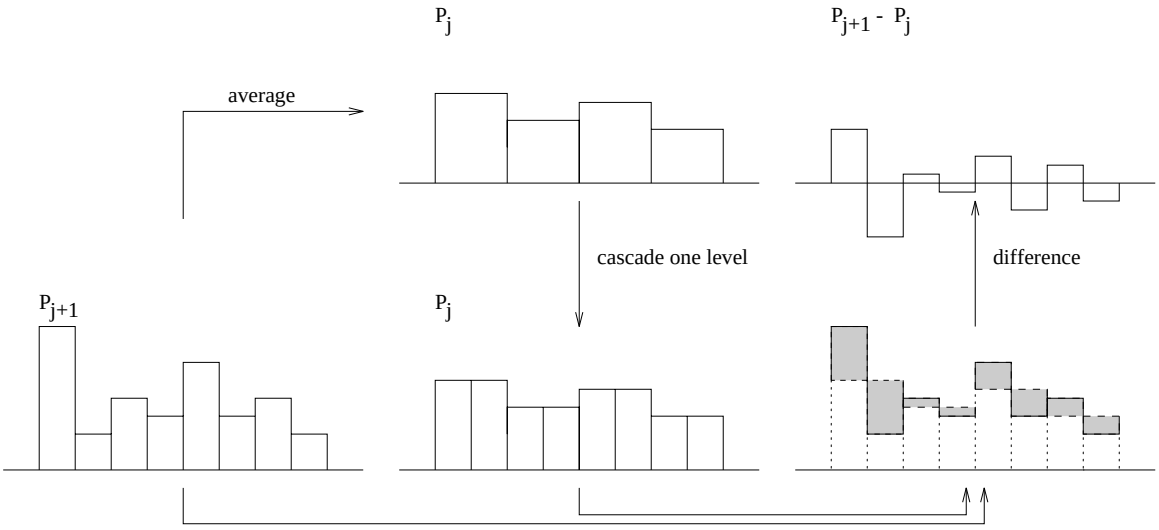

Figure III.14: On the left we begin with the piecewise constant approximation at level $j+1$. After averaging we arrive at the piecewise constant approximation at level j. Cascading the latter out again to $j+1$ we can take the difference with the original to quantify the detail lost (right side). This detail can be written as a linear combination of Haar wavelets.

where $\varphi_{j,k} = \varphi(2^j x - k)$ and $\varphi(x) = \chi_{[0,1)}$, the function which is 1 on $[0,1)$ and zero elsewhere. The dual functions are given by $\tilde{\varphi}_{j,k} = 2^j \varphi(2^j x - k)$ (see Section 5). This implies (see Equation 2) that a coarser approximation is found by

$$\lambda_{j,k} \;=\; 1/2\,(\lambda_{j+1,2k} + \lambda_{j+1,2k+1}). \tag{7}$$

Let us next try to find the wavelet. We use the same idea as in the previous section and simply calculate $P_{j+1} - P_j$, see Figure III.14. Taking

$$\lambda_{j+1,2k}\,\varphi_{j+1,2k} + \lambda_{j+1,2k+1}\,\varphi_{j+1,2k+1} \;=\; \lambda_{j,k}\,\varphi_{j,k} + \gamma_{j,k}\,\psi_{j,k},$$

and filling in the refinement relation for $\varphi_{j,k} = \varphi_{j+1,2k} + \varphi_{j+1,2k+1}$ and (7) we find that

$$\begin{aligned}\gamma_{j,k}\,\psi_{j,k} &= 1/2\,(\lambda_{j+1,2k} - \lambda_{j+1,2k+1})\,\varphi_{j+1,2k} + 1/2\,(\lambda_{j+1,2k+1} - \lambda_{j+1,2k})\,\varphi_{j+1,2k+1} \\ &= 1/2\,(\lambda_{j+1,2k} - \lambda_{j+1,2k+1})\,(\varphi_{j+1,2k} - \varphi_{j+1,2k+1}).\end{aligned}$$

Comparing both sides we see that the wavelet coefficients are calculated as

$$\gamma_{j,k} \;=\; 1/2\,(\lambda_{j+1,2k} - \lambda_{j+1,2k+1}),$$

and that $\psi_{j,k} = \psi(2^j x - k)$ with

$$\psi(x) \;=\; \chi_{[0,1/2)} - \chi_{[1/2,2)} \;=\; \varphi(2x) - \varphi(2x-1).$$

This is the famous Haar wavelet. The formulas for inverse transform in this case are

$$\begin{aligned}\lambda_{j+1,2k} &= \lambda_{j,k} + \gamma_{j,k} \\ \lambda_{j+1,2k+1} &= \lambda_{j,k} - \gamma_{j,k}.\end{aligned}$$

Note that the pure subdivision scheme with $N = 1$ is simply the inverse wavelet transform with all wavelet coefficients equal to zero.

Let us next discuss a higher order example ($N = 3$). We would like to build scaling functions that can reproduce polynomials up to degree 2. Instead of building such scaling functions directly, the lifting scheme first constructs a new dual wavelet which has 3 vanishing moments. This should be equivalent (see our earlier remarks).

Again the dual wavelet is the sum of an old dual wavelet (the Haar) and dual scaling functions on the same level. Let $\tilde{\varphi} = \chi_{[0,1)}$ then

$$\tilde{\psi}(x) \;=\; \overbrace{\tilde{\varphi}(2x) - \tilde{\varphi}(2x-1)}^{\text{old dual wavelet}} - A\,\tilde{\varphi}(x+1) - B\,\tilde{\varphi}(x) - C\,\tilde{\varphi}(x-1).$$

It is easy to see that for the dual wavelet to have 3 vanishing moments, we need to choose $A = 1/8$, $B = 0$, and $C = -1/8$. Thus

$$\tilde{\psi}_{j,m} \;=\; \tilde{\varphi}_{j+1,2m} - \tilde{\varphi}_{j+1,2m+1} - 1/8\,\tilde{\varphi}_{j,m-1} + 1/8\,\tilde{\varphi}_{j,m+1}.$$

Given the fact that the dual lifting scheme does not change the dual scaling function, the coarser $\lambda_{j,k}$ coefficients are still given by

$$\lambda_{j,k} \;=\; 1/2\,(\lambda_{j+1,2k} + \lambda_{j+1,2k+1}).$$

The wavelet coefficients are now found by first calculating the Haar coefficients

$$\gamma_{j,k} \;=\; 1/2\,(\lambda_{j+1,2k} - \lambda_{j+1,2k+1}),$$

and then using the scaling function coefficients on the *same* level to find the new wavelet coefficients

$$\gamma_{j,m} \mathrel{+}= -1/8\,\lambda_{j,m-1} + 1/8\,\lambda_{j,m+1}.$$

The calculation of a coarser level now involves ***first*** the calculation of the $\lambda_{j,k}$ values and ***secondly*** the update of the $\gamma_{j,m}$ using the $\lambda_{j,k}$. The inverse transform first undoes the update of the wavelet coefficients and then does an inverse Haar step.

Now what happened to the primal wavelet and scaling function? The lifting scheme says that the coefficients of the primal wavelet in the refinement relation do not change, thus

$$\psi(x) = \varphi(2x) - \varphi(2x-1).$$

The new scaling function is given by

$$\varphi(x) = \varphi(2x) + \varphi(2x-1) - 1/8\,\psi(x+1) + 1/8\,\psi(x-1).$$

By filling in the refinement relation of the wavelet, we realize that this is exactly the same scaling function as generated with the average-interpolation scheme with $N = 3$. Indeed the filter coefficients are $\{-1/8, 1/8, 1, 1, 1/8, -1/8\}$.

7.5 Wavelets and Average-Interpolation: Formal description*

Let us again start with the simplest example, namely if $N = 1$. We already saw that

$$\varphi_{j,k} = \chi_{I_{j,k}} \text{ and } \tilde{\varphi}_{j,k} = \chi_{I_{j,k}}/|I_{j,k}|$$

How do we find the wavelets? They are piecewise constant functions with a vanishing integral. The dual wavelets are

$$\tilde{\psi}_{j,m} = \tilde{\varphi}_{j+1,2m} - \tilde{\varphi}_{j+1,2m+1}.$$

The fact that they have a zero integral follows immediately from the fact that the dual scaling functions are normalized to have integral 1. The primal wavelets are given by

$$\psi_{j,m} = |I_{j+1,2m+1}|/|I_{j,m}|\,\varphi_{j+1,2m} - |I_{j+1,2m}|/|I_{j,m}|\,\varphi_{j+1,2m+1},$$

and again have one vanishing moment. These wavelets are called the generalized biorthogonal Haar wavelets.

Now how does this connect with the average-interpolation scheme? Again we use the dual lifting scheme to start from the biorthogonal Haar multiresolution analysis and build a dual wavelet with N vanishing moments and thus a scaling function which can reproduce N polynomials. Take $N = 3$. We build a new dual wavelet of the form

$$\tilde{\psi}_{j,m} = \tilde{\varphi}_{j+1,2m} - \tilde{\varphi}_{j+1,2m+1} - A_{j,m}\,\tilde{\varphi}_{j,m-1} - B_{j,m}\,\tilde{\varphi}_{j,m} - C_{j,m}\,\tilde{\varphi}_{j,m+1}.$$

Here the coefficient $A_{j,m}$, $B_{j,m}$ and $C_{j,m}$ are chosen such that $\tilde{\psi}_{j,m}$ has 3 vanishing moments. The dual scaling function is still a box function. The new scaling function after lifting satisfies a refinement relation of the form

$$\varphi_{j,k} = \varphi_{j+1,2k} + \varphi_{j+1,2k+1} + C_{j,m-1}\,\psi_{j,m-1} + B_{j,m}\,\psi_{j,m} + A_{j,m+1}\,\psi_{j,m+1}.$$

The new wavelet after lifting is given by

$$\psi_{j,m} = |I_{j+1,2m+1}|/|I_{j,m}|\,\varphi_{j+1,2m} - |I_{j+1,2m}|/|I_{j,m}|\,\varphi_{j+1,2m+1}.$$

Figure III.15 show the wavelets affected by the boundary in both the interpolating and average-interpolation case. In the average-interpolation case $N = 3$ and the wavelets have $\tilde{N} = 1$. In the interpolating case $N = 4$ and the wavelets, built with lifting, have $\tilde{N} = 2$ vanishing moments.

In the next section we will describe how to build the fast wavelet transform.

8 Fast wavelet transform

In this section we describe the implementation of the fast wavelet transform with the use of the lifting scheme. The fast wavelet transform is a linear algorithm to, given the $\lambda_{n,k}$ coefficients, calculate the $\gamma_{j,m}$ wavelet coefficients with $0 \leqslant j < n$ and the coarsest level coefficients $\lambda_{0,k}$. The inverse transform does the opposite. The transform works level wise and on each level splits coefficients $\{\lambda_{j+1,l} \mid l\}$ into $\{\lambda_{j,k} \mid k\}$ and $\{\gamma_{j,m} \mid m\}$. The inverse transform does the opposite. The overall structure is given by the following

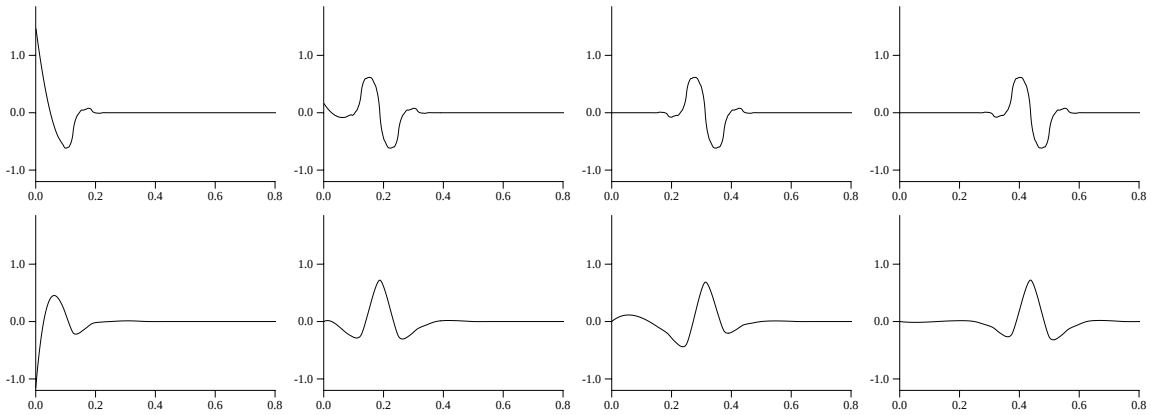

Figure III.15: Examples of wavelets affected by a boundary. On the top wavelets with $\tilde{N} = 1$ vanishing moment and $N = 3$ at $j = 3$ and $k = 0, 1, 2, 3$. On the bottom the wavelets with $\tilde{N} = 2$ vanishing moments and $N = 4$ at $j = 3$ and $k = 0, 1, 2, 3$.

algorithm

Forward wavelet transform

```
For j = n-1 downto 0
    Forward(j)
```

Inverse wavelet transform

```
For level = 0 to n-1
    Inverse(j)
```

One of the nice features of the lifting scheme is that once we write down the forward transform, the inverse transform can simply be found by reversing the steps and undoing what the forward transform did in each step. In the interpolation case, we first subsample the scaling function coefficients, then calculate the wavelet coefficients $\gamma_{j,m}$, and finally of use the wavelet coefficients to update the scaling function coefficients $\lambda_{j,k}$. The algorithms for forward and inverse transform are given by

```
Forward(j):
```

For $0 \leqslant k \leqslant 2^j$: $\lambda_{j,k} := \lambda_{j+1,2k}$

For $0 \leqslant m < 2^j$: $\gamma_{j,m} := \lambda_{j+1,2m+1} - \sum_k h_{j,k,2m+1}\, \lambda_{j,k}$

For $0 \leqslant k \leqslant 2^j$: $\lambda_{j,k} \mathrel{+}= A_{j,k}\, \gamma_{j,k} + B_{j,k-1}\, \gamma_{j,k-1}$

```
Inverse(j):
```

For $0 \leqslant k \leqslant 2^j$: $\lambda_{j,k} \mathrel{-}= A_{j,k}\, \gamma_{j,k} + B_{j,k-1}\, \gamma_{j,k-1}$

For $0 \leqslant m < 2^j$: $\lambda_{j+1,2m+1} := \gamma_{j,m} + \sum_k h_{j,2m+1,k}\, \lambda_{j,k}$

For $0 \leqslant k \leqslant 2^j$: $\lambda_{j+1,2k} := \lambda_{j,k}$

In the average-interpolation case we first calculate one step in the generalized Haar transform, and then update the $\gamma_{j,m}$ coefficients with the help of the $\lambda_{j,k}$ coefficients. We give the algorithms for $N = 3$. Higher N are done similarly.

```
Forward(j):
For 0 ⩽ k < 2^j :

  λ_{j,k}  :=  (|I_{j+1,2k}| λ_{j+1,2k} + |I_{j+1,2k+1}| λ_{j+1,2k+1})/|I_{j,k}|
  γ_{j,k}  :=  λ_{j+1,2k} − λ_{j+1,2k+1}

For 0 ⩽ m < 2^j :

      γ_{j,m} −= A_{j,m} λ_{j,m−1} + B_{j,m} λ_{j,m} + C_{j,m} λ_{j,m+1}
```

```
Inverse(j):
For 0 ⩽ m < 2^j :

      γ_{j,m} += A_{j,m} λ_{j,m−1} + B_{j,m} λ_{j,m} + C_{j,m} λ_{j,m+1}

For 0 ⩽ k < 2^j :

          λ_{j+1,2k}   :=  λ_{j,k} + |I_{j+1,2k+1}|/|I_{j,k}| γ_{j,k}
          λ_{j+1,2k+1} :=  λ_{j,k} − |I_{J+1,2k}|/|I_{j,k}| γ_{j,k}
```

Note how the A, B, C relate back to the average-interpolation subdivision scheme. Simply substitute $\gamma_{j,m}$ into the right hand side of the $\lambda_{j+1,2k}$ and $\lambda_{j+1,2k+1}$ computation. For $N > 3$ the same reasoning can be applied to make this connection.

9 Examples

In this section we describe results of some experiments involving the ideas presented earlier. The examples were generated with a simple C code whose implementation is a direct transliteration of the algorithms described above. The only essential piece of code imported was an implementation of Neville's algorithm from Numerical Recipes [156]. All examples were computed on the unit interval, that is all constructions are adapted to the boundary as described earlier. The only code modification to accommodate this is to insure that the moving window of coefficients does not cross the left or right end point of the interval. The case of a weight function required somewhat more machinery which we describe in that section.

9.1 Interpolation of Randomly Sampled Data

The first and simplest generalization concerns the use of $x_{j_0,k}$ placed at random locations. Figure III.16 shows the scaling functions (left) and wavelets (right) which result for such a set of random locations. The scaling functions are of order $N = 4$ (interpolating subdivision) and the wavelets have $\tilde{N} = 2$ vanishing moments (using lifting). In this case we placed 7 uniformly random samples between $x_{3,0} = 0$ and $x_{3,8} = 1$. These locations are discernible in the graph as the unique points at which all scaling functions have a root save for one which takes on the value 1. Sample points at finer levels were generated recursively by simply adding midpoints, i.e., $x_{j+1,2k+1} = 1/2\,(x_{j,k} + x_{j,k+1})$ for $j > 3$.

An interesting question is how the new sample points should be placed. A disadvantage of always adding midpoints is that imbalances between the lengths of the intervals are maintained. A way to avoid this is to

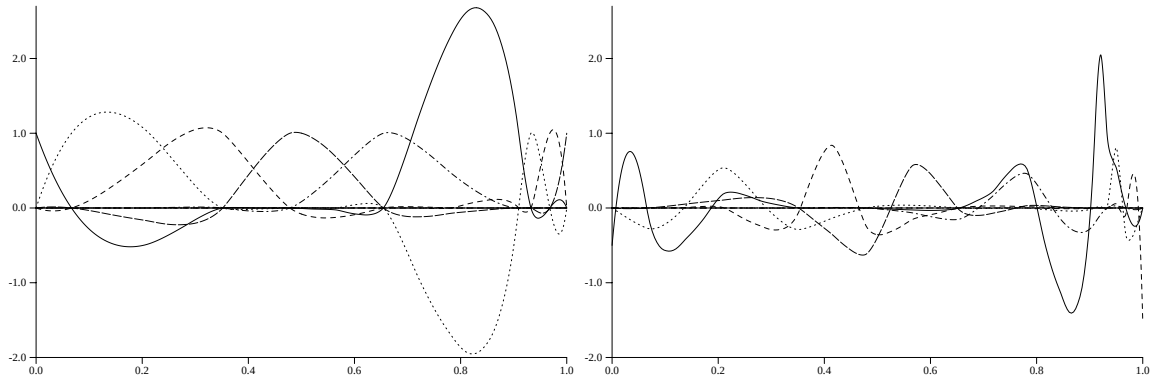

Figure III.16: Example of scaling functions (left) with $N = 4$ (interpolating subdivision) and wavelets (right) with $\tilde{N} = 2$ (lifting) adapted to irregular sample locations. The original sample locations $x_{3,k}$ can be discerned as the locations where all scaling functions but one are zero.

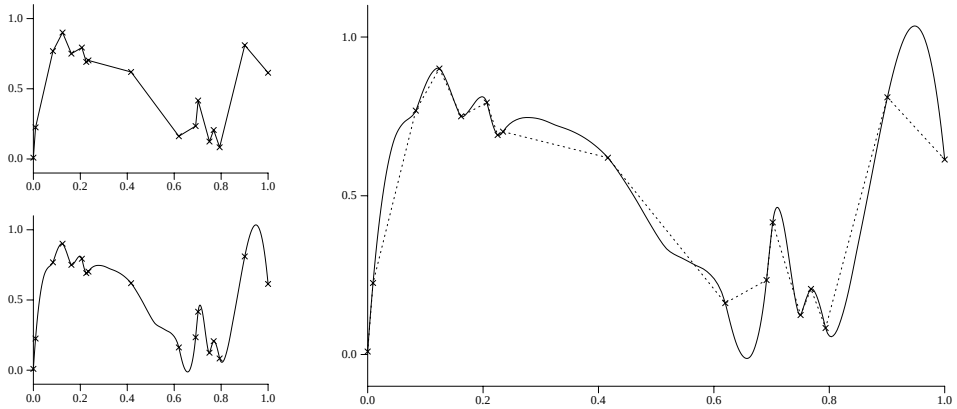

Figure III.17: Example of data defined at random locations $x_{4,k}$ on the unit interval and interpolated with interpolating subdivision of order $N = 2$ and 4 respectively.

place new sample points only in intervals whose length is larger than the average interval length. Doing so repeatedly will bring the ratio of largest to smallest interval length ever closer to 1.

Another possible approach would add new points such that the length of the intervals varies in a smooth manner, i.e., no large intervals neighbor small intervals. This can be done by applying an interpolating subdivision scheme, with integers as sample locations, to the $x_{j,k}$ themselves to find the $x_{j+1,2k+1}$. This would result in a smooth mapping from the integers to the $x_{j,k}$. After performing this step the usual interpolating subdivision would follow. Depending on the application one of these schemes may be preferable.

Next we took some random data over a random set of 16 sample locations and applied linear ($N = 2$) and cubic ($N = 4$) interpolating subdivision to them. The resulting interpolating functions are compared on the right side of Figure III.17. These functions can be thought of as a linear superposition of the kinds of scaling functions we constructed above for the example $j = 3$.

Note how sample points which are very close to each other can introduce sharp features in the resulting function. We also note that the interpolation of order 4 exhibits some of the overshoot behavior one would expect when encountering long and steep sections of the curve followed by a reversal of direction. This

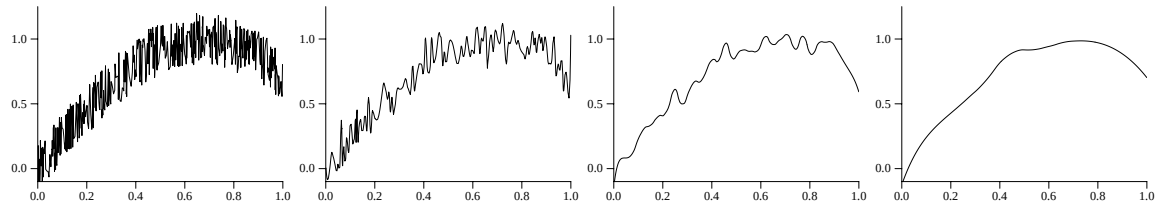

Figure III.18: A sine wave with additive noise sampled at uniformly distributed random locations in the unit interval and reconstructed with quintic average-interpolation and successive smoothings of the original data.

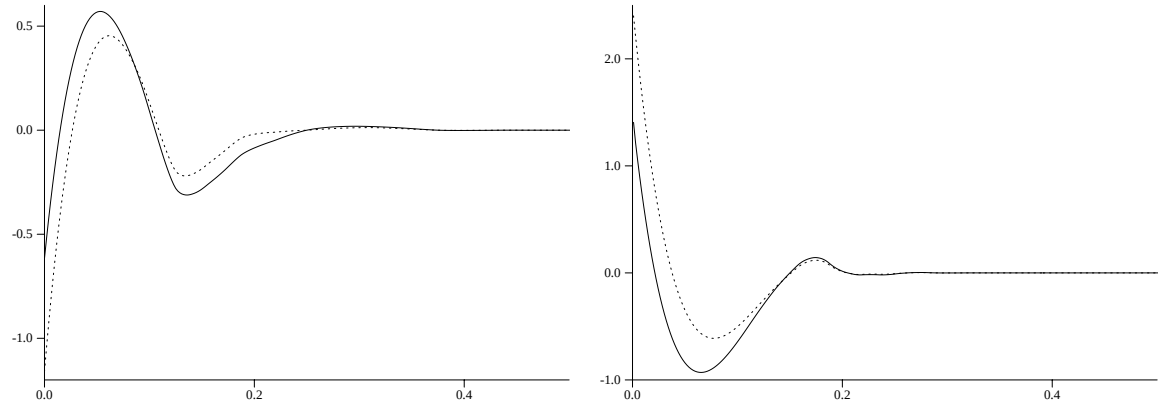

Figure III.19: Comparison of weighted (solid line) and unweighted (dotted line) wavelets at the left endpoint of the interval where the weight function $x^{-1/2}$ becomes singular. On the left 2 primal vanishing moments and 4 dual vanishing moments; on the right 1 primal vanishing moment and 5 dual vanishing moments. Note how the weighted wavelets take on smaller values at zero in order to adapt to the weight function whose value tends to infinity.

behavior gets worse for higher order interpolation schemes. These experiments suggest that it might be desirable to enforce some condition on the ratio of the largest to the smallest interval in a random sample construction.

9.2 Smoothing of Randomly Sampled Data

A typical use for wavelet constructions over irregular sample locations is smoothing of data acquired at such locations. As an example of this we took 512 uniformly random locations on the unit interval (V_9) and initialized them with averages of $\sin(3/4\pi x)$ with $\pm 20\%$ additive white noise. The resulting function is plotted on the left of Figure III.18 at level 9. The scaling functions used were based on average-interpolation with $N = 5$ and $\tilde{N} = 1$. Smoothing was performed by going to coarser spaces (lower index) and subdividing back out. This is the linear approximation algorithm described in Section 5.8 and is equivalent to setting wavelet coefficients below a certain level to zero. From left to right these were V_9, V_7, V_5, and V_3.

We hasten to point out that this is is a very simple and naive smoothing technique. Depending on the application and knowledge of the underlying processes much more powerful smoothing operators can be constructed [65, 66]. This example merely serves to suggest that such operations can also be performed over irregular samples.

9.3 Weighted Inner Products

When we discussed the construction of scaling functions and wavelets we pointed out how a weight function in the inner product can be incorporated to construct bases biorthogonal with respect to a weighted inner product. The only complication is that we cannot cast the average-interpolation problem into the form of a Neville interpolation problem anymore. Instead we first explicitly construct the polynomial p in the subdivision and use it to find the filter coefficients. This implies solving the underlying linear system which relates the coefficients of p to the observed weighted averages. We thus need to know the weighted moments of the dual (box) scaling functions. Similarly when lifting the interpolating wavelets to give them 2 vanishing moments the weighted moments of the primal scaling function enters. In both of these cases the construction of weighted bases requires additional code to compute moments and solve the linear systems involved in finding the filters. Moment calculations can be performed recursively from the finest level on up by using the refinement relationship for the scaling function (dual scaling function respectively) during the wavelet transform. Without going into much detail we point out that moment calculations and the solution of the linear system to find p can be numerically delicate. The stability essentially depends on which polynomial basis is used. For example, we found the linear systems that result when expressing everything with respect to global monomial moments so ill-conditioned as to be unsolvable even in double precision. The solution lies in using a local polynomial, i.e., a basis which changes for each interval. A better choice might be a basis of local orthogonal polynomials.

In our experiments we used the weight function $x^{-1/2}$ which is singular at the left interval boundary. For the moment computations local monomials were used, resulting in integrals for which analytic expressions are available.

Figure III.19 shows some of the resulting wavelets. In both cases we show the left most wavelet, which is most impacted by the weight function. Weighted and unweighted wavelets further to the right become ever more similar. Part of the reason why they look similar is the normalization. For example, both weighted and unweighted scaling functions have to satisfy $\sum_k \varphi_{j,k} = 1$. The images show wavelets with $N = 4$ (interpolating) and $\tilde{N} = 2$ vanishing moments (lifting) on the left and wavelets with $N = 5$ (average-interpolation) and $\tilde{N} = 1$ primal vanishing moment on the right. In both cases the weighted wavelet is shown with a solid line and the unweighted case with a dotted line.

The weighted and unweighted wavelets are only slightly different in shape. However, when applied to the expansion of some function they can make a dramatic difference. As an example we applied both types of wavelets to the function $f(x) = \sin(4\pi x^{1/2})$, which has a divergent derivative at zero. With unweighted wavelets the convergence will be slow close to the singularity, typically $O(h)$ with $h = 2^{-j}$ independent of N. In other words, there is no gain in using higher order wavelets. However, if we build weighted wavelets for which the weight function times f is an analytic function, we can expect $O(h^N)$ behavior everywhere again. For our example we can take $w(x) = x^{-1/2}$. This way the weighted wavelets are adapted to the singularity of the function f. Figure III.20 shows the error in the resulting expansions with $N = 1$, 3, 5, and 7 (average-interpolation) dual vanishing moments and $\tilde{N} = 1$ primal vanishing moment. For unweighted wavelets higher order constructions only get better by a constant factor, while the weighted wavelets show higher order convergence when going to higher order wavelets.

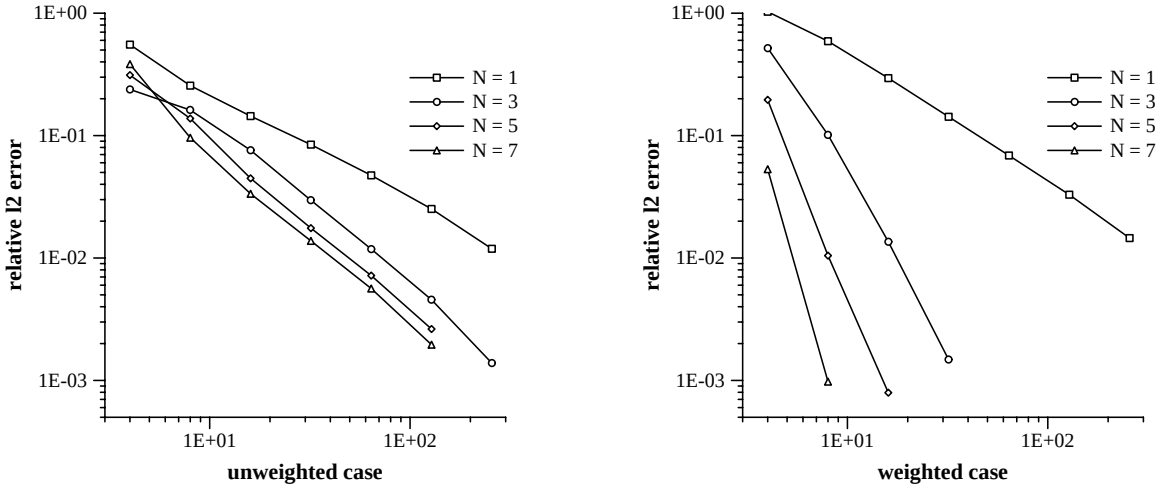

Figure III.20: Comparison of approximation error when expanding the function $\sin(4\pi x^{1/2})$ over $[0, 1/2]$ using wavelets biorthogonal with respect to an unweighted inner product (left) and a weighted inner product with weight $x^{-1/2}$ (right). The number of dual vanishing moments was 1, 3, 5, and 7.

10 Warning

Like every "do it yourself at home" product this one comes with a warning. Most of the techniques we presented here are straightforward to implement and before you know it you will be generating wavelets yourself. However, we did not discuss most of the deeper underlying mathematical properties which assure that everything works like we expect it to. These address issues such as: What are the conditions on the subdivision scheme so that it generates smooth functions? or: Do the resulting scaling functions and wavelets generate a stable, i.e., Riesz basis? These questions are not easily answered and require some heavy mathematics. One of the fundamental questions is how properties, such as convergence of the cascade algorithm, Riesz bounds, and smoothness, can be related back to properties of the filter sequences. This is a very hard question and at this moment no general answer is available to our knowledge.

We restrict ourselves here to a short description of the extent to which these questions have been answered. In the classical case, i.e., regular samples and no weight function, everything essentially works. More precisely if the wavelet and dual wavelet have at least 1 vanishing moment, we have stable bases. The regularity of the basis functions varies linearly with N. In the case of the interval, regular samples, and no weight function, again the same results hold. This is because the boundary basis functions are finite linear combinations of the ones from the real line. In the case of regular samples with a weight function, it can be shown that with some minimal conditions on the weight function, the basis functions have the same regularity as in the unweighted case. In the case of irregular samples, little is known at this moment. Everything essentially depends on how irregular the samples are. It might be possible to obtain results under the conditions that the irregular samples are not too far from the regular samples, but this has to be studied in detail in the future.

Recent results concerning general multiscale transforms and their stability were obtained by Wolfgang Dahmen and his collaborators. They have been working (independently from [179, 181]) on a scheme which is very similar to the lifting scheme [18, 47]. In particular, Dahmen shows in [44] which properties in addition to biorthogonality are needed to assure stable bases. Whether this result can be applied to the bases constructed here needs to be studied in the future.

11 Outlook

So far we have only discussed the construction of second generation wavelets on the real line or the interval. Most of the techniques presented here such as polynomial subdivision and lifting extend easily to much more general sets. In particular domains in $\mathbf{RR}^n$, curves, surfaces, and manifolds.

One example is the construction of wavelets on the sphere [168]. There we use the lifting scheme to construct locally supported, biorthogonal spherical wavelets and their associated fast transforms. The construction starts from a recursive triangulation of the sphere and is parameterization independent. Since the construction does not rely on any specific properties of the sphere it can be generalized to other surfaces. The only question which needs to be addressed is what the right replacement for polynomials is. Polynomials restricted to a sphere are still a natural choice because of the connection with spherical harmonics, but on a general surface this is no longer the case.

A further application of these techniques is to scattered data processing in the plane. Imagine the original $x_{j,k}$ sample locations as being in the plane. A Delauney triangulation of the sample locations can then be used to go to finer levels by midpoint subdivision or a smoother subdivision method. The coarser levels can be constructed using standard computational geometry coarsening techniques. For smooth interpolating subdivision methods on triangles, we refer to [72].

IV: Wavelets, Signal Compression and Image Processing

Wim SWELDENS

University of South Carolina

1 Wavelets and signal compression

1.1 The need for compression

As we know, the amount of information stored, transmitted, and handled by computers has been growing exponentially over the last decades. Two recent development have particularly contributed to this effect. One development is the breakthrough of multi-media systems along with its spin-off to numerous applications. The time when computers handled only numbers and text is long gone and has been replaced by an era of sound, images, movies and virtual reality. Another development is the increased availability of the Internet, which has made this information available to a large body of users. These two developments are synthesized in the so-called World Wide Web, an interactive, multi-media, hyper-text based information network.

This development was only possible because of the rapid evolution on the hardware side. The performance of cpu's, disks, and transmission channels has grown tremendously. However, there is still a way to go as can be understood from the following examples:

1. To store a moderately large image, say a 512×512 pixels, 24 bit color image, takes about 0.75 MBytes. A video signal typically has around 30 frames per second.
2. A standard 35mm photograph digitized at 12 μm resolution requires about 18 MBytes.
3. One second of NTSC color video takes 23 MBytes.

This shows that one can easily find examples where the current hardware is inadequate (either technically or economically). Compression techniques, which are presented in this chapter, provide a solution. The reasoning behind attempting compression is straightforward. If we can represent the information in a compressed format, we can obviously:

1. save storage,
2. save cpu-time,
3. save transmission time.

Most of the information we use is highly correlated. In other works, it inherently contains redundancy. Thus it seems possible to use compression without losing information. The major requirement from the compression is that one can quickly switch between the original and compressed data.

1.2 General idea

There are two basic kinds of compression schemes: lossless and lossy. In the case of lossless compression one is interested in reconstructing the data exactly, without any loss of information. Lossless compression is often used for text files.

In the case of lossy compression we allow an error as long as the quality after compression is acceptable. A lossy compression scheme has the advantage that one can achieve much higher compression ratios than with lossless compression; however, it can only be used in case one can replace the original data with an approximation which is easier to compress. We have to be specific in what we mean by an "acceptable" representation. For example, in image compression an acceptable approximation of an image is one that is visually indistinguishable from the original image.

The underlying idea of any compression scheme is to remove the correlation present in the data. Correlated data is characterized by the fact that one can, given one part of the data, fill in the missing part.

Several types of correlation exist. We give some examples:

1. Spatial correlation: One can often predict the value of a pixel in an image by looking at the neighbouring pixels.
2. Spectral correlation: The Fourier transform of a signal is often smooth. This means that one can predict one frequency component by looking at the neighbouring frequencies.
3. Temporal correlation: In a digital video, most pixels of two neighbouring frames change very little in the time direction (e.g. the background).

One of the standard procedures for lossy compression is through transform coding, as indicated in Figure IV.1. The idea is to represent the data using a different mathematical basis in the hope that this new representation will reveal or unravel the correlation. By this we mean that in the new basis, the majority of the coefficients are so small they can be set to zero. The information is thus packed into a small number of coefficients. Compression is achieved by calculating the transform associated with this basis, setting coefficients below a threshold to zero, and lossless encoding of the non-zero coefficients.

In case one knows precisely the correlation present in a data set, it is possible to find the optimal transform. It is the so-called Karhunen-Loève representation. The optimal basis, i.e. that one with the best information packing quality, is given by the eigenvectors of the correlation matrix. This theoretical optimal representation, however, has several practical disadvantages:

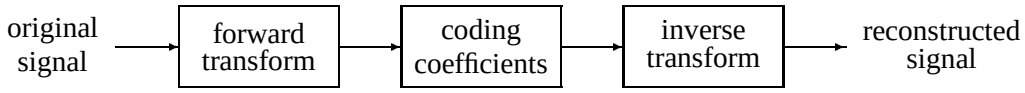

Figure IV.1: Transform coding.

1. In most cases the correlation matrix is not known.
2. The algorithm to calculate the eigenvectors of a matrix has cubic complexity. Given the fact that the dimension of the problem in the case of image compression is e.g. 512×512, we realize that it is impossible to compute the Karhunen-Loève basis.
3. Suppose one knows the optimal basis, calculating the transform is a quadratic algorithm, which in most cases still is unacceptable.
4. The basis depends on the data set. It can thus only be used in case one knows precisely which set the data belong to.

This tells us that we need a transform with the following properties:

1. The transform is independent of the data set.
2. A fast (linear or linear-logarithmic) algorithm to calculate the transform exists.
3. The transform is capable of removing the correlation for a large, general set of data.

A possible candidate for a transform is the Fast Fourier Transform (FFT). It definitely has the first two properties. However, it does not always have the third property. The basis functions are perfectly local in frequency, but not local at all in time. Therefore, it is unable to reveal local temporal correlation. Most signals have both local frequency and spatial correlation. We need a transform that is adapted to this behavior. More precisely, we need a basis which is local in time *and* frequency. There are two ways to construct such a basis.

1. One can divide the spatial domain into pieces and use a Fourier series on each piece separately. This way one gets a local trigonometric basis.
2. One can use a wavelet basis.

Both these methods result in a transform, which is data-independent, fast, and which yields a compact representation for a large, general set of data.

In both cases, one can allow some limited, but quite powerful data-dependency. This is done by not simple considering one basis, but a family of closely related bases, out of which one can select the best one. This process is called best basis selection [43]. In the case of local trigonometric bases, one builds a family of

bases by allowing domains to be joined, while in the wavelet case one uses wavelet packets [42]. These two basis families are closely related as, roughly speaking, one can be seen as the Fourier transform of the other [74]. One could say that using the first basis family corresponds to using the second one on the Fourier transform of the data.

1.3 Error measure

For any lossy compression scheme we need to measure the quality of the compressed data in order to be able to compare different methods. For example, in the case of image compression one usually wants the compressed image to be of the same visual quality as the original. Since such comparisons are subjective, one often turns to quantitative measures.

Let us be more specific. Suppose we are given a set of N data samples $\{f_i\}$ where i belongs to some suitable index range. Take $\{\tilde{f}_i\}$ to be the lossy compressed data. The compression ratio is defined as the number of bits it takes to store the f_i divided by the number of bits required to store the $\tilde{f}_i$. We use the following measures to compare f_i and $\tilde{f}_i$:

1. Root Mean Square Error:
$$\text{RMSE} \;=\; \sqrt{\frac{1}{N}\sum_{i=1}^{N}(f_i - \tilde{f}_i)^2}\,.$$

2. Peak Signal-to-Noise Ratio (in dB):
$$\text{PSNR} \;=\; 20\log_{10}\frac{\max_i |f_i|}{\text{RMSE}}\,.$$
For example, if we use 8 bits per sample the numerator is 255.

1.4 Theory of wavelet compression

We discuss here compression from an approximation problem point of view [58, 59]. More specifically, let us fix an orthogonal wavelet ψ. Given an integer $M \geqslant 1$, we try to find the "best" approximation of f by using a representation
$$f_M(x) \;=\; \sum_{kl} d_{j,k}\,\psi_{j,k}(x) \quad \text{with } M \text{ non-zero coefficients } d_{j,k}. \tag{1}$$

The basic reason why this potentially might be useful is that each wavelet picks up information about the function f essentially at a given location and at a given scale. Where the function has more interesting features, we can spend more coefficients, and where the function is nice and smooth we can use fewer and still get good quality of approximation. In other words, the wavelet transform allows us to focus on the most relevant parts of f.

As mentioned above, we are interested in finding an optimal approximation minimizing the RMSE. Because of the orthogonality of the wavelets this is equivalent to minimizing
$$\left(\sum_{j,k} |\,\langle f, \psi_{j,k}\rangle - d_{j,k}|^2\right)^{1/2}.$$

A moment's thought reveals that the best way to pick M non-zero coefficients $d_{j,k}$, making the error as small as possible, is by simply picking the M coefficients with largest absolute value, and setting $d_{j,k} = \langle f, \psi_{j,k} \rangle$ for these numbers. This yields the optimal approximation f_M^{opt}.

Another fundamental question is which images can be approximated well by using the procedure just sketched. Let us take this to mean that the error satisfies

$$\|f - f_M^{\text{opt}}\|_{L^2} = \mathcal{O}(M^{-\beta}), \tag{2}$$

for some $\beta > 0$. The larger β, the faster the error decays as M increases and the fewer coefficients are generally needed to obtain an approximation within a given error. The exponent β can be found easily, in fact it can be shown that

$$\left(\sum_{M \geq 1} (M^{\beta} \|f - f_M^{\text{opt}}\|_{L^2})^p \frac{1}{M} \right)^{1/p} \approx (\sum_{j,k} |\langle f, \psi_{j,k} \rangle|^p)^{1/p} \tag{3}$$

with $1/p = 1/2 + \beta$. The maximal β for which (2) is valid can be estimated by finding the smallest p for which the right-hand side of (3) is bounded.

If follows from this reasoning that a wide range of images can accurately be approximated by using only a few wavelet coefficients. In other words, wavelets are a good choice as basis in a transform coding scheme.

1.5 Image compression

One of the most commonly used algorithms for image compression is JPEG. It essentially uses a local trigonometric basis in a transform coding scheme. It divides an image into blocks of 8×8 pixels and uses a Discrete Cosine Transform on each block [192].

This idea has the disadvantage that the compressed image sometimes reveals the blocks and that one cannot exploit correlation among the blocks. The first disadvantage can be solved by using smooth cutoff functions to split the image into blocks and fold the overlapping parts back into the blocks in a clever way. This idea was first proposed in [40] and [136]. It was used in image compression in [1] and [111].

We focus on wavelet based compression. Some of the material is borrowed from [105], we refer the interested reader to the original paper for more details. We start out with a simple example illustrating the power of the wavelet transform. Figure IV.2 shows the histogram of the image before and after transformation. While the distribution of the coefficients before the transformation is spread out, the majority of the wavelet coefficients is neglectably small.

Algorithm

A wavelet compression algorithm essentially consists of three steps: transform, quantization, and encoding, see Figure IV.3.

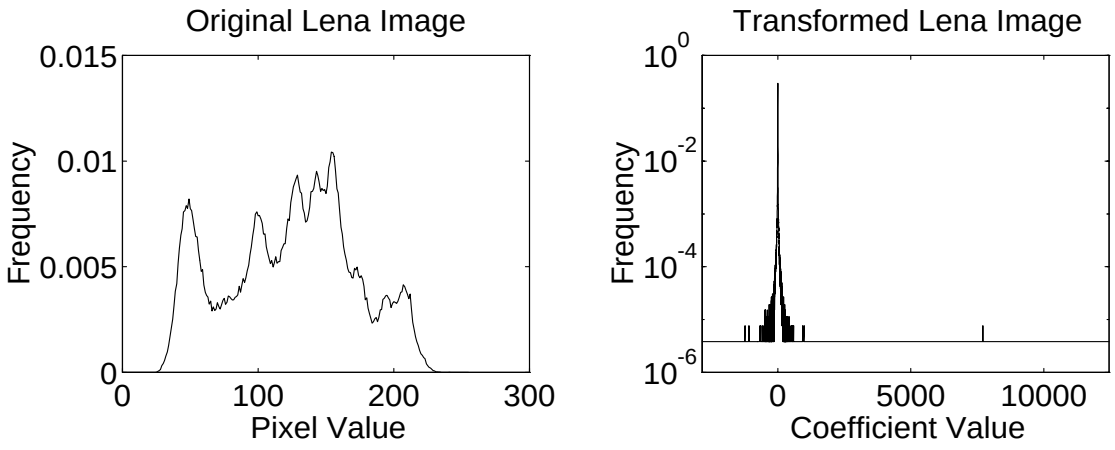

Figure IV.2: Histogram before and after transform

Wavelet transform

The wavelet transform and its implementation in 1D is commented on in other sections of these lecture notes. The transformation in 2D can be derived in a straightforward manner from the 1D one. In each step it involves applying the 1D transform to the rows and columns of a matrix, see Figure IV.4. After one step, one ends up with 4 subbands: one average image f_{LL}, and 3 detail images f_{LH}, f_{HL}, and f_{HH}. The next step of the algorithm does the same decomposition on f_{LL}. For the inverse transform, see the scheme in Figure IV.5.

In choosing a particular wavelet one has to consider the following issues:

1. Compact support: If the scaling function and wavelet are compactly supported, the filters are finite impulse response filters.

2. Rational coefficients: When using filters with rational coefficients or, even better, dyadic rationals, floating point operations can be avoided.

3. Smoothness: As we saw, compression is achieved by setting small coefficients $d_{j,l}$ to zero, and thus leaving out a component $d_{j,l}\,\psi_{j,l}$ from the original function. If the original function represents an image and the wavelet is not smooth, the error can easily be visually detected. Note that the smoothness of the wavelets is much more important to this aspect than the smoothness of the dual wavelets. Also, a higher degree of smoothness corresponds to better frequency localization of the filters.

4. Number of vanishing moments of the dual wavelet: The number of vanishing moments determines the convergence rate of wavelet approximations of smooth functions. Where the image is smooth more vanishing moments lead to smaller wavelet coefficients. On the other hand, where the image is non-smooth more vanishing moments lead to more large wavelet coefficients. Also, the number of vanishing moments of the dual wavelet is connected to the smoothness of the wavelet (and vice versa).

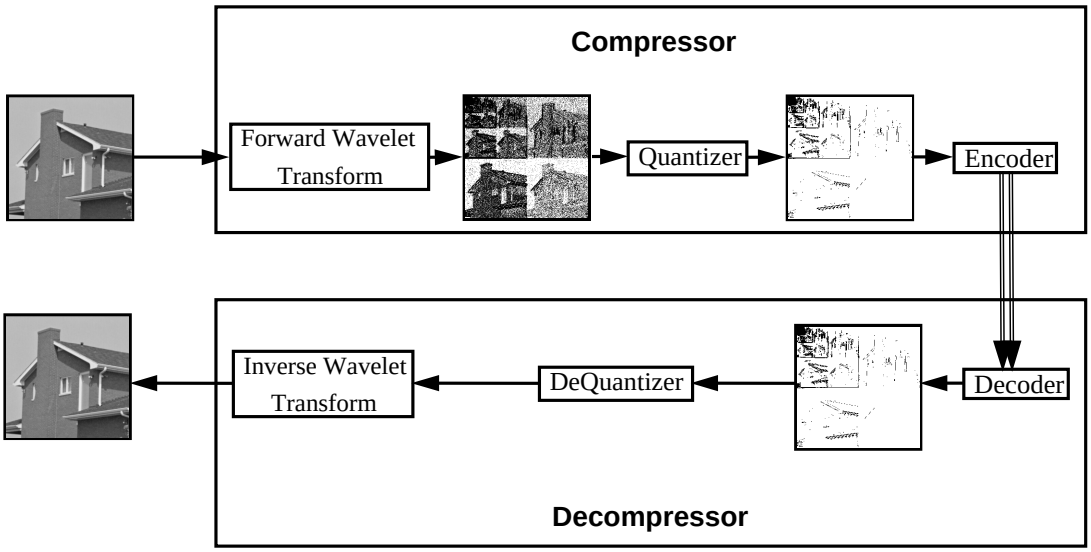

Figure IV.3: Scheme of wavelet encoding/decoding

5. Length of the filters: Obviously short filters are preferable. However, there is a trade-off between short filter lengths on one hand and the smoothness and number of vanishing moments on the other hand. As mentioned in Chapter 2, smoothness and vanishing moments are proportional to the length of the filter.

The most popular wavelets used in image compression are the orthogonal Daubechies' wavelets with 3 vanishing moments, and the biorthogonal wavelets with 2 vanishing moments for the wavelet and dual wavelet. The first one has filters of length 6, while the second has filters with lengths 3 and 5.

Quantization

A problem that hinders efficient encoding is the fact that the transform coefficients can have nearly arbitrary values. The purpose of quantization is to restrict the values of the coefficients to a limited number of possibilities.

One can distinguish two kinds of quantization: vector and scalar. In the case of scalar quantization, one divides the real axis in a number of non-overlapping intervals, each corresponding to a symbol k_i. Each coefficient is now replaced by the symbol k_i associated with the interval to which it belongs. The intervals and symbols are kept in a quantization table.

A more powerful variant is vector quantization [89]. Here one replaces a group of coefficients (a vector) with one symbol. The key is to find the right way of grouping the coefficients, such that as few symbols as possible are needed. One idea is to group wavelet coefficients of different bands associated with the same

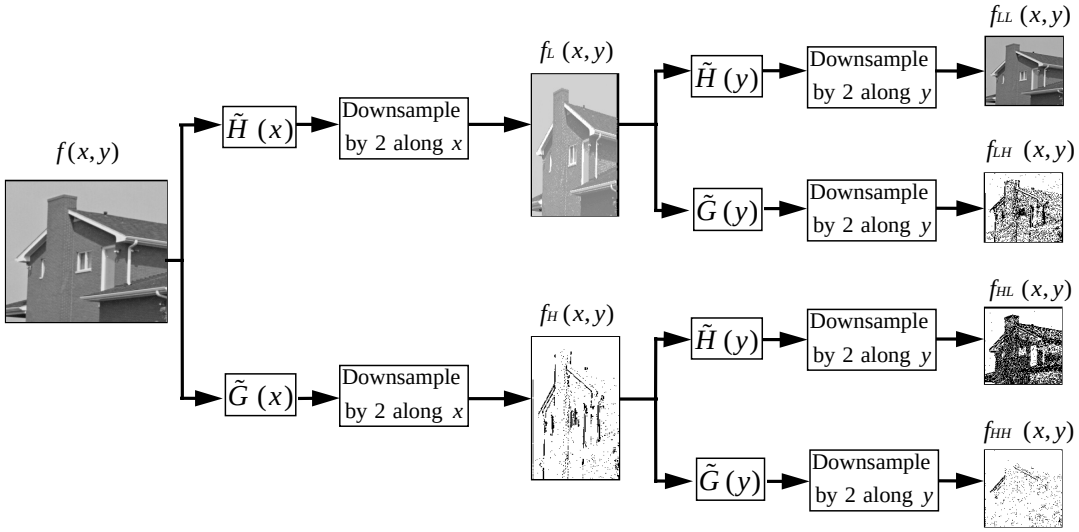

Figure IV.4: Forward wavelet transform.

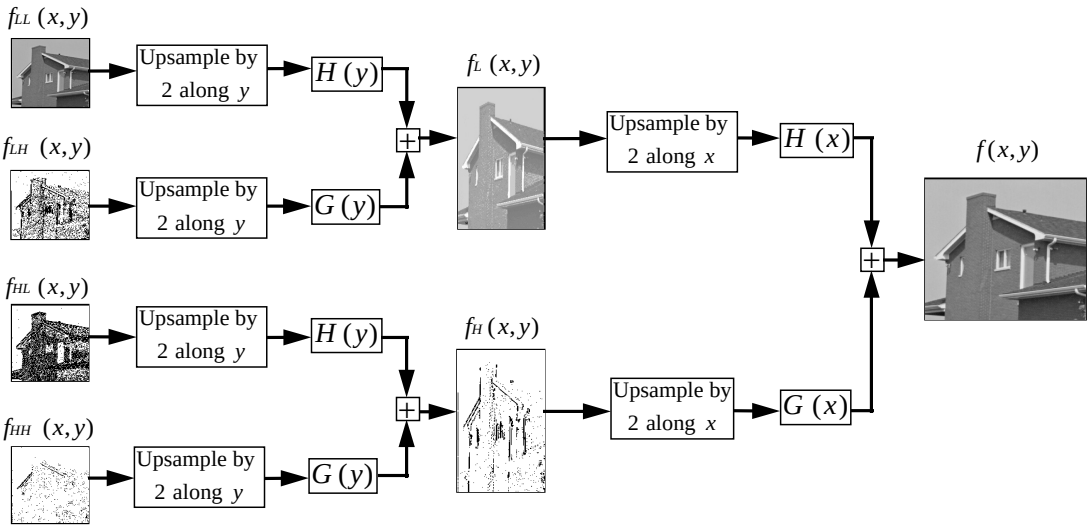

Figure IV.5: Inverse wavelet transform.

spatial location. For more details on vector quantization in combination with wavelets we refer to [5]. To design a quantization scheme one has to study the statistical behavior of the transform together with the properties of the human visual system [138]. To get optimal results, one uses different quantization tables for each level.

Encoding

The encoding step involves replacing, in a reversible way, the string of inputs symbols coming from the quantizer by a bit stream.

The two major categories are fixed length (FLC) and variable length coding (VLC). In a fixed length coder each symbol is replaced with the same number of bits. It is therefore essential to use a good quantizer. An example is the Lloyd-Max algorithm that can be used to construct a table that gives the minimal quantization error (in the mean square norm) [140]. With an empirical estimated probability density function for the coefficients, one can build the quantizer. Usually one takes longer code words for the coefficients on the coarser levels.

A more powerful variant uses variable length coding. The idea here is to assign shorter codewords to the more frequent symbols and longer to the less frequent. Suppose that a codeword k_i has a probability p_i with

$$\sum_i p_i = 1.$$

The "information content" or entropy is now given by

$$H = -\sum_i p_i \log_2 p_i,$$

and this is the theoretical minimum amount of bits needed per codeword. The problem is that H is not necessarily a natural number.

Variable length coders (or entropy coders) try to get as close as possible to this minimum. The two most popular methods are Huffman and arithmetic coding. For more details and references we refer to [157].

One has to bear in mind that these entropy encoders are only optimal in case the probabilities p_i are known. In practice one usually has to estimate the p_i either based on the data or on some a priori information.

Evidently, the position of the coefficients that were set to zero has to also be encoded. This can be done by run length encoding, i.e. replacing every string of zeros by its length [155]. This is usually followed by entropy encoding of the run lengths.

A technique that has proven particularly useful in combination with wavelets is so-called zero tree encoding. It exploits the self similarity between the different wavelet bands. For example, if a wavelet coefficient on a level is set to zero, it is likely that the wavelet coefficients corresponding to the same locations on the finer levels are set to zero as well. With this technique it is possible to greatly improve the performance of a wavelet encoder. An example is Shapiro's zero tree encoding [170].

One has to realize that any encoder represents a tradeoff between speed, memory and quality. For example Shapiro's encoder outperforms most other but is much slower.

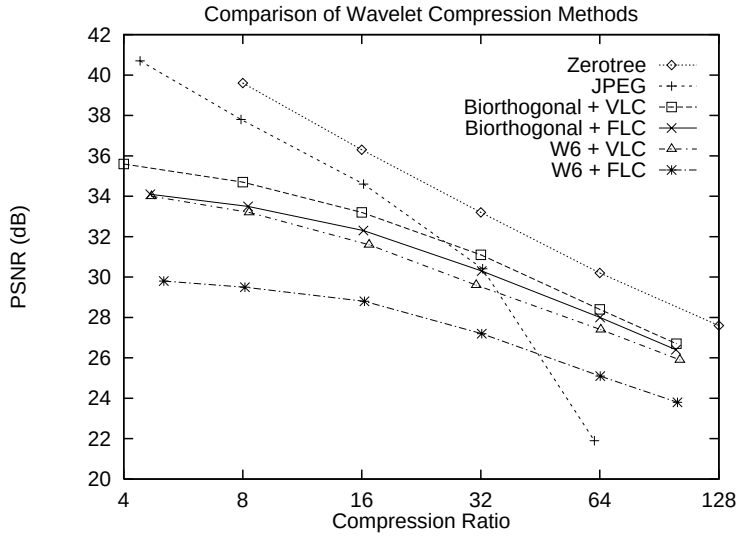

Figure IV.6: Comparison of wavelet compression.

When speed is important usually run-length encoding the zero coefficients is preferable.

Results

For a comparison between JPEG and several wavelet based encoders, we refer one to Figure IV.6 (which is borrowed from [110]). The JPEG coder used is the one from Version 2.21 of the `xview` program.

Finally, we include some results from commercial packages. One is a wavelet based coder from Summus, Ltd, while the other is Leadview, a JPEG based coder. Images `lena-4.tif` till `lena-9.tif` are compressed with the Summus code at ratios 4, 8, 16, 32, 64, and 128 respectively. Images `lena-10.tif` till `lena-13.tif` are compressed with the Leadview code at ratios 4, 8, 16, and 32 respectively. Summus's compression outperforms Leadview's in PSNR over the whole range of compression ratios. The execution times are comparable.

1.6 Video compression

In this section we discuss how wavelets can be used for video compression. A naive approach would be just to use still image compression on each frame. However, much higher compression ratios can be achieved if we also exploit the temporal redundancy. From that point of view, video compression is easier than image compression. However, an additional requirement with video compression is that the encoding and decoding has to be done in real time. A first problem is that the regular wavelet transform on a PC cannot be performed at frame rate (typically 30 frames/second; on a 66-Mhz 80486 processor the wavelet transform takes 1/4 seconds). Second, in many situations one cannot work with multiple frames at the same time because of memory constraints.

We present here an example of a simple wavelet video compression scheme based on the following two ideas:

– In order to remove the temporal redundancy we simply take the difference between two adjacent frames, see Figures IV.7 and IV.8. Consequently, we only need to have two frames at the time in the memory. The difference image is often sparse and can be compressed efficiently with wavelet based methods.

– Since the difference images are sparse, there is no need to calculate the whole wavelet transform. It suffices to only calculate the coefficients that are non-zero. For more details on this scheme we refer to [4]. For a compression of 20:1, this can speed up the calculation of the wavelet transform by a factor of 4.

Other wavelet based video encoders use wavelets also in the temporal domain or techniques such as motion estimation. More details can be found in [119] and [200].

We give an example from a commercial program by Summus, Ltd. It concerns 30 frames of a person speaking. We give the original sequence (`video-original`) and the compressed (70:1) sequence (`video-compressed`).

2 Wavelets and image processing

2.1 General idea

The general idea behind wavelets and image processing is simply to look at the wavelet coefficients as an alternative representation of the image. So instead of performing operations on the pixels we can work with the wavelet coefficients. This gives us the opportunity to take advantage of their multiresolution structure and their time-frequency localization.

A typical example is edge detection. As we know, the wavelet coefficients on each level represent a band pass filtering of the original image; thus, they naturally provide an edge map on different scales. We will come back to this later.

A simple application where wavelets can be useful is the following. Often one wants to resize an image. Simple subsampling to reduce the size or pixel duplication to increase the size usually gives poor quality results. Wavelets can be useful here in the following way. Suppose the original image can be seen as an element of the space V_9. Smaller size image now can simply be found by taking the projections in V_i with $i < 9$. These can be calculated with the fast wavelet transform. Larger size images can be constructed by looking at the image as an element in V_i with $i > 9$. The coefficients in those spaces can be calculated by using the inverse wavelet transform where the wavelet coefficients in the spaces W_i with $i \geqslant 8$ are set to zero. This is in fact a subdivision scheme. In case we use an interpolating scaling function, the original pixel values are not altered.

2.2 Multiscale edge detection and reconstruction

Mallat's wavelet maxima representation

One of the major drawbacks of wavelets in pattern recognition is that the transform is not translation invariant. In other words, when the input signal is shifted, the wavelet coefficient are not shifted, but instead can change completely. An idea of Mallat and co-workers is not to work with the (discrete) wavelet

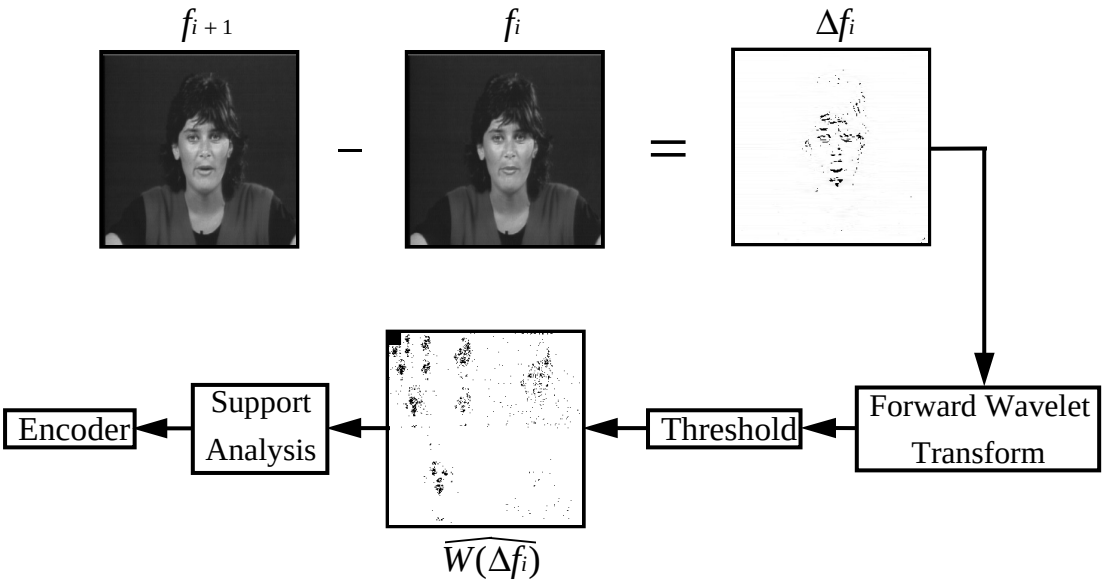

Figure IV.7: Video encoding.

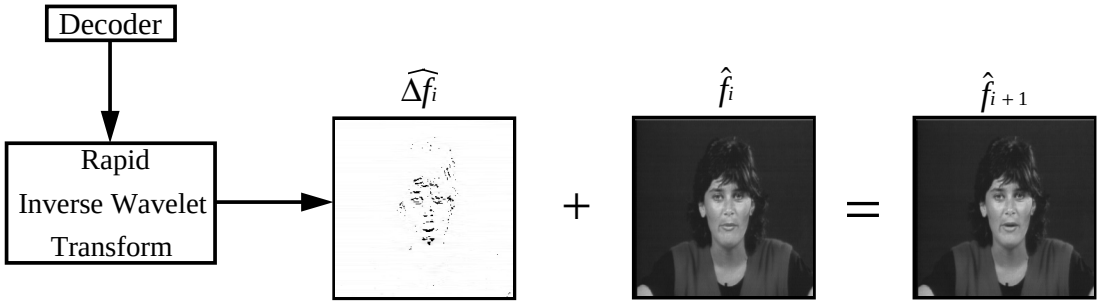

Figure IV.8: Video decoding.

coefficients but rather with the local maxima of each (continuous) wavelet band $WF_a^1(t)$, see Section 7.8 of Chapter 1. These local maxima somehow correspond to the edges of the image. For a specific class of wavelets this leads to the classic Canny edge detector [17].

The nice thing is that one can use these maxima not only for image analysis but also for the *representation* of images. This idea goes back to a conjecture of David Marr concerning computer vision in [138], where he claims that images can be reconstructed from their multiscale edges.

Mallat and co-workers have developed an elegant framework for these problems. In [131] they show how one can use the wavelet transform to characterize the local smoothness of an image. Edges typically correspond to locations where the image is non-smooth or where it has singularities. With the wavelet transform it is possible to precisely characterize the kind of singularity (i.e. its algebraic degree or more precisely, its Hölder regularity).

In [133] they present an algorithm to reconstruct an image from the wavelet maxima. It relies on an iteration between two subspaces: on one hand the subspace of all possible dyadic wavelet transforms (there is a one-to-one mapping from this space to the space of all images) and on the other hand the space of all functions having the same maxima. By repeatedly projecting back and forth between the two spaces, one approaches the intersection of the two spaces. This way one finds the reconstructed image. However, there is no theoretical proof of the convergence nor of the fact that the solution is unique. As a matter of fact, Meyer has been able to find an (exotic) counterexample.

Nevertheless, the algorithm works fine in practice. We include here two examples of a 256×256 Lena images reconstructed from its wavelet maxima. The first one (`lena-1.tif`) is obtained after 8 iterations of the algorithm and has an PSNR of 41dB. The second one (`lena-2.tif`) is obtained after 20 iterations and has a PSNR of 43dB.

One can also use this representation for compression purposes. To illustrate its feasibility, we give an example of the Lena image reconstructed with 8 iterations and after omitting every wavelet maximum below the threshold of 8 (`lena-3.tif`, PSNR 35dB). We see that the fine details and textures are lost, but the main edges are preserved and sharp. The typical blurring effect that many compression schemes have can be avoided with this technique. Mallat proposed an encoding algorithm that first connects the wavelet maxima into chains and then uses a thresholding based on the length of the chain and the average modulus.

Note:
The software from Mallat and co-workers (source code) can be obtained with anonymous ftp to the machine cs.nyu.edu (128.122.140.24). The files are /pub/wave/wave1.tar.Z (1D) and /pub/wave/wave1.tar.Z (2D).

Wavelet probing

Another implementation of the same idea exists and is called wavelet probing. It is based on the construction of wavelets on closed sets. We explain it first in two dimensions. For more details we refer one to [4] and [55]. Suppose we are given a signal. Instead of using the standard wavelet transform on the whole signal, it sometimes is useful to split the signal into several segments and perform the wavelet transform on each segment. The latter can be done using wavelets on an interval, see Chapter 2.

The question now is: how do we find the optimal splitting locations? The answer is given by wavelet

probing. The idea is to simply try every possible splitting location and check whether it pays off to put a segmentation point there. This can be done based on a criterion that depends on the application. For example, in the case of compression, one could simply count and compare the number of wavelet coefficients bigger than a certain threshold with and without a splitting point. Using a method called split and merge, checking one splitting point takes only a number of operations proportional to the number of levels in the wavelet transform. The whole algorithm thus takes only $N \log(N)$ operations. To understand why this is potentially useful, consider the following example. Take a signal which is smooth except for a jump discontinuity at one point. Where the signal is smooth, the wavelet coefficients decay rapidly to zero. However the discontinuity is "expensive" in terms of wavelet coefficients since it leads to large wavelet coefficients on every level. By simply putting a splitting point at the discontinuity, one obtains two pieces, which each are smooth; this thsu lead to small wavelet coefficients everywhere.

This idea can be generalized to 2D. It then leads to an alternative way of picking the natural "edges" in an image. The advantage is that the reconstruction is not iterative and thus can be performed very fast.

We here include a simple example of how it can be used in image compression. In this example we do not use the full wavelet probing algorithm but merely a simple edge detector to find the edges. We then calculate the wavelet transform over the domains defined by those edges. This can be done using a tensor product version of wavelets on an interval. Note that these domains need not be closed. Next, we can achieve compression by simply thresholding the wavelet coefficients. The original image is a 512×512 color image of the F16 jet. The regular wavelet compressed (at roughly 400:1) is given in `f16-3.tif`. The one compressed with this edge technique (again at roughly 400:1) is given ins `f16-4.tif`. The edge map is give in `f16-5.tif`. Again we have the effect that the main edges are preserved while texture and fine details disappear.

2.3 Enhancement

When using wavelets for approximation and compression, one most often works with the L^2 norm. This is straightforward as the L^2 norm of a function f and the discrete ℓ^2 norm of its wavelet coefficients $d_{j,k}$ are closely related. In the case of orthogonal wavelets, one even has an equality in the sense that

$$\|f\| \;=\; \sqrt{\sum_{j,k} d_{j,k}^2}.$$

However, one can add a tremendous amount of flexibility by using more general norms. We introduce a new norm that makes use of some weights $w_{j,k}$ and let

$$\|f\|_w \;=\; \sqrt{\sum_{j,k} w_{j,k}^2\, d_{j,k}^2}.$$

By choosing these weights carefully, one can direct attention to very specific features. We give two examples:

1. By choosing the weights as $w_{j,k} = 2^{j\alpha}$, one obtains a so-called Sobolev norm. This is a norm that measures the smoothness (or differentiability) of a function up to order α. The Sobolev norm gives more weight to the higher frequencies. This makes sense because the smoothness of a function corresponds to the decay of its Fourier transform.

2. By choosing the weights of wavelet coefficients associated with a certain region larger than the other ones, one can pay more attention to this region. Assuming that the mother wavelet is centered around the origin, a wavelet coefficient $d_{j,k}$ is associated with a certain region if, roughly speaking, $2^{-j}k$ belongs to that region. This way one can "focus" on one particular part of an image.

Evidently, one can also combine these two methods. This way one makes full use of the time-frequency localization of the wavelets.

We illustrate this with two examples taken from [110]. Image `f16-1.tif` is a picture of a F-16 jet compressed at 100:1. Many features of the jet are lost. Suppose one is mainly interested in the jet and not so much in the background, this technique can be used to focus on the airplane. In this example, it is done by multiplying the coefficients corresponding to the jet by a factor of 5. Image `f16-2.tif` is the same picture, compressed at 100:1, but with focusing on the jet. Much more details of the jet are preserved. Unavoidably, details of the background are lost.

The next example concerns the image of a map. Image `map-1.tif` is the map compressed at 15:1. Image `map-2.tif` is the map compressed at 15:1 using a Sobolev norm, and thus paying more attention to the high frequencies. It is obvious that this one contains much more fine detail. The weight factors used are $w_{8,k} = 2.5$, $w_{7,k} = 1.5$ and the others are equal to 1.

2.4 Others

Many other applications of wavelets in image processing exist. However, space does not permit us to further expand here. We simply mention two other areas.

The first one involves noise removal. In some sense noise removal is closely related to compression as both try to eliminate non-correlated components. Noise by definition is uncorrelated. Several schemes for noise removal are presented by Donoho and Johnstone. We refer one to [64], [65], [66], and [67] for more details.

Another direction involves high level image processing tasks such as shape from shading and stereo matching. Most of these can be reformulated as a minimization problem or as a partial or integral differential equation. We refer one to the section on differential equations for more details. One problem is that some of these equations are non-linear and at this moment it is not clear yet how wavelets will be most useful in their solution.

Disclaimer

Discussion of any specific product in these notes is provided to reference a particular capability and is not intended to be a recommendation.

Acknowledgement

The author would like to thank Björn Jawerth, Michael Hilton, and Terry Huntsberger for letting him use material from their papers, Prasanjit Panda for his help in installing and using Mallat's software, and Summus, Ltd for providing several of the examples concerning image and video compression.

filename	description
`lena.tif`	512x512 original lena
`lena-1.tif`	Mallat 20 iterations
`lena-2.tif`	Mallat 8 iterations
`lena-3.tif`	Mallat 8 iterations after threshold
`lena-4.tif`	Summus 4:1
`lena-5.tif`	Summus 8:1
`lena-6.tif`	Summus 16:1
`lena-7.tif`	Summus 32:1
`lena-8.tif`	Summus 64:1
`lena-9.tif`	Summus 128:1
`lena-10.tif`	Leadview 4:1
`lena-11.tif`	Leadview 8:1
`lena-12.tif`	Leadview 16:1
`lena-13.tif`	Leadview 32:1
`f16.tif`	512x512 original F16
`f16-color.tif`	512x512 original F16 (color)
`f16-1.tif`	compressed 100:1
`f16-2.tif`	compressed 100:1 and focused
`f16-3.tif`	compressed 400:1 (color)
`f16-4.tif`	compressed 400:1 with edge preservation
`f16-5.tif`	edge map
`map.tif`	512x512 original map
`map-1.tif`	compressed 15:1
`map-2.tif`	compressed 15:1 with fine detail emphasized
`video-original`	original movie (30 frames of 360x288)
`video-compressed`	Summus 70:1

Table IV.1: List of images.

V: Curves and Surfaces

Tony D. DEROSE
University of Washington

Michael LOUNSBERY
Alias Research

Leena-Maija REISSELL
University of British Columbia

1 Wavelet representation for curves (Leena-Maija Reissell)

1.1 Introduction

Hierarchical representation methods for curves and surfaces are popular because of their obvious advantages: they allow efficient geometric computations at selected accuracy levels, rapid data classification, fast display, and multiresolution surface design. Since wavelets give rise to hierarchical representations and are also successful at many general tasks such as de-noising, compression and discontinuity detection, it is natural to apply them to curve and surface representation.

For instance, wavelets can be used to represent parametric curves and surfaces simply by computing the wavelet decomposition of each coordinate function separately. The wavelets should be suitably adapted to intervals. This method has been used in [161]. Wavelets can also be defined intrinsically on curves and surfaces; more on this approach can be found in other chapters.

The general advantages of using wavelets include:

– Good, well understood approximation properties.

The wavelet coefficients provide a precise measure of the approximation error. This error behavior is well understood in terms of the number of vanishing moments of the wavelet. By contrast, other hierarchical representation schemes often do not provide an analysis of the approximation error.

– Space-frequency localization.

– Fast, robust numerical calculations.

– Compression algorithms for compact data storage.

– Hierarchical curve/surface representation and analysis tools.

These include the usual wavelet compression and multiresolution tools. However, if the wavelets are chosen appropriately, the scaling coefficients can also be used selectively, via wavelet compression algorithms, to provide compact hierarchical representations. The scaling coefficient representation is well suited for input to other operations, such as display and intersection. This is particularly useful in large scale applications which benefit from good piecewise linear approximations.

The wavelet coefficients can also be used to partition the curve or surface into areas of varying complexity for use in other operations or geometric algorithms.

There are some general requirements on the wavelets used in geometric applications. In many areas wavelet regularity and symmetry are not very important, but here any lack of those properties will show very clearly. For instance, using the Daubechies wavelet with 4 vanishing moments, D_8, will lead to the "smoothed" curve in Figure V.1. The corresponding curve with the P_4 wavelet, constructed here, is shown next to it. In general, good choices for the underlying multiresolution include different B-spline-based scaling functions, box splines for surfaces, and interpolating scaling functions.

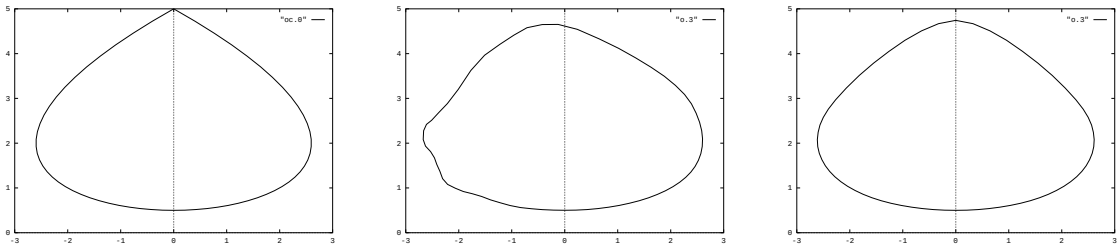

Figure V.1: Original curve; D_8 smoothed curve; P_4 smoothed curve

In this section, we will give examples of wavelet use in parametric curve/surface applications and construct specific wavelets, *pseudocoiflets* ([161]), with good properties and with interpolating scaling functions. Our construction actually yields a family of wavelets P_{2N}, for even numbers of vanishing moments $2N$. The construction provides an example of using the biorthogonal wavelet framework to build "customized" wavelets.

Pseudocoiflets are constructed to provide scaling coefficients which approximate the original curve or surface well. When combined with a wavelet compression approach, this provides simple, accurate approximations to the original curve using a small number of points. These approximations can be piecewise linear. Such *adaptive scaling coefficient approximations* can then be used in, for instance, intersection algorithms. In Section 3.2 we give examples of adaptive scaling coefficient approximations of a brain scan curve.

Wavelets can also be used to analyze surfaces for relative smoothness. This has applications to motion planning, for instance. An example of rough terrain path planning for mobile robots [151], using pseudocoiflets, is presented in Section 3.2.

The following figure illustrates some of the basic properties of pseudocoiflets. Selected levels of multiresolution approximations and scaling coefficients, based on the pseudocoiflets P_4, are shown. The scaling coefficients form good approximations of the original curve.

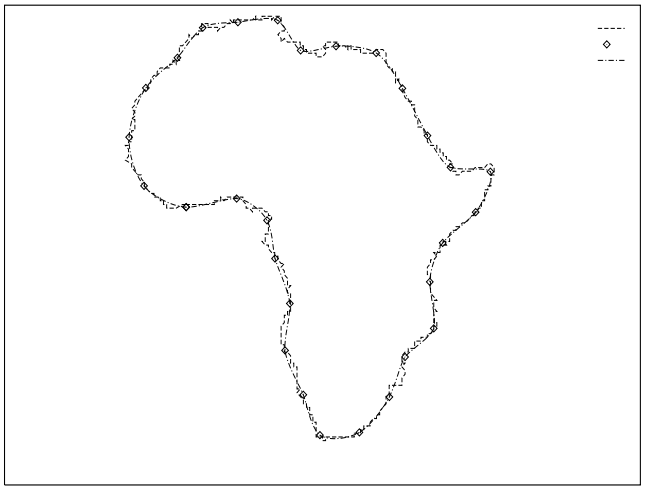

Figure V.2: P_4 scaling coefficients and multiresolution approximation curve, overlaid on original data.

We will focus here on the wavelet decomposition of curves. The formal extensions to parametric surfaces are analogous. Much of the material is from [161].

1.2 Parametric wavelet decomposition notation

We will first consider curves C from $[0,1]$ into $\mathbb{R}^n$ defined by the component functions

$$x_k = f^k(t), \quad k = 0, \ldots, n-1.$$

with the restriction that these functions are in L^2. Suppose also that we have a biorthogonal wavelet family determined by the analyzing scaling function φ and wavelet ψ, and the corresponding reconstruction functions $\tilde{\varphi}$ and $\tilde{\psi}$. Apart from the switch in the roles of dual and primal filters, we adopt the conventions of the previous sections. The wavelet family for ψ is defined as

$$\psi_{m,n}(x) = \sqrt{2^m}\, \psi(2^m x - n),$$

and analogous notation is used for the families generated by the other functions. The fact that the data is defined on an interval is dealt with by adapting the chosen wavelets to intervals, for instance by using periodic wavelets for cyclic data or via the methods of ([35]). We then represent the curve componentwise

by the wavelet decomposition in the basis chosen. Other than the parametrization, there are no restrictions on the kinds of curves represented this way (closed, open, nonmanifold . . .). The basic notation is given below:

– The *scaling coefficients* of the curve are given by the scaling coefficients for each coordinate $s^k_{ij} = 2^{-i/2} \langle f^k, \varphi_{i,j} \rangle$.

  Here the s^k are normalized as if they were coefficients for the L^∞-normalized scaling functions – the advantage is that the scaling coefficients are close to the original function this way. The discrete set of points defined by the scaling coefficients of C at level i, $\{(s^0_{ij}, s^1_{ij}, ...) : j \in \mathbb{Z}\}$, can also be thought to form a sampled curve, $\mathcal{S}_i(C)$.

– The *approximating* curve $\mathcal{A}_i(C)$ at level i consists of the projections of C to the multiresolution spaces and it is constructed from the scaling coefficients by

$$P_i f^k(t) = \sum_j \; d^k_{ij} \; \tilde{\varphi}_{ij}(t), \quad k < n,$$

  where n is the dimension of the underlying space. For orthonormal wavelets, each component of the approximating curve is the least squares approximant from the i^{th} level multiresolution space.

  The coefficient curve is useful for instance when piecewise linear approximations to the approximating curves $\mathcal{A}_i(C)$ are needed (piecewise linear curves cannot approximate as well as higher order curves, but since operations on them are very fast, the trade-off is often worth it.) Under certain conditions, the coefficient curves provide good approximations of the original curve.

– The *wavelet decomposition* of the curve C is the collection of wavelet decompositions of each coordinate function $f^k = \sum \langle f^k, \psi_{i,j} \rangle \, \tilde{\psi}_{i,j}$.

  The k^{th} component of the error between approximations at level i is, as usual, $\sum_j \; w^k_{ij} \; \tilde{\psi}_{ij}$, where $w^k_{ij} = \langle f^k, \psi_{i,j} \rangle$ are the wavelet coefficients of the curve.

In practice, the curve C will be given as a collection of uniformly sampled coordinates, and it is represented by a set of discrete points. The sampled points are transformed to a representation of the curve C at the finest multiresolution level considered. This is often done by using the samples themselves as initial coefficients, giving potentially an initial approximation error.

The wavelet decomposition and reconstruction for the sampled curve are now obtained as usual from the initial coefficients via the Mallat tree algorithm; the analyzing filter pair is applied separately to each coordinate. – If the wavelet filters used are finite, all computations of the coefficients and of points on the scaling curve $\mathcal{S}_i(C)$ and on the approximating curve $\mathcal{A}_i(C)$ are local.

1.3 Basic properties of the wavelet decomposition of curves

The parametric wavelet decomposition of curves respects basic geometric operations, such as translation, rotation, and scaling:

– $\mathbf{Op}(\mathcal{S}_i(C)) = (\mathcal{S}_i(\mathbf{Op}(C))), \qquad \mathbf{Op}(\mathcal{A}_i(C)) = (\mathcal{A}_i(\mathbf{Op}(C))).$
  where $\mathbf{Op}$ is a translation, rotation or scaling.

The proofs are simple, and follow from the bilinearity of inner products and the definitions.

The wavelet decomposition is *not* preserved under reparametrization.

Vanishing moments.

Define as usual the $n-$moment of f, $n = 0, 1, \ldots$, to be $\int t^n f(t)dt$. The number of vanishing moments of the wavelet determines its approximation properties. For instance, this number influences the preservation of polynomials in successive multiresolution approximations: more precisely, if the analyzing wavelet has N vanishing moments, polynomial curves and Bézier curves of degree $N-1$ are not changed by successive wavelet approximations. In addition, the scaling coefficient curves of polynomial curves are also polynomial, with the same degree.

In addition to the vanishing moments of the wavelet, it is useful to consider the vanishing moments of the scaling function: we say that the *first N moments of the scaling function $\tilde{\varphi}$ vanish*, if the $1, \ldots, N$ moments of $\tilde{\varphi}$ are 0. (The 0^{th} moment can never vanish in this case.)

In order to use scaling coefficients to approximate the original curves, Daubechies constructed orthonormal wavelets, called *coiflets*, which have these vanishing moment properties for both the scaling function and the wavelet. Coiflets produce "good" scaling coefficients: for instance, the initial sampling can be used with only a small penalty as the initial coefficients of the wavelet decomposition, since the dyadic function samples now satisfy

$$f(2^i k) = 2^{-i/2} \langle f, \varphi_{i,k} \rangle + O(h^N), \tag{1}$$

where N is the number of vanishing moments and φ is the scaling function with the coiflet property (see [50]).

Here, we will call biorthogonal wavelets with N vanishing moments for both wavelets and one scaling function *coiflet-like*. We will construct coiflet-like wavelets with interpolating scaling functions; interpolation allows for instance the *error free* use of initial function samples as scaling coefficients.

1.4 Choosing a wavelet

We end this section with a review of some desirable properties for wavelets used in representing geometric objects:

- Symmetry and smoothness.
- Small oscillation in the scaling function.
- Short support.

  The computation time in wavelet algorithms is proportional to the size of filter used, and so to the support of the wavelet or scaling function. However, the approximation properties of wavelets tend to improve with support length, resulting in a tradeoff.
- Good space-frequency localization.

In addition, it is useful to consider wavelets with additional properties:

- Moment conditions and interpolation.

  Interpolating scaling functions allow:

  - Use of data samples as initial scaling coefficients.
  - Fast, local schemes for curve and surface interpolation.
  - Interchanging control points and curve points.
  - Natural use of scaling coefficients in curve and surface approximation.

  The simplest interpolating scaling function is the hat function. The pseudocoiflets constructed here also give higher order interpolating scaling functions. These higher order wavelets allow better approximation when the data is relatively smooth.

Some examples of good wavelets

- Biorthogonal and semiorthogonal B-spline based wavelets.
- Wavelets based on B-splines with arbitrary knots (for instance, [127]).
- Wavelets with smooth interpolating scaling functions ([161]).

Another construction is the more general:

- Box spline based, wavelet-like error decomposition for surfaces, using nonorthogonal projections into multiresolution spaces. [59].

2 Wavelets with interpolating scaling functions

We will outline the construction ([161]) of compactly supported symmetric biorthogonal wavelets, for which one of the scaling functions, say, the dual scaling function, is interpolating. The construction is based on the methods of Cohen, Daubechies, and Feauveau [33]. This example also illustrates the ease of specific biorthogonal wavelet building. Similar biorthogonal wavelets have been constructed independently in [165].

The interpolating dual scaling functions are Deslauriers-Dubuc functions ([57]), which are smooth. Since it turns out that the resulting wavelets automatically must have coiflet-like moment properties, we will call the biorthogonal wavelets we construct *pseudocoiflets*, after the coiflet family of orthonormal wavelets constructed by Daubechies ([50]).

More specifically, we will build a family P_{2N} of scaling functions $(\varphi, \tilde{\varphi})$ and corresponding wavelets satisfying the exact reconstruction condition (see [33]) and with the following properties:

- The scaling functions φ and $\tilde{\varphi}$ are symmetric.

– The first 2N moments for ψ and $\tilde{\psi}$ vanish.

– $\tilde{\varphi}$ satisfies the scaling function vanishing moment condition for 2N.

– φ , ψ , $\tilde{\varphi}$, and $\tilde{\psi}$ are compactly supported.

– $\tilde{\varphi}$ is interpolating and smooth.

According to the methods of [33], for a given N, we find the appropriate trigonometric polynomials $m_0(\xi)$ and $\tilde{m}_0(\xi)$ corresponding to φ and $\tilde{\varphi}$.

2.1 The construction

We assume first that both $m_0(\xi)$ and $\tilde{m}_0(\xi)$ correspond to filters which are symmetric and consist of an odd number of elements. The moment conditions on the wavelet and the scaling function for such a filter transfer function m_0 can then be rewritten in the following way:

$$m_0(\xi) = (1 + \cos\xi)^{N_1} P_1(\cos\xi). \tag{2}$$

$$m_0(\xi) = 1 + (1 - \cos\xi)^{N_2} P_2(\cos\xi) \tag{3}$$

The factorization is implied by the moment conditions. Here, both P_1 and P_2 are trigonometric polynomials of cos ξ, and $2N_1$ and $2N_2$ are the numbers of vanishing moments required. We will note that (2) is the only form the trigonometric polynomial $\tilde{m}_0$ can take if $\tilde{\varphi}$ is to be interpolating.

2.1.1 The interpolation condition

We will first observe that interpolating scaling functions can be obtained as a special case from the construction of coiflet-like scaling functions. For these scaling functions, it turns out that both moment conditions (3) and (2) are satisfied for $N = N_1 = N_2$.

A scaling function φ corresponding to a multiresolution is *interpolating* if the representation of a function f using the translates of φ , $f(x) = \sum_i d_i \varphi(x - i)$, interpolates the coefficients d_i. The multiresolution is of necessity not an orthonormal one. For interpolation the coefficients h_j in the refinement equation for φ should satisfy

$$h_{2j} = \frac{1}{\sqrt{2}} \delta_{j,0}. \tag{4}$$

An equivalent condition is requiring that the corresponding filter transfer function $m_0(\xi) = \frac{1}{\sqrt{2}} \sum h_j e^{-ij\xi}$ has the property

$$m_0(\xi) + m_0(\xi + \pi) = 1. \tag{5}$$

2.1.2 Coiflet-like wavelets

Assume first that both $m_0(\xi)$ and $\tilde{m}_0(\xi)$ correspond to filters which are symmetric and consist of an odd number of elements. The number of vanishing moments imposed is N. The requirement that the construction is coiflet-like can then be expressed as follows, using the factorization of (3) and (2) with $N = N_1 = N_2$:

$$(1+x)^N P_1(x) - (1-x)^N P_2(x) = 1, \tag{6}$$

where $x = \cos\xi$. This equation has the solution

$$P_1(x) = \frac{1}{2^N} \sum_0^{N-1} \begin{pmatrix} N-1+k \\ k \end{pmatrix} \frac{1}{2^k}(1-x)^k \; + \; (1-x)^N F(x), \tag{7}$$

$$P_2(x) = -P_1(-x) \tag{8}$$

where F is an arbitrary odd polynomial. For $F = 0$ these P_1 correspond to functions studied by Deslauriers and Dubuc (see [57], [50]).

In addition, interpolating scaling functions are also obtained this way by the following observation ([161]):

- If the trigonometric polynomial $\tilde{m}_0$ is coiflet-like, symmetric, and consists of an odd number of filter elements, and has $2N$ vanishing moments, $\tilde{m}_0$ is interpolating.
- Conversely, compactly supported symmetric interpolating scaling functions are coiflet-like, have an even number of vanishing moments, and the corresponding filter consists of an odd number of elements.

This relies on the fact that the equations (5) and (6) have the same solutions. For details, see [161].

2.1.3 The biorthogonality conditions

The interpolating trigonometric polynomials $\tilde{m}_0$ obtained in the above way are then inserted into the biorthogonality conditions of [33] to find the dual trigonometric polynomials m_0. The necessary condition for biorthogonality for m_0 and $\tilde{m}_0$ is

$$m_0(\xi)\overline{\tilde{m}_0(\xi)} + m_0(\xi+\pi)\overline{\tilde{m}_0(\xi+\pi)} = 1. \tag{9}$$

Here we assume that the corresponding wavelets will be built from the scaling functions by using mirror filters, as usual. For m_0 and $\tilde{m}_0$ as in (3) and (2), with $2N$ and $2\tilde{N}$ giving the numbers of vanishing moments, the biorthogonality condition can be expressed as

$$(1+x)^{N+\tilde{N}} \tilde{P}(x) P(x) + (1-x)^{N+\tilde{N}} \tilde{P}(-x) P(-x) = 1. \tag{10}$$

The biorthogonality condition can always be satisfied if $\tilde{m}_0$ is a solution of the coiflet equation (6) ([161]):

– If $\tilde{P}(x)$ is a solution (7) for P_1 to the coiflet equation (6), then there is a polynomial P such that P and $\tilde{P}$ solve the biorthogonality equation (10) with $N = \tilde{N}$. The unique minimum degree solution P corresponding to the minimum degree $\tilde{P}$ has degree $3N - 2$.

In practice, finding the polynomial P only involves solving a linear system, which can be done when $\tilde{P}(x)$ and $\tilde{P}(-x)$ have no common zeros. In our case, the polynomials never have common zeros ([161]).

2.2 The pseudocoiflet family P_{2N}

The family of pseudocoiflets P_{2N}, a wavelet family $(\varphi, \psi),\ (\tilde{\varphi}, \tilde{\psi})$ satisfying the necessary biorthogonality condition (10), is now obtained by the following procedure.

Construction of pseudocoiflets P_{2N}

1. Let $\tilde{P}$ and P be the trigonometric polynomials $m_0(\xi) = (1 + \cos\xi)^N P(\cos\xi)$ and $\tilde{m}_0(\xi) = (1 + \cos\xi)^{N_1}\tilde{P}(\xi)$.
2. Find the minimal degree solution (7) for $\tilde{P}$ by letting $\tilde{P} = P_1$.
3. Find the minimal degree solution P for the given $\tilde{P}$ using the linear system in (10). This solution exists by the above result.
4. Evaluate the filter coefficients from P and $\tilde{P}$.

The above construction implies that there is an exact reconstruction filtering scheme corresponding to the functions $(\varphi, \psi),\ (\tilde{\varphi}, \tilde{\psi})$. It does not yet guarantee that the constructed functions $(\varphi, \psi),\ (\tilde{\varphi}, \tilde{\psi})$ are in L^2, or that the wavelets derived from $\psi, \tilde{\psi}$ form a dual basis. A necessary and sufficient condition for the functions $(\varphi, \psi),\ (\tilde{\varphi}, \tilde{\psi})$ to define a true biorthogonal L^2-wavelet family has been given by Cohen in [33]. This condition can be easily shown to hold for the first few members of the family P_{2N}, and so we have L^2-biorthogonal wavelet bases corresponding to these N.

The following properties of the pseudocoiflets ψ and $\tilde{\psi}$ follow immediately from the construction:

Properties of pseudocoiflets P_{2N}

– The pseudocoiflets ψ and $\tilde{\psi}$ have $2N$ vanishing moments, as does the scaling function $\tilde{\varphi}$.

– The reconstructing scaling function $\tilde{\varphi}$ is interpolating.

– The scaling functions are symmetric.

– The degrees of $\tilde{m}_0$ and m_0 are $N - 1$ and $3N - 2$, respectively.

– The lengths of the pseudocoiflet P_{2N} reconstructing and analyzing filters are $4N-1$ and $6N-1$, respectively.

We note that it is possible to choose different values of $\tilde{N}$ and N in (10), leading to a construction of a family $P_{2\tilde{N},2N}$ of pseudocoiflets consisting of a family of analyzing functions, depending on N, for each reconstructing scaling function with moment properties given by $\tilde{N}$. Other variations of the construction can also be obtained, for instance, by considering longer than minimal length reconstructing filters.

2.3 Examples

The filter coefficients for the pseudocoiflets with $N=1$ and $N=2$ are listed below in Table V.1. The coefficients are exact. The pseudocoiflet for $N=1$ has the hat function as the reconstructing scaling function and the filter pair equals the corresponding spline-based biorthogonal filter of [33]. The pseudocoiflet scaling functions for $N=2$ are pictured in Figure V.3.

analyzing filter N = 1 multiply by $\frac{1}{\sqrt{2}}$	reconstructing filter N = 1 multiply by $\sqrt{2}$	analyzing filter N = 2 multiply by $\frac{1}{\sqrt{2}}$	reconstructing filter N = 2 multiply by $\sqrt{2}$
		-0.00390625	
		0	
		0.0703125	
		-0.0625	-0.03125
-0.25		-0.24609375	0
0.5	0.25	0.5625	0.28125
1.5	0.5	1.359375	0.5
0.5	0.25	0.5625	0.28125
-0.25		-0.24609375	0
		-0.0625	-0.03125
		0.0703125	
		0	
		-0.00390625	

Table V.1: Scaling filter coefficients for pseudocoiflets with $N=1,2$.

The wavelet filter coefficients are obtained by the mirror filter construction from the scaling filters. The analyzing wavelet is obtained from the reconstructing scaling function, and vice versa. The wavelet coefficients for $N=2$ are, for the analyzing filter,

$$(0.03125,\quad 0,\quad -0.28125,\quad 0.5,\quad -0.28125,\quad 0,\quad 0.03125)$$

multiplied by $\sqrt{2}$, and, for the reconstructing wavelet filter,

$$(-0.00390625,\quad 0,\quad 0.0703125,\quad 0.0625,\quad -0.24609375,\quad -0.5625,\quad 1.359375,$$

$$-0.5625,\quad -0.24609375,\quad 0.0625,\quad 0.0703125,\quad 0,\quad -0.00390625)$$

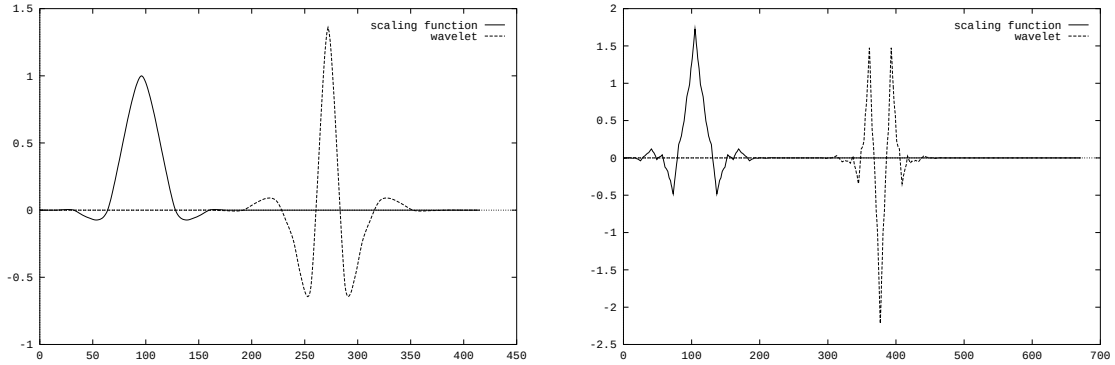

Figure V.3: Pseudocoiflet P_2 scaling function, wavelet and the duals

multiplied by $\frac{1}{\sqrt{2}}$. Note that the application of the analyzing wavelet filter to data has to be shifted by one step from the application of the scaling filter to achieve exact reconstruction.

Examples of the multiresolution approximation and scaling coefficient curves obtained using P_4 are shown in Figure V.4 and below. The approximations obtained using the scaling coefficients are close to the original, at this resolution, at levels 3 and 4 (corresponding to 12.5 % and 6.25 % of the original points). Of course, by using wavelet or scaling coefficients from different levels adaptively, we can approximate more effectively – see the example in Section 3.2.

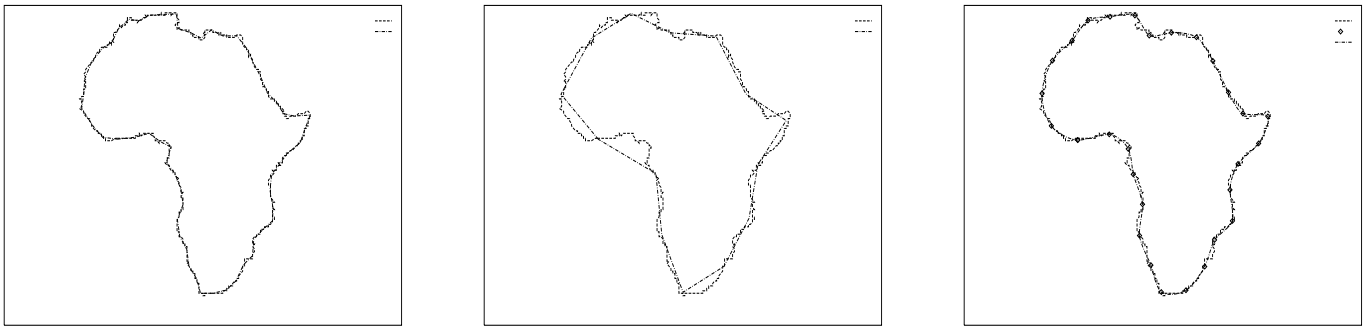

Figure V.4: Selected scaling coefficient curves (levels 3, 5), overlaid on original curve. Level 4 scaling coefficients and multiresolution approximation curve.

3 Applications

3.1 Adaptive scaling coefficient representation

The compact representation of curves and surfaces for use in operations such as display and interference detection presents requirements which are somewhat different from those in data compression. Rather than give a pure wavelet transform as input to these operations, it is useful to approximate the curve or surface by a minimal amount of simple, possibly nonuniform, segments, which can be processed fast. The approximations can be piecewise linear or low order polynomial. The wavelet decomposition is now used to build such compact representations.

A curve can be approximated adaptively using those scaling coefficients which correspond to areas where *all higher level wavelet coefficients are* $< \epsilon$, where ϵ is an arbitrary small threshold (Figure V.5). This means that portions of multiresolution approximation curves from different levels, given by the scaling coefficients as "control points", are pieced together to give an approximation to the whole curve. This approximation is an *adaptive scaling coefficient approximation*.

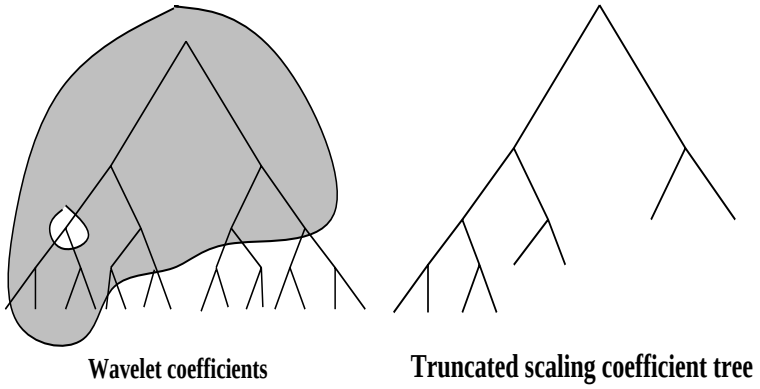

Figure V.5: Wavelet coefficients with large coefficients shaded; corresponding truncated scaling coefficient tree. Isolated small wavelet coefficients have been included in the scaling coefficient representation.

In the worst case, storing the scaling coefficients requires more space than the standard wavelet compression scheme. But for most naturally occurring geometric data, there is little or no difference in compression levels, since areas with small coarse level wavelet coefficients generally tend to have small finer level coefficients as well.

If the threshold changes, the scaling coefficient approximation can now be refined fast by simply adding finer level wavelet coefficients where required by the new threshold. The new scaling coefficients are computed in these areas – scaling coefficients in other areas will not have to be updated, since no coarser level wavelet coefficients are changed.

If the curve has smooth regions, the number of these compressed scaling coefficients can be much smaller than the number of original curve samples. We should note that the number of scaling coefficient "control points" required to accurately represent smooth curve portions decreases with larger numbers of vanishing moments for the underlying wavelet.

If the wavelet is suitably chosen, the scaling coefficients themselves can also constitute good approximations. In this case, an adaptive approximation to the whole curve can be obtained by piecing together portions of the

linearly interpolated scaling coefficients from different levels, as determined by the wavelet decomposition and the given compression threshold. This is a piecewise linear adaptive scaling coefficient approximation.

Again, the number of linear segments approximating the curve is usually much smaller than the original sample size; further, this approximation compares well with standard schemes for the nonuniform subdivision of curves into piecewise linear segments (the scaling coefficient approximation does not constitute an actual subdivision of the curve). The pseudocoiflets P_{2N} of the previous section are good wavelets for use in this application.

The underlying data structure for an adaptive scaling coefficient approximation is a truncated binary tree, the *segment tree*, where the segments are associated with scaling coefficients. The tree corresponds to an adaptive subdivision of the parameter space. Each segment on a given level corresponds to a unique section of the underlying curve or surface; these sections are nested across the scales. The leaves of the truncated scaling coefficient tree represent the underlying compressed surface. This compressed surface can be recovered at the original sampling density by extending the tree to its full binary form (either by point evaluation or by carrying out the complete reconstruction algorithm).

3.2 Example of adaptive approximation using scaling coefficients

The above method effectively sections the curve or surface into regions of different complexity, and allows the curve to be approximated by piecewise linear scaling coefficient curve segments at different levels of refinement. This adaptive approximation is most effective for nonhomogeneous curves, with both smooth segments and areas with significant small resolution detail. Instead of calculating the compressed surface from the scaling coefficients at the original sampling density, the coefficients can be used by themselves in a piecewise approximation. This approximation consists of linear pieces (at the boundaries between regions corresponding to different levels, the endpoints can be equated, since the error of doing this is within the error bound for the approximation).

Figures V.6, V.7 give examples of an adaptive, piecewise linear scaling coefficient approximation to a $\approx$ 5000-point curve obtained from brain scan data[1], using the pseudocoiflet P_4.

The first figure is an illustration. For clarity, the error allowed is large, and only two levels of wavelet decomposition are used. To show the areas from different levels better, the regions have not been connected to one piecewise linear curve.

Wavelet coefficients for both coordinates are used to determine the appropriate scaling coefficient blocks. Most of the curve can be adequately approximated using the lower resolution level, but some sharper corners require the use of higher resolution scaling coefficients. The original curve has 4992 points.

Figure V.7 gives an adaptive scaling coefficient representation of the same 5000 point brain data curve, superimposed on the original data. The number of points in the adaptive representation is 245, for compression of less than 5 %.

[1]Data courtesy of Peter Cahoon, UBC.

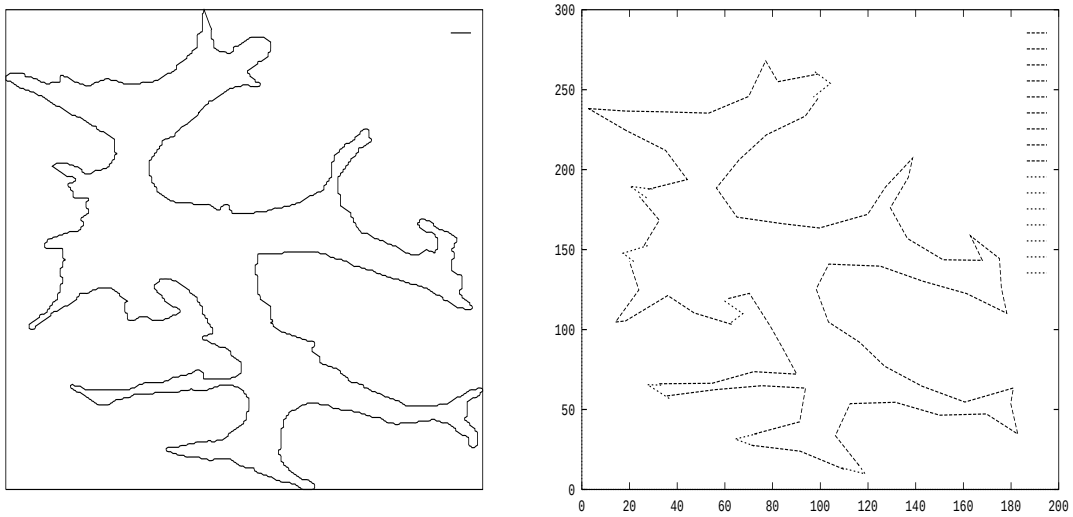

Figure V.6: Original curve and a 2-level adaptive scaling coefficient approximation. Some sections of the curve are approximated with the sparser low resolution scaling coefficients, sharper corners need higher resolution coefficients.

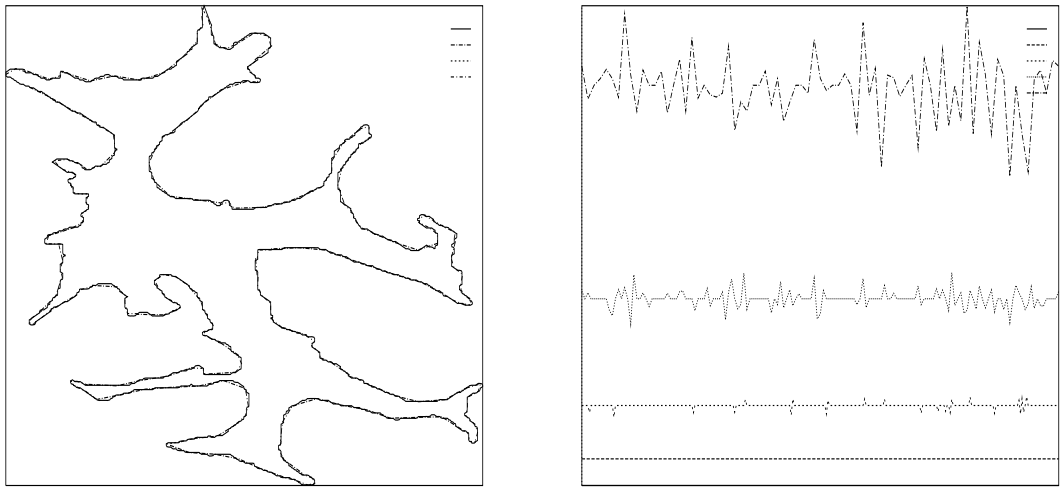

Figure V.7: The original curve superimposed on the adaptive scaling coefficient representation for 5 % compression. Selected levels of the corresponding compressed wavelet coefficients.

3.3 Finding smooth sections of surfaces; natural terrain path planning

The size of the wavelet coefficients can be used to analyze the curve or surface for relative "smoothness". Smooth sections are the ones for which higher level wavelet coefficients are small, that is, the sections which are approximated well by coarser level data.

Figure V.8 shows an example of identifying the smooth sections of a surface representing real terrain data[2]. The sections are found by determining where the finer level coefficients are small. The smooth sections are shown on a coarse level by the marked rectangles. The wavelet used is the pseudocoiflet P_4.

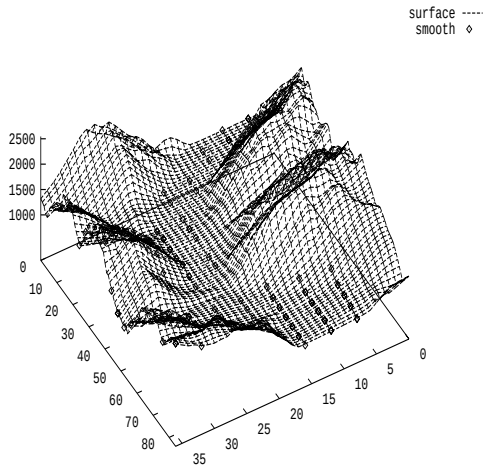

Figure V.8: Identifying smooth surface sections - original surface and smoother sections marked on coarse level scaling coefficients.

A similar idea is used in [151] to hierarchically plan mobile robot paths through natural terrain. Hierarchical planning is a must in these problems due to the large size of the search space. Using wavelets, we can in addition zero in on "nice" terrain sections, while still searching only a coarse data level, and so reduce planning time further. The wavelet coefficients are used to compute hierarchical terrain costs in each region; the costs are a measure of terrain smoothness. These terrain costs, together with a new, nonscalar path measure, are then used to find paths which prefer smoother terrain sections. The cost function can be modified with robot- or terrain-dependent obstacles, and it can be extended to related motion planning problems.

Figure V.9 shows paths planned hierarchically using the real terrain data of the previous example:

3.4 Error estimation

We end with a note on the calculation of error boxes for the adaptive scaling coefficient representation of Section 3.1.

Many operations with curves and surfaces require error boxes for selected regions (this is especially important for intersection and interference detection).

[2]Data from Bob Woodham, UBC.

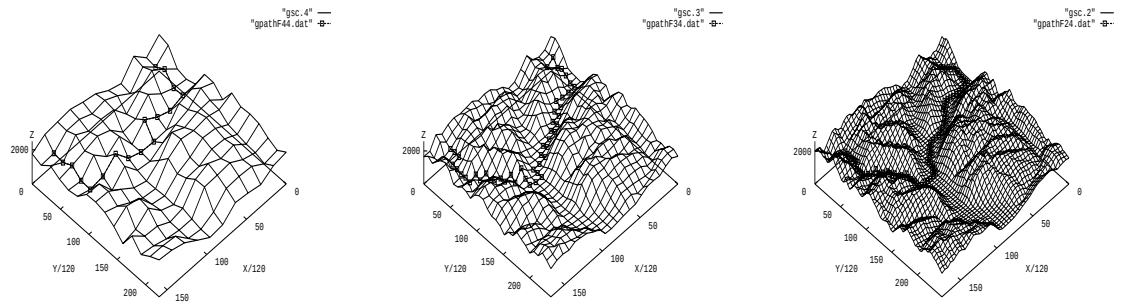

Figure V.9: Hierarchical rough terrain path planning.

There are methods for L^∞ compression, as well as L^p compression for other p ([60]) – but in practice the L^2 approximation and compression obtained by wavelet procedures also gives excellent L^∞ approximations, especially in the absence of discontinuities. We can estimate an upper bound for the distance error from the wavelet coefficients. We briefly discuss this and other methods of determining error boxes here.

3.4.1 Error bounds from wavelet coefficients

Conservative error bounds for a replacing a given curve segment s by an approximating curve on level i can be obtained from the L^∞ errors of the coordinate functions, so we need only look at the approximation errors for a function f of one variable. An upper bound for the L^∞ error of approximating a function f by its multiresolution approximation is obtained very easily from the wavelet coefficients:

Suppose that the component function is f and its wavelet coefficients corresponding to the region s on level i are denoted by $w_i(s) = (w_{ij} : j \in A(s,i))$. These are the coefficients entering into calculations about s. This set is restricted to a set of indices $A(s,i)$, which is determined by the filter length used.

The coefficients of the error in terms of the next level scaling functions, are $w_i^*(s) = \tilde{G} w_i(s)$, where $\tilde{G}$ is the reconstructing wavelet filter. The new coefficients are similarly restricted to a subset of all the coefficients w^*. Let $f_i(s)$ denote the approximation f_i on the segment s, and let $\tilde{\varphi}$ be the reconstructing scaling function. Then the error between a segment and its refinement by one level is given by

$$\text{error}_i(s) \;=\; \|f_{i-1}(s) - f_i(s)\|_\infty \;=\; \max_j \Big| \sum_{j \in A(s,i)} w_{ij} \tilde{\varphi}_{ij} \Big|$$

$$\leqslant\; (\max_j |w_{ij}^*(s)|) \sum_j |\tilde{\varphi}_{ij}|.$$

The quantity $U(\tilde{\varphi}) = \sum_j |\tilde{\varphi}_{ij}|$ can be estimated or calculated for general scaling functions and we have

$$\text{error}_i(s) \leqslant U(\tilde{\varphi})\; \max_j |(w_{ij}^*(s))|.$$

The total error at level i is now bounded simply as

$$\text{TotalError}_i(s) = \sum_{i' \leqslant i} \text{error}_{i'}(s).$$

For positive scaling functions, such as B-splines, $\sum_j |\tilde{\varphi}_{ij}| = 1$, by the partition of unity property, and $\text{error}_i \leqslant \max_j |(w^*_{ij}(s))|$. That is, the error is obtained by adding the maximum reconstructed wavelet coefficient norms on each level.

For pseudocoiflets, the maximum real errors on each level are almost the same as the maximum reconstructed coefficient norms: as can be seen from an example in Figure V.10, the wavelet coefficients, with one step of the reconstruction algorithm performed, give a good approximation of the real error.

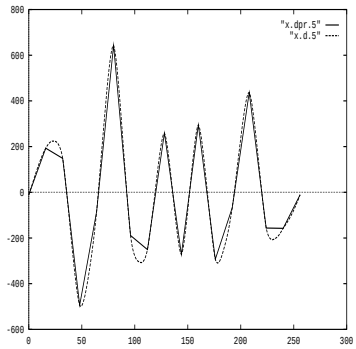

Figure V.10: Real error compared to wavelet coefficients with 1 step reconstruction, using pseudocoiflets

The maximum reconstructed coefficient norm $a = \max_j |w^*_{ij}(s)|$ can also be estimated from the wavelet coefficient maximum $b = \max_j |w_{ij}(s)|$ directly: in the worst case, $a = \sqrt{2}\, b$. This worst case is usually not attained. This procedure gives reasonable (but not minimal) error bounds, especially for smoother sections of curves.

3.4.2 Linearization error

The previous error estimate was valid for approximation curves. For the piecewise linear scaling coefficient curves, the effect of linearizing the approximation curve has to be estimated as well. This linearization error is usually not as large as the error from the wavelet coefficients.

The linearization error can also be computed from the wavelet transform by looking at the difference functions between the real approximation curve and the piecewise linear scaling coefficient curve. The scaling coefficient curve can be formally obtained by applying the hat function as a reconstructing function to the scaling coefficients.

So, the difference functions are obtained by looking at the difference "basis" function $\tilde{\varphi} - \varphi_{\text{hat}}$, where $\tilde{\varphi}$ is the reconstructing scaling function, and φ_{hat} the hat function. Estimating the max norm of this "basis" function, and applying this to the scaling coefficients, gives a bound for the linearization error.

In cases where the above wavelet coefficient estimates do not give sufficiently tight bounds, minimal error regions for replacing a curve section with scaling coefficients can be computed as follows. For

two consecutive scaling coefficients on level L, find the 2^L points on the original curve corresponding to these scaling coefficients, and compute a minimal box aligned with the line segment between the scaling coefficients (the line in the figure), and containing the points ("X"):

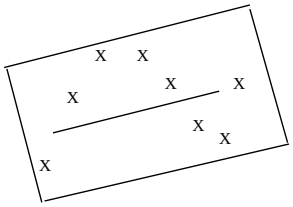

4 Conclusion

We constructed specific wavelets P_{2N}, *pseudocoiflets* ([161]), with interpolating scaling functions. These wavelets are well suited for curve and surface representation. The construction can also be viewed as an example of using the biorthogonal wavelet framework to build "customized" wavelets.

Pseudocoiflets were constructed to provide scaling coefficients which approximate the original curve or surface well. When combined with a wavelet compression approach, this provides simple, accurate approximations using a small number of points. These approximations can be piecewise linear. Such *adaptive scaling coefficient approximations* can then be used in, for instance, display and intersection algorithms. Examples of adaptive scaling coefficient approximations for a curve from brain scan data are given in Section 3.2.

Other applications of wavelets include the analysis of curves and surfaces for relative smoothness. This fact can be used in motion planning: an algorithm for natural terrain path planning for mobile robots using pseudocoiflets has been derived in [151]. We briefly illustrate some results in Section 3.2.

5 Multiresolution Analysis for Surfaces of Arbitrary Topological Type

(Tony D. DeRose, Michael Lounsbery, Joe Warren)

5.1 Introduction

As explained in previous chapters, the simplest setting for multiresolution analysis and wavelets is for representing functions defined on $\mathbb{R}^1$, the entire real line. In most practical applications — including curve modeling — the functions of interest are defined only over a bounded interval $[a, b]$ of the real line, leading various investigators to formulate bounded interval wavelets [29, 50, 75].

Two-dimensional wavelets are important for a variety of applications including image compression. They are generally constructed by forming tensor products of univariate wavelets [50], in much the same way that tensor product B-spline surfaces are formed by products of univariate B-splines. A tensor product of unbounded univariate wavelets leads to wavelets defined on all of $\mathbb{R}^2$; wavelets on a bounded rectangle can likewise be created using a tensor products of bounded interval wavelets. It is also possible to create tensor product wavelets on cylinders and tori by using periodic univariate wavelets in one or both parametric directions.

There also exist non-tensor product constructions for wavelets on $\mathbb{R}^2$ [50, 114], but none of these methods – tensor product or non-tensor product — are applicable to functions defined on more general topological domains, such as spheres or surfaces of genus larger than one. Thus, existing methods are not well suited for decomposing and compressing surfaces such as the ones shown in Color Plates 1 and 2, since they are described by parametric functions on the sphere.

In this chapter we sketch some of the ideas necessary for extending multiresolution analysis and wavelets to surfaces of arbitrary topological type.[3] (For a more complete description of the work, see Lounsbery *et al.* [125].) Our extension is based on the use of subdivision surfaces, the first instances of which were introduced in 1978 by Catmull and Clark [19] and simultaneously by Doo and Sabin [69, 68].

The generalization of wavelets to arbitrary topological surfaces considerably extends the class of applications to which multiresolution analysis can be applied, including:

- Continuous level-of-detail control. When a complex shape is rendered in an animation, a fully detailed representation of the shape contains much more detail than is required for all but the closest view. Using a compressed wavelet representation of complex objects, it is possible to greatly reduce the number of polygons in a scene without significantly impacting the visible detail (see Color Plate 1). Moreover, it is possible to smoothly vary the detail, avoiding the discontinuous jumps that occur when suddenly switching between distinct models. This application is discussed in more detail in Section 5.7.
- Compression of functions defined on surfaces. Consider the situation shown in Color Plate 2 where a globe (a geometric sphere) is pseudo-colored according to elevation. The pseudo-coloring can be thought of as a function that maps each point on the sphere to an *RGB* triple. A straightforward method for storing the function is to store its value at a large number of regularly distributed points; in this case more than one million points were used. The methods in this paper can be used to create compressed wavelet approximations of varying complexity. (The mesh lines on the original surface are so dense that the image shown in Color Plate 2(h) is nearly black.)

[3] The topological type of a two-dimensional surface refers to its genus, presence of boundary curves, etc.

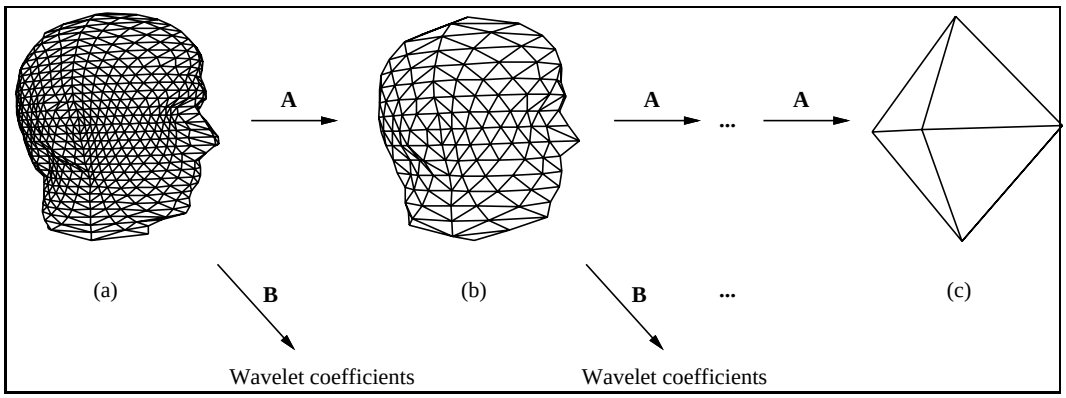

Figure V.11: Decomposition of a polyhedral surface.

– Multiresolution editing of surfaces. Hierarchical B-splines, as introduced by Forsey and Bartels [82], provide a powerful mechanism for editing shapes at various levels of detail. However, hierarchical B-splines can only represent a restricted class of surface topologies. The methods described here provide an alternative to hierarchical B-splines, and are capable of representing smooth multiresolution surfaces of arbitrary topological type. Editing at fractional levels of detail can also be achieved by using the methods developed by Finkelstein and Salesin [75].

5.2 A preview of the method

Although the mathematical underpinnings of multiresolution analysis of surfaces are somewhat involved, the resulting algorithms are relatively simple. Before diving into the mathematical details, we give here a brief description of how the method can be applied to decompose the polyhedral object shown in Figure V.11(a). (Although all our examples use C^0 surfaces, the theory works equally well for C^1 subdivision surfaces.)

As described in previous chapters, a main idea behind multiresolution analysis is the decomposition of a function (in this case a polyhedron expressed as a parametric function on the sphere) into a low resolution part and a "detail" part. The low resolution part of the polyhedron in Figure V.11(a) is shown in Figure V.11(b). The vertices in (b) are computed as certain weighted averages of the vertices in (a). These weighted averages essentially implement a low pass filter denoted as $\mathbf{A}$. The detail part naturally consists of a collection wavelet coefficients, computed as weighted differences of the vertices in (a). These differencing weights form a high-pass filter $\mathbf{B}$. The decomposition process (often referred to as *analysis*), can be used to further split (b) into an even lower resolution version and corresponding wavelet coefficients, resulting in a typical filter bank procedure.

The analysis filters $\mathbf{A}$ and $\mathbf{B}$ are constructed so that the original polyhedron can be recovered exactly from the low resolution version and the wavelet coefficients. Recovery (often called *synthesis*) proceeds by refining each triangle of (b) into four subtriangles by introducing new vertices at edge midpoints, followed by perturbing the resulting collection of vertices according to the wavelet coefficients. The refining and perturbing steps are described by two synthesis filters $\mathbf{P}$ (the refining filter) and $\mathbf{Q}$ (the perturbing filter).

The trick is to develop the four analysis and synthesis filters so that: (1) the low resolution versions are good approximations to the original object (in a least-squares sense), (2) the magnitude of a wavelet coefficient

reflects a coefficient's importance by measuring the error introduced when the coefficient is set to zero, and (3) analysis and synthesis filter banks should have time complexity linear in the number of vertices.

5.3 Our view of multiresolution analysis

To formulate multiresolution analysis for surfaces of arbitrary topological type, we must use a fairly general, but unfortunately abstract, view of multiresolution analysis. The bare essence of multiresolution analysis is contained in two basic ingredients: an infinite chain of nested linear function spaces $V^0 \subset V^1 \subset V^2 \subset \cdots$ and an inner product $\langle f, g \rangle$ defined on any pair of functions $f, g \in V^j$, for some $j < \infty$.

The inner product is used to define the orthogonal complement or *wavelet spaces* W^j as

$$W^j := \{f \in V^{j+1} \mid \langle f, g \rangle = 0 \ \forall g \in V^j\}.$$

The following terminology is now standard: scaling functions, denoted by φ's, refer to bases for the spaces V^j, and wavelets, denoted by ψ's, refer to bases for the wavelet spaces W^j. Note that we do not require the scaling functions or wavelets to form orthonormal bases. As shown in Section 5.6.3, the analysis and synthesis filters are determined by considering various ways of changing bases between scaling functions and wavelets.

5.4 Nested linear spaces through subdivision

When formulating multiresolution analysis on the entire real line, the nested sequence of linear spaces required by multiresolution analysis are generally obtained by defining a single scaling function $\varphi(x)$ that satisfies a refinement equation of the form

$$\varphi(x) = \sum_i p_i \, \varphi(2x - i)$$

for some fixed constants p_i. The refinement equation (sometimes called a two-scale relation) guarantees that the spaces defined as

$$V^j := \text{Span}\{\varphi(2^j x - i) \mid i = -\infty, ..., \infty\}$$

are nested. In other words, the nested spaces are generated by translations and dilations of a single refinable function $\varphi(x)$.

To generalize these ideas to domains of arbitrary topological type one could attempt to make definitions for what it means to dilate and translate a function on an arbitrary topological domain. One could then try to find a refinable scaling function and proceed as before to define orthogonal complements, wavelets, and so on. We have instead chosen what appears to be a simpler approach.

In this section, we use recursive subdivision to define a collection of functions $\varphi_i^j(\mathbf{x})$ that are refinable in the sense that each function with superscript j lies in the span of the functions with superscript $j + 1$; the argument $\mathbf{x}$ is a point that ranges over a domain 2-manifold of arbitrary topological type. In one respect, this is a generalization of the approach taken by Daubechies in that her locally supported orthogonal scaling functions are also defined through a recursive subdivision procedure. Although in general the $\varphi^{j+1}(\mathbf{x})$ are not simple dilates of the $\varphi^j(\mathbf{x})$, we can nonetheless use them to define a sequence of nested spaces.

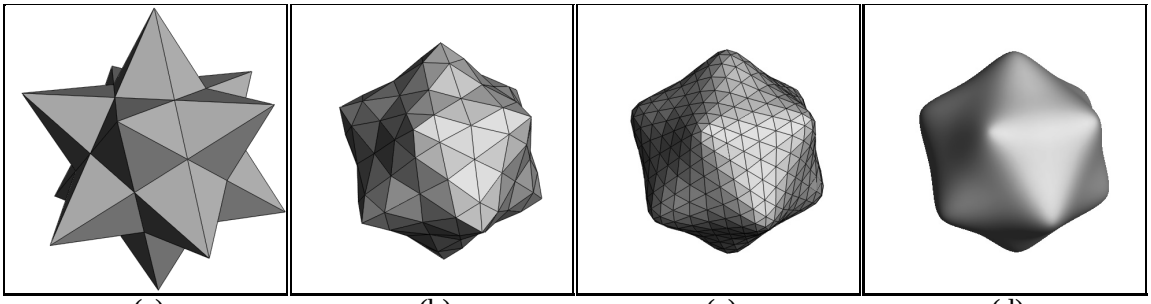

Figure V.12: Loop's subdivision scheme: (a) the control mesh M^0, (b) the mesh M^1 after one subdivision step, (c) the mesh M^2, (d) the limit surface.

5.4.1 Subdivision surfaces

Intuitively speaking, subdivision surfaces are defined by iteratively refining a control polyhedron M^0 so that the sequence of increasingly faceted polyhedra $M^1, M^2, ...$ converge to some limit surface $S = M^\infty$. In each subdivision step, the vertices of M^{j+1} are computed as affine combinations of the vertices of M^j. Thus, if $\mathbf{V}^j$ is a matrix whose i-th row consists of the x, y, and z coordinates of vertex i of M^j, there exists a non-square matrix of constants $\mathbf{P}^j$ such that

$$\mathbf{V}^{j+1} = \mathbf{P}^j \mathbf{V}^j. \tag{11}$$

The matrix $\mathbf{P}^j$ therefore characterizes the subdivision method. The beauty of subdivision surface schemes is that the entries of $\mathbf{P}^j$ depend only on the connectivity of the vertices in M^0, not on the geometric positions of the vertices.

The simplest example of such a scheme is polyhedral subdivision. Given a polyhedron M^0 with triangular faces, a new polyhedron M^1 is built by splitting each triangular face of M^0 into four subfaces as in Figure V.13. The matrix $\mathbf{P}^0$ characterizing the first subdivision step is also shown in Figure V.13. Running this subdivision scheme for j steps on an initial triangular mesh M^0 produces a mesh M^j. M^j includes the vertices of M^0 together with new vertices introduced through subdivision.

Polyhedral subdivision converges to the original polyhedron M^0, that is, to a C^0 surface. However, other schemes have been developed that converge to C^1 limit surfaces that either approximate or interpolate the vertices of M^0. Subdivision schemes can be further categorized as being either *primal* or *dual*. A subdivision scheme is primal if the faces of the mesh are split into subfaces by the refinement procedure. Catmull-Clark subdivision [19, 100] is a primal scheme based on subdivision of quadrilateral faces. Polyhedral subdivision, the butterfly scheme of Dyn, Gregory, and Levin [72] and Loop's method [106, 123] are primal schemes based on subdivision of triangular faces. A scheme is dual if the structure of the refined mesh is obtained by doing a primal subdivision followed by taking the polyhedral dual of the result. Doo-Sabin subdivision [69, 68] is a dual scheme based on quadrilaterals. For simplicity we shall restrict the discussion to primal triangular subdivision schemes, although our results hold more generally for any primal scheme.

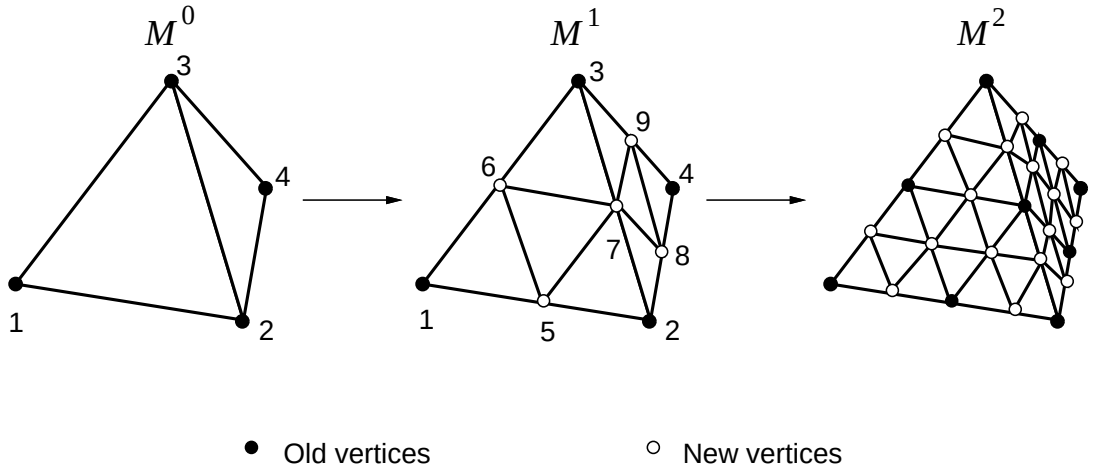

$$\mathbf{P}^0 = \begin{pmatrix} \mathbf{O}^0 \\ \hline \mathbf{N}^0 \end{pmatrix} = \left(\begin{array}{cccc} 1 & 0 & 0 & 0 \\ 0 & 1 & 0 & 0 \\ 0 & 0 & 1 & 0 \\ 0 & 0 & 0 & 1 \\ \hline \frac{1}{2} & \frac{1}{2} & 0 & 0 \\ \frac{1}{2} & 0 & \frac{1}{2} & 0 \\ 0 & \frac{1}{2} & \frac{1}{2} & 0 \\ 0 & \frac{1}{2} & 0 & \frac{1}{2} \\ 0 & 0 & \frac{1}{2} & \frac{1}{2} \\ \frac{1}{2} & 0 & 0 & \frac{1}{2} \end{array}\right) \quad \mathbf{Q}^0 = \begin{pmatrix} -\frac{3}{8} & -\frac{3}{8} & \frac{1}{8} & \frac{1}{8} & \frac{1}{8} & -\frac{3}{8} \\ -\frac{3}{8} & \frac{1}{8} & -\frac{3}{8} & -\frac{3}{8} & \frac{1}{8} & \frac{1}{8} \\ \frac{1}{8} & -\frac{3}{8} & -\frac{3}{8} & \frac{1}{8} & -\frac{3}{8} & \frac{1}{8} \\ \frac{1}{8} & \frac{1}{8} & \frac{1}{8} & -\frac{3}{8} & -\frac{3}{8} & -\frac{3}{8} \\ \frac{5}{8} & -\frac{1}{8} & -\frac{1}{8} & -\frac{1}{8} & \frac{1}{8} & -\frac{1}{8} \\ -\frac{1}{8} & \frac{5}{8} & -\frac{1}{8} & \frac{1}{8} & -\frac{1}{8} & -\frac{1}{8} \\ -\frac{1}{8} & -\frac{1}{8} & \frac{5}{8} & -\frac{1}{8} & -\frac{1}{8} & \frac{1}{8} \\ -\frac{1}{8} & \frac{1}{8} & -\frac{1}{8} & \frac{5}{8} & -\frac{1}{8} & -\frac{1}{8} \\ \frac{1}{8} & -\frac{1}{8} & -\frac{1}{8} & -\frac{1}{8} & \frac{5}{8} & -\frac{1}{8} \\ -\frac{1}{8} & -\frac{1}{8} & \frac{1}{8} & -\frac{1}{8} & -\frac{1}{8} & \frac{5}{8} \end{pmatrix}$$

$$\begin{pmatrix} \mathbf{A}^0 \\ \hline \mathbf{B}^0 \end{pmatrix} = \left(\begin{array}{cccccccccc} \frac{7}{16} & -\frac{1}{16} & -\frac{1}{16} & -\frac{1}{16} & \frac{3}{8} & \frac{3}{8} & -\frac{1}{8} & -\frac{1}{8} & -\frac{1}{8} & \frac{3}{8} \\ -\frac{1}{16} & \frac{7}{16} & -\frac{1}{16} & -\frac{1}{16} & \frac{3}{8} & -\frac{1}{8} & \frac{3}{8} & \frac{3}{8} & -\frac{1}{8} & -\frac{1}{8} \\ -\frac{1}{16} & -\frac{1}{16} & \frac{7}{16} & -\frac{1}{16} & -\frac{1}{8} & \frac{3}{8} & \frac{3}{8} & -\frac{1}{8} & \frac{3}{8} & -\frac{1}{8} \\ -\frac{1}{16} & -\frac{1}{16} & -\frac{1}{16} & \frac{7}{16} & -\frac{1}{8} & -\frac{1}{8} & -\frac{1}{8} & \frac{3}{8} & \frac{3}{8} & \frac{3}{8} \\ \hline -\frac{1}{2} & -\frac{1}{2} & 0 & 0 & 1 & 0 & 0 & 0 & 0 & 0 \\ -\frac{1}{2} & 0 & -\frac{1}{2} & 0 & 0 & 1 & 0 & 0 & 0 & 0 \\ 0 & -\frac{1}{2} & -\frac{1}{2} & 0 & 0 & 0 & 1 & 0 & 0 & 0 \\ 0 & -\frac{1}{2} & 0 & -\frac{1}{2} & 0 & 0 & 0 & 1 & 0 & 0 \\ 0 & 0 & -\frac{1}{2} & -\frac{1}{2} & 0 & 0 & 0 & 0 & 1 & 0 \\ -\frac{1}{2} & 0 & 0 & -\frac{1}{2} & 0 & 0 & 0 & 0 & 0 & 1 \end{array}\right)$$

$$\mathbf{I}^0 = \begin{pmatrix} 1 & \frac{1}{3} & \frac{1}{3} & \frac{1}{3} \\ \frac{1}{3} & 1 & \frac{1}{3} & \frac{1}{3} \\ \frac{1}{3} & \frac{1}{3} & 1 & \frac{1}{3} \\ \frac{1}{3} & \frac{1}{3} & \frac{1}{3} & 1 \end{pmatrix} \quad \boldsymbol{\alpha}^0 = \begin{pmatrix} \frac{3}{8} & \frac{3}{8} & -\frac{1}{8} & -\frac{1}{8} & -\frac{1}{8} & \frac{3}{8} \\ \frac{3}{8} & -\frac{1}{8} & \frac{3}{8} & \frac{3}{8} & -\frac{1}{8} & -\frac{1}{8} \\ -\frac{1}{8} & \frac{3}{8} & \frac{3}{8} & -\frac{1}{8} & \frac{3}{8} & -\frac{1}{8} \\ -\frac{1}{8} & -\frac{1}{8} & -\frac{1}{8} & \frac{3}{8} & \frac{3}{8} & \frac{3}{8} \end{pmatrix}$$

Figure V.13: Polyhedral subdivision of a tetrahedron and various associated filters

5.4.2 Basis functions from subdivision

All subdivision schemes we have mentioned converge to either C^0 or C^1 surfaces. In such a case, it is possible to show that the resulting limit surface can be parametrized using a function $S(\mathbf{x})$, where $\mathbf{x}$ is a point that ranges over the faces of the initial mesh M^0 [125]. The initial mesh M^0 therefore serves as the parameter domain for the limit surface. Specifically, it can be shown [125] that for any $j \geqslant 0$, and any point $\mathbf{x}$ on some face of M^0, $S(\mathbf{x})$ can be written as

$$S(\mathbf{x}) = \sum_i v_i^j \varphi_i^j(\mathbf{x}), \tag{12}$$

where v_i^j denotes the i-th vertex of M^j. The scaling functions $\varphi_i^j(\mathbf{x})$ depend on the subdivision rules used, and in general are defined through a limiting procedure. Although they are well defined and continuous if the subdivision scheme converges to a C^0 surface, they generally cannot be expressed as polynomials, or in any other closed form.

It is generally helpful to write Equation 12 in matrix form as

$$S(\mathbf{x}) = \mathbf{\Phi}^j(\mathbf{x})\ \mathbf{V}^j \tag{13}$$

where $\mathbf{\Phi}^j(\mathbf{x})$ denotes the row matrix of scaling functions $\varphi_i^j(\mathbf{x})$, and where $\mathbf{V}^j$ is as in Equation 11. These scaling functions can also be shown to satisfy the *refinement relation*

$$\mathbf{\Phi}^j(\mathbf{x}) = \mathbf{\Phi}^{j+1}(\mathbf{x})\ \mathbf{P}^j. \tag{14}$$

For primal subdivision schemes, it is convenient to express Equation 14 in block matrix form by writing $\mathbf{\Phi}^{j+1}(\mathbf{x})$ as

$$\mathbf{\Phi}^{j+1}(\mathbf{x}) = (\mathcal{O}^{j+1}(\mathbf{x})\ \ \mathcal{N}^{j+1}(\mathbf{x})) \tag{15}$$

where $\mathcal{O}^{j+1}(\mathbf{x})$ consists of all scaling functions $\varphi_i^{j+1}(\mathbf{x})$ associated with the "old" vertices of M^j (the black vertices in Figure V.13) and $\mathcal{N}^{j+1}(\mathbf{x})$ consists of the remaining scaling functions associated with the "new" vertices added when obtaining M^{j+1} from M^j (the white vertices in Figure V.13). Equation 14 can now be expressed in block matrix form:

$$\mathbf{\Phi}^j(\mathbf{x}) = (\mathcal{O}^{j+1}(\mathbf{x})\ \ \mathcal{N}^{j+1}(\mathbf{x})) \begin{pmatrix} \mathbf{O}^j \\ \mathbf{N}^j \end{pmatrix}. \tag{16}$$

The block matrix decomposition of $\mathbf{P}^0$ for the example tetrahedron appears in Figure V.13.

5.4.3 Nested linear spaces

Given these relations, a chain of nested linear spaces $V^j(M^0)$ associated with a mesh M^0 can now be defined as follows:

$$V^j(M^0) := \text{Span}(\mathbf{\Phi}^j(\mathbf{x}))$$

Equation 14 implies that these spaces are indeed nested; that is,

$$V^0(M^0) \subset V^1(M^0) \subset \cdots.$$

The notation $V^j(M^0)$ is to emphasize that the linear spaces are adapted to M^0 in that they consist of real-valued functions having M^0 as the domain.

5.5 Inner products over subdivision surfaces

Given a chain of nested linear spaces, the other necessary ingredient for the creation of a multiresolution analysis is the existence of an inner product on these spaces. In this section, we define an inner product and describe at a high level a simple method for computing the inner product of functions defined through subdivision. A detailed treatment is presented in Lounsbery *et al.* [125].

5.5.1 Definition

Given two functions $f, g \in V^j(M^0)$, $j < \infty$, (with some foresight) we define their inner product to be

$$\langle f, g \rangle := \sum_{\tau \in \Delta(M^0)} \frac{1}{\text{Area}(\tau)} \int_{\mathbf{x} \in \tau} f(\mathbf{x})\, g(\mathbf{x})\, d\mathbf{x}$$

where $d\mathbf{x}$ is a differential area, and where $\Delta(M^0)$ denotes the set of triangular faces of M^0.

This definition of inner product implies that the faces of M^0 are weighted equally; that is, the inner product is independent of the geometric positions of the vertices of M^0. This has an important practical consequence: the wavelet spaces are invariant of the geometry of the mesh, meaning that a significant amount of precomputation of inner products and wavelets can be done.

An alternative definition is to weight the inner product by areas of triangles in M^0; however, such an approach has the practical drawback that much less precomputation is possible.

5.5.2 Computation

For any given f, g, one could estimate the inner product $\langle f, g \rangle$ using numerical cubature. It turns out, however, that it is possible to compute $\langle f, g \rangle$ *exactly* if f and g are given as expansions in φ_i^j:

$$f(\mathbf{x}) = \sum_i f_i^j \varphi_i^j(\mathbf{x}) \qquad\qquad g(\mathbf{x}) = \sum_i g_i^j \varphi_i^j(\mathbf{x}).$$

Bi-linearity of the inner product allows $\langle f, g \rangle$ to be written in matrix form as

$$\langle f, g \rangle = \mathbf{g}^T \mathbf{I}^j \mathbf{f}, \tag{17}$$

where $\mathbf{f}$ and $\mathbf{g}$ are column matrices consisting of the coefficients of f and g, respectively, and where $\mathbf{I}^j$ is the square matrix whose i, i'-th entry is $(\mathbf{I}^j)_{i,i'} = \langle \varphi_i^j, \varphi_{i'}^j \rangle$. The inner product matrix $\mathbf{I}^0$ for the example tetrahedron appears in Figure V.13.

If the subdivision matrices $\mathbf{P}^j$ are sparse, the scaling functions in $\mathbf{\Phi}^j(\mathbf{x})$ will be locally supported, meaning that $\mathbf{I}^j$ is also sparse. We show in Lounsbery *et al.* [125] that the entries of $\mathbf{I}^j$ can be computed exactly simply by solving a system of linear equations. This result is somewhat surprising since there is no closed form expression for the scaling functions — they are known only as limit functions defined through subdivision.

Without going too far into the details, the basic idea behind the exact integration procedure is to establish

the following linear recurrence that relates $\mathbf{I}^j$ to $\mathbf{I}^{j+1}$:

$$\mathbf{I}^j = (\mathbf{P}^j)^T \, \mathbf{I}^{j+1} \, \mathbf{P}^j, \qquad j = 0, ...$$

Since $\mathbf{P}^j$ is known, the only unknowns in the above equation are the entries of the $\mathbf{I}$s. It turns out that the infinite chain of recurrences has only a finite number of distinct entries (up to a common scale factor), meaning that a finite linear system can be solved to determine these entries.

Once the entries of each of the inner product matrices have been determined, an arbitrary integral such as $\langle f, g \rangle$ can be be computed exactly using Equation 17.

5.6 Multiresolution analysis based on subdivision

Having established nested linear spaces and an inner product, we are now in a position to define our wavelets spaces as

$$W^j(M^0) \; := \; \{f \in V^{j+1}(M^0) \mid \langle f, g \rangle = 0 \;\; \forall g \in V^j(M^0)\}.$$

and to construct wavelets, that is, sets of functions $\mathbf{\Psi}^j(\mathbf{x}) = (\psi_1^j(\mathbf{x}), \psi_2^j(\mathbf{x}), ...)$ spanning the spaces $W^j(M^0)$. (The elements of $\mathbf{\Psi}^j(\mathbf{x})$ we construct are not mutually orthogonal. Some authors, including Chui [26], refer to such functions as *pre-wavelets*.)

5.6.1 The construction

Our construction consists of two steps. First, we build a basis for $V^{j+1}(M^0)$ using the scaling functions $\mathbf{\Phi}^j(\mathbf{x})$ and the "new" scaling functions $\mathcal{N}^{j+1}(\mathbf{x})$ in $V^{j+1}(M^0)$. It is straightforward to show that the $\mathbf{\Phi}^j(\mathbf{x})$ and $\mathcal{N}^{j+1}(\mathbf{x})$ together span $V^{j+1}(M^0)$ if and only if the matrix $\mathbf{O}^j$ is invertible. Most primal subdivision methods such as polyhedral subdivision and the butterfly method have this property.[4] Given a function $S^{j+1}(\mathbf{x})$ in $\mathbf{V}^{j+1}(M^0)$ expressed as an expansion in the basis $(\mathbf{\Phi}^j(\mathbf{x}) \;\; \mathcal{N}^{j+1}(\mathbf{x}))$, an approximation in $V^j(M^0)$ can be obtained by *restriction to* $\mathbf{\Phi}^j(\mathbf{x})$, that is, by setting to zero the coefficients corresponding to $\mathcal{N}^{j+1}(\mathbf{x})$. However, this generally does not produce the best least-squares approximation.

To ensure the best least-squares approximation after restriction to $\mathbf{\Phi}^j(\mathbf{x})$, we orthogonalize the new basis functions $\mathcal{N}^{j+1}(\mathbf{x})$ by computing their projection into $W^j(M^0)$. The resulting functions $\mathbf{\Psi}^j(\mathbf{x})$ are wavelets since they form a basis for $W^j(M^0)$. Expressed in matrix form,

$$\mathcal{N}^{j+1}(\mathbf{x}) = \mathbf{\Psi}^j(\mathbf{x}) + \mathbf{\Phi}^j(\mathbf{x}) \, \boldsymbol{\alpha}^j, \tag{18}$$

where $\boldsymbol{\alpha}^j$ is a matrix of yet to be determined coefficients. Figure V.14 is a plot of one such wavelet for the case of polyhedral subdivision. If $S^{j+1}(\mathbf{x})$ is expanded in terms of $\mathbf{\Phi}^j(\mathbf{x})$ and $\mathbf{\Psi}^j(\mathbf{x})$, then the restriction of $S^{j+1}(\mathbf{x})$ to $\mathbf{\Phi}^j(\mathbf{x})$ is guaranteed to be the best approximation to $S^{j+1}(\mathbf{x})$ in $V^j(M^0)$ in a least-squares sense.

[4] One notable exception is Catmull-Clark subdivision for vertices with three incident edges. However, the subdivision rule for such vertices can be easily modified to produce an invertible matrix.

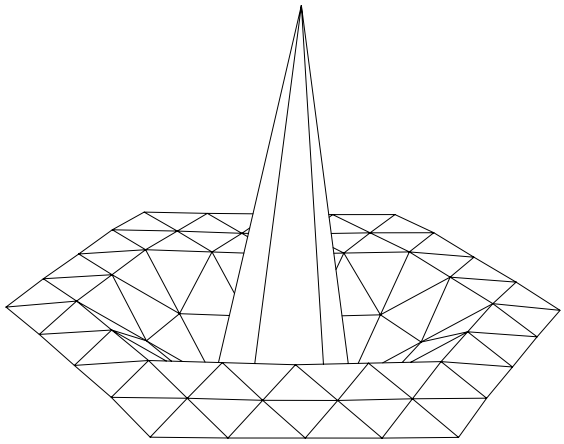

Figure V.14: A polyhedral wavelet centered on a vertex with 6 incident edges.

5.6.2 Computation of wavelets

The coefficients $\boldsymbol{\alpha}^j$ are the solution to the linear system formed by taking the inner product of each side of Equation 18 with $\boldsymbol{\Phi}^j(\mathbf{x})$:

$$\begin{aligned} \langle \boldsymbol{\Phi}^j(\mathbf{x}), \boldsymbol{\Phi}^j(\mathbf{x}) \rangle \, \boldsymbol{\alpha}^j &= \langle \boldsymbol{\Phi}^j(\mathbf{x}), \mathcal{N}^{j+1}(\mathbf{x}) \rangle, \\ &= (\mathbf{P}^j)^T \, \langle \boldsymbol{\Phi}^{j+1}(\mathbf{x}), \mathcal{N}^{j+1}(\mathbf{x}) \rangle \end{aligned} \tag{19}$$

where $\langle \mathbf{F}, \mathbf{G} \rangle$ stands for the matrix whose i, i'-th entry is $\langle (\mathbf{F})_i, (\mathbf{G})_{i'} \rangle$. The matrix $\langle \boldsymbol{\Phi}^j(\mathbf{x}), \boldsymbol{\Phi}^j(\mathbf{x}) \rangle$ is therefore simply $\mathbf{I}^j$, and the matrix $\langle \boldsymbol{\Phi}^{j+1}(\mathbf{x}), \mathcal{N}^{j+1}(\mathbf{x}) \rangle$ is a submatrix of $\mathbf{I}^{j+1}$ consisting of those columns corresponding to members of $\mathcal{N}^{j+1}(\mathbf{x})$. The matrix $\boldsymbol{\alpha}^0$ for the example tetrahedron appears in Figure V.13.

Two difficulties arise in solving this system of equations. First, the inner product matrix $\mathbf{I}^j$ must be inverted. Second, the inverse of $\mathbf{I}^j$ is dense even though $\mathbf{I}^j$ is sparse. As a consequence, the resulting wavelets are globally supported on M^0, implying that straightforward implementations of filter bank decomposition and reconstruction algorithms would require quadratic time. We currently do not know of a construction leading to unique locally supported wavelets, nor do we know if such a construction always exists. Our approach for now, which is relatively common in practice and has worked very well in our level-of-detail control experiments described in Section 5.7, is to obtain locally supported functions by relaxing the condition that the $\psi_i^j(\mathbf{x})$'s lie exactly in $W^j(M^0)$. Instead, we construct them to span a space W_*^j that is some (non-orthogonal) complement of $V^j(M^0)$ in $V^{j+1}(M^0)$. We show below that it is possible to make $W_*^j(M^0)$ close to $W^j(M^0)$, at the expense of increasing the supports of the quasi-wavelets.

Our wavelets are constructed by selecting their supports *a priori*. For each $\psi_i^j(\mathbf{x})$, those members of $\boldsymbol{\Phi}^j(\mathbf{x})$ whose supports are sufficiently distant from the support of $(\mathcal{N}^{j+1})_i$ have their corresponding coefficients in the i-th column of $\boldsymbol{\alpha}^j$ set to zero. The remaining non-zero coefficients can be found by solving a smaller, local variant of Equation 19. By allowing more of the coefficients of $\boldsymbol{\alpha}^j$ to be non-zero, the supports grow, and $W_*^0(M^0)$ approaches $W^0(M^0)$.

5.6.3 A filter bank algorithm

Analysis and synthesis filters for multiresolution analysis on the infinite real line are spatially invariant, meaning that they can be represented by a convolution kernel, that is, by a sequence of real numbers. This is not the case for multiresolution analysis on arbitrary topological domains. The filter coefficients in general must vary over the mesh, so the filters are represented by (hopefully sparse) matrices.

The analysis and synthesis filters can be conveniently expressed using block matrix equations. Let $\mathbf{\Psi}^j(\mathbf{x})$ denote the row matrix of wavelets spanning $W_*^j(M^0)$. For any multiresolution analysis the synthesis filters are defined by the relation

$$\left(\mathbf{\Phi}^j(\mathbf{x}) \;\; \mathbf{\Psi}^j(\mathbf{x})\right) = \mathbf{\Phi}^{j+1}(\mathbf{x}) \begin{pmatrix} \mathbf{P}^j & \mathbf{Q}^j \end{pmatrix}, \tag{20}$$

and the analysis filters are obtained from the inverse relation

$$\begin{pmatrix} \mathbf{A}^j \\ \mathbf{B}^j \end{pmatrix} = \begin{pmatrix} \mathbf{P}^j & \mathbf{Q}^j \end{pmatrix}^{-1}. \tag{21}$$

For our construction it is again convenient to write $\mathbf{\Phi}^{j+1}(x)$ in block form as $(\mathcal{O}^{j+1}(\mathbf{x})\, \mathcal{N}^{j+1}(\mathbf{x}))$. It then follows from Equation 18 that our synthesis filters can be written in block form as

$$\begin{pmatrix} \mathbf{P}^j & \mathbf{Q}^j \end{pmatrix} = \begin{pmatrix} \mathbf{O}^j & -\mathbf{O}^j\, \boldsymbol{\alpha}^j \\ \mathbf{N}^j & \mathbf{1} - \mathbf{N}^j\, \boldsymbol{\alpha}^j \end{pmatrix}, \tag{22}$$

where $\mathbf{1}$ denotes the identity matrix. The analysis filters are obtained from Equation 21. Examples are shown for the tetrahedron in Figure V.13.

From a practical standpoint, it is critical that the analysis and synthesis matrices are sparse. To achieve linear time decomposition and reconstruction, they must each have a constant number of non-zero entries in each row. If $\mathbf{P}^j$ and $\boldsymbol{\alpha}^j$ are sparse, then $\mathbf{Q}^j$ is sparse. Unfortunately, the analysis filters derived from Equation 21 need not be sparse. For interpolating subdivision schemes such as polyhedral subdivision and the C^1 "butterfly" scheme of Dyn et. al. [72], the situation is much improved. Such interpolating schemes have the property that $\mathbf{O}^j$ is the identity matrix. Equation 22 in this case simplifies greatly; the resulting filters are

$$\begin{pmatrix} \mathbf{P}^j & \mathbf{Q}^j \end{pmatrix} = \begin{pmatrix} \mathbf{1} & -\boldsymbol{\alpha}^j \\ \mathbf{N}^j & \mathbf{1} - \mathbf{N}^j\, \boldsymbol{\alpha}^j \end{pmatrix} \qquad \begin{pmatrix} \mathbf{A}^j \\ \mathbf{B}^j \end{pmatrix} = \begin{pmatrix} \mathbf{1} - \boldsymbol{\alpha}^j\, \mathbf{N}^j & \boldsymbol{\alpha}^j \\ -\mathbf{N} & \mathbf{1} \end{pmatrix}.$$

If $\mathbf{P}^j$ and $\boldsymbol{\alpha}^j$ are sparse, then all four filters are also sparse. The situation is less desirable for methods related to B-splines, such as Loop's scheme and Catmull-Clark surfaces. For these subdivision schemes, the synthesis filters are sparse, but the analysis filters are dense. Making these methods efficient for multiresolution analysis is a topic of future research.

The analysis filters can be used to decompose a surface $S^{j+1}(\mathbf{x})$ in $V^{j+1}(M^0)$ given by

$$S^{j+1}(\mathbf{x}) = \sum_i v_i^{j+1} \varphi_i^{j+1}(\mathbf{x}) \tag{23}$$

into a lower resolution part in $V^j(M^0)$ plus a detail part in $W_*^j(M^0)$

$$S^{j+1}(\mathbf{x}) = \sum_i v_i^j \varphi_i^j(\mathbf{x}) + \sum_i w_i^j \psi_i^j(\mathbf{x})$$

as follows. Let $\mathbf{V}^j$ be as in Equation 13, and let $\mathbf{W}^j$ denote the corresponding matrix of wavelet coefficients w_i^j. We can rewrite Equation 23 in matrix form and substitute the definition of the analysis filters:

$$\begin{aligned} S^{j+1}(\mathbf{x}) &= \mathbf{\Phi}^{j+1}(\mathbf{x})\ \mathbf{V}^{j+1} \\ &= \left(\mathbf{\Phi}^j(\mathbf{x})\ \mathbf{\Psi}^j(\mathbf{x})\right) \begin{pmatrix} \mathbf{A}^j \\ \mathbf{B}^j \end{pmatrix} \mathbf{V}^{j+1} \\ &= \mathbf{\Phi}^j(\mathbf{x})\mathbf{A}^j\ \mathbf{V}^{j+1} + \mathbf{\Psi}^j(\mathbf{x})\mathbf{B}^j\ \mathbf{V}^{j+1} \end{aligned}$$

and therefore

$$\mathbf{V}^j = \mathbf{A}^j\ \mathbf{V}^{j+1} \qquad\qquad \mathbf{W}^j = \mathbf{B}^j\ \mathbf{V}^{j+1}.$$

Of course, the analysis filters $\mathbf{A}^{j-1}$ and $\mathbf{B}^{j-1}$ can now be applied to $\mathbf{V}^j$ to yield $\mathbf{V}^{j-1}$ and $\mathbf{W}^{j-1}$ and so on. A similar argument shows that $\mathbf{V}^{j+1}$ can be recovered from $\mathbf{V}^j$ and $\mathbf{W}^j$ using the synthesis filters:

$$\mathbf{V}^{j+1} = \mathbf{P}^j\ \mathbf{V}^j + \mathbf{Q}^j\ \mathbf{W}^j.$$

5.7 Examples

In this section, we apply our theory to two compression problems: the compression of a polyhedral model consisting of over 32,000 triangles, and compression of a piecewise linear representation of a color function defined on over one million points on the globe.

The input for the first example (shown in Color Plate 1(a)) is a polyhedral mesh consisting of 32,768 triangles created from laser range data provided courtesy of Cyberware, Inc. The triangulation was created by recursively subdividing an octahedron six times. The octahedron therefore serves as the domain mesh M^0, with the input triangulation considered as a parametric function $S(\mathbf{x}), \mathbf{x} \in M^0$ lying in $V^6(M^0)$. More precisely, if v_i^6 denote the vertices of the input mesh, $S(\mathbf{x})$ can be written as

$$S(\mathbf{x}) = \mathbf{\Phi}^6(\mathbf{x})\mathbf{V}^6, \qquad \mathbf{x} \in M^0$$

where the scaling functions $\mathbf{\Phi}^6(\mathbf{x})$ are the (piecewise linear) functions defined through polyhedral subdivision.

The wavelets $\psi_i^j(\mathbf{x})$ for this example are chosen to be supported on 2-discs. (The k-disc around a vertex v of a triangulation is defined to be the set of all triangles whose vertices are reachable from v by following k or fewer edges of the triangulation.) The filter bank process outlined in Section 5.6.3 can be applied in linear time to rewrite $S(\mathbf{x})$ in the form

$$S(\mathbf{x}) = \mathbf{\Phi}^0(\mathbf{x})\ \mathbf{V}^0 + \sum_{j=0}^{5} \mathbf{\Psi}^j(\mathbf{x})\ \mathbf{W}^j.$$

The first term describes a base shape as the projection of $S(\mathbf{x})$ into $V^0(M^0)$, which in this case is an approximating octahedron with vertex positions given by the eight rows of $\mathbf{V}^0$.

Approximations to the original mesh $S(\mathbf{x})$ can be easily obtained from the wavelet expansion by adding to the base shape only those wavelet coefficients w_i^j whose size is greater than some threshold ϵ. The accuracy of the approximations can be controlled by varying ϵ, as shown in Color Plate 1(d), (g), and (j). These models correspond to compressions of 99%, 88%, and 70%, respectively. Notice that this simple rule causes the mesh to refine in areas of high detail, while leaving large triangles in areas of relatively low detail.

Color Plate 1 also illustrates the use of wavelet approximations for automatic level-of-detail control in rendering. Images of the full-resolution mesh at various distances are shown in the left column. When viewing the input polyhedron at these distances, it is inefficient and unnecessary to render all 32,000 triangles. The approximations shown in the second column may instead be used without significantly degrading image quality.

Suddenly switching between models of different detail in an animation often produces a noticeable jump. This problem is easily mended by using a wavelet expansion where the wavelet coefficients are treated as continuous functions of the viewing distance. This simple technique allows the object geometry to smoothly change its appearance as the viewing distance changes. The effect of this type of continuous level-of-detail control is demonstrated in an accompanying video.

Color Plate 2 demonstrates another application of our method, that of compressing a function on the sphere. In this example, elevation and bathymetry data obtained from the U.S. National Geophysical Data Center was used to create a piecewise linear pseudo-coloring of the sphere. The resulting color function contained 2,097,152 triangles and 1,048,578 vertices. The full resolution pseudo-coloring was too large to be rendered on an SGI Indigo Extreme with 128MB of memory, and is therefore not shown in its entirety in Color Plate 2. An appreciation for the density of the data can be gotten from Color Plate 2(h), where even at close range the mesh lines are so close that the image is almost completely black.

The approximations shown in Color Plate 2(a)-(f) were produced using our method. Color Plate 2(a) shows a distant view of the Earth using a 99.9% compressed approximation (the mesh is shown in (b)). Likewise, Color Plates 2(c) and (d) show the result of a 98% compression for a medium-range view. At close range the 90% compression model in (e) is nearly indistinguishable from the full resolution model in (g). A comparison of the meshes shown in (f) and (h) reveals the striking degree of compression achieved in this case.

5.8 Summary

In this section we have sketched some of the ideas necessary for extending multiresolution analysis to surfaces of arbitrary topological type. Subdivision surfaces were shown to play an important role in this theory, making them an even more attractive method modeling complex surfaces.

The theory and constructions we have described hold for any primal subdivision scheme such as polyhedral subdivision, the butterfly method [72], Loop's method [123], and Catmull-Clark surfaces [19]. The results also hold for piecewise smooth subdivision as described in Hoppe *et al.* [106], and for open surfaces possessing boundary curves. While all these subdivision schemes possess linear time synthesis algorithms, our analysis algorithms are linear time only for the polyhedral and butterfly schemes.

There are numerous areas for future work:

- Our surface decomposition retains the topological type of the input surface. When the input is a relatively simple object with many small holes, it is more often desirable to decompose the input into a "topologically simpler" surface, that is, one with lower genus, fewer boundary curves, etc.
- Straightforward analysis algorithms for bounded interval B-spline wavelets [29] require quadratic time. Quak and Weyrich [159] have recently given a linear time algorithm. It may be possible to adapt the Quak-Weyrich technique to produce linear time analysis for Catmull-Clark and Loop's surfaces.
- To use our method for level-of-detail control as described in Section 5.7, the object O to be viewed must first be projected into a space $V^j(M^0)$, for some j, and for some (hopefully simple) mesh M^0 homeomorphic to O. Stated less abstractly, our filter bank algorithms can only be run on meshes that result from recursively subdividing a simple base mesh M^0. Often one knows a parametrization $F(\mathbf{x})$ for O, as was the case for the two examples presented in Section 5.7. Knowledge of the scaling function and wavelet and duals should allow $F(\mathbf{x})$ to be efficiently projected into an appropriate space $V^j(M^0)$. We are therefore interested in finding convenient representations for the duals.
- The images in Color Plates 1 and 2 were created by simply adding the wavelet coefficients in order of largest to smallest magnitude. We are currently investigating view-dependent error measures designed to produce improved image quality using even coefficients and hence fewer triangles.

VI: Wavelet Radiosity: Wavelet Methods for Integral Equations




Peter SCHRÖDER

Princeton University

1 Introduction

In this chapter we will explain how wavelets can be used to solve integral equations. The example we use is an important integral equation in graphics, the radiosity equation. The radiosity equation governs the transport of light between surfaces under the assumption that all reflection occurs isotropically. The resulting integral equation is linear and can be analyzed as a linear operator. Since wavelets can be used as bases for function spaces, linear operators can be expressed in them. If these operators satisfy certain smoothness conditions—as radiosity does—the resulting matrices are approximately sparse and can be solved asymptotically faster if only finite precision is required of the answer.

We develop this subject by first introducing the Galerkin method which is used to solve integral equations. Applying the method results in a linear system whose solution approximates the solution of the original integral equation. This discussion is kept very general. In a subsequent section the realization of linear operators in wavelet bases is discussed. There we will show why the vanishing moment property of wavelets results in (approximately) sparse matrix systems for integral operators satisfying certain kernel estimates. After these foundations we change gears and describe some techniques recently introduced in the radiosity literature. A technique, known as Hierarchical Radiosity, is shown to be equivalent to the use of the Haar basis in the context of solving integral equations. Treating this example in more detail allows us to fill many of the mathematical definitions with geometric intuition. Finally we discuss the implementation of a particular wavelet radiosity algorithm and the construction of an oracle function which is crucial for a linear time algorithm.

In general we will concentrate on the arguments and intuition behind the use of wavelet methods for integral equations and in particular their application to radiosity. Many of the implementation details will be deliberately abstracted and they can be found by the interested reader in the references ([166, 94, 102]).

1.1 A Note on Dimensionality

The final application of the developments in this chapter will be to the problem of radiosity in 3D, i.e., the light transport between surfaces in 3D. Consequently all functions will be defined over 2D parameter domains. Initially we will discuss only 1D parameter domains to simplify the exposition. The chief advantage of this reduction in dimensionality lies in the fact that many quantities, which we have to manipulate, have a number of subscripts or superscripts which is directly proportional to the dimensionality of the problem. It is easy to loose sight of the essential ideas unless we limit ourselves to the 1D domain case. The 1D domain case corresponds to what is known as flatland radiosity [103], i.e., the exchange of light between line segments in the plane. Aside from dimensionality there is no essential difference between the integral equations governing 3D or flatland radiosity. Where appropriate we will be explicit about the changes necessary to go to 2D domains. In general the differences are limited to more indices to manipulate, or in the case of a program, more array dimensions to iterate over.

2 Galerkin Methods

Galerkin methods are a class of algorithms designed to solve integral equations of a particular kind [54]. In this section we begin with an introduction to the radiosity equation as a particular example of an integral equation which can be solved efficiently with a Galerkin method. This is followed by a detailed description of the quantities which need to be computed when applying a Galerkin scheme to such an equation.

2.1 The Radiosity Equation

The computation of radiosity, i.e., power per unit area $[\frac{W}{m^2}]$, on a given surface is a widely used technique in computer graphics to solve for the illumination in an environment. Radiosity is governed by an integral equation which arises from a more general integral equation known as the rendering equation [115] when one assumes that all reflection occurs isotropically. Solving the underlying integral equation exactly is not possible in general. Thus numerical approximations must be employed leading to algorithms which are generally very expensive. The fundamental reason for the high cost of numerical approximations is that all surfaces in a given scene can potentially influence all other surfaces via reflection.

Radiosity $B(y)$ is a function defined over all surfaces $\mathrm{M}^2 \subset \mathbf{R}^3$ which make up a given scene. It is governed by a Fredholm integral equation of the second kind

$$B(y) = B^e(y) + \rho(y) \int_{\mathrm{M}^2} G(x,y) B(x)\, dx, \tag{1}$$

which describes radiosity as a sum of an emitted part (light sources) and the product of irradiance, computed by the integral, multiplied with the local reflectance $\rho(y)$, i.e., the fraction of light reemitted. Irradiance accounts for radiosities originating at all other surfaces weighted by a geometry term $G(x,y) = c \cos\theta_x \cos\theta_y r_{xy}^{-d} V(x,y)$ consisting of the cosines made by the local surface normals with a vector connecting two points, a normalization constant c, the distance r_{xy} between the two points, and a visibility function whose value is in $\{0,1\}$ depending whether the line between the two surface points x and y is obscured or unobscured respectively (see Figure VI.1). The points x and y are functions of some parameter. For flatland radiosity the parameter domain is 1D with $d = 1$, and the normalization constant $c = 1/2$. For full 3D radiosity the domain is 2D, $d = 2$ and the normalization constant is $c = \pi^{-1}$. In all the following derivations d, c, and x and y will be defined according to their context (1D or 2D).

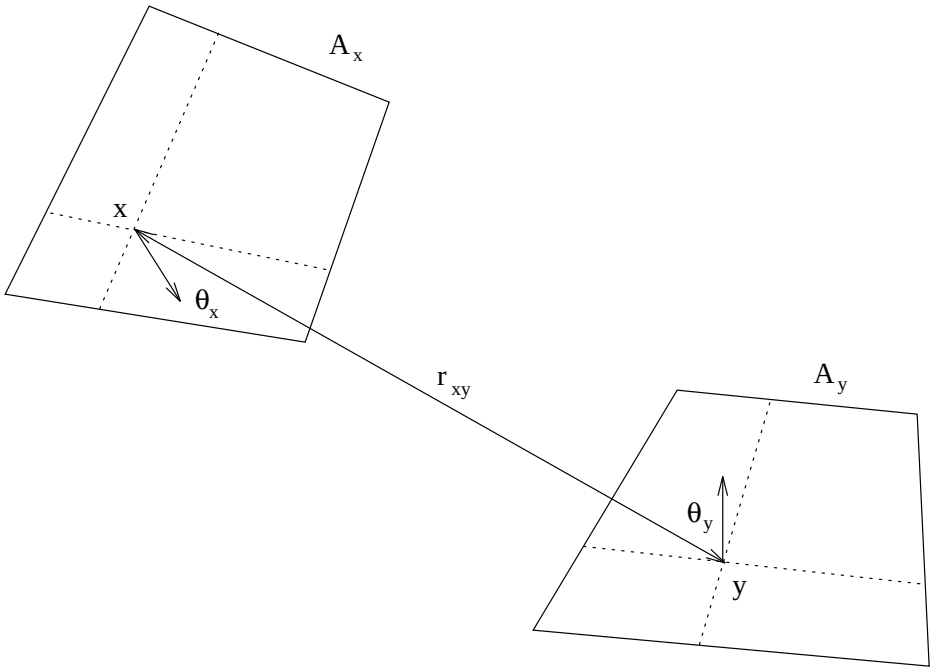

Figure VI.1: Geometry for the transport between two surfaces. θ denotes the angles that the vector connecting two points on the surfaces (x and y) makes with the local surface normals.

In the context of integral equations we refer to the function G as the *kernel* of the integral operator $\mathcal{G}(f) = \int G(x,.)f(x)\,dx$. Using operator notation we can express the equation to be solved as

$$(I - \rho\mathcal{G})B = B^e.$$

This particular integral operator has a number of properties which will be important later on. G is singular because the r factor in its denominator becomes zero for surfaces that touch. Nonetheless $\mathcal{G}$ is a bounded operator and closed on all L^p spaces [7]. We are mostly interested in its action on L^2, i.e., the space which contains all finite energy functions. Since ρ is strictly less than one for physically realistic environments we also know that the spectral radius of $\rho\mathcal{G}$ is strictly less than one, insuring the convergence of various iterative schemes. In particular we can compute, at least formally, the solution to the operator equation by a Neumann series

$$B = (I - \rho\mathcal{G})^{-1}B^e = \sum_{i=0}^{\infty}(\rho\mathcal{G})^i B^e = B^e + (\rho\mathcal{G})B^e + (\rho\mathcal{G})^2 B^e \ldots,$$

which gives the solution as the sum of directly emitted light, light that bounced through the environment once, twice, and so forth. While not a practical prescription for computation as such, it is nonetheless a basis for a number of algorithms to compute the solution to such operator equations. In particular in our case the physical system is generally so damped (small ρ) and the falloff is so quick (r^2 in 3D) that iterative schemes need to compute only a few terms in the above series until (numerical) convergence.

The task then is to find an efficient representation of both B and $\rho\mathcal{G}$ which facilitates the computation of terms in the Neumann series. In what follows we will assume that ρ is piecewise constant so that we only have to concentrate on the realization of $\mathcal{G}$. This is an often made assumption, but it is not necessary [88].

Once again we make it to simplify our exposition.

2.2 Projections

A canonical solution technique for integral equations such as the radiosity equation (1) is the weighted residual method [54], often referred to as finite elements. Historically radiosity algorithms were derived from power balance arguments [91, 150] and only recently [103] was the traditional mathematical framework brought to bear on the radiosity problem. However, all previous algorithms can be analyzed in the framework of the weighted residual method. For example, Classical Radiosity (CR) [91, 150] can be analyzed as a finite element method using piecewise constant basis functions.

A Galerkin method is an instance of a weighted residual method in which the original operator equation is *projected* into some subspace. We then seek an approximation $\widehat{B}$ of B in this subspace such that the residual

$$r(y) = \widehat{B}(y) - B^e(y) - \rho(y) \int_{\mathrm{M}^2} G(x, y)\widehat{B}(x)\, dx,$$

i.e., the difference between the left and right hand sides of the original integral equation with $\widehat{B}$ in place of B is orthogonal to the chosen subspace. To understand the projection of our operator $\mathcal{G}$ into a subspace we first consider writing the operator with respect to a basis for the entire space.

Let $\{N_i\}_{i\in\mathbf{Z}}$ be some basis for L^2. Using this basis the radiosity function B is characterized by a set of coefficients b_i such that $B(x) = \sum_i b_i N_i(x)$. The coefficients b_i can be found by projecting the function B with respect to the dual basis $\{\tilde{N}_i\}_{i\in\mathbf{Z}}$ which is defined by the property

$$\langle N_i, \tilde{N}_j \rangle = \int N_i(x)\tilde{N}_j\, dx = \delta_{ij}.$$

Using this fact we can write

$$B(x) = \sum_i b_i N_i(x) = \sum_i \langle B, \tilde{N}_i \rangle N_i(x).$$

Since the dual basis is a basis as well—whose dual is the original (primal) basis—we can also write

$$B(x) = \sum_j \tilde{b}_j \tilde{N}_j(x) = \sum_j \langle B, N_j \rangle \tilde{N}_j(x).$$

From the study of linear operators we know that a linear operator is fully specified if only we know its action on a basis set. In our case the resulting vectors are $\{\mathcal{G}(N_j)\}_{j\in\mathbf{Z}}$. These vectors, living in our space, are subject to being described with respect to our basis as well, leading us to consider

$$G_{ij} = \langle \mathcal{G}(N_j), \tilde{N}_i \rangle.$$

Arranging these coefficients in a tableaux we arrive at an infinite sized matrix equation which represents the original integral operator

$$\forall i: \; b_i = b_i^e + \rho_i \sum_j G_{ij} b_j. \tag{2}$$

The coefficients of this system are integrals of the form

$$G_{ij} = \int\int G(x,y)N_j(x)\tilde{N}_i(y)\,dx\,dy. \tag{3}$$

These coefficients are often called couplings or interactions to remind us that they have the physical interpretation of measuring how much one basis function physically interacts or couples with another across the integral operator. Note that the well known form factors of CR arise as $F_{ij} = G_{ij}$ when $\tilde{N}_i = \chi_{A_i}/A_i$ and $N_j = \chi_{A_j}$ ($\chi_A(x)$ is the function which takes on the value 1 for $x \in A$ and 0 otherwise).

In practice we have to deal with finite sized matrices. This corresponds to ignoring all but a finite sub-square of the infinite matrix, or said differently, the use of a finite basis. Doing this we in effect fix some subspace $V \subset L^2$ spanned by the corresponding finite basis. There are many choices for V (and its associated basis). For example one choice is the space of functions piecewise constant over fixed intervals, and one basis for that space is the set of "box" functions. Other examples are spaces spanned by "hat" functions or B-splines of higher orders. It is important to remember the difference between a choice of subspace and a choice of basis for this subspace. Once we make a choice of subspace, e.g., all functions which are piecewise linear, we still have considerable freedom in choosing a basis for this space. In particular we will consider wavelet bases.

When choosing a *finite* primal basis $\{N_j\}_{j=1,\ldots,n}$ and associated dual basis $\{\tilde{N}_i\}_{i=1,\ldots,n}$ we need to be careful as to the spaces specified by these. The subspace span$\{N_j\}$ is not necessarily the same as the space span$\{\tilde{N}_i\}$. If they are the same we say that $\{N_j\}$ and $\{\tilde{N}_i\}$ are *semi-orthogonal* and in particular they are *orthogonal* if $N_j = \tilde{N}_j$. In either of these cases we still have a Galerkin technique. The more general case arises when we consider biorthogonal bases $\{N_j\}$ and $\{\tilde{N}_i\}$ in which case we have a Petrov-Galerkin method. In what follows we will quietly ignore this distinction and collectively refer to the resulting algorithms as Galerkin methods.

Once we have chosen finite subsets $\{N_j\}_{j=1,\ldots,n}$ and $\{\tilde{N}_i\}_{i=1,\ldots,n}$ of our basis we have in effect restricted the integral equation to a subspace. To analyze these restrictions further we define the projection operator for this space by

$$\widehat{B} = P_V B = \sum_{i=1}^{n} \langle B, \tilde{N}_i \rangle N_i.$$

Since the span of the primal basis is not necessarily the same as the span of the dual basis, we have $P_V \neq P_{\tilde{V}}$.

Limiting the original integral equation to this subspace we arrive at

$$(I - \rho P_V \mathcal{G} P_V)B = P_V B^e,$$

which is now characterized by a finite linear system $(G_{ij})_{i,j=1,\ldots,n}$. In this way we have reduced our task to one of solving a finite linear system in order to find coefficients b_i for a function which is an approximation to the actual solution. The quality of this approximation depends on the approximation properties of the space V. Generally these spaces contain piecewise polynomial functions up to some order $M-1$. In this case it is easy to see that the error in our computed answer $|\widehat{B} - B|$ can be[1] $O(h^M)$, where h is the sidelength of some discretization imposed on the original geometry. There are other sources of error due to imprecise geometry or boundary conditions for example, which we will not consider here (for a careful analysis of these see Arvo *et al.*[7]).

[1] If the numerical techniques employed properly account for the singularity in the kernel function.

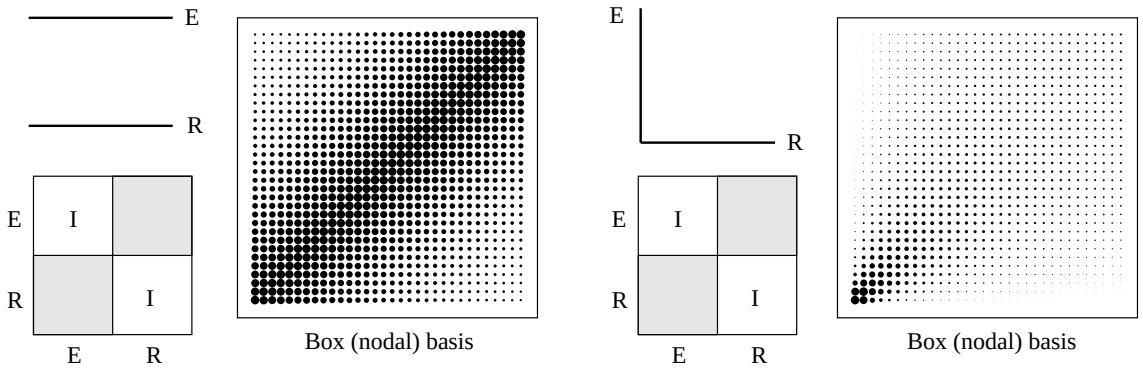

Figure VI.2: Two simple environments in flatland, two parallel line segments (left), and two perpendicular line segments (right), and the resulting matrix of couplings using piecewise constant functions. (Adapted from [166].)

Since wavelets can be used as bases for function spaces it makes sense to consider them in the context of a Galerkin method to solve an integral equation. In the next section we turn to a detailed study of $P_V \mathcal{G} P_V$ and the associated coefficients G_{ij} in the case that the space V is some space V_j in a multiresolution analysis and the basis set $\{N_i\}_{i=1,\ldots,n}$ is a wavelet basis.

3 Linear Operators in Wavelet Bases

In the previous section we showed why the object $P_V \mathcal{G} P_V$ is central to our study. This projected version of the integral operator $\mathcal{G}$ has some special properties which wavelets can exploit to yield efficient algorithms.

Consider CR which uses piecewise constant functions at some (finest) level V_L of meshing. Two examples of the resulting matrices $(G_{ij})_{i,j=1,\ldots,32}$ are illustrated in Figure VI.2. The figure shows two flatland radiosity scenarios. On the left is the flatland environment of two parallel line segments (upper left hand corner; denoted E and R). The resulting matrix of $(I - \rho\mathcal{G})$ has a block diagonal form. The diagonal blocks are identity matrices while one of the off diagonal blocks is shown enlarged. The size of dots is proportional to the magnitude of the coupling coefficient G_{ij}. Similarly on the right we see the resulting matrix for an environment with two line segments meeting in a corner, for which the domain contains the singularity. Notice how smooth and coherent the resulting matrices are. This is due to the smoothness of the kernel function itself. Suppose now we treat these matrices as pictures and apply a lossy wavelet compression to them. We can expect a high compression ratio while maintaining a good representation of the matrix, i.e., incurring only a small error in our computed answer. This is the essence of the use of wavelet bases for integral operators with smooth kernels (such as radiosity).

To understand the meaning of a lossy compression scheme in the context of linear algebra computations we need to connect the wavelet transform of a picture (matrix) to a vector space basis change. Since the Galerkin method uses projections we define projection operators for a multiresolution hierarchy. For the space V_i we define

$$P_i = \sum_{k=0}^{2^i-1} \langle\, . \,, \tilde{\varphi}_{i,k} \rangle\, \varphi_{i,k},$$

while the wavelet spaces W_i have projection operators

$$Q_i = P_{i+1} - P_i = \sum_{k=0}^{2^i-1} \langle\, .\, , \tilde{\psi}_{i,k} \rangle\, \psi_{i,k}.$$

Armed with these we describe—in the context of linear algebra—the first version of a wavelet transform, which is known as the *standard basis*.

3.1 Standard Basis

As we saw earlier there are alternative ways of writing some finest resolution space V_L using wavelets. Writing $V_L = V_0 + \sum_{i=0}^{L-1} W_i$ corresponds to writing the projection operator as $P_L = P_0 + \sum_{i=0}^{L-1} Q_i$. Using this identity we have

$$\begin{aligned} P_L \mathcal{G} P_L &= (P_0 + \sum_{i=0}^{L-1} Q_i)\mathcal{G}(P_0 + \sum_{i=0}^{L-1} Q_i) \\ &= P_0\mathcal{G}P_0 + \sum_{i=0}^{L-1} P_0\mathcal{G}Q_i + \sum_{i=0}^{L-1} Q_i\mathcal{G}P_0 + \sum_{i,l=0}^{L-1} Q_i\mathcal{G}Q_l. \end{aligned}$$

This decomposition corresponds to a particular two dimensional basis construction. Given a one dimensional wavelet basis $\{\varphi_0, \psi_{i,k}\}$, $i = 0, \ldots, L-1, k = 0, \ldots, 2^i - 1$ we can build a two dimensional basis via a tensor product construction $\{\tilde{\varphi}_0, \tilde{\psi}_{i,k}\} \times \{\varphi_0, \psi_{l,m}\}$, $i, l = 0, \ldots, L-1, k = 0, \ldots, 2^i - 1$, and $m = 0, \ldots, 2^l - 1$. This is often referred to as the standard realization of the integral operator [15].

The pyramid algorithms that were mentioned earlier for transforming a function of a single variable between a basis of V_L and the bases in $V_0 + \sum_{i=0}^{L-1} W_i$ can be applied to matrices (functions of two variables). In particular the standard decomposition corresponds to applying such a pyramid transform to all rows (transforming the right hand side P_L) followed by a transform of all row transformed columns. This transformation of the coefficients corresponds exactly to a change of basis as is often done with matrices for various reasons. The remarkable property of the change to the wavelet basis is that it can be performed in time proportional to the number of basis functions, $O(n^2)$. In general expressing a matrix of size $O(n^2)$ with respect to another basis entails a transform of cost $O(n^3)$.

Figure VI.3 shows the effects of transforming form factor matrices expressed originally in the piecewise constant nodal basis (see Figure VI.2) into different wavelet bases. On the left the Haar basis was used, while on the right the Flatlet basis with two *vanishing moments* [94] was used. The top row gives matrices for the example of two parallel line segments, while the bottom row shows the case of two perpendicular line segments. Notice how many of the coefficients are small in magnitude (small disks). As the number of vanishing moments increases from one to two (left to right) we can observe many more entries becoming small. This demonstrates for two particular cases how more vanishing moments lead to more (approximate) sparsity in the matrices. In the next section we will explain why vanishing moments are so important for the compression (sparsification) of matrices which arise from smooth integral operators.

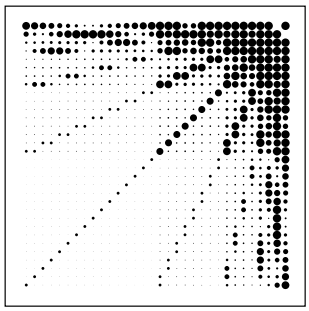

Haar basis (1 vanishing moment)

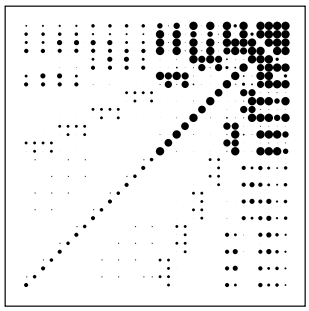

Flatlet basis (2 vanishing moments)

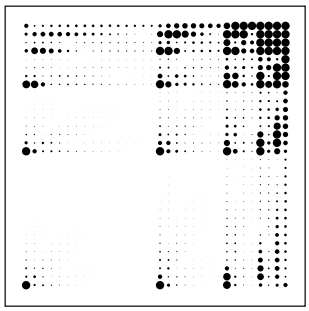

Haar basis (1 vanishing moment)

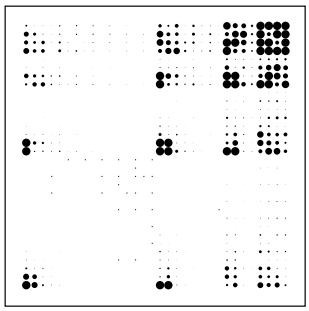

Flatlet basis (2 vanishing moments)

Figure VI.3: Coupling matrices for two flatland environments (see Figure VI.2) expressed in wavelet bases. The top row shows the coupling matrix for two parallel line segments expressed in the Haar basis (top left) and in the $\mathcal{F}_2$ (Flatlet) basis [94] (top right), which has 2 vanishing moments but remains piecewise constant at the finest level. The bottom row shows the same bases applied to the form factor matrix for two perpendicular lines segments. (Adapted from [166].)

3.2 Vanishing Moments

We begin with the definition of vanishing moments. A function ψ is said to have M vanishing moments if its projection against the first M monomials vanishes

$$\langle \psi, x^i \rangle = 0 \;\; i = 0, \ldots, M-1.$$

The Haar wavelet for example has 1 vanishing moment. Other wavelets can be constructed to have more vanishing moments.

To see why this leads to small coefficients in general consider some function $f \in L^2$. Suppose we want to write it with respect to a wavelet basis. The coefficients of such an expansion can be found by taking inner products against the dual basis functions

$$f(x) = \sum_{i,j} \langle f, \tilde{\psi}_{i,j} \rangle \psi_{i,j}.$$

We want to show that for smooth f many of the coefficients $f_{i,j} = \langle f, \tilde{\psi}_{i,j} \rangle$ are small. If f is smooth we

can apply Taylor's theorem to expand it about some point x_0 (for simplicity, let $x_0 = 0$) to get

$$f(x) = \sum_{i=0}^{M-1} \frac{f^{(i)}(0)}{i!} x^i + \frac{f^{(M)}(\xi)}{M!} x^M,$$

for some $\xi \in [0, x]$. Now consider computing $f_{i,j}$. To simplify the argument we consider the inner product necessary to compute $f_{0,0}$, i.e., the inner product with $\tilde{\psi}$ (all others being related by translations and scalings). Suppose that the dual basis functions have vanishing moments, then we can bound the resulting coefficient as follows

$$\begin{aligned} |f_{0,0}| &= \left| \int f(x) \tilde{\psi}(x)\, dx \right| \\ &= \left| \int \frac{f^{(M)}(\xi)}{M!} x^M \tilde{\psi}(x)\, dx \right| \\ &\leqslant \left| \frac{f^{(M)}(\xi)}{M!} \right| I_x^M \int |\tilde{\psi}(x)|\, dx \\ &= C_M \sup_{\xi \in I_x} \left| f^{(M)}(\xi) \right| I_x^M, \end{aligned} \tag{4}$$

where I_x is the size of the interval of support of $\tilde{\psi}$. From this bound we can see that the associated coefficient will be small whenever either I_x is small or the M^{th} derivative of f is small. Similar arguments can be made for functions of more than one variable, for example the kernel function of an integral operator.

This bound allows us to argue that many of the entries in a matrix system arising from an integral operator will be very small and can be ignored, leading to a sparse matrix system. Recall that integral operators led to linear systems whose coefficients are integrals of the kernel function against the chosen basis functions (primal as well as dual). In the case of radiosity this led to the G_{ij} (Equation 3). Suppose that the basis functions for the integral operator are chosen to be wavelets and that these wavelets (both primal and dual) have vanishing moments. If G is smooth then many of the G_{ij} will be quite small because of the vanishing moment property, and can be ignored without incurring too much error. Below we will make this argument mathematically precise.

3.3 Integral Operators and Sparsity

In a paper published in 1991 Beylkin *et al.*[15] showed that for a large class of integral operators the resulting linear system, when using wavelet bases, is approximately sparse. More specifically they showed that for a class of integral operators satisfying certain kernel estimates and any $\epsilon > 0$ a $\delta(\epsilon)$ exists such that all but $O(n \log n)$ of the matrix entries will be below δ and can be ignored without incurring more than an error of ϵ in the computed answer.

The requirements on the kernel of the integral operator are given as estimates of "falloff away from the diagonal"

$$\begin{aligned} |K(x, y)| &\leqslant \frac{1}{|x - y|^d} \\ |\partial_x^M K| + |\partial_y^M K| &\leqslant \frac{C_M}{|x - y|^{d+M}}, \end{aligned} \tag{5}$$

for some $M > 0$, and $K : \mathbf{R}^d \times \mathbf{R}^d \rightarrow \mathbf{R}$ the kernel function of the integral operator in question. Note that the kernel G of the radiosity integral operator satisfies a falloff property of this type if we replace $|x - y|$ with r. Since the parameterizations which we use for our surfaces are well behaved (bounded derivative) this distinction from the classical case does not matter. Examining the matrices in Figure VI.3 we can immediately see the $O(n \log n)$ structure. There are approximately $\log n$ bands visible, each of length approximately equal to n. This is particularly noticeable in the case of two parallel lines and the Haar basis (upper left in Figure VI.3). We will not give a proof here, but give a geometric argument for the case of radiosity later on. The geometric argument is equivalent to the mathematical proof (for the radiosity operator), but provides more intuition.

Beylkin *et al.*[15] proceeded to analyze the $\log n$ dependence in the number of non-negligible entries in the matrix and showed that by decoupling all the scales it is possible to reduce the number of needed entries to $O(n)$ (for certain classes of operators). It is interesting to note that the original Hierarchical Radiosity (HR) algorithm [102] (see below) already gave a proof of the $O(n)$ complexity based purely on geometric arguments using a construction which does decouple the scales in a way very close to the Beylkin *et al.* argument. This so called *non-standard construction* is also the basis of later wavelet radiosity work [94, 166]. We will describe this construction next.

3.4 Non-Standard Basis

We saw earlier how the decomposition $P_L = P_0 + \sum_{i=0}^{L-1} Q_i$ applied to $P_L \mathcal{G} P_L$ on both sides resulted in a realization of $\mathcal{G}$ in the wavelet basis. The resulting sum consisted of terms involving all possible combinations of subspaces $\{P_0, Q_i\}_{i=0,\ldots,L-1}$ on either side of $\mathcal{G}$. Said differently, the operator was expressed as a sum of contributions between subspaces at *all* resolutions. To remove this coupling across levels we use a telescoping sum argument to write

$$\begin{aligned} P_L \mathcal{G} P_L &= P_0 \mathcal{G} P_0 + \sum_{i=0}^{L-1} (P_{i+1} \mathcal{G} P_{i+1} - P_i \mathcal{G} P_i) \\ &= P_0 \mathcal{G} P_0 + \sum_{i=0}^{L-1} Q_i \mathcal{G} P_i + \sum_{i=0}^{L-1} P_i \mathcal{G} Q_i + \sum_{i=0}^{L-1} Q_i \mathcal{G} Q_i, \end{aligned}$$

using the fact that $P_{i+1} = P_i + Q_i$ and rewriting each summand in turn as

$$\begin{aligned} P_{i+1} \mathcal{G} P_{i+1} - P_i \mathcal{G} P_i &= (P_i + Q_i) \mathcal{G} (P_i + Q_i) - P_i \mathcal{G} P_i \\ &= P_i \mathcal{G} Q_i + Q_i \mathcal{G} P_i + Q_i \mathcal{G} Q_i. \end{aligned}$$

The main difference to the earlier decomposition is the fact that the subspaces occurring on either side of $\mathcal{G}$ in the final sums all have the same index, i.e., only spaces at the *same* level interact. This is referred to as the *non-standard realization*, since it corresponds to a realization of the operator in a basis which requires an over representation for the functions to which the operator is applied. The over representation occurs because for each i both P_i and Q_i occur on either side of $\mathcal{G}$. However, the total number of functions that occur is still only n^2, but they cannot be written as a cross product of one dimensional bases. This set of functions, $\{\tilde{\varphi}_0 \varphi_0, \tilde{\varphi}_{i,m} \psi_{i,j}, \tilde{\psi}_{i,m} \varphi_{i,j}, \tilde{\psi}_{i,m} \psi_{i,j}\}$, $i = 0, \ldots, L-1$, and $j, m = 0, \ldots, 2^i - 1$, is also referred to as the *non-standard basis*.

Figure VI.4 shows the non-standard realizations of the operators for the two flatland environments considered earlier (Figure VI.2). Each level consists of three blocks. The sets of triples consist of the $Q_i \mathcal{G} Q_i$ block

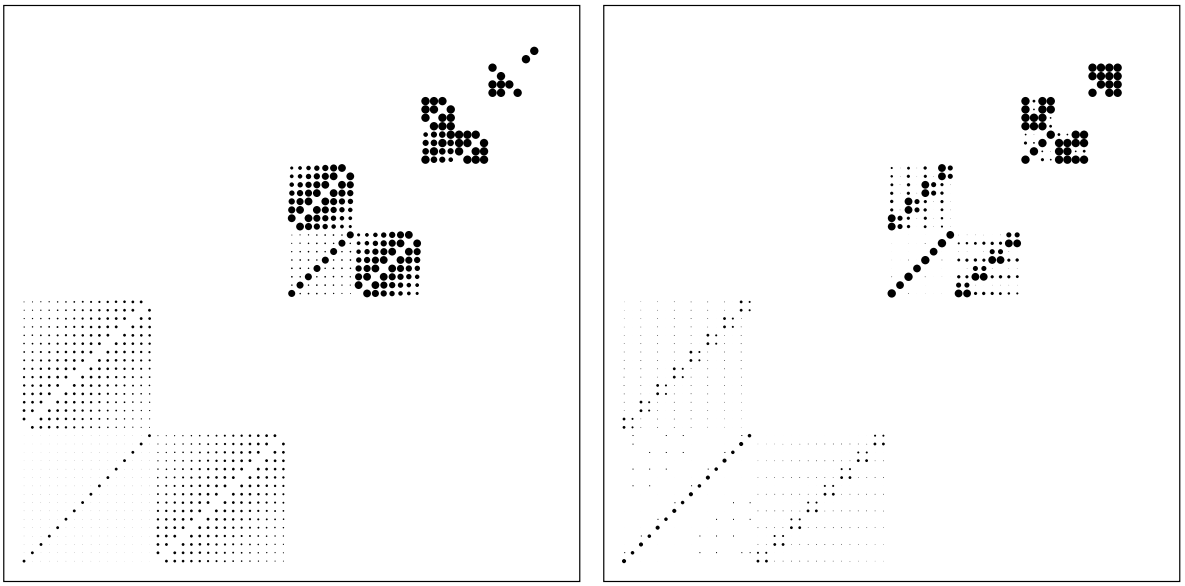

Non-standard Haar Non-standard Flatlet 2

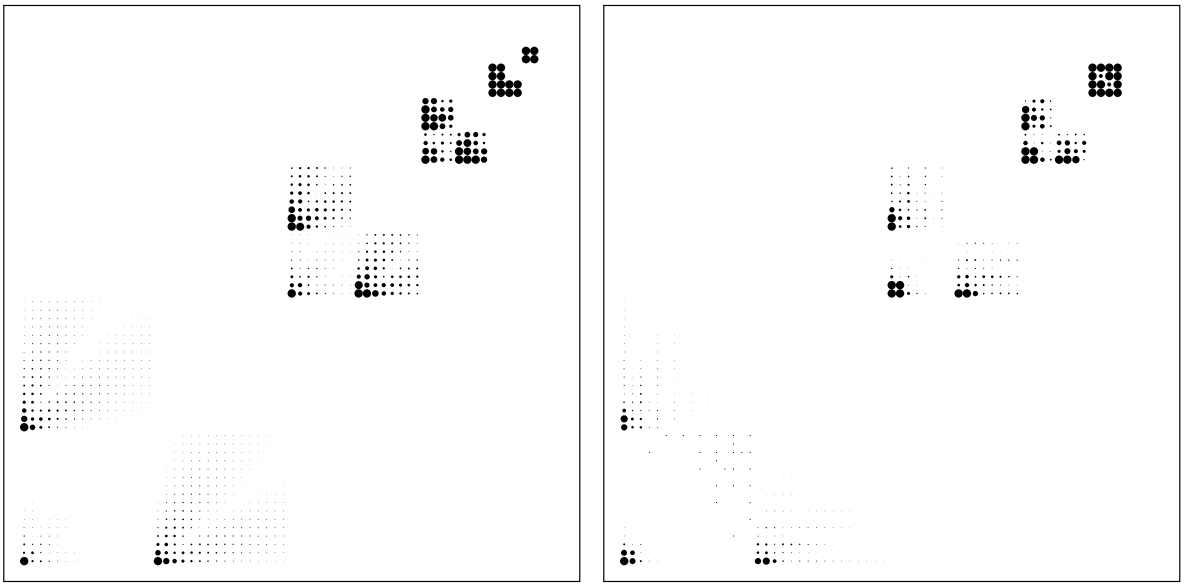

Non-standard Haar Non-standard Flatlet 2

Figure VI.4: Coupling matrices for two flatland environments (see Figure VI.2) expressed in wavelet bases using the non-standard operator realization. The top row shows the coupling matrix for two parallel line segments expressed in the Haar basis (top left) and in the $\mathcal{F}_2$ basis [94] (top right). The bottom row shows the same bases applied to the coupling matrix for two perpendicular line segments. (Adapted from [166].)

in the lower left, the $P_i\mathcal{G}Q_i$ block in the upper left and the $Q_i\mathcal{G}P_i$ block in the lower right. The empty quadrant would have corresponded to $P_i\mathcal{G}P_i$, however this is the block that the recursion (telescoping sum) occurs on. This last observation also suggests how to transform a matrix from the nodal basis into the non-standard realization. Instead of performing complete pyramid transforms on each row, followed by complete transforms on each column, the non-standard realization can be achieved by interleaving the

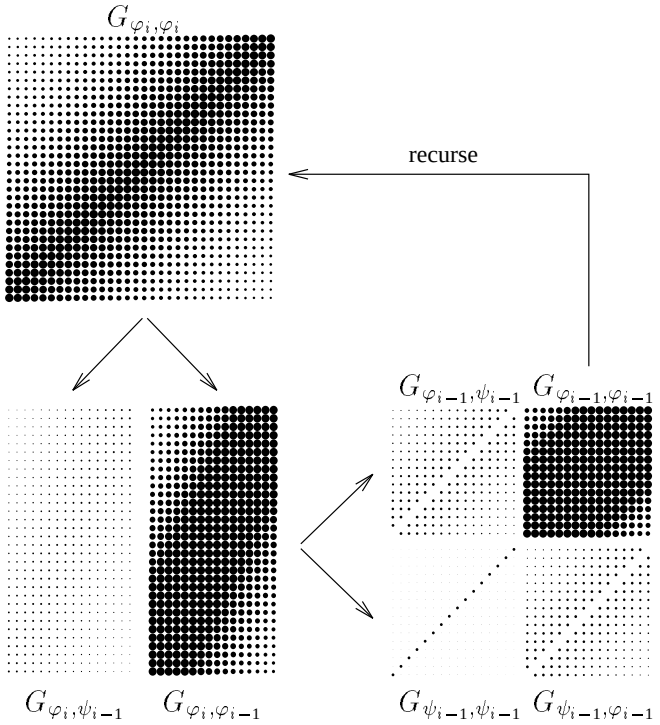

Figure VI.5: The 2D non-standard Pyramid Algorithm is applied to coupling coefficients taken from the flatland radiosity environment consisting of two parallel line segments. One step in the transform is shown. (Adapted from [94].)

individual transforms. First all rows are split into high pass and low pass bands (a single level application of the two scale relation), then all columns are subjected to a single level transform. Now recurse on the low pass/low pass quadrant $P_i \mathcal{G} P_i$ (see Figure VI.5). When writing this out as a matrix suitable for matrix/vector multiplies the matrices in Figure VI.4 result.

4 Wavelet Radiosity

Wavelet Radiosity (WR) was first introduced by Gortler *et al.*[94] and Schröder *et al.*[166]. Their algorithm unifies the benefits of higher order Galerkin Radiosity (GR) [103, 104, 199, 188] and HR [102]. HR was the first method to fully exploit a multilevel hierarchy to gain an asymptotic improvement in the efficiency of radiosity computations. It also corresponds directly to the use of a Haar wavelet basis for radiosity.

In the next section we first give a quick review of GR to motivate the desire to extend the ideas of HR to higher order basis functions. This latter extension was realized with the use of wavelets. Approaching the description of the final algorithm in this way also allows us to argue the correctness of the method with very direct geometric means.

4.1 Galerkin Radiosity

GR, first introduced by Heckbert [103, 104] aims to increase the order of basis functions used in radiosity algorithms. In this context CR [91, 150] is seen to be a Galerkin method using piecewise constant functions.

The original goal of applying higher order Galerkin methods to radiosity was to improve the quality of the answers computed, as well as the efficiency of the computations. In particular using higher order basis functions allows the use of much coarser meshes than CR required while still meeting a requested error bound. In his original work Heckbert applied these ideas in a flatland environment using piecewise linear basis functions. More recently Troutman and Max [188] and Zatz [199] have applied higher order basis functions to the computation of 3D radiosity. Zatz in particular has pushed the ideas to their extreme by leaving many surfaces unmeshed. Instead he increased the polynomial order of the basis functions so that the radiosity even over large surfaces, such as entire walls, could be computed with high accuracy without any subdivision.

4.2 Hierarchical Radiosity

The first use of hierarchies was made by Cohen *et al.*[38] who introduced a two level hierarchy known as sub-structuring. They observed that a fine subdivision was only necessary on the receiver of a transport of light, while a coarser subdivision was sufficient on the source. Since the roles of receivers and sources are reversible a two level hierarchy over each geometric primitive resulted. These ideas were developed further in a paper by Hanrahan *et al.*[102]. They introduced HR, which applied some arguments from the n-body literature [6, 98, 11] to CR. In their approach a possibly very deeply nested subdivision hierarchy was imposed on every primitive. Light transport was allowed to occur throughout these hierarchies. They showed that to within some user selectable error tolerance a linear number of interactions amongst all possible interactions was sufficient to compute an accurate answer. Because the algorithms up to that point always used a quadratic number of interactions HR improved the performance of radiosity computations considerably.

4.2.1 A Note on Performance Analyses

To put these two techniques and their respective advantages into perspective we need to look at their costs. Given k input surfaces, say polygons[2], any one of the above algorithms will use some number of basis functions n defined over the totality of input surfaces. For example in the case of CR the surfaces are typically subdivided into many elements with each element carrying an associated constant basis function (whose support is exactly the element itself). In this case n elements correspond to n basis functions. Similarly for higher order Galerkin methods we will probably do some meshing into elements as well, albeit not as fine a mesh. Each resulting element will then typically carry some number of basis functions. For example, if we are using piecewise linear basis functions each surface (2D) element will typically have four basis functions associated with it. For each parameter axis we need two basis functions (constant and linear) and we have two parameter axes for a total of four combinations. In general an $M-1$ order piecewise polynomial basis will have M^2 basis functions defined over each (2D) element. Counting in this manner it makes sense to talk about n basis functions in total for n/M^2 elements.

Once we have a set of n basis functions the Galerkin method will give rise to a linear system relating all of these basis functions with each other resulting in a system of size $O(n^2)$ (see Equation 2). This linear system needs to be solved to find the coefficients of all the basis functions. Using some iterative solver the solution cost is proportional to $O(n^2)$. Our linear systems are very well behaved due to the r^{-d} falloff in the kernel of the operator. As a result, iterative schemes typically converge within very few iterations.

[2]To simplify our exposition we will stick to polygons, in particular quadrilaterals. However, there is no fundamental mathematical limitation preventing us from using more general parametric surfaces such as bicubic or triangular patches, for example.

GR, by going to higher order bases, manages to decrease n and thus get efficiency gains. Even though the number of bases per element increases (M^2) the number of elements necessary for a given overall accuracy falls faster for a net gain. To see why this is, we use the fact that a Galerkin method using a piecewise polynomial basis of order $M-1$ will have an accuracy of $O(h^M)$[3]. Where h gives the sidelength of the elements in the mesh [54, 116]. To make this concrete, suppose we are willing to allow an error proportional to $1/256$. Using piecewise constant basis functions, h would have to be on the order of $1/256$ to meet our goal. Now consider piecewise linear functions. In this case h would only need to be on the order of $\sqrt{1/256} = 1/16$. So even though the number of basis functions per element goes up, we still come out ahead. In the case of flatland there are two linear basis functions per element and we go from $n = 256$ to $n = 2 \cdot 16$ bases total. In 3D radiosity where we have $2 \cdot 2$ linear basis functions per element n goes from 256^2 down to $(2 \cdot 16)^2$ basis functions overall.

We have seen that for n basis functions we have $O(n^2)$ interactions in general. It is also immediately clear on an intuitive level that not all interactions are equally important. HR makes this statement precise and takes advantage of it to reduce the number of interactions, which need to be computed, to $O(n)$. For example, "far" interactions do not need as much subdivision as "close" interactions. The exact argument as to why $O(n)$ elements are enough will be given below. However, even if we can make statements about the number of elements generated during meshing, and how they will interact, we still need to consider at least one interaction between each pair of the original set of incoming surfaces. Consequently the work of an HR algorithm will be $O(k^2 + n)$. Even though there still is a k^2 dependence we will often have $n >> k$ resulting in significant savings. Note that in a case in which the original set of k surfaces is presented premeshed as n elements HR will be reduced to CR. Thus it will perform no worse, but in practice often dramatically better, than CR. We will take up the issue of the k^2 dependence in the last section when we consider clustering.

4.3 Algorithms

All radiosity algorithms have roughly two components for purposes of this discussion. These can be described as setting up the equations, i.e., *computing* the entries of the linear system, and *solving* the linear system. The latter typically invokes some iterative solution scheme, for example Jacobi or Gauss Seidel iteration [175], or Southwell relaxation [96]. In actual implementations these two phases are often intermixed, for example when refining a subdivision mesh (adding basis functions) during successive iterations. Nonetheless we can distinguish these two fundamental operations in our algorithms. Since iterating, i.e., performing row updates, or matrix/vector multiplies is conceptually straightforward we will first focus on the aspect of setting up the equations.

The simplest version of a wavelet radiosity algorithm would compute the initial matrix of coupling coefficients at some finest level V_L (see Figure VI.2), followed by the transformation of this matrix into the non-standard form (see Figure VI.4). Eliminating all entries less than some threshold would leave us with a sparse system for which $O(n)$ solution techniques exist. The major disadvantage of this algorithm is the cost of setting up the initial set of equations. Computing the full matrix to begin with consumes $O(n^2)$ time. Recall that our eventual goal is an $O(n)$ algorithm. The only way to achieve this goal is to compute only the entries in the transformed matrix which will be larger than the allowed threshold. The difficulty is that it is not a-priori clear where these entries are.

[3] This assumes that the singularity in the kernel function is treated correctly. If this is not done the method will have much worse behavior.

The HR algorithm addressed this concern in an elegant way which we now turn to. Studying this example gives us a somewhat unusual approach to the non-standard wavelet basis, since only scaling functions appear in the formulation of HR. The advantage of this approach is that it has a clear and provably correct way to enumerate just those interactions which are above the threshold. In the process it provides a constructive, geometric proof for the $O(n)$ claims of general wavelet methods for certain integral operators. In a later section we will relate the HR construction back to the more general theory, but first we give a detailed exposition of HR.

4.3.1 Hierarchical Radiosity

HR considers the possible set of interactions in a recursive enumeration scheme. We want to insure that every transport, i.e., every surface interacting with other surfaces, is accounted for once and only once. Physically speaking we want to neither miss power, nor introduce it into the simulation multiple times. To do this we call the following procedure for every input surface with every other input surface as a second argument (once again we consider the problem over 1D domains)

```
ProjectKernel( Element i, Element j )
   error = Oracle( i, j );
   if( Acceptable( error ) || RecursionLimit( i, j ) )
      G_ij = Quadrature( i, j );
   else
      if( PreferredSubdivision( i, j ) == i )
         ProjectKernel( LeftChild( i ), j );
         ProjectKernel( RightChild( i ), j );
      else
         ProjectKernel( i, LeftChild( j ) );
         ProjectKernel( i, RightChild( j ) );
```

This procedure consists of several parts which we discuss in turn.

First we call a function `Oracle`, which is capable of estimating the error across a proposed interaction between elements `i` and `j`. If this estimated error satisfies the predicate `Acceptable`, the required coefficient is created by calling a quadrature routine which evaluates the integral of Equation 3. We have in effect created an entry in the matrix system, as well as implicitly decided on a particular basis function. Even if the error is not acceptable yet, resource limitations may require us to terminate the recursion. This predicate is evaluated by `RecursionLimit`. For example, we may decide that we cannot afford to subdivide input elements to a size smaller than some minimum. Of course the hope is that this predicate will never be the cause of recursion termination.

If the error is too high we recurse by subdividing, i.e., by going to a finer space V_{j+1} over the particular element. Typically we will find that the benefit in terms of error reduction is not equal for the two elements in question. For example, one element might be much larger than the other and it will be more helpful to subdivide the larger one in order to reduce the overall error. This determination is made by `PreferredSubdivision` and a recursive call is initiated on the child interactions which arise from splitting one of the parent elements. For 2D elements there would typically be four recursive calls each, not two. The preferred element would be split into four children (quadrants).

As mentioned earlier, the process of iterating and subdividing is not typically separated in a real implementation. For example, we could imagine that the predicate `Acceptable` takes into account the brightness of the sender (brightness refinement [102]) and maybe the importance of the receiver (importance refinement [174]) vis-a-vis some global error threshold ϵ. The error threshold may itself become smaller upon successive iterations (multigridding [102]), creating a fast but inaccurate solution first and using it as the starting point for successive solutions with lesser error. Any of these techniques we might refer to as refinement. Thus we will typically reexamine interactions created in an earlier iteration when iterating again.

In an implementation this is easily done by keeping a list of all G_{ij} created and calling a modified version of `ProjectKernel` on these before the next iteration. If none of the parameters which influence `Acceptable` has changed, `ProjectKernel` would simply return; otherwise it would delete the interaction G_{ij} because it has too much error and replace it with a set of finer interactions. This would correspond to replacing some set of basis functions (and their interactions) with a new and finer set of basis functions (and their interactions).

From the structure of the recursion, it is clear that every transport will be accounted for once and only once. The remaining task is to show that for a strictly positive amount of allowable error[4] we will create only a linear number of interactions amongst all the (implicit in the subdivision) basis functions created. Furthermore we need to show that the function `Oracle` can be implemented in an efficient way.

4.3.2 Bounding the Error

We proceed by analyzing the function `ProjectKernel` more closely to understand how many recursive calls it will generate. Again in order to streamline the presentation we first analyze the case of radiosity defined over 1D domains (flatland radiosity). When we used the name `ProjectKernel` we already anticipated one meaning of the G_{ij} coefficients which we will now use to analyze the relationship between allowed error and number of interactions necessary.

Recall the definition of G_{ij} (Equation 3). We may interpret the G_{ij} as expansion coefficients of G as follows

$$\begin{aligned} G_{ij} &= \int\int G(x,y)\, N_j(x) \tilde{N}_i(y)\, dx\, dy \\ &= \langle \langle G, N_j \rangle, \tilde{N}_i \rangle \\ G(x,y) &\approx \widehat{G}(x,y) = \sum_{i,j=1}^{n} G_{ij} \tilde{N}_j(x) N_i(y). \end{aligned}$$

In other words, computing some set of G_{ij} is equivalent to approximating the function $G(x,y)$ with a projected version $\widehat{G}(x,y)$.

Using the fact that the radiosity integral operator is bounded and strictly less than 1 for physically realistic reflectances [7], the error in our computed solution $\widehat{B}$ can be bound vis-a-vis the actual solution B as

$$|\widehat{B} - B| \leqslant C_{\mathcal{G}} |\widehat{G} - G|,$$

where the norms are between functions, and C is some constant associated with the input (geometry,

[4] Imagine `Acceptable` always returns `False`. In this case the recursion would always bottom out and in fact all n bases at the finest level of meshing, as determined by `RecursionLimit` would interact, resulting in n^2 interactions.

reflectances, and right hand side), but independent of the basis functions used. Clearly given a user selectable $\epsilon > 0$ the error in the computed solution can be forced below ϵ by making $\widehat{G}$ sufficiently close to G.

So far we only have a global statement on the error. We next need to show that we can keep the global error, in some suitable error norm, under control by making local decisions. There are many possible ways to derive such bounds. We consider only a very simple one, not necessarily the tightest. Observe that the difference between $\widehat{G}$ and G is simply given by all the terms in the infinite expansion of G which are not accounted for by the finite number of terms used for $\widehat{G}$. In a wavelet expansion all the coefficients in this difference have a level number associated with them. Now consider the 1-norm of these coefficients within each level and the sup norm accross levels. We would like to argue that the resulting norm will fall off as we consider more and more levels. Away from the singularity this follows easily since there even the 2-norm of the coefficients will fall off as $2^{-i(\alpha+n/2)}$ ($n = 2$ in flatland and $n = 4$ in 3D radiosity), with α the local Lipschitz exponent and i the level number. Note that this is sufficient even for discontiuities due to visibility where $\alpha = 0$. Only the behavior at the singularity actually forces us to use the 1-norm. This follows from the fact that the form factor will stay constant ($\alpha = -d$), but the throughput (1-norm), i.e., area times formfactor, will fall off exponentially with the level number at the singularity. Consequently any strategy which considers the 1-norm within each level and stops refining, i.e., going deeper, when some threshold has been undercut (the sup-norm estimate is satisfied) will be capable of insuring that the resulting error in the solution is below some desirable ϵ.

Now we already know that the simplest version (no brightness, importance, or multigridding refinements) of the function `Acceptable` is a comparison of `error` against δ.

4.3.3 Bounding the Number of Interactions

Suppose now that we stay in the framework of CR in so far that we only allow constant basis functions (as HR does [102]) and that we simply set $\widehat{G} = G(x_0, y_0)$ where x_0 and y_0 are the midpoints of the respective intervals (areas) we are considering. In the language of wavelets our scaling functions are "box" functions and the associated wavelet is the Haar function. Using the fact that

$$|G(x\,,y)| < \frac{C}{r^d},$$

we get, over the support of two elements I_x and I_y, which do not intersect

$$\begin{aligned} |\widehat{G} - G| &\leqslant \int_{I_y}\int_{I_x} |G(x_0, y_0) - G(x\,,y)|\, dx\, dy \\ &\leqslant C\, I^2 \left(\frac{I}{r}\right)^{d+1}, \end{aligned}$$

through an application of the mean value theorem. I denotes the length of the maximum edge of any of the involved domains (two 1D domains in flatland, four 1D domains in 3D). The bound given above is small whenever the ratio of sizes to distances is small. In particular it will fall as a second power (even faster in 3D) of the ratio of the largest edge length to the distance. From this follow two observations

1. I always needs to be less than r to get the bound below our error threshold;

2. the involved elements should be of comparable size, since nothing is gained by making one smaller but not the other.

Below we will see that this is enough to argue that for every element I_x there are a constant number of elements I_y which satisfy these criteria.

The bound given above is only useful when $r > 0$. When the two elements meet, a more careful analysis must be applied. The difficulty arises because of the r^{-d} nature of the radiosity kernel. In other words, the bound given above holds everywhere so long as we exclude an arbitrarily small region around the intersections of any of the elements. To deal with these remaining regions we need the boundedness of our original operator. For this small region around the intersection set $\widehat{G} = 0$ to get

$$|\widehat{G} - G| = |G| \leqslant C I_y F_{I_y, I_x}$$

(in 3D the factor I_y is replaced by A_y). Since the form factor $F_{I_y, I_x} \leqslant 1$ we can force $|\widehat{G} - G|$ below any desired threshold by making I_y (A_y respectively) small enough.

Taking both bounds together we can make the distance between G and its approximation arbitrarily small by making the ratio of size to distance small or, when we are at the singularity, by simply making the size itself small. The region over which we have to employ the second bound can be made arbitrarily small, and with it the bound itself. For sake of our argument we allocate $\epsilon/2$ of our total allowed error to the regions touching the singularity and continue to consider only the case of elements which are separated. Their error must now be kept below $\epsilon/2$, for a total of the given ϵ.

Given that we have a remaining error budget of $\epsilon/2$ we need to show that for this allowable error any recursive call will create at most a constant number of calls to the function `Quadrature`. From the above error bound we see that an interaction will be created whenever the size to distance ratio is smaller than some threshold. How many elements can there be for which this is true? To answer this question we interpret the size to distance ratio geometrically as a measure of angle subtended. In other words, this ratio is proportional to the angle that one element subtends from the point of view of the other element.

On the initial call to `ProjectKernel` there can at most be k elements (the original input surfaces) less than this threshold (hence the k^2 in the overall performance analysis). Suppose that some of those initial input surfaces are too large, i.e., their angle subtended is above our threshold. These surfaces will result in recursive calls. How many can there be? Since the total angle subtended above a given element is bounded there can at most be a constant number of elements larger than some minimum on any given recursive call. Suppose that at the next recursion level, due to subdivision, all of these elements have fallen below the threshold. In this case they all interact with our element, i.e., this element interacts with a constant number of other elements. Suppose instead that not all elements have fallen below the threshold due to the subdivision. Once again, there can be at most a constant number of such "too-large" elements.

In either case each element—below the top level call to `ProjectKernel`—interacts at most with a constant number of other elements. This means that the total number of interactions created due to recursive calls is proportional to the total number of elements. The constant of proportionality is a function of the problem definition and error requested, but not of the discretization itself.

4.3.4 Oracle

From the above arguments, we have seen that the function `Oracle` can be implemented by estimating the ratio of size to distance, or in the vicinity of the singularity, simply the size itself. In the case of radiosity with constant basis functions, measuring the ratio is particularly simple since it is given by the point to finite area form factor, a quantity for whose computation many formulas are known (see for example [171] or [146]). This was the oracle used in the original HR algorithm [102]. For higher order methods a simple form factor estimate is sufficient to argue the asymptotic bounds, but does not take full advantage of the information present. There are other, more direct methods to estimate the quantity $|\widehat{G} - G|$ discussed in the next section.

4.3.5 Higher Orders

Consider again the argument used above to show that HR constructs only a linear number of interactions. There was nothing particular in the argument which ties it to constant basis functions. Suppose we wish to employ a Galerkin scheme with higher order basis functions. In this case each interaction between two elements entails a number of quadratures. For constant basis functions there was simply one coefficient G_{ij} for elements `i` and `j`. We will continue to use the indexing G_{ij}, but think of the quantity G_{ij} as consisting of an array of numbers describing all the possible coupling terms over the given elements due to higher order basis functions. For example, in the case of piecewise linear basis functions we have two basis functions along each dimension. In flatland G_{ij} now consists of $2 \cdot 2$ couplings and in 3D G_{ij} has $2^2 \cdot 2^2$ numbers associated with it. If $M - 1$ is the order of basis functions used we will abstract $M \cdot M$ (flatland) and $M^2 \cdot M^2$ (3D) couplings respectively into G_{ij}.

The basic reasoning of the recursion count argument still holds. $|\widehat{G} - G|$ is still the quantity which needs to be kept below some $\delta(\epsilon)$, however $\widehat{G}$ is not constant anymore. The form factor argument to measure angle subtended does not take full advantage of the power of higher order basis functions. However, it is still sufficient to argue the asymptotic bound. In practice we will of course want to take advantage of the higher order nature of the basis functions. One way to do this is to have the function `Oracle` use an estimate of the G_{ij} to construct a polynomial and measure how well this polynomial interpolates the real kernel G over the support of the two elements in question. This type of oracle was employed in the case of wavelet radiosity [94, 166] and estimates the quantity $|\widehat{G} - G|$ directly.

4.3.6 Iterative Solvers

As pointed out earlier there are two parts to a complete algorithm, setting up the equations, and solving them. Above we described how to set up the equations and argued why there are $O(k^2 + n)$ interactions total for any given finite accuracy requirement. To complete the algorithm we need the iteration function. This function corresponds to the matrix/vector multiply in an iterative solver. In HR this was referred to as `Gather`, a function which moves radiosity from element `j` across G_{ij} to element `i`, multiplying it with the factor G_{ij} (the form factor for constant basis functions). Once this has occurred we still need a function referred to as `PushPull` in [102].

For each input surface (element) `i`, `ProjectKernel` is called with all other input surfaces (elements) `j`. As pointed out above, the choice of interactions G_{ij} actually created corresponds to an implicit choice of basis functions. Consequently when `ProjectKernel` was called on, say `i` and $\mathtt{j}_0$, versus `i` and $\mathtt{j}_1$, different basis functions may have been constructed on `i` for those two calls. Put differently, irradiance at

a surface will be computed at different levels of the hierarchy, due to different sources. These incoming irradiances need to be consolidated.

Consider the function `PushPull` as proposed in Hanrahan *et al.*[102]. Irradiance of a parent in the subdivision hierarchy is added to the children on a downward pass, while on an upward pass the radiosity at a parent is the area average of the radiosity at the children

```
PushPull( Element i )
   if( !Leaf( i ) )
      i.children.E += i.E; //Push
      ForAllChildren( i.c )
         PushPull( i.c );
      i.B = AreaAverage( i.children.B ); //Pull
   else
      i.B = i.Be + ApplyRho( i.E );
```

where we used the symbols `B` to denote radiosity, `E` to denote irradiance, and `Be` for the emitted part of radiosity.

The summing of irradiance on the way down follows immediately from the physical meaning of irradiance. The irradiance at a given element is the sum of all the irradiances received at the element itself and all its ancestor elements. The area averaging on the way up follows directly from the definition of constant radiosity, which is a density quantity per area.

How to extend this `PushPull` reasoning to the higher order hierarchical algorithm briefly outlined above is not immediately clear. This is where wavelets come in since they not only generalize the notion of higher order hierarchical basis sets, but also the attendant notions of pushing (pyramid down) and pulling (pyramid up) throughout such a hierarchy.

4.4 $O(n)$ Sparsity

The abstract mathematical proof of the $O(n)$ sparsity claim for certain integral operators given by Beylkin *et al.*[15] is the exact analog of the constructive geometric argument we gave above for the $O(n)$ claim of HR. The main difference is that the abstract proof argues that *all but* $O(n)$ entries in the resulting matrix system are below the threshold, while HR argues the complement: *only* $O(n)$ entries are above the threshold.

In HR we argued that for a given allowable error of ϵ we can permit some amount of error (δ) across each link and that there would only be a linear number of such links. In fact we used scaling functions (piecewise polynomial) as basis functions. Saying that there is an error of δ for one such approximation is equivalent to saying that the associated wavelet coefficient is less than δ (for sufficiently smooth kernels). Recall that the wavelet coefficient measures the difference between one level of approximation and the next finer level (recursive splitting) of approximation.

While we used an "angle subtended" argument to limit the number of coefficients thusly created the classical falloff property (Equation 5) is the abstract analog of this geometric statement. Recall the bound we gave on the coefficients of ψ for a smooth function f (Equation 4). It bounds the magnitude by interval (area) size raised to the M^{th} power multiplied with the derivative. But for integral operators we have a bound on these derivatives of the form $|x - y|^{-d-M}$. In other words the coefficients are bounded by a power

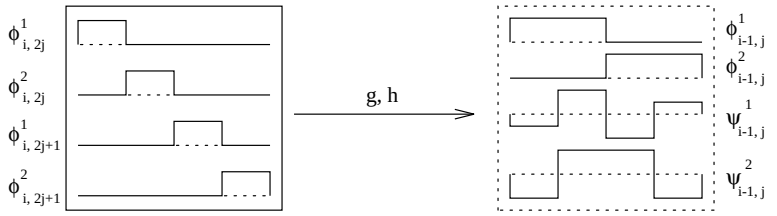

Figure VI.6: The $\mathcal{F}_2$ wavelet construction. $\mathcal{F}_2$ bases have two different wavelet functions. Both of them have two vanishing moments (from [94]).

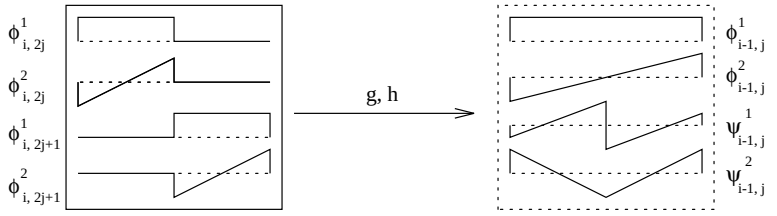

Figure VI.7: The $\mathcal{M}_2$ wavelet construction whose scaling functions are the first two Legendre polynomials. Both of the wavelet functions (lower right) have two vanishing moments (from [94]).

of a size (interval or area) to distance ($|x - y|$) ratio. The same argument we used earlier in the context of radiosity, except this time made on purely mathematical grounds with no reference to the surrounding geometry. In this way the classical argument of Beylkin *et al.* generalizes to other integral operators an idea that is perhaps more obvious in the geometrical context of graphics.

One issue remains. The abstract theory of integral operators has us use the scaling *and* wavelet functions to construct the sparse linear system. WR [94] (or higher order hierarchical methods) only use the scaling functions.

Consider again the Haar example. Suppose we are using the Haar basis for a non-standard realization of our operator (see Figure VI.4 left column). If we ignore all entries in the matrix less than some threshold we will be left with some set of entries corresponding to couplings between a mixture of scaling and wavelet functions. In the Haar case we can transform this set of couplings into a set of couplings involving *only* scaling functions by exploiting the two scale relationship. Simply replace all occurrences of $\psi_{i,j}$ with $2^{-1/2}\varphi_{i+1,2j} - 2^{-1/2}\varphi_{i+1,2j+1}$. The remaining set of couplings involves only scaling functions.

The reason the Haar basis allowed us to do this simplification lies in the fact that the scaling functions in the Haar system do not overlap. For more general wavelets there is overlap between neighboring functions. Consequently the above substitution, while still possible [92], is not as straightforward. The problem arises with overlapping basis functions because some regions may be accounted for multiple times, in effect introducing the same power more than once into the system. The wavelets that were used in the original WR work [94, 166] did not suffer from this problem because they were tree wavelets. In a tree wavelet the filter sequences do not overlap.

The Haar basis is a tree wavelet basis. When trying to extend these ideas to more vanishing moments we have to allow more than one wavelet (and scaling) function over a given interval to keep the filter sequences from overlapping. In essence neighboring intervals are decoupled. This is not a classical construction because there are multiple generators of the MRA. WR used so called Flatlets, which are still piecewise constant, but combine more than two box functions to increase the number of vanishing moments (Figure VI.6 shows the

shape of Flatlets with two vanishing moments). Another set of wavelets explored for WR was introduced by Alpert [2] under the name multi-wavelets. Over each interval a set of Legendre polynomials up to some order $M-1$ is used and a wavelet hierarchy is imposed. Here too, neighboring intervals decouple giving multi-wavelets the tree property as well (see Figure VI.7 for a multi-wavelet with two vanishing moments). Details regarding these functions in the context of WR can be found in [94, 166].

Using tree wavelets and the substitution of all wavelet functions by sequences of scaling functions leads to an obvious simplification of the code and follows naturally from the historical development. It also results in a straightforward procedure to enumerate all "important" couplings and circumvents all issues associated with boundaries. Instead of specializing a wavelet constructed for the real line to one usable for an interval the multi-wavelets and Flatlets have the interval property right from the start.

There are other practical issues which are taken up in the original papers and the interested reader is referred to them for more details ([94, 166]). For example, in some wavelet constructions only the primal (or dual) bases have vanishing moments. Recall that the G_{ij} (Equation 3) had both primal and dual bases under the integral sign. If only one of these has vanishing moments, say the primal basis, it is desirable to use a projection into the dual basis on the left hand side of the original operator, $P_{\tilde{V}}\mathcal{G}P_V$. This was the case in [94, 166] for the so called Flatlets. Doing this requires a basis change back to the primal basis after each iteration of the operator. This is easily absorbed into the `PushPull` procedure, though.

5 Issues and Directions

In our treatment so far we have deliberately left out a number of issues arising in a real implementation for purposes of a clear exposition of the general principles. We now turn to some of these issues as well as to a discussion of extensions of the basic ideas.

5.1 Tree Wavelets

Both HR and WR used scaling functions which do not maintain continuity across subdivision boundaries. While convergence of the computed answers is assured in some weighted error norm, there is nothing in the algorithm which will guarantee continuity between adjacent elements. This has undesirable consequences for purposes of displaying the computed answers. Discontinuities in value or even derivative lead to visually objectionable artifacts (e.g., Mach bands).

These discontinuities arose from a desire to use tree wavelets. Recall that in classical wavelet constructions with more than 1 vanishing moment the supports of neighboring scaling functions overlap. In this way continuity between neighboring mesh elements up to some order (depending on the wavelet used) can be assured. Two difficulties arise if one wants to use such wavelets: (A) They need to be modified at the boundary of the original patch since overlap onto the outside of the patch is not desirable (it is not even physically meaningful); (B) sparse representations, i.e., partially refined subdivisions, are difficult to build with such wavelets. To appreciate the latter point consider the scaling function associated with the subdivision child of some element. If the neighboring element does not get subdivided, i.e., does not have children itself, the former scaling function will again overlap a "niece" element which does not exist. Tree wavelets avoid both of these issues. Since they inherently live on the interval no overlap outside the interval or over "niece" elements, which do not exist, can occur. Furthermore every wavelet can be replaced immediately by a linear combination of its constituent scaling functions, resulting in a much streamlined program which only needs to deal with scaling functions. This convenience comes at a cost of higher storage.

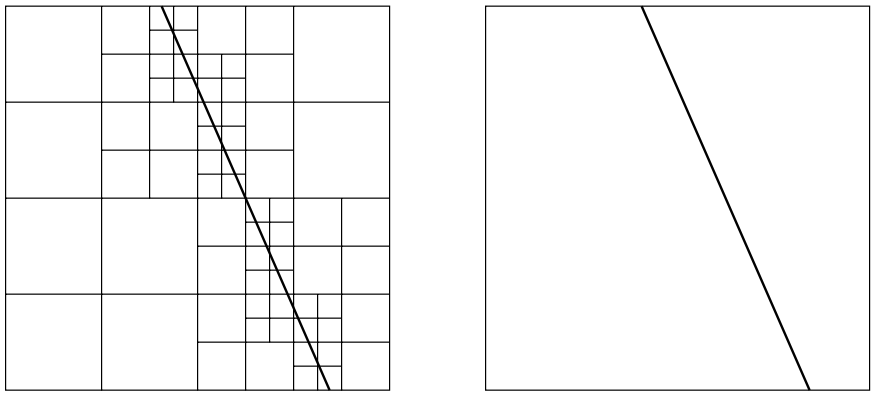

Figure VI.8: Subdivision around a feature line (bold diagonal line). On the left a restricted quadtree subdivision bracketing the feature line to within some grid resolution. On the right subdivision is induced immediately along the feature line, representing it perfectly and resulting in far fewer elements.

Whenever an element is subdivided we do not just simply add a single new coefficient to the representation of the kernel, but rather a chunk. Consider 3D radiosity and wavelets with M vanishing moments. In this case every G_{ij} actually consists of $(M^2)^2$ coefficients (one for each possible combination of bases over the two elements). For cubic bases the refinement of an existing interaction into 4 child interactions results in $3 \cdot 256$ additional floating point coupling coefficients.

Preliminary experiments with classical wavelets for radiosity have recently been reported by Pattanaik and Bouatouch [152]. They used Coiflets [52] as well as interpolating scaling functions [63]. However, they ignored issues associated with the boundary of patches, the singularity, and only gave an algorithm which does uniform refinement when the error criterion is not met (resulting in an $O(n^2)$ algorithm).

Clearly more research is needed for an algorithm which uses overlapping scaling functions of higher regularity and properly addresses boundary and adaptive subdivision issues.

5.2 Visibility

The basic premise on which the sparsification arguments for integral operators rest is the smoothness of the kernel function. However, in the case of radiosity the kernel function contains a non-smooth component: the visibility function $V(x, y)$. Clearly the kernel is still piecewise smooth so the arguments certainly hold piecewise. Alternatively, the arguments can be approached with a notion of smoothness as defined in the Besov space sense. However, the complexity analysis is considerably more complicated. To our knowledge no such analysis has yet been performed. We hypothesize that the total number of coefficients will have a component which is in some sense proportional to the "length" of the discontinuity.

In practice two basic approaches have emerged to address the discontinuities in the kernel function. HR [102] and WR [166, 94] use regular quadtree subdivision of quadrilaterals. Thus they in effect resolve the resulting features in the computed radiosity function by approximating them with successively smaller rectangles (see the left side of Figure VI.8). Since the oracle is based on estimating how well the kernel is approximated by a low order polynomial over the support of the two elements in question, it will automatically "zoom" in on these feature boundaries. This follows trivially from the fact that the discontinuity in the kernel is not well approximated by a low order polynomial. Another approach has been put forward by Lischinski *et al.*[121]. They take the feature lines due to discontinuities in the visibility function explicitly into account

with *discontinuity meshing*. Instead of using regular subdivision they introduce subdivisions along lines of discontinuities in the computed answer (see the right side of Figure VI.8). As a result they generate far fewer elements and discontinuity features are resolved exactly. The disadvantage of their approach lies in the considerably more complicated global visibility analysis necessary to find all such feature lines. Another difficulty arises from the fact that such an approach needs wavelets over irregularly subdivided domains. Lischinski *et al.*[121] stayed within the HR, i.e., constant basis function, framework. In this case the filter coefficients for `PushPull` are still just simple area ratios. Piecewise polynomial triangular elements could be accommodated as well in a straightforward extension of the use of multi-wavelets in [94]. The feasibility of this approach was recently examined by Bouatouch and Pattanaik [16]. Classical wavelets however, have only recently been adapted to irregular meshes [126, 168] and they have not yet been applied to wavelet radiosity algorithms with explicit (or implicit) discontinuity meshing.

5.3 Radiance

The basic ideas behind HR and WR can also be applied to the computation of *radiance,* i.e., global illumination in the presence of reflection which is no longer uniform with respect to direction. In this case the physical quantity of interest has units $[\frac{W}{m^2 sr}]$ and the basic integral equation to solve becomes

$$L(y,z) = L^e(y,z) + \int_{\mathbf{M}^2} f_r(x,y,z) G(x,y) L(x,y)\, dx.$$

Here $L(y,z)$ is the unknown radiance function describing the flow of power from y to z, f_r is the bidirectional reflectance distribution function (BRDF), and G accounts for geometry as before (with $c = 1$). The BRDF gives the relation at y between incoming radiance from x and outgoing radiance towards z.

Aupperle and Hanrahan [8] were the first to give a hierarchical finite element algorithm for radiance computations. They extended their earlier work [102] in a straightforward manner by considering triple interactions from A_x via A_y towards A_z (as opposed to the case of radiosity with interactions from A_x towards A_y). The complexity arguments are similar to the ones we gave for the case of radiosity with the difference that the overall complexity is now $O(k^3 + n)$ since initially all triples of surfaces have to be accounted for. This work was extended to higher order multi-wavelet methods in [167].

In both of these approaches [8, 167] radiance was parameterized over pairs of surfaces. Christensen *et al.*[23] pursued a different avenue. They treated radiance as a function of a spatial and *directional* argument given by the corresponding integral equation

$$L(y,\omega_o) = L^e(y,\omega_o) + \int_{\mathbf{H}^2} f_r(\omega_i, y, \omega_o) \cos\theta_i L_i(y,\omega_i)\, d\omega_i,$$

where $L_i(y,\omega_i) = L(x,-\omega_i)$ is the incoming radiance at y from direction ω_i, which is identical to the outgoing radiance at some point x visible from y in the direction ω_i. The integration is now performed over the hemisphere of incoming directions. The chief advantage of this formulation is the fact that recursive coupling coefficient enumeration needs to consider only all *pairs* of input surfaces. As a basis they used the Haar basis for the spatial support. For the directional part of the domain they constructed a basis by parametrically mapping the Haar basis over the unit square onto the hemisphere. For a more detailed discussion of some of the differences between these two approaches the reader is referred to [167].

Computing solutions to the radiance integral equations is notoriously expensive due to the higher dimensionality of the involved quantities, 4D functions interacting across a 6D integral operator with 4D functions.

Naive finite element methods are hopeless, but even hierarchical methods based on wavelets still require enormous amounts of space and time and more research is needed before these techniques become truly practical.

5.4 Clustering

In all our discussions so far we have only considered the intelligent *subdivision* of surfaces. Ironically the historical roots of HR lie in n-body algorithms [98], which are all about clustering, not subdivision. This difference moves most clearly into focus when considering the complexity analysis we gave earlier. There we argued that HR and WR have a complexity of $O(k^2 + n)$ where k is the number of input surfaces and n the number of elements they are meshed into. In order to remove the k^2 dependence the hierarchy of interactions must be extended "upward". A number of such clustering algorithms have recently appeared in the literature [163, 173, 172, 22].

The main difficulty with clustering in the context of radiosity is due to visibility. For example, the light emitted by a cluster of elements is not equal to the sum of the individual emissions. Similarly, the reflective behavior of a cluster is not uniform in all directions even though each individual reflection is uniform in the hemisphere above the respective surface.

Sillion [172] realizes clustering of surfaces by imposing an octree partition on the entire scene and treating all surfaces within one of the octree nodes as an approximate volume density. In the limit with surfaces very small and uniform in each cube of the octree the resulting approximation is correct. The resulting datastructure can be built in time linear in the number of surfaces and the only modification to an existing HR solver is the introduction of volume elements characterized by their averaged behavior. As observed by Sillion even in the case of purely diffuse reflection the aggregate behavior of any volume is generally not diffuse (uniform in all directions). In order to account for this observation a correct system needs to be able to deal with directionally dependent quantities.

Smits *et al.*[173] give a clustering extension to HR with a complexity of $O(k \log k + n)$ by introducing higher level links between clusters of surfaces. The main task is to set up an error estimator usable by the oracle, which is conservative but tight for such links. They too deal only with isotropic approximations of clusters. Noting this deficiency Christensen *et al.*[22] give a clustering algorithm which addresses the more general radiance case. Each cluster is treated as a point source (and receiver) whose behavior is characterized as a function of direction with a small number of discretized directions. In this way the resulting algorithm is more closely related to the multipole based algorithm of Greengard [98] rather than a wavelet method.

All of the above clustering algorithms compute an approximation of the radiosity or radiance at such a coarse level that a final reconstruction step (also referred to as final gather) needs to be added to produce an acceptable looking final image. This final step is generally very expensive and better techniques are clearly desirable.

6 Conclusion

We have seen that the Galerkin method for integral equations gives rise to a linear system which needs to be solved to find an approximation to the original integral equation solution. The linear system has entries which are the coefficients of the kernel function itself with respect to some basis (standard or non-standard). As such they possess properties which derive directly from the kernel function itself. Using wavelets as

basis functions the resulting matrix system is approximately sparse if the kernel function is smooth. A wide class of operators whose kernel functions satisfy certain "falling off with distance" estimates have the right properties. By ignoring all entries below some threshold the resulting linear system has only $O(n)$ remaining entries leading to fast solution algorithms for integral equations of this type. To realize an algorithm which is $O(n)$ throughout a function `Oracle` is needed to help enumerate the important entries in the matrix system.

HR was described in this context as an application of the Haar basis to the radiosity integral equation. We argued that HR needs only a linear number of interactions between elements to achieve an a-priori accuracy claim. The argument used geometric reasoning which corresponds exactly to the abstract arguments given by Beylkin *et al.*[15]. In this way we in effect gave a constructive, geometric proof of the sparsity claim for somewhat more benign operators than are treated in the general case. The development of these arguments led to a WR algorithm which has been shown to perform exceedingly well in practice under many circumstances [102, 166, 94, 88, 184].

The original method [166, 94] used tree wavelets (multi-wavelets and Flatlets) which simplify many implementation issues and are a natural extension from the historical development out of HR. As such the exploration of interesting basis functions from the wide variety of available wavelet bases has only begun and we look forward to further developments in this area.

VII: More Applications

Michael F. COHEN
Princeton University

Wim SWELDENS
University of South Carolina

Alain FOURNIER
University of British Columbia

1 Hierarchical Spacetime Control of Linked Figures
(Michael F. Cohen, Zicheng Liu, Steven J. Gortler)

These course notes are excerpted from *Hierarchical Spacetime Control*, by Zicheng Liu, Steven J. Gortler, and Michael F. Cohen, *SIGGRAPH, 1994*.

1.1 Introduction

The spacetime constraint method, proposed in 1988 by Witkin and Kass [195], and extended by Cohen [37], has been shown to be a useful technique for creating physically based and goal directed motion of linked figures. The basic idea of this approach can be illustrated with a three-link arm and a ball (see Figure VII.1). The problem statement begins with specifying *constraints*, examples being specifying the position of the arm at a given time, requiring the ball to be in the hand (end effector) at time t_0, and that the arm is to throw the ball at time t_1 to land in a basket at time t_2. In addition, the animator must specify an *objective* function, such as to perform the tasks specified by the constraints with minimum energy or some other style consideration. The solution to such a series of specifications is a set of functions through time (or *trajectories*) of each degree of freedom (DOF), which in this case are the joint angles of the arm. Thus the unknowns span both space (the joint angles) and time, and have led to the term *spacetime constraints*.

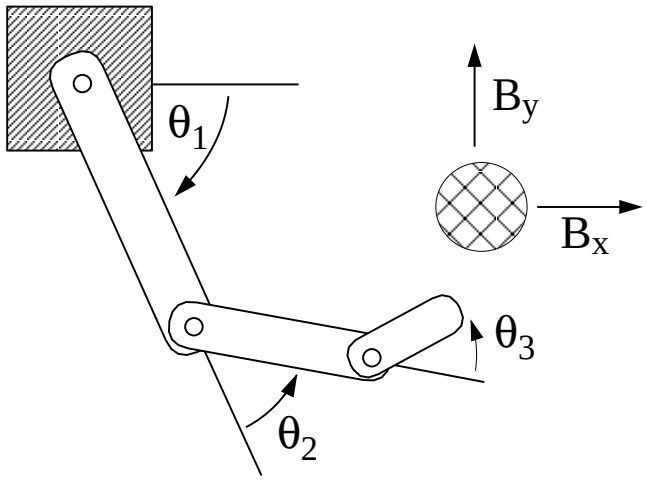

Figure VII.1: A planar three-link arm.

Related approaches to the spacetime constraint paradigm are reported in [189, 149]. In each of these papers, feedback control strategies are the fundamental unknown functions rather than DOF trajectories. The goal is set, for example, for the creature to move in some direction as far as possible in 10 seconds, and a *score* for a particular motion is defined as the distance traveled. An initial control strategy is selected, a dynamic simulation is run and the results are scored. Iterations change the control strategy, as opposed the motion curves, producing a simulation that, hopefully, has a higher score. The results of these studies are encouraging, however, they are distinctly different from that in the previous spacetime constraint work (and the work described in this paper) in which the aim is to provide the animator with the overall control of the motion.

The spacetime constraint formulation leads to a non-linear constrained variational problem, that in general, has no closed form solution. In practice, the solution is carried out by reducing the space of possible trajectories to those representable by a linear combination of basis functions such as cubic B-splines. Finding the finite number of coefficients for the B-splines involves solving the related constrained optimization problem, (i.e., finding the coefficients to create motion curves for the DOF that minimize the objective while satisfying the constraints). Unfortunately, general solutions to such a non-linear optimization problem are also unknown.

Based on this observation, Cohen developed an interactive spacetime control system using hybrid symbolic and numeric processing techniques [37]. In this system, the user can interact with the iterative numerical optimization and can *guide* the optimization process to converge to an acceptable solution. One can also focus attention on subsets or *windows* in spacetime. This system produces physically based and goal directed motions, but it still suffers from a number of computational difficulties, most notably as the complexity of the creature or animation increases.

An important difficulty in the spacetime system is that the user is required to choose the discretization of the B-spline curves. If not enough control points are selected, there may be no feasible solution (i.e., one that meets all constraints), or the restriction to the curve is so severe, that the resulting motion curves have a much higher objective cost than necessary. If too many control points are selected, then the computational complexity is increased unnecessarily due to the larger number of unknowns as well as the resulting ill-

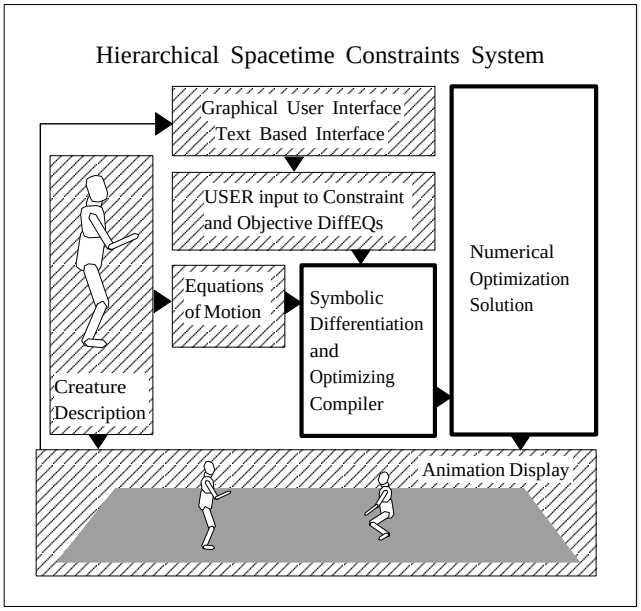

Figure VII.2: The Hierarchical Spacetime Constraints System. This paper focuses on the Symbolic Differentiation and Optimizing Equation Compiler, and the Numerical Optimization System

conditioning of the linear subproblems that arise in the solution [185]. This complexity issue is addressed by reformulating the DOF functions in a *hierarchical* basis, in particular, in a B-spline wavelet (B-wavelet) basis. Wavelets provide a natural and elegant means to include the proper amount of local detail in regions of spacetime that require the extra subdivision without overburdening the computation as a whole.

1.2 System overview

The interactive spacetime control system is shown in Figure VII.2. Input to the system includes user defined constraints and objectives and a creature description from which the symbolic equations of motion are generated automatically. The equations of motion define the torque at each joint as a function of the position and velocity of all joints as well as physical properties such as mass and length of the links. These expressions for torque are central to the definition of a minimum energy objective. The expressions are next symbolically differentiated and compiled to create concise evaluation trees.

The main focus of the current discussion is on the next section, the numerical process that solves for the coefficients of the chosen B-spline or hierarchical wavelet basis. Finally, the intermediate and final animations are displayed graphically. The animator can simply watch the progress of the optimization procedure or can interact directly with the optimization by creating starting motion curves for the DOF and/or by modifying intermediate solutions.

1.3 Wavelets

An elegant and concise hierarchical basis, and one that leads naturally to an adaptive basis, is offered by a *wavelet* construction. This section concentrates on the advantages of wavelets and wavelet formulations in the spacetime animation problem.

The wavelet construction results in a non-redundant basis that provides the means to begin with a low resolution basis and then *adaptively refine* the representation layer by layer when necessary without changing the representation above. If refinements are required in only part of the interval, then only those coefficients whose bases have support in this region need to be added.

Since the wavelet coefficients encode differences, in smooth portions of the trajectory the coefficients encoding finer scale detail will be zero. Thus, only those basis functions with resulting coefficients greater than some ϵ will have a significant influence on the curve and the rest can be ignored. In other words, given an *oracle* function [97, 93], that can predict which coefficients will be above a threshold, only the corresponding subset of wavelets needs to be included.

Solutions to the non-linear spacetime problem, involve a series of quadratic subproblems for which the computational complexity depends on the number of unknown coefficients. The smaller number of significant unknown coefficients in the wavelet basis provide faster iterations. In addition, the wavelet basis provides a better conditioned system of equations than the uniform B-spline basis, and thus requires less iterations. The intuition for this lies in the fact that there is no single basis in the original B-spline basis that provides a global estimate of the final trajectory (i.e., the locality of the B-spline basis is, in this case, a detriment). Thus, if the constraints and objective do not cause interactions across points in time, then information about changes in one coefficient travels very slowly (in $O(n)$ iterations) to other parts of the trajectory. In contrast, the hierarchical wavelet basis provides a shorter ($O(\log(n))$) "communication" distance between any two basis functions. This is the basic insight leading to *multigrid* methods [185], and the related hierarchical methods discussed here.

The wavelet representation also allows the user to easily lock in the coarser level solution and only work on details simply by removing the coarser level basis functions from the optimization. This provides the means to create small systems that solve very rapidly to develop the finest details in the trajectories.

1.3.1 B-wavelets

In the literature, there are many wavelet constructions, each with its own particular functions φ an ψ, with varying degrees of orthogonality, compactness, and smoothness. The particular wavelet construction used in this work are derived in [26], and were chosen because of the semi-orthogonality of the basis, the associated φ is a cubic B-spline (i.e., C^2), and the wavelet function ψ is symmetric with compact support.

1.3.2 Wavelets on the Interval

In a classical wavelet construction, the domain goes from $-\infty \ldots \infty$. In an animation context, only functions over some fixed finite interval of time need to be expressed, and it is important to only deal with a finite number of basis functions. Therefore, the function space V_L used here is defined to be the space of all C^2 functions defined over the interval $[0 \ldots 2^L]$ that are piecewise cubic between adjacent integers (simple knots at the inner integers and quadruple knots at the boundaries). A basis for V_L is made up of *inner* basis functions, which are just those translational B-spline basis functions $\varphi_{L,j}$ whose support lies completely within the interval, as well as three special *boundary* B-spline basis functions at each end of the interval. For the boundary basis functions, one may either choose to include the translational basis functions $\varphi_{L,j}$ themselves whose support intersects the boundaries by just truncating those basis functions at the boundary, or else one may use the special boundary basis functions that arise from placing quadruple knots at the boundaries [13]. This complete set of basis functions will be denoted $\varphi_{L,j}$ with j in $\{-3 \ldots 2^L - 1\}$, where

it is understood that the first and last three basis functions are the special boundary B-spline basis functions.

A two-part basis for V_L can be constructed with the wider B-spline functions $\varphi_{L-1,j}$ with j in $\{-3 \ldots 2^{L-1} - 1\}$ where again the first and last three basis functions are scaled versions of the special boundary B-splines functions. The two-part basis is completed with the wavelet functions $\psi_{L-1,j}$ with j in $\{-3 \ldots 2^{L-1} - 4\}$. Here too, the *inner* wavelet basis functions are just those translational functions $\psi_{L-1,j}$ that do not intersect the boundaries, while the first three and the last three interval wavelet basis functions must be specially designed to fit in the interval and still be orthogonal to the $\varphi_{L-1,j}$. A full description of this construction is given in [29, 159].

1.3.3 Completing the Wavelet Basis

The reasoning that was used to construct the two-part basis can now be applied recursively $L-3$ times to construct a multilevel *wavelet basis*. Noting that roughly half of the basis functions in the two-part basis are themselves B-spline basis functions (only twice as wide), to continue the wavelet construction, keep the basis functions $\psi_{L-1,j}$ and recursively apply the reasoning above to replace the $\varphi_{i,j}$ with $\{\varphi_{i-1,j}, \psi_{i-2,j}\}$.

Each time this reasoning is applied, the number of B-spline functions in the hierarchical basis is cut in half (roughly), and the new basis functions become twice as wide. After $L-3$ applications, the wavelet basis

$$\{\varphi_{3,k}, \psi_{i,j}\} \tag{1}$$

is obtained, with i in $\{3 \ldots L-1\}$, k in $\{-3 \ldots 7\}$ and j in $\{-3 \ldots 2^i - 4\}$, where the inner basis functions are defined by

$$\begin{aligned} \varphi_{i,j}(t) &= \varphi(2^{(i-L)}t - j) \\ \psi_{i,j}(t) &= \psi(2^{(i-L)}t - j) \end{aligned} \tag{2}$$

This basis is made up of eleven wide B-splines, and translations (index j) and scales (index i) of the wavelet shape (as well as scales of the boundary wavelet basis functions).

The wavelet basis is an alternate basis for V_L, but unlike the B-spline basis, it is an $L-3$ level hierarchical basis. At level 3 there are eleven broad B-splines, and eight broad wavelets. These basis functions give the coarse description of the function. At each subsequent level going from level 3 to $L-1$, the basis includes twice as many wavelets, and these wavelets are twice as narrow as the ones on the previous level. Each level successively adds more degrees of detail to the function.

Since each wavelet coefficients represents the amount of local detail of a particular scale, *if the function is sufficiently smooth in some region, then very few non-zero wavelet coefficients will be required in that region*[1].

1.3.4 Scaling

One final issue is the scaling ratio between the basis functions. Traditionally [26] the wavelet functions are defined with the following scaling:

[1] In this case, non-zero can be defined to be having an absolute value greater than some epsilon without incurring significant error in the representation.

$$\begin{aligned} \varphi_{i,j}(t) &= 2^{(i-L)/2}\, \varphi(2^{(i-L)}t - j) \\ \psi_{i,j}(t) &= 2^{(i-L)/2}\, \psi(2^{(i-L)}t - j) \end{aligned} \tag{3}$$

This means that at each level up, the basis functions become twice as wide, and are scaled $\frac{1}{\sqrt{2}}$ times as tall. While in many contexts this normalizing may be desirable, for optimization purposes it is counter productive. For the optimization procedure to be well conditioned [45] it is advantageous to emphasize the coarser levels and hence use the scaling defined by

$$\begin{aligned} \varphi_{i,j}(t) &= 2^{L-i}\, \varphi(2^{(i-L)}t - j) \\ \psi_{i,j}(t) &= 2^{L-i}\, \psi(2^{(i-L)}t - j) \end{aligned} \tag{4}$$

where the wider functions are also taller.

1.4 Implementation

The input to the wavelet spacetime problem includes the creature description, the objective function (i.e., symbolic expressions of joint torques generated from the creature description), and user defined constraints specifying desired actions (throw, catch, etc.), and inequality constraints such as joint limits on the elbow.

Each trajectory of a DOF, $\theta(t)$, is represented in the uniform cubic B-spline basis. The unknowns are then the B-spline coefficients, $\mathbf{b}$, or the equivalent wavelet coefficients, $\mathbf{c}$, scaling the individual basis functions. This finite set of coefficients provide the information to evaluate the $\theta(t)$, $\theta\dot{(}t)$, and $\theta\ddot{(}t)$ at any time t, that comprise the leaves of the DAGs. This finite representation transforms the variational problem into a constrained non-linear optimization problem. An unconstrained problem can then be derived by penalizing violations to the constraints.

A quasi-Newton method, BFGS [79], is used to solve the resulting non-linear problem. Iterations begin with a user provided initial guess of wavelet coefficients (that can be derived from B-spline coefficients) and a guess of the inverse of the Hessian (usually an identity matrix leading to the first iteration being a simple gradient descent).

Each subsequent iteration involves finding the gradient of the modified constraint/objective function and performing a matrix-vector multiply. The newly obtained solution is then transformed into B-spline coefficients and sent to the graphical user interface for display.

If the initial function space is restricted to a coarse representation consisting of the broad B-splines and a single level of wavelets, after each iteration a simple *oracle* function adds wavelets at finer levels only when the wavelet coefficient above exceeds some tolerance. This procedure quickly approximates the optimal trajectory and smoothly converges to a final answer with sufficient detail in those regions that require it.

An important feature of the system discussed in [37] is also available in the current implementation. The user can directly modify the current solution with a simple key frame system to help *guide* the numerical process. This is critical to allow the user, for example, to move the solution from an underhand to an overhand throw, both of which represent local minima in the same optimization problem. The next iteration then begins with these new trajectories as the current guess.

1.5 Results

A set of experiments was run on the problem of a three-link arm and a ball (see Figure VII.1). The goal of the arm is to begin and end in a rest position hanging straight down, and to throw the ball into a basket. The objective function is to minimize energy, where energy is defined as the integral of the sum of the squares of the joint torques. Gravity is active.

The four graphs in Figure VII.3 show the convergence of five different test runs of the arm and ball example. Each plot differs only in the starting trajectories of the arm DOF. Each run converged to either an underhand or overhand throw into the basket. The full B-spline basis contained 67 basis functions for each of the three DOF, thus there were 201 unknown coefficients to solve for. Iterations took approximately 7 seconds each on an SGI workstation with an R4000 processor. Convergence was achieved on each, but only after many iterations due to the ill-conditioning of the B-spline formulation.

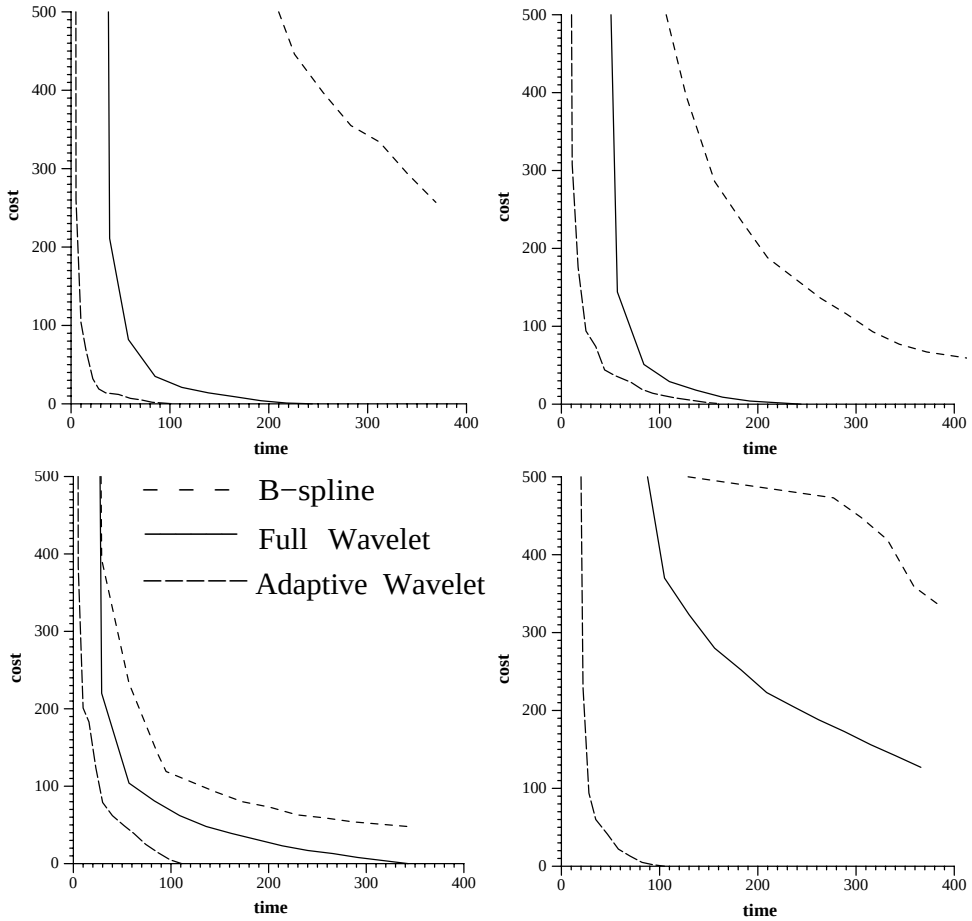

Figure VII.3: Convergence of Arm and Ball example for 4 different starting trajectories. The first and fourth examples resulted in underhand throws, and the rest overhand. Time is in seconds, and the cost is a weighted sum of constraint violations and energy above the local minimum.

The full wavelet basis also contained 67 basis function per DOF (11 B-splines at the top level and 56 wavelets below), thus iterations also took approximately the same 7 seconds. Figure VII.3 clearly shows the improved convergence rates of the wavelet formulations over the B-spline basis, due to better conditioned linear systems. The adaptive wavelet method with the oracle was the fastest since the number of unknowns was small in early iterations, leading to a very fast approximation of the final trajectories, in addition to the better conditioning provided by the hierarchical basis. The final few iterations involved more wavelets inserted by the oracle to complete the process. Note that in each case, a good approximation to the complete animation was achieved in less than a minute of computation.

1.6 Conclusion

The spacetime constraint system first suggested by Witkin and Kass [195] for animating linked figures has been shown to be an effective means of generating goal based motion. Cohen enhanced this work by demonstrating how to focus the optimization step on *windows* of spacetime and methodologies to keep the user in the optimization loop. These notes discuss extentions to this paradigm by removing two major difficulties.

A major improvement lies in the representation of the trajectories of the DOF in a wavelet basis. This resulted in faster optimization iterations due to less unknown coefficients needed in smooth regions of the trajectory. In addition, even with the same number of coefficients, the systems become better conditioned and thus less iterations are required to settle to a local minimum. Results are shown for a planar three-link arm.

Acknowledgements

The authors owe a debt to Charles Rose who implemented the user interface for this work. This research was supported in part by the National Science Foundation, Grant CCR-9296146.

2 Variational Geometric Modeling with Wavelets

(Michael F. Cohen, Steven J. Gortler)

These course notes are excerpted from “Hierarchical and Variational Geometric Modeling with Wavelets”, by Steven J. Gortler and Michael F. Cohen, 1995 Symposium on Interactive 3D Graphics.

2.1 Abstract

This portion of the notes discusses how wavelet techniques may be applied to a variety of geometric modeling tools. In particular, wavelet decompositions are shown to be useful for B-spline control point or least squares editing. In addition, direct curve and surface manipulation methods using an underlying geometric variational principle can be solved more efficiently by using a wavelet basis. Because the wavelet basis is hierarchical, iterative solution methods converge rapidly. Also, since the wavelet coefficients indicate the degree of detail in the solution, the number of basis functions needed to express the variational minimum can be reduced, avoiding unnecessary computation. An implementation of a curve and surface modeler based on these ideas is discussed and experimental results are reported.

2.2 Introduction

Wavelet analysis provides a set of tools for representing functions hierarchically. These tools can be used to facilitate a number of geometric modeling operations easily and efficiently. In particular, these notes outline three paradigms for free-form curve and surface construction: control point editing, direct manipulation using least squares, and direct manipulation using variational minimization techniques. For each of these paradigms, the hierarchical nature of wavelet analysis can be used to either provide a more intuitive modeling interface or to provide more efficient numerical solutions.

In control point editing, the user sculpts a free-form curve or surface by dragging a set of control points. A better interface allows the user to directly manipulate the curve or surface itself, which defines a set of constraints. In a *least squares* paradigm, given a current curve or surface, the modeling tool returns the curve or surface that meets the constraints by changing the current control points by the least squares amount [12, 86].

The behavior of the modeling tool is determined by the type of control points and *basis functions* used to describe the curve or surface. With the uniform cubic B-spline basis, for example, the user's actions result in local changes at a predetermined scale. This is not fully desirable; at times the user may want to make fine changes of detail, while at other times he may want to easily make broad changes. Hierarchical B-splines offer a representation that allows both control point and least squares editing to be done at multiple resolutions [80]. Hierarchical B-splines, though, form an over-representation for curves and surface (i.e., any curve has multiple representations using hierarchical B-splines). As a result, the same curve may behave differently to a user depending on the particular underlying representation. In contrast, B-spline wavelets form a basis for the space of B-spline curves and surfaces in which every object has a unique representation. Wavelet methods in conjunction with B-splines provide a method for constructing a useful geometric modeling interface. This approach is similar to the one described by Finkelstein and Salesin [76]. In these notes we will discuss some of the various issues that are relevant to building such a modeling tool.

Variational modeling is a third general paradigm for geometric modeling[21, 194, 147]. In this setting, a user alters a curve or surface by directly manipulation, as above, defining a set of constraints. The variational modeling paradigm seeks the "best" solution amongst all answers that meet the constraints. The notion of best, which is formally defined as the solution that *minimizes some energy function*, is often taken to mean the *smoothest* solution.

In theory, the desired solution is the curve or surface that has the minimum energy of *all* possible curves or surfaces that meet the constraints. Unfortunately there is little hope to find a closed form solution [2]. Therefore, in practice, the "space" of parametric curves or surfaces is restricted to those represented by a linear combination of a fixed set of basis functions such as cubic B-splines. Given a set of n basis functions, the goal of finding the best curve or surface is then reduced to that of finding the best set of n coefficients. This reduction is referred to as the *finite element method* [187].

The general case requires solving a non-linear optimization problem. In the best case, the energy function is quadratic and the constraints are linear leading to a single linear system to solve. But even this can be costly when n is large since direct methods for matrix inversion require $O(n^3)$ time. To accelerate this process it is tempting to use gradient-type iterative methods to solve the linear system; these methods only take $O(n)$ time per iteration, due to the $O(n)$ matrix sparsity created by the finite element formulation. Unfortunately, the linear systems arising from a finite element formulation are often expensive to solve

[2] But see [141].

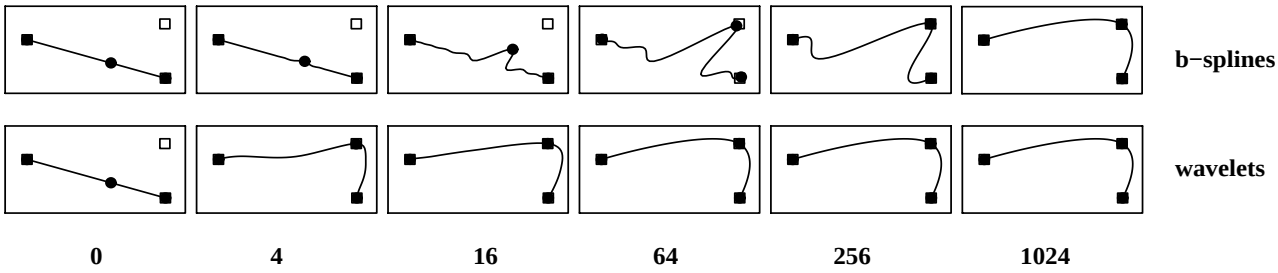

Figure VII.4: Minimum energy solutions subject to three constraints, found by the B-spline and wavelet methods after various numbers (0-1024) of iterations. (65 variables, 3 constraints). This illustrates the ill conditioning of the B-spline optimization problem.

using iterative methods. This is because the systems are ill-conditioned, and thus require many iterations to converge to a minimum [186, 182]. Intuitively speaking this occurs because each basis function represents a very narrow region of the answer; there is no basis function which can be moved to change the answer in some broad manner. For example, changing one coefficient in a cubic B-spline curve during an iteration alters the curvature in a local region only. In order to produce a broad smooth curve, the coefficients of the neighboring B-splines will move in next few iterations. Over the next many iterations, the solution process will affect wider and wider regions, and the effect will spread out slowly like a wave moving along a string. The result is very slow convergence (see Figure (VII.4)). One method used to combat this problem is multigridding [186, 81], where a sequence of problems at different resolution levels are posed and solved.

An alternative approach, is to use a *wavelet* basis instead of a standard finite element basis [182, 158, 109, 154]. In a wavelet basis, the answer is represented hierarchically. This allows the solution method to alter the answer at any desired resolution by altering the proper basis function, and thus the ill-conditioning is avoided. We will show how to use a wavelet construction, which is based on cubic B-splines, to quickly solve variational modeling problems in an elegant fashion.

Another problem with the finite element approach is choosing the density of the basis functions. If too few basis functions (too few B-spline segments or tensor product B-spline patches) are used then the solution obtained will be far from the actual minimum. If too many basis functions are used then unnecessary computation will be performed during each iteration (n is too big). In order to successfully choose a proper density, one must know how much detail exists in the variational minimum answer. Since, a priori, this is unknown, an efficient solver must be able to adaptively change the basis during the solution process [194], one needs an easy way to detect that too many or too few basis functions are being used. In addition, one needs a basis for which adding more detail, (i.e., refinement), is easy. Wavelets offer a basis where this task can be accomplished quickly and elegantly.

The work presented here combines the wavelet approaches of [182], [94], and [122]. Like [182], we use hierarchical basis functions as a pre-conditioner, so that fewer iterations are needed for convergence. Similar to [94] and [122], wavelets are also used as a method for limiting the solution method to the proper level of detail.

2.3 Geometric Modeling with Wavelets

The styles of interactive control discussed in the introduction will be revisited in the context of parametric representations. *Multiresolution modeling* allows the user to interactively modify the curve or surface at

different resolution levels. This allows the user to make broad changes while maintaining the details, and conversely detailed changes while maintaining the overall shape. Two types of manipulation are considered, control point dragging and a direct manipulation involving solving a least squares problem.

In contrast, *variational modeling* allows the user to directly manipulate the curve or surface with the curve or surface maintaining some notion of overall smoothness subject to user imposed constraints. This physically based paradigm provides an intuitive means for shape control. Each of these paradigms will be explored in the context of wavelet bases which will be shown to provide the required hooks for such interaction and/or significant computational savings.

2.3.1 Multiresolution Modeling

A multiresolution representation such as a B-spline or wavelet representation may be used to implement a multiresolution modeling system. This section explores the choices that must be made when designing a multiresolution tool. Two related methods are described; direct control point manipulation and a least squares solver.

In control point modeling, the user is allowed to directly alter the coefficient values, by clicking and dragging on control points. In the least squares scheme [12, 86], the user can click and drag directly on the curve or surface, defining interpolation and tangent constraints, linear with respect to the control points. The system returns the curve or surface that satisfies these linear constraints, by changing the coefficients by the least squares amount. Least square solutions can be found very inexpensively using the pseudoinverse [86]. The least squared problem can also be posed as a minimization problem [194], whose solution can be found by solving a sparse, well conditioned, linear system.

In multiresolution versions of these two schemes, the user chooses the resolution level i, and then only the quantities of basis functions on level i are altered. The locality of the effect on the curve or surface is directly tied to the chosen level i. In control point modeling, the control polygon at level i is manipulated by the user. In a least squares scheme, the user is provided a direct handle on the curve or surface itself, and the least squares solution is found only using the basis functions on level i. The least-squares approach offers a much more intuitive interface, and (for curves) works at interactive speeds.

One decision to be made is whether to expose the user to hierarchical B-splines or to wavelets. It is easy to see that manipulating wavelet basis functions does not produce an intuitive interface. Moving such a control point, and thus changing the amount of some wavelet basis function used, changes the solution in a "wave" like fashion. In contrast, it is more intuitive to move a B-spline control point which changes the solution in a "hump" like fashion. Thus the user in this case should manipulate the hierarchical B-spline functions.

An important tool to implement the ideas in these notes is the ability to find the closet (in some sense) lower resolution curve or surface to one constructed at a higher resolution. This process is called *projection*. The inverse process, *refinement*, takes a low resolution curve or surface and adds additional degrees of freedom, in general without changing the shape.

There are many ways to obtain a lower resolution version of some object. For example, given an object at some resolution of detail, one could obtain a lower resolution version by throwing away every other control point. Subsampling is not a true projection; starting with a smooth curve and then expressing that smooth curve in the higher resolution B-spline basis basis and finally subsampling the control points will not return the original smooth curve we began with.

Another way of obtaining a smoothed version of the object is by *orthogonally* projecting the object from a space defined by a larger set of basis functions to a smaller (i.e., lower resolution) space spanning linear combinations of fewer basis functions. The orthogonal projection is the object in the lower resolution space that is closest to object in the higher resolution space using the L^2 measure. In general, this involves a sort of low-pass filtering. This is the approach used in [76]. Although this is a very elegant way of obtaining a lower resolution version of an object, it has a few drawbacks. The particular filter sequence used is infinite in length (although it does decay rapidly from its centers) and so performing this task efficiently can be troublesome. Also, because these sequences are not local, then a single change to one B-spline coefficient at some level will alter all of the coefficients of the projection at the next courser level.

One good compromise between these two extremes (subsampling, and orthogonal projection), is to use the filter sequence given for the non-orthogonal wavelet construction by Cohen et al. [34]. This projection in non-orthogonal, but it is entirely local. This is the choice we have used in our multiresolution modeling tool.

When one projects a curve or surface to a lower resolution, the detail may be lost. One can, however, explicitly store this lost detail, perhaps to be added back in later, or to be added to another curve or surface to give it a similar quality.

What set of basis functions should be used to represent the detail. If a wavelet projection is used to define the lower resolution versions of the object, then the detail can be represented by using the corresponding wavelet functions. The other option is to represent the detail using hierarchical B-spline functions. The disadvantage of using hierarchical B-splines is that there are roughly $2n$ B-splines in the hierarchy, and only n wavelets.

The advantage of using hierarchical B-splines however is that they maintain the relationship between the detail and the local orientation (captured by the local tangent, normal, and binormal frame) better. When the user changes the broad sweep of the curve, changing the orientation, the detail functions are remixed. If the detail functions are wavelet functions, then changing the normal and tangent frame remixes "wave" shaped functions introducing non-intuitive wiggles. If the detail functions are B-spline basis functions, then "hump" shaped functions get remixed, yieding more intuitive changes. Also if the detail functions are B-splines, then because there are twice as many B-splines than wavelets, the tangent and normal directions are computed at twice as many sample points allowing the detail to follow the orientation with more fidelity.

2.4 Variational Modeling

The variational modeling paradigm generalizes the least squares notion to any *objective* function minimization, typically one representing minimizing curvature. The variational problem leads to a non-linear optimization problem over a finite set of variables when cast into a given basis.

There are a variety of objective functions used in geometric modeling [147, 160] In our implementation we have used the *thin-plate* measure which is based on minimizing the parametric second derivatives [187, 21, 194]. If the vector of unknown coefficients are denoted by $\mathbf{x}$, and the linear position and tangent constraints imposed by the user's action are given by the set of equations $\mathbf{A}\mathbf{x} = \mathbf{b}$, then the thin plate minimum may be found by solving the following linear system [194].

$$\begin{vmatrix} \mathbf{H} & \mathbf{A}^{\mathbf{T}} \\ \mathbf{A} & \mathbf{0} \end{vmatrix} \begin{vmatrix} \mathbf{x} \\ \lambda \end{vmatrix} = \begin{vmatrix} \mathbf{0} \\ \mathbf{b} \end{vmatrix} \tag{5}$$

Where $\mathbf{H}$ is the Hessian matrix defined by the thin plate functional, and λ are Lagrange variables.

2.4.1 Hierarchical Conditioning

Wavelets can be used in the context of variational modeling so that the solution may be obtained more efficiently.

In the B-spline basis, the optimization procedure resulted in the linear system given by Equation (5). In the wavelet basis, a different linear system results. If the wavelet filter sequences defining the wavelet transform are contained in the matrix $\mathbf{W}$, then an equivalent linear system is given by

$$\left| \begin{array}{cc} \bar{\mathbf{H}} & \bar{\mathbf{A}}^T \\ \bar{\mathbf{A}} & \mathbf{0} \end{array} \right| \left| \begin{array}{c} \bar{\mathbf{x}} \\ \lambda \end{array} \right| = \left| \begin{array}{c} \mathbf{0} \\ \mathbf{b} \end{array} \right| \tag{6}$$

where the bars signify that the variables are wavelet coefficients, $\bar{\mathbf{x}} = \mathbf{W}\mathbf{x}$, and the Hessian and constraint matrix are expressed with respect to the wavelet basis. To see the relationship with the B-spline system, the new system can also be written down as

$$\left| \begin{array}{cc} \mathbf{W}^{-\mathbf{T}}\mathbf{H}\mathbf{W}^{-1} & \mathbf{W}^{-\mathbf{T}}\mathbf{A}^{\mathbf{T}} \\ \mathbf{A}\mathbf{W}^{-1} & \mathbf{0} \end{array} \right| \left| \begin{array}{c} \bar{\mathbf{x}} \\ \lambda \end{array} \right| = \left| \begin{array}{c} \mathbf{0} \\ \mathbf{b} \end{array} \right| \tag{7}$$

Although Equation (5) and Equation (6/7) imply each other, they are two distinct linear systems of equations. Because the wavelet system (6/7) is hierarchical it will not suffer from the poor conditioning of the B-spline system of Equation (5). For a rigorous discussion of the relevant theory see [46].

The scaling of the basis functions is very significant for the behavior of the optimizing procedures. Traditionally the wavelet functions are defined with the scaling defined in [135, 154]. At each level moving up, the basis functions become twice as wide, and are scaled $\frac{1}{\sqrt{2}}$ times as tall. While in many contexts this normalizing may be desirable, for optimization purposes it is counter productive.

For the optimization procedure to be well conditioned [109, 46] it is essential to emphasize the coarser levels. The correct theoretical scaling depends on both the energy function used, and the dimension of problem. For a fuller discussion, see the Appendix in [95]. In the experiments described below a different scaling was used.

As one goes one level down, the basis functions become twice as wide, and $1/2$ as tall. In the pyramid code, this is achieved by multiplying all of the scaling and wavelet filter coefficients by 2, and all of the dual coefficients by $1/2$ The proper scaling is essential to obtain the quick convergence of the wavelet method when steepest descent or conjugate gradient iteration is used. Scaling is not important with Gauss-Seidel iteration, which will perform the same sequence of iterations regardless of scale.

There is now a choice to make. In an iterative conjugate gradient solver, the common operation is multiplication of a vector times the wavelet matrix given in Equations (6/7). There are two ways to implement this.

One approach, the *explicit* approach, is to compute and store the wavelet Hessian matrix $\bar{\mathbf{H}}$ and the wavelet constraint matrix $\bar{\mathbf{A}}$ (Equation (6)). These can be computed directly from a closed form (piecewise polynomial) representation of the wavelet functions. Unfortunately, these matrices are not as sparse as the B-spline Hessian and constraint matrices.

Alternatively, there is the *implicit* approach [198, 182] which only computes and stores the entries of the B-spline matrices $\mathbf{H}$ and $\mathbf{A}$ (Equation (7)). Multiplication by the $\mathbf{W}$ matrices is accomplished using a linear time pyramid transform procedure.

The advantage of this approach is that the whole multiply remains $O(n)$ in both time and space, since the pyramid procedures run in linear time, and the matrices $\mathbf{H}$ and $\mathbf{A}$ are $O(n)$ sparse. Even though one of the methods explicitly uses wavelet terms while the other uses B-spline terms, these two methods are mathematically equivalent, and so both will have the same condition properties.

2.4.2 Adaptive Oracle

By limiting the possible surfaces to only those that can be expressed as a linear combination of a fixed set of basis functions, one obtains an approximation of the true optimal surface. As more basis functions are added, the space of possible solutions becomes richer and a closer approximation to the true optimal surface can be made. Unfortunately, as the space becomes richer, the number of unknown coefficients increases, and thus the amount of computation required per iteration grows. A priori, it is unknown how many basis functions are needed. Thus, it is desirable to have a solution method that adaptively chooses the appropriate basis functions. This approach was applied using hierarchical B-splines in [194]. When refinement was necessary, "thinner" B-splines basis functions were added, and the redundant original "wider" B-splines were removed. With wavelets, all that must be done is to add in new "thinner" wavelets wherever refinement is deemed necessary. Since the wavelets coefficients correspond directly to local detail, all previously computed coefficients are still valid.

The decision process of what particular wavelets to add and remove is governed by an `oracle` procedure which is called after every fixed number of iterations. The oracle must decide what level of detail is required in each region of the curve or surface.

When some region of the solution does not need fine detail, the corresponding wavelet coefficients are near zero, and so the first thing the `oracle` does is to deactivate the wavelet basis functions whose corresponding coefficients are below some small threshold. The `oracle` then activates new wavelet basis functions where it feels more detail may be needed. There are two criteria used. If a constraint is not being met, then the oracle adds in finer wavelet functions in the region that is closest in parameter space to the unmet constraint. Even if all the constraints are being met, it is possible that more basis functions would allow the freedom to find a solution with lower energy. This is accomplished by activating finer basis functions near those with coefficients above some maximum threshold.

To avoid cycles, a basis function is marked as being `dormant` when it is removed from consideration. Of course, it is possible that later on the solution may really need this basis function, and so periodically there is a `revival` phase, where the `dormant` marks are removed.

2.4.3 User Interface

A user of the system is first presented with a default curve or surface. Constraints can then be introduced by clicking on the curve or surface with the mouse. The location of the mouse click defines a parametric position t (and s) on the curve (or surface). The user can then drag this point to a new location to define an interpolation constraint. Tangent constraints at a point can also be defined by orienting "arrow" icons at the point. Once the constraint is set, the solver is called to compute the minimum energy solution that satisfies the constraints placed so far and the result is displayed.

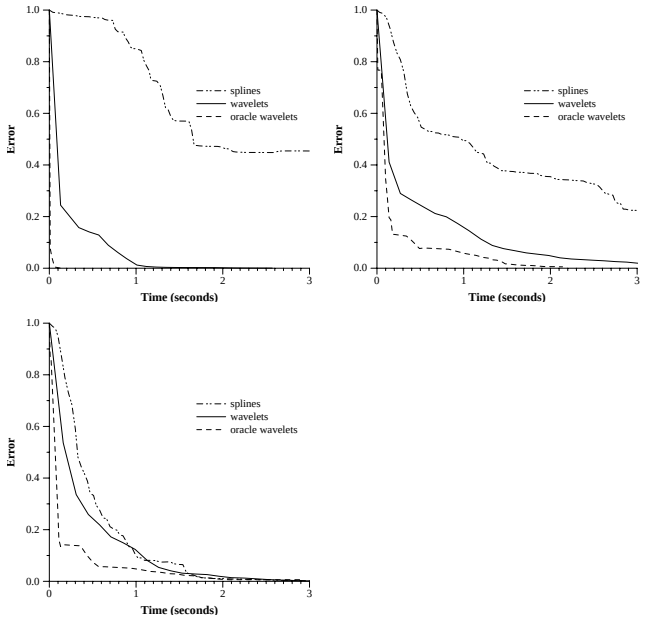

Figure VII.5: Error per time. Curve with 65 control points, 3, 7, and 13 constraints.

When the solution is completed, the result provides information for not only the curve or surface satisfying the specific value of the new constraint, but for all curves or surfaces with respect to any value of this constraint. Once the linear system (Equation (6/7)) with the newest constraint has been solved, the solver stores the delta vector

$$\frac{\Delta \bar{\mathbf{x}}}{\Delta \mathbf{b_m}} \tag{8}$$

where m is the index of the newest constraint, and b_m is the constraint value (i.e., the position or tangent specified by the user). This vector stores the change of the coefficient vector due to a unit change in the new constraint $\Delta \mathbf{b_m}$, essentially a column of the inverse matrix. The user is now free to interactively move the target location of the constraint without having to resolve the system since, as long as the parameters s, and t of the constraints do not change, the matrix of the system, and thus its inverse, do not change. However, as soon as a new constraint is added (or a change to the parameters s and t is made) there is fresh linear system that must be solved, and all of the delta vectors are invalidated. The ability to interactively change the value of a constraint is indicated to the user by coloring the constraint icon.

2.4.4 Variational Modeling Results

A series of experiments were conducted to examine the performance of the wavelet based system compared to a B-spline basis. In the curve experiments, the number of levels of the hierarchy, L, was fixed to 6, and in the surface experiments, L was fixed as 5. The optimization process was then run on problems with different numbers of constraints. The results of these tests are shown in Figures VII.5 and VII.6. These graphs show the convergence behavior of three different methods, solving with the complete B-spline basis, solving with the complete wavelet basis, and solving with an adaptive wavelet basis that uses an oracle. (The wavelet results shown here are using the *implicit* implementation). If $\mathbf{x^{(m)}}$ is the computed solution expressed as B-spline coefficients at time m, and $\mathbf{x}^*$ is the correct solution of the complete linear system [3]

[3] computed numerically to high accuracy

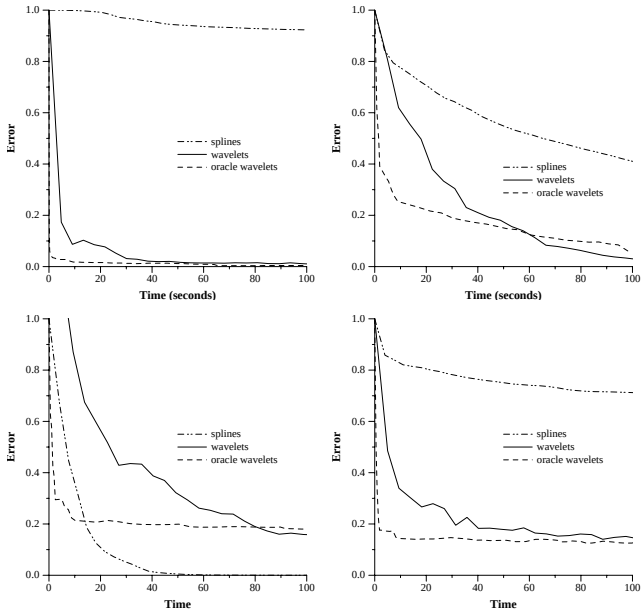

Figure VII.6: Error per time. Surface with 1089 control points, 11,23,64 evenly space constraints, and 62 constraints along the boundary.

(i.e., the complete system with $2^L + 1$ variables, and no adaptive oracle being used) then the error at time m is defined as

$$\frac{\sum_j \mid x_j^* - x_j^{(m)} \mid}{\sum_j \mid x_j^* - x_j^{(0)} \mid} \tag{9}$$

To obtain the starting condition $\mathbf{x^{(0)}}$, two constraints were initialized at the ends of the curve, and the minimal thin plate solution (which in this case is a straight line) was computed. (For surfaces, the four corners were constrained.) All times were taken from runs on an SGI R4000 reality engine. [4]

When there are large gaps between the constraints, the B-spline method is very poorly conditioned, and converges quite slowly while the wavelet method converges dramatically faster. In these problems, the oracle decides that it needs only a very small active set of wavelets and so the adaptive method converges even faster. As the number of constraints is increased, the solution becomes more tightly constrained, and the condition of the B-spline system improves. (Just by satisfying the constraints, the B-spline solution is very close to minimal energy). Meanwhile the oracle requires a larger active set of wavelets. Eventually, when enough constraints are present, the wavelet methods no longer offer an advantage over B-splines.

Experiments were also run where all the constraints were along the boundary of the surface. In these experiments there are many constraints, but the since the constraints are along the boundary, much of the surface is "distant" from any constraint. In these problems, the wavelets also performed much better than the B-spline method.

[4] In the curve experiments, each B-spline iteration took 0.0035 seconds, while each iteration of the implicit wavelet method took 0.011 seconds. For the surface experiments, each B-spline iteration took 0.68 seconds while each iteration of the implicit wavelet method took 0.85 seconds. (The wavelet iterations using the explicit representation took about 10 times as long).

2.5 Conclusion

These notes have explored the use of wavelet analysis in a variety of modeling settings. It has shown how wavelets can be used to obtain multiresolution control point and least squares control. It has shown how wavelets can be used to solve variational problems more efficiently.

Future work will be required to explore the use of higher order functionals like those given in [147, 160]. Because the optimization problems resulting from those functionals are non-linear, they are much more computationally expensive, and it is even more important to find efficient methods. It is also important to study optimization modeling methods where constraint changes only have local effects.

Many of these concepts can be extended beyond the realm of tensor product uniform B-splines. Just as one can create a ladder of nested function spaces using uniform cubic B-splines of various resolutions, one can also create a nested ladder using non-uniform B-splines [128].

Subdivision surfaces are a powerful technique for describing surfaces with arbitrary topology [101]. A subdivision surface is defined by iteratively refining an input control mesh. As explained by Lounsbery et al. [124], one can develop a wavelet decomposition of such surfaces. Thus, many of the ideas developed above may be applicable to that representation as well.

Acknowledgements

We are grateful to James H. Shaw for developing the graphical interface to the optimization program.

3 Wavelets and Integral and Differential Equations (Wim Sweldens)

3.1 Integral equations

Interest in wavelets historically grew out of the fact that they are effective tools for studying problems in partial differential equations and operator theory. More specifically, they are useful for understanding properties of so-called Calderón-Zygmund operators.

Let us first make a general observation about the representation of a linear operator T and wavelets. Suppose that f has the representation

$$f(x) \;=\; \sum_{j,k} \langle\, f, \psi_{j,k} \,\rangle\, \psi_{j,k}(x).$$

Then,

$$Tf(x) \;=\; \sum_{j,k} \langle\, f, \psi_{j,k} \,\rangle\, T\psi_{j,k}(x),$$

and, using the wavelet representation of the function $T\psi_{j,k}(x)$, this equals

$$\sum_{j,k} \langle\, f, \psi_{j,k} \,\rangle \sum_{i,l} \langle\, T\psi_{j,k}, \psi_{i,l} \,\rangle\, \psi_{i,l}(x) \;=\; \sum_{i,l} \left(\sum_{j,k} \langle\, T\psi_{j,k}, \psi_{i,l} \,\rangle\; \langle\, f, \psi_{j,k} \,\rangle \right) \psi_{i,l}(x).$$

In other words, the action of the operator T on the function f is directly translated into the action of the infinite matrix $A_T = \{\, \langle\, T\psi_{j,k}, \psi_{i,l} \,\rangle \,\}_{i,l,j,k}$ on the sequence $\{\, \langle\, f, \psi_{j,k} \,\rangle \,\}_{j,k}$. This representation of T as the matrix A_T is often referred to as the "standard representation" of T [15]. There is also a "nonstandard representation". For virtually all linear operators there is a function (or, more generally, a distribution) K such that

$$Tf(x) \;=\; \int K(x,y) f(y)\, dy.$$

The nonstandard representation of T is now simply the decomposition one gets by considering K as an image and calculate the 2D wavelet transform.

Let us briefly discuss the connection with Calderón-Zygmund operators. Consider a typical example. Let H be the Hilbert transform,

$$Hf(x) \;=\; \frac{1}{\pi} \int_{-\infty}^{\infty} \frac{f(s)}{x-s}\, ds.$$

The basic idea now is that the wavelets $\psi_{j,k}$ are approximate eigenfunctions for this, as well as for many other related (Calderón-Zygmund) operators. We note that if $\psi_{j,k}$ were exact eigenfunctions, then we would have $H\psi_{j,k}(x) = s_{j,k}\psi_{j,k}(x)$, for some number $s_{j,k}$ and the standard representation would be a diagonal "matrix":

$$A_H \;=\; \{\, \langle\, H\psi_{i,l}, \psi_{j,k} \,\rangle \,\} \;=\; \{ s_{i,l}\, \langle\, \psi_{i,l}, \psi_{j,k} \,\rangle \,\} \;=\; \{ s_{i,l}\, \delta_{i-l,j-k} \}.$$

This is unfortunately not the case. However, it turns out that A_T is in fact an almost diagonal operator, in the appropriate, technical sense, with the off diagonal elements quickly becoming small. To get some idea why this is the case, note that for large $|x|$, we have, at least heuristically,

$$H\psi_{j,k}(x) \;\approx\; \frac{1}{\pi x} \int \psi_{j,k}(y)\, dy.$$

A priori, the decay of the right-hand side would thus be $\mathcal{O}(1/x)$, which of course is far from the rapid decay

of a wavelet $\psi_{j,k}$ (remember that some wavelets are even zero outside a finite set). Recall, however, that $\psi_{j,k}$ has at least one vanishing moment so the decay is in fact much faster than just $\mathcal{O}(1/x)$, and the shape of $H\psi_{j,k}(x)$ resembles that of $\psi_{j,k}(x)$. By expanding the kernel as a Taylor series,

$$\frac{1}{x-s} \;=\; \frac{1}{x}\left(1+\frac{s}{x}+\frac{s^2}{x^2}\cdots\right),$$

we see that the more vanishing moments ψ has, the faster the decay of $H\psi_{j,k}$ is.

Thus for a large class of operators, the matrix representation, either the standard or the nonstandard, has a rather precise structure with many small elements. In this representation, we then expect to be able to compress the operator by simply omitting small elements. In fact, note that this is essentially the same situation as in the case of image compression with the "image" now being the kernel $K(x,y)$. Hence, if we could do basic operations, such as inversion and multiplication, with compressed matrices rather than with the discretized versions of T, then we may significantly speed up the numerical treatment. This program of using the wavelet representations for the efficient numerical treatment of operators was initiated in [15]. We also refer to [3, 2] for related material and many more details.

3.2 Differential equations

In a different direction, because of the close similarities between the scaling function and finite elements, it seems natural to try wavelets where traditionally finite element methods are used, e.g. for solving boundary value problems [108]. There are interesting results showing that this might be fruitful; for example, it has been shown [15, 45] that for many problems the condition number of the $N \times N$ stiffness matrix remains bounded as the dimension N goes to infinity. This is in contrast with the situation for regular finite elements where the condition number in general tends to infinity.

One of the first problems we have to address when discussing boundary problems on domains is how to take care of the boundary values and the fact that the problem is defined on a finite set rather than on the entire Euclidean plane. This is similar to the problem we discussed with wavelets on an interval, and, indeed, the techniques discussed there can be often used to handle these two problems [4, 9].

Wavelets have also been used in the solution of evolution equations [90, 129]. A typical test problem here is Burgers' equation:

$$\frac{\partial u}{\partial t}+u\,\frac{\partial u}{\partial x} \;=\; \nu\,\frac{\partial^2 u}{\partial x^2}.$$

The time discretization is obtained here using standard schemes such as Crank-Nicholson or Adams-Moulton. Wavelets are used in the space discretization. Adaptivity can be used both in time and space [10].

One of the nice features of wavelets and finite elements is that they allow us to treat a large class of operators or partial differential equations in a unified way, allowing for example general PDE solvers to be designed. In specific instances, though, it is possible to find particular wavelets, adapted to the operator or problem at hand. In some cases one can construct functions that diagonalize a 1D differential operator [112]. This leads to a fast, non-iterative algorithm for the solution of ordinary differential equations with various kinds of boundary values.

4 Light Flux Representations (Alain Fournier)

Since the introduction of global illumination computations in computer graphics in 1984 [91] most such computations have been based on *radiosity* computations [39]. While very successful and still intensively investigated, it has serious limitations. Most of the drawbacks of radiosity come from the fact that it is *patch-driven*, and introduces the light only after the form factors have been computed (even though that has been addressed recently), and from the fact it really works only for separable sources and reflectors. It is a global illumination solution which critically depends on a limiting assumption about the local behaviour of light. Hybrid solutions also invariably have problems because there is no neat dichotomy between specular and diffuse reflection, and real reflection/refraction is a continuum between these two extremes.

An alternative is a *light-driven* approach, where the global illumination problem is solved by propagating the light from sources (we use "source" in the broadest sense of anything radiating light) to other parts of the environment to the eye. Another important criterion is that the amount of effort spent on each part of the scene is somehow related to how much light will come from it. There is no need to compute much about the whole content of a closet whose door remains closed, even less need to compute anything if all the lights are off. That leads therefore, to a *light-driven, volume-oriented* approach.

The essential paradigm is as follows. Consider a volume **V** within the environment to render, with a boundary surface S. If we know for every point of S the flux of light crossing it in any direction, then we can study separately the illumination inside and outside of **V**. Furthermore, even if we do not know the true situation at the boundary, but only some amount of light emitted inside **V** and the amount of light coming into **V**, and if we know how to solve the global illumination problem inside **V**, then we can assign to points of S the correct amounts of outgoing light. The outside of **V** can then be treated without considering **V** unless it is found that more light comes into **V** from outside. In this case we can solve the global illumination problem inside **V** again *independently* of the previous solution if we assume (and it is the only serious restriction) the *linearity* of the light effects. After dealing with a volume, all the incoming light energy has been accounted for, being transmitted to the neighbours or absorbed within the volume. If we cannot solve the global illumination problem for **V**, we can partition it into two or more sub-volumes, and so on recursively until each section is simple enough so that we can deal with it.

Once a volume has been dealt with, the result is a description of the flux of light coming through S to the outside. Adjacent volumes are then assigned that flux (added to any already incoming) as incoming flux. An untreated volume will be unbalanced in energy, since it receives light energy not yet accounted for inside. The basic algorithm is then to examine the unbalanced volumes and treat them. In the initial state no power is exchanged between volumes, and the only unbalanced volumes are the ones containing a light source. After balancing any of these volumes, new volumes will become unbalanced because their energy balance will become positive. If when dealing with a volume we are careful not to "create" energy, that is we have a local illumination and transmission model with some physical credibility, then a "treated" volume will be balanced, and remain so until new light is transmitted into it from an adjacent volume. This amount of light cannot be more than its neighbour received (in power), and in fact will be less after any reflection/refraction, so we are guaranteed to eventually reach a state where all volumes are balanced. In particular we will not become trapped in local minima, and general global optimization algorithms are not necessary.

The first implementation of this approach was described in [84] and a parallel version in [70].

The second implementation of this paradigm is in progress, the work of Bob Lewis and Alain Fournier. There are of course many interesting issues, dealing with space subdivision, local illumination and propa-

gation in particular, but the one especially relevant to this course is *light flux representation*. The crucial implementation decision is how to represent light as it enters and leaves the cell. If we examine the requirements for the light flux representation, we find that at each point on the surface of the volume (for the nonce we will assume that this surface is a rectangle, which is the case in our current implementation since we use an octree subdivision of the space) we need to know the radiance going through for every direction. This means that we need a four-variable function in the continuous case (two spatial, two directional). This function can be very smooth (for instance when the whole flux comes from a point light source), smooth spatially but not directionally (for instance if the whole flux comes from a directional light source; it is a δ function in direction), or highly discontinuous in every way (after being blocked, reflected and refracted by thousands of objects. We need a coarse description sometimes or some places, a detailed description some other times, and the ability to simplify the representation as the light propagates from volume to volume. Another way to look at it is to consider that in a given direction the light flux representation is essentially a picture description, and we want a compact, multi-resolution representation of such. Clearly a wavelet representation seems indicated, and that is what we are currently implementing. The practical questions are:

- which wavelet basis to choose
- is the relatively high dimensionality a problem
- which data structure to choose to balance compactness and efficiency of computation
- can the wavelet representation be used directly to propagate the light
- can the wavelet representation be used directly to compute the local illumination, possibly using a similar representation for the BRDF and/or the object surface description.

To test our representation, and as an interesting application in its own right, we can use the representation so obtained as a compact multiresolution storage of a set of views of an object. For a simple example, if we consider all the orthographic projections of a given object on planes not intersecting it, they constitute only scalings and translations of a canonical 4-D array of radiance values, which is exactly what our light flux representation is. In a context of so-called *fish tank virtual reality* [193], where the head position of a user is tracked to display the appropriate view of objects on the screen (with or without stereo), this can be used to precompute and display the views of objects which otherwise would be too expensive to display by conventional methods (such as volumetric data) or whose models are not available (such as real objects). For real objects the data is obtained by digitizing multiple views (in our case taken by a camera held by a robot arm programmed to sample the sphere of directions). We are exploring the more interesting aspects of this approach. The built-in multiresolution is especially useful to give coarse images while the viewer's head is moving fast, or motion-blurred images (there is a difference).

5 Fractals and Wavelets (Alain Fournier)

5.1 Fractal Models

The term and most of the concepts and methods of *fractal* were introduced by Benoit Mandelbrot during the last 20 years. The universe of fractals is by now very large, but for our purposes here they can be divided into deterministic fractals, from Koch curves to the ubiquitous Mandelbrot set, and stochastic fractals, where the fractal properties apply to the various characteristics of random variables. We will only consider here one such stochastic fractal process, *fractional Brownian motion* (fBm). It has been introduced by Mandelbrot and Van Ness [137] as a generalization of Brownian motion, which itself has fractal properties. It has been of interest in graphics because as a first approximation it is a useful model for terrain.

5.2 Fractional Brownian Motion

Fractional Brownian motion, as a stochastic process $B_H(t)$ has one parameter $0 \leqslant H \leqslant 1)$ and can be characterized by its *self-similarity*. If we consider a scale parameter $a > 0$, the process $(B_H(t+a\tau)-B_H(t))$ has the same moments than $(a^H B_H(\tau))$. It is a *non-stationary* process, that is its covariance function is a function of t

$$E[B_H(t)B_H(s)] = (V_H/2)[|t|^{2H} + |s|^{2H} - |t-s|^{2H}]$$

$$V_H = \Gamma(1-2H)\frac{\cos \pi H}{\pi H}$$

The variance of the process is then:

$$\text{Var}[B_H(t)] = V_H|t|^{2H}$$

Even though fBm does not have a spectrum in the usual sense, one can define an average spectrum [78]:

$$S_H(f) = \frac{V_H}{|f|^{2H+1}}$$

The main advantage of fBm as a model of terrain is a remarkable compactness of representation. Depending on how much deterministic data is included, the data base can be from two numbers to a few hundreds, to represent terrain that ultimately contains thousands or million of polygons. The second big advantage, due to its fractal nature, is that unlimited amounts of details can be generated. The disadvantages include the fact that to generate a surface pure recursive subdivision is not sufficient, and that will complicate somehow the subdivision algorithms, and that it has limited flexibility, with basically only one parameter to be adjusted to generate different terrains.

5.3 Stochastic Interpolation to Approximate fBm

There have been numerous methods published for stochastic subdivisions. The criteria to evaluate them have to depend on what they claim to accomplish and their intended use. The techniques to approximate specifically fractional Brownian motion [85] [191] have been well described. The paper by Fournier, Fussell and Carpenter [85] puts their methods into the context of computer graphics, and emphasizes the problems of integrating the generation of approximations to fBm with traditional graphics modelling.

The methods used in this paper are all based on *stochastic interpolation*, that is an interpolation method where stochastic variables are used to approximate samples of a known stochastic process. They use *recursive subdivision*, which has the advantage of being a known and common method in computer graphics, especially in conjunction with parametric surfaces. Since in the case of fBm, the expected position of the mid-point between two existing sample points is the arithmetic mean of these points, the only problem is to determine the variance. But the influence of scale (and therefore of level of subdivision) on the variance is given directly by the definition of fBm. As a function of one variable this gives directly an acceptable algorithm to generate fBm. Note that it has most of the required properties: it is adaptive, it is fast, and the cost is proportional to the number of sample points actually generated. When applied to the two-variable case, that is surfaces, we have to deal with the non-Markovian property of fBm. Straight recursive subdivision, especially on triangles has been used extensively. The obvious attraction is that most hardware/firmware/software rendering systems deal efficiently with triangles. The possible artefacts created by the non-stationarity of the samples generated (usually seen as "creases", that is boundaries where the slope changes is higher than in the neighbourhood) can be controlled. The easiest way is to reduce the scale factor applied to the displacement value obtained. This is however conceptually unsatisfactory. In the same paper an alternative, a form of interwoven quadrilateral subdivision, was proposed and illustrated. In this scheme, the subdivision scheme proceeds by using information not only from the boundaries, but from neighbours across it, and the distribution information is spread in a non-Markovian fashion. It is interesting to note that it is quite close to the quincunx subdivision scheme [50] used for two-dimensional wavelet transforms.

For many applications it is important to realize a true stochastic "interpolation", that is a constraint is not to modify the points already computed at later stages of subdivision. Methods recently proposed by Voss [153], Saupe [153] and Musgrave, Kolb and Mace [148] do not respect that constraint, while trying to be more flexible or more faithful to the process simulated (generally fBm). The latter is especially interesting as it uses *noise synthesis* in the spatial domain with Perlin type noise functions. An interesting work by Szeliski and Terzopoulos [183] describes how to use constrained splines to fit an initial discrete set of points, and then use the energy function used for minimization to derive the probability distribution of the stochastic element. This, when properly implemented, generates *constrained fractal* surfaces, and seems a very useful modelling tool. Depending on the modalities of implementation, one can obtain varying level of details through a multi-grid approach, and true interpolation by sacrificing some of data-fitting aspect of the method. To go back to stochastic interpolation proper, a paper by Miller [144] proposes a solution which can be interpreted as smoothing over the already generated values with a small filter.

5.4 Generalized Stochastic Subdivision

The most comprehensive answer to the problem of stochastic interpolation is *generalized stochastic subdivision* by J. Lewis [120]. In his method each new interpolated value is computed by adding noise of known variance to the weighted sum of the current values in a neighbourhood of size $2S$:

$$\widehat{V}_{t+\frac{1}{2}} = \sum_{k=1-S}^{S} a_k V_{t+k}$$

Note the difference between this and the method in [85], where the value used is just the average of V_t and V_{t+1}. In other words, $S = 1$ and $a_0 = a_1 = \frac{1}{2}$. The correct coefficients a_k are those which make $\widehat{V}_{t+\frac{1}{2}}$ the best estimation of the interpolated value. It can be shown that if the auto-correlation function:

$$R(\tau) = \mathbf{E}[V(t)V(t+\tau)]$$

is known, then the a_k can be computed from the relation:

$$R(m - \frac{1}{2}) = \sum_{k=1-S}^{S} a_k R(m-k) \quad for \;\; 1 - S \leqslant m \leqslant S$$

The computation of the a_k requires a matrix inversion (the above formula is of course a shorthand for $2S$ equations with $2S$ unknowns) but only has to be done once for a stationary process. The method permits the approximation of a wide range of processes, Markovian as well as non-Markovian, and even oscillatory. The choice of the correct size of neighbourhood is related to the process to be approximated.

5.5 Wavelet Synthesis of fBm

Since the main characteristics of fBm is to be non-stationary (even though its increments are stationary) and self-similar, wavelet analysis seems to be an appropriate tool to study it. Non-stationarity requires a time-dependent analysis, and self-similarity requires a scale-dependent analysis, two features wavelet analysis possesses.

Indeed we can easily recouch the basic recursive subdivision approach to fBm synthesis as a wavelet reconstruction. At level j in the process, if $a_{j+1}(i)$ are the values already computed and $d_{j+1}(i)$ the mid-point displacements, then the new values are:

$$a_j(i) = a_{j+1}(i/2)$$

when i is even, and

$$a_j(i) = 1/2(a_{j+1}((i-1)/2) + a_{j+1}((i+1)/2)) + d_{j+1}((i+1)/2)$$

when i is odd. This corresponds to the wavelet reconstruction:

$$a_j(i) = \sum_k [\, a_{j+1}(k)\, h[-i+2k] + d_{j+1}(k)\, g[-i+2k]\,]$$

with for filter coefficients $h(-1) = h(1) = 1/2$, $h(0) = 1$, $g(1) = 1$ and all other coefficients 0, and the detail values generated as uncorrelated Gaussian variables with variance $V_H(2^j)^{2H+1}$.

It is now easier to examine the characteristics of such a construction from the wavelet analysis standpoint. There is by now a large literature on wavelet analysis and synthesis of fractals, but the following is based mainly on papers by P. Flandrin [77] [78] and G. W. Wornell [196] [197].

If we conduct an orthonormal wavelet decomposition of some sample $B_H(t)$ of fBm, the detail coefficients $d_j(k)$ are equal to:

$$d_j(k) \;=\; 2^{-j/2} \int_{-\infty}^{\infty} B_H(t)\, \psi_(2^{-j}t - k)\, dt$$

The smooth, or average coefficients are similarly equal to:

$$a_j(k) \;=\; 2^{-j/2} \int_{-\infty}^{\infty} B_H(t)\, \varphi(2^{-j}t - k)\, dt$$

As used many times in earlier chapters, this is not in practice the way the coefficients are computed. Instead they are computed recursively from the coefficients of the discrete filters associated with the two functions, $h[i]$ with $\varphi(t)$ and $g[i]$ with $\psi(t)$.

$$a_j(i) = \sum_k a_{j+1}(k)\, h[-i + 2k]$$

$$d_j(i) = \sum_k a_{j+1}(k)\, g[-i + 2k]$$

with the reconstruction formula given above. The reconstruction formula will provide us with a way to synthesize fBm, if we can obtain information about the statistics of the coefficients and they are easy to approximate. The central result, showed in [78] is that

1. The time sequence of detail coefficients at the same level $d_j(i)$ and $d_j(k)$ is self-similar and stationary; the covariance of the coefficients properly scaled is a unique function of $(k - i)$.

2. The scale sequence of detail coefficients for the same "time", $d_j(i)$ and $d_l(k)$, such that $k = 2^{j-l}i$ suitably scaled is stationary as well; the covariance of the coefficients is a unique function of $(j - l)$.

The non-stationarity of fBm is therefore not present in the detail coefficients. It can be shown that it is indeed in the smooth coefficients $a_j(i)$, which are self similar and time dependent, as predictable, since they constitute an approximation of the whole process.

The ideal case for construction would be if the detail coefficients are all uncorrelated (covariance = 0). Then we would only have to generate coefficients with the right variance to obtain an approximation to fBm.

The variance of the detail coefficients is given by

$$\text{Var}[d_j(i)] = V_H/2\; V_\psi(H) 2^{j(2H+1)} \tag{10}$$

where $V_\psi(H)$ is a function of H characteristic of the wavelet used.

In general it can be shown that the correlation between detail coefficients decays quite rapidly as a function of the time distance (same level) and the level distance. For example in the case of the Haar wavelet and $H = 1/2$ (ordinary Brownian motion), the correlation at the same level is 0, with:

$$\text{Var}[d_j(i)] = \frac{V_H}{2}\, \frac{1}{6}\, 2^{2j}$$

and the correlation between levels for synchronous positions is:

$$E[d_j(i)d_k(2^{j-k}i)] = \frac{V_H}{2}\frac{1}{4}\,2^{2j}\,2^{5(k-j)/2}$$

It is also 0 outside a specific time-scale domain. When H takes different values, the situation becomes more complex, and the interested reader should consult [78] for details.

When considering wavelets other than Haar, it turns out that the crucial factor is the number of vanishing moments N (see chapter II for a definition of N). Asymptotically the correlation is given by:

$$E[d_j(i)d_k(l)] = O(|l-s|^{2(H-N)})$$

So the larger the number of vanishing moment the wavelet has, the more uncorrelated the coefficients are, both between and within levels.

It follows [196] that for the purpose of approximation, one can generate the detail coefficients as uncorrelated Gaussian samples with the variance given in (10) and be guaranteed that at the limit the process obtained has a time-averaged spectrum $S_H(f)$ such that:

$$\gamma_1\frac{V_H}{|f|^{2H+1}} \;\leqslant\; S_H(f) \;\leqslant\; \gamma_2\frac{V_H}{|f|^{2H+1}}$$

where γ_1 and γ_2 are constant depending on the wavelet.

Since the filter coefficients used in the original midpoint displacement scheme are far from the desirable properties for such filters (see section 1 in Chapter II), one can try better filters without sacrificing too much of the convenience of the method. A good choice is to keep the values for $h()$: $h(-1) = h(1) = 1/2$, $h(0) = 1$ and choose for $g(\cdot)$: $g(0) = g(2) = 1/2$, $g(1) = -1$, and all other coefficients 0. These of course correspond to the linear B-spline (the *hat* smoothing function. They have all the properties required except orthogonality to their translates. In this application, however, we only need the reconstruction filters, and a biorthogonal scheme is sufficient (we do not even have to know the dual filters). The filters now means that at each stage all the new smooth values are modified, and we have lost the interpolating property.

If the correlation function between detail coefficients is known, and if the range for which it is non-negligible is rather small (as would be the case with a wavelet with high number of vanishing moments) then using Lewis' generalized stochastic subdivision to generate coefficients with the right correlation is appropriate. The great simplification that the wavelet analysis allows is that since the detail coefficients are stationary and self-similar, the matrix inversion involved in computing the best estimate of the variance has to be computed only once.

To conclude this section we should stress that the trade-off between interpolation and and approximation also involves the question of what process we assume to sample the coarse values. Interpolation correspond to point-sampling, while most wavelet schemes correspond to some form of filtering. The latter is good for smooth transitions between the levels. It is problematic, however, it we do not pay close attention to the fact that the rendering process is not a linear operation, and the averages obtained might be grossly unrepresentative under some conditions.

VIII: Pointers and Conclusions

1 Sources for Wavelets

Obviously this field is rapidly expanding. The rate of apparition of new results and applications is astounding. The bibliography that follows is not meant to be exhaustive. The must-have books are by Daubechies [50] and Chui [26]. Good survey articles are by Strang [177], Chui [25], Rioul and Vetterli [162], Devore and Lucier [61] and Jaworth and Sweldens [113]. A recent tutorial by Stollnitz, DeRose and Salesin is concerned specifically about applications in computer graphics [176]. All of these references are pointers to considerably more.

An important source of information available on the internet is the Wavelet Digest, from the University of South Carolina. To quote from it:

Subscriptions for Wavelet Digest: E-mail to wavelet@math.scarolina.edu with "subscribe" as subject. To unsubscribe, e-mail with "unsubscribe" followed by your e-mail address as subject. To change address, unsubscribe and resubscribe.

Archive site, preprints, references and back issues: Anonymous ftp to maxwell.math.scarolina.edu (129.252.12.3), directories /pub/wavelet and /pub/imi_93.

Gopher and Xmosaic server: bigcheese.math.scarolina.edu.

2 Code for Wavelets

The Wavelet Digest and the sources mentioned above contain numerous pointers to sources of code. An interesting package from Yale, originally from V. Wickerhause and R.R Coifman, is the Wavelet Packet Laboratory, available as an X version as XWPL from pascal.math.yale.edu. A commercial version of such also exists, running among other things under PC Windows. Other packages are based on MATLAB (Matlab is a trademark of The MathWorks Inc.) such as WavBox from Carl Taswell (taswell@sccm.stanford.edu).

The latest edition of the popular *Numerical Recipes in C* [157] has a new section on wavelets, and contains many useful routines.

The CD-ROM version of these notes includes the code for the UBC Wavelet Library (version 1.3) as a shar file, by Bob Lewis. It is a lean but useful library of functions to compute multi-dimensional transforms with a wide variety of wavelet bases. To quote from the accompanying blurb:

Announcing wvlt: The Imager Wavelet Library – Release 1.3 ————————————————————-

I am putting in the public domain Release 1.3 of "wvlt", the Imager Wavelet Library. This is a small library of wavelet-related functions in C that perform forward and inverse transforms and refinement. Support for 15 popular wavelet bases is included, and it's easy to add more.

The package also includes source for a couple of shell-level programs to do wavelet stuff on ASCII files and some demo scripts. (The demos require "gnuplot" and "perl" to be installed on your system.) The code has been compiled and tested under IBM RS/6000 AIX, Sun SPARC SunOS, and SGI IRIX, and should port to other systems with few problems.

The package is available as a shell archive ("shar" file) either by ftp (node: `ftp.cs.ubc.ca`*, file:* `/pub/local/bobl/wvlt/wvlt_r1_3.shar`*) or the World Wide Web via the Imager Home Page (*`http://www.cs.ubc.ca/nest/imager/imager.html`*). There is also a link to it from the Wavelet Digest (*`http://www.math.scarolina.edu:80/ wavelet/`*) pages as well.*

Future releases are under development and will include both speedups and increased functionality. They will be available by the same mechanisms.

I produced this package and hereby release it to the public domain. Neither I nor the University of British Columbia will be held responsible for its use, misuse, abuse, or any damages arising from same. Any comments regarding this package may, nevertheless, be sent to: Bob Lewis (`bobl@cs.ubc.ca`.

3 Conclusions

Nobody should walk out of this course thinking that they became an expert on wavelets. What we hope you will carry out is the certainty that wavelets are worth knowing, and that on many occasions (not always) they are worth using. Many of the concepts associated with wavelets, such as multiresolution, hierarchical analysis, recursive subdivision, spatio-temporal analysis, have been known and used before, some of them for decades if not centuries. Wavelets brought us a formal framework and a powerful analytical tool to understand the possibilities and limitations. It is not often than we in computer graphics are presented with such a gift and we should be thankful.

Bibliography

[1] AHARONI, G., AVERBUCH, A., COIFMAN, R., AND ISRAELI, M. Local Cosine Transform — A Method for the Reduction of the Blocking Effect in JPEG. *J. Math. Imag. Vision 3* (1993), 7–38.

[2] ALPERT, B. A Class of Bases in L^2 for the Sparse Representation of Integral Operators. *SIAM J. Mathematical Analysis 24*, 1 (January 1993), 246–262.

[3] ALPERT, B., BEYLKIN, G., COIFMAN, R., AND ROKHLIN, V. Wavelet-Like Bases for the Fast Solution of Second-Kind Integral Equations. *SIAM J. Sci. Comp. 14*, 1 (1993), 159–184.

[4] ANDERSSON, L., HALL, N., JAWERTH, B., AND PETERS, G. Wavelets on Closed Subsets of the Real Line. In [169]. pp. 1–61.

[5] ANTONINI, M., BARLAUD, M., MATHIEU, P., AND DAUBECHIES, I. Image Coding using the Wavelet Transform. *IEEE Trans. Image Process. 1*, 2 (1992), 205–220.

[6] APPEL, A. An Efficient Program for Many Body Simulation. *SIAM J. Scientific and Statistical Computing 6*, 1 (1985), 85–103.

[7] ARVO, J., TORRANCE, K., AND SMITS, B. A Framework for the Analysis of Error in Global Illumination Algorithms. In *Computer Graphics (Proc. SIGGRAPH)* (July 1994), ACM. To appear.

[8] AUPPERLE, L., AND HANRAHAN, P. A Hierarchical Illumination Algorithm for Surfaces with Glossy Reflection. In *Computer Graphics Annual Conference Series 1993* (August 1993), Siggraph, pp. 155–162.

[9] AUSCHER, P. Wavelets with Boundary Conditions on the Interval. In [27]. pp. 217–236.

[10] BACRY, E., MALLAT, S., AND PAPANICOLAOU, G. A Wavelet Based Space-Time Adaptive Numerical Method for Partial Differential Equations. *RAIRO Mathematical Modelling and Numerical Analysis 26*, 7.

[11] BARNES, J., AND HUT, P. A Hierarchical $O(n \log n)$ Force Calculation Algorithm. *Nature 324* (1986), 446–449.

[12] BARTELS, R., AND BEATTY, J. A Technique for the Direct Manipulation of Spline Curves. In *Graphics Interface 1989* (1989), pp. 33–39.

[13] BARTELS, R. H., BEATTY, J. C., AND BARSKY, B. A. *An Introduction to Splines for Use in Computer Graphics and Geometric Modeling.* Morgan Kaufmann Publishers, Inc., 1987.

[14] BEAUCHAMP, K. G. *Applications of Walsh and Related Functions*. Academic Press, 1984.

[15] BEYLKIN, G., COIFMAN, R., AND ROKHLIN, V. Fast Wavelet Transforms and Numerical Algorithms I. *Comm. Pure and Applied Mathematics 44* (1991), 141–183.

[16] BOUATOUCH, K., AND PATTANAIK, S. N. Discontinuity Meshing and Hierarchical Multi-Wavelet Radiosity. In *Proceedings of Graphics Interface* (1995).

[17] CANNY, J. A Computational Approach to Edge Detection. *IEEE Trans. Pattern Analysis and Machine Intelligence 8*, 6 (1986), 679–698.

[18] CARNICER, J. M., DAHMEN, W., AND PEÑA, J. M. Local decompositions of refinable spaces. Tech. rep., Insitut für Geometrie und angewandete Mathematik, RWTH Aachen, 1994.

[19] CATMULL, E., AND CLARK, J. Recursively Generated B-spline Surfaces on Arbitrary Topological Meshes. *Computer Aided Design 10*, 6 (1978), 350–355.

[20] CAVARETTA, A., DAHMEN, W., AND MICCHELLI, C. Subdivision for Computer Aided Geometric Design. *Memoirs Amer. Math. Soc. 93* (1991).

[21] CELNIKER, G., AND GOSSARD, D. Deformable Curve and Surface Finite-Elements for Free-From Shape Design. *Computer Graphics 25*, 4 (July 1991), 257–266.

[22] CHRISTENSEN, P. H., LISCHINSKI, D., STOLLNITZ, E., AND SALESIN, D. Clustering for Glossy Global Illumination. TR 95-01-07, University of Washington, Department of Computer Science, February 1995. `ftp://ftp.cs.washington.edu/tr/1994/01/UW-CSE-95-01-07.PS.Z`.

[23] CHRISTENSEN, P. H., STOLLNITZ, E. J., SALESIN, D. H., AND DEROSE, T. D. Wavelet Radiance. In *Proceedings of the 5th Eurographics Workshop on Rendering* (Darmstadt, June 1994), pp. 287–302.

[24] CHUI, C., AND QUAK, E. Wavelets on a Bounded Interval. In *Numerical Methods of Approximation Theory* (1992), D. Braess and L. L. Schumaker, Eds., Birkhäuser-Verlag, Basel, pp. 1–24.

[25] CHUI, C. K. An Overview of Wavelets. In *Approximation Theory and Functional Analysis*, C. K. Chui, Ed. Academic Press, 1991, pp. 47–71.

[26] CHUI, C. K. *An Introduction to Wavelets*, vol. 1 of *Wavelet Analysis and its Applications.* Academic Press, Inc., Boston, MA, 1992.

[27] CHUI, C. K., Ed. *Wavelets: A Tutorial in Theory and Applications*. Academic Press, San Diego, 1992.

[28] CHUI, C. K., MONTEFUSCO, L., AND PUCCIO, L., Eds. *Conference on Wavelets: Theory, Algorithms, and Applications*. Academic Press, San Diego, CA, 1994.

[29] CHUI, C. K., AND QUAK, E. Wavelets on a Bounded Interval. In *Numerical Methods of Approximation Theory, Vol. 9*, D. Braess and L. L. Schumaker, Eds. Birkhauser Verlag, Basel, 1992, pp. 53–75.

[30] CHUI, C. K., AND WANG, J. Z. An Overview of Wavelets. Tech. Rep. CAT 223, Center for Approximation Theory, Department of Mathematics, Texas A&M University, 1990.

[31] CHUI, C. K., AND WANG, J. Z. A General Framework of Compactly Supported Splines and Wavelets. *J. Approx. Theory 71*, 3 (1992), 263–304.

[32] COHEN, A. Ondelettes, Analyses Multiresolutions et Filtres Miroirs en Quadrature. *Ann. Inst. H. Poincaré, Anal. Non Linéaire 7*, 5 (1990), 439–459.

[33] COHEN, A., DAUBECHIES, I., AND FEAUVEAU, J. Bi-orthogonal Bases of Compactly Supported Wavelets. *Comm. Pure and Applied Mathematics 45* (1992), 485–560.

[34] COHEN, A., DAUBECHIES, I., AND FEAUVEAU, J. C. Biorthogonal Bases of Compactly Supported Wavelets. *Communication on Pure and Applied Mathematics 45* (1992), 485–560.

[35] COHEN, A., DAUBECHIES, I., JAWERTH, B., AND VIAL, P. Multiresolution Analysis, Wavelets and Fast Algorithms on an Interval. *Comptes Rendus de l'Acad. Sci. Paris I*, 316 (1993), 417–421.

[36] COHEN, A., DAUBECHIES, I., AND VIAL, P. Multiresolution analysis, wavelets and fast algorithms on an interval. *Appl. Comput. Harmon. Anal. 1*, 1 (1993), 54–81.

[37] COHEN, M. F. Interactive Spacetime Control for Animation. *Computer Graphics (Proc. SIGGRAPH) 26*, 2 (July 1992), 293–302.

[38] COHEN, M. F., GREENBERG, D. P., IMMEL, D. S., AND BROCK, P. J. An Efficient Radiosity Approach for Realistic Image Synthesis. *IEEE Computer Graphics and Applications 6*, 3 (March 1986), 26–35.

[39] COHEN, M. F., AND WALLACE, J. R. *Radiosity and Realistic Image Synthesis*. Academic Press, 1993.

[40] COIFMAN, R., AND MEYER, Y. Remarques sur l'Analyse de Fourier à Fenêtre. *Comptes Rendus de l'Acad. Sci. Paris I*, 312 (1991), 259–261.

[41] COIFMAN, R. R., AND MEYER, Y. Orthonormal Wave Packet Bases. Preprint.

[42] COIFMAN, R. R., MEYER, Y., QUAKE, S., AND WICKERHAUSER, M. V. Signal Processing and Compression with Wave Packets. In *Proceedings of the International Conference on Wavelets, Marseille* (1989), Y. Meyer, Ed., Masson, Paris.

[43] COIFMAN, R. R., AND WICKERHAUSER, M. L. Entropy Based Algorithms for Best Basis Selection. *IEEE Trans. Information Theory 38*, 2 (1992), 713–718.

[44] DAHMEN, W. Stability of multiscale transformations. Tech. rep., Institut für Geometrie und angewandete Mathematik, RWTH Aachen, 1994.

[45] DAHMEN, W., AND KUNOTH, A. Multilevel Preconditioning. *Numer. Math. 63*, 2 (1992), 315–344.

[46] DAHMEN, W., AND KUNOTH, A. Multilevel Preconditioning. *Numerische Mathematik 63* (1992), 315–344.

[47] DAHMEN, W., PRÖSSDORF, S., AND SCHNEIDER, R. Multiscale methods for pseudo-differential equations on smooth manifolds. In [28]. pp. 385–424.

[48] DAUBECHIES, I. Orthonormal Bases of Compactly Supported Wavelets. *Comm. Pure and Applied Mathematics 41* (1988), 909–996.

[49] DAUBECHIES, I. The Wavelet Transform, Time-Frequency Localization of and Signal Analysis. *IEEE Trans. Information Theory 36*, 5 (September 1990), 961–1005.

[50] DAUBECHIES, I. *Ten Lectures on Wavelets*, vol. 61 of *CBMS-NSF Regional Conference Series on Applied Mathematics*. SIAM, Philadelphia, PA, 1992.

[51] DAUBECHIES, I. *Ten Lectures on Wavelets*. No. 61 in CBMS-NSF Series in Applied Mathematics. SIAM, Philadelphia, 1992.

[52] DAUBECHIES, I. Orthonormal bases of compactly supported wavelets II: Variations on a theme. *SIAM J. Math. Anal. 24*, 2 (1993), 499–519.

[53] DAUBECHIES, I., AND LAGARIAS, J. C. Two-scale Difference Equations I. Existence and Global Regularity of Solutions. *SIAM J. Mathematical Analysis 22*, 5 (1991), 1388–1410.

[54] DELVES, L. M., AND MOHAMED, J. L. *Computational Methods for Integral Equations*. Cambridge University Press, 1985.

[55] DENG, B., JAWERTH, B., PETERS, G., AND SWELDENS, W. Wavelet Probing for Compression Based Segmentation. In *Mathematical Imaging: Wavelet Applications in Signal and Image Processing* (1993), A. F. Laine, Ed., SPIE Proceedings Series, Vol. 2034, pp. 266–276.

[56] DESLAURIERS, G., AND DUBUC, S. Interpolation dyadique. In *Fractals, dimensions non entières et applications*. Masson, Paris, 1987, pp. 44–55.

[57] DESLAURIERS, G., AND DUBUC, S. Symmetric Iterative Interpolation Processes. *Constr. Approx. 5*, 1 (1989), 49–68.

[58] DEVORE, R. A., JAWERTH, B., AND LUCIER, B. J. Image Compression Through Wavelet Rransform Coding. *IEEE Trans. Information Theory 38*, 2 (1992), 719–746.

[59] DEVORE, R. A., JAWERTH, B., AND LUCIER, B. J. Surface Compression. *Computer Aided Geometric Design 9*, 3 (1992), 219–239.

[60] DEVORE, R. A., JAWERTH, B., AND POPOV, V. Compression of Wavelet Decompositions. *Amer. J. Math. 114* (1992), 737–785.

[61] DEVORE, R. A., AND LUCIER, B. J. Wavelets. In *Acta Numerica 1* (1991), Cambridge University Press, pp. 1–56.

[62] DONOHO, D. L. Smooth Wavelet Decompositions with Blocky Coefficient Kernels. In [169]. pp. 259–308.

[63] DONOHO, D. L. Interpolating wavelet transforms. Preprint, Department of Statistics, Stanford University, 1992.

[64] DONOHO, D. L. Unconditional Bases are Optimal Bases for Data Compression and for Statistical Estimation. *Appl. Comput. Harmon. Anal. 1*, 1 (1993), 100–115.

[65] DONOHO, D. L., AND JOHNSTONE, I. M. Adapting to Unknown Smoothness by Wavelet Shrinkage. Preprint Department of Statistics, Stanford University, 1992.

[66] DONOHO, D. L., AND JOHNSTONE, I. M. Ideal Spatial Adaptation via Wavelet Shrinkage. Preprint Department of Statistics, Stanford University, 1992.

[67] DONOHO, D. L., AND JOHNSTONE, I. M. New Minimax Theorems, Thresholding, and Adaptation. Preprint Department of Statistics, Stanford University, 1992.

[68] DOO, D. *A Recursive Subdivision Algorithm for Fitting Quadratic Surfaces to Irregular Polyhedrons*. PhD thesis, Brunel University, 1978.

[69] DOO, D., AND SABIN, M. Behaviour of Recursive Division Surfaces Near Extraordinary Points. *Computer Aided Design 10*, 6 (1978), 356–360.

[70] DRETTAKIS, G., FIUME, E., AND FOURNIER, A. Tightly-Coupled Multiprocessing for a Global Illumination Algorithm. In *Eurographics '90* (September 1990), C. Vandoni and D. Duce, Eds., North-Holland, pp. 387–398.

[71] DYN, N., GREGORY, A., AND LEVIN, D. A 4-point Interpolatory Subdivision Scheme for Curve Design. *Computer Aided Geometric Design 4* (1987), 257–268.

[72] DYN, N., LEVIN, D., AND GREGORY, J. A Butterfly Subdivision Scheme for Surface Interpolation with Tension Control. *ACM Trans. on Graphics 9*, 2 (April 1990), 160–169.

[73] EIROLA, T. Sobolev Characterization of Solutions of Dilation Equations. *SIAM J. Mathematical Analysis 23*, 4 (1992), 1015–1030.

[74] FANG, X., AND SÉRÉ, E. Adaptive Multiple Folding Local Trigonometric Transforms and Wavelet Packets. Preprint.

[75] FINKELSTEIN, A., AND SALESIN, D. Multiresolution Curves. In *Computer Graphics (Proc. SIGGRAPH)* (July 1994), ACM. To appear.

[76] FINKELSTEIN, A., AND SALESIN, D. Multiresolution Curves. In *Computer Graphics, Annual Conference Series, 1994* (1994), Siggraph, pp. 261–268.

[77] FLANDRIN, P. On the Spectrum of Fractional Brownian Motions. *IEEE Trans. Information Theory 35*, 1 (January 1989), 197–199.

[78] FLANDRIN, P. Wavelet Analysis and Synthesis of Fractional Brownian Motion. *IEEE Trans. Information Theory 38*, 2 (1992), 910–917.

[79] FLETCHER, R. *Practical Methods of Optimization 1*. John Wiley and Sons, 1980.

[80] FORSEY, D., AND BARTELS, R. Hierarchical B-Spline Refinement. *Computer Graphics 22*, 4 (August 1988), 205–212.

[81] FORSEY, D., AND WENG, L. Multi-resolution Surface Approximation for Animation. In *Graphics Interface* (1993).

[82] FORSEY, D. R., AND BARTELS, R. H. Hierarchical B-spline Refinement. *Computer Graphics (Proc. SIGGRAPH) 22*, 4 (1988), 205–212.

[83] FORSEY, D. R., AND BARTELS, R. H. Tensor Products and Hierarchical Surface Approximation. *ACM Trans. on Graphics* (To appear.).

[84] FOURNIER, A., FIUME, E., OUELLETTE, M., AND CHEE, C. K. FIAT LUX: Light Driven Global Illumination. Technical Memo DGP89–1, Dynamic Graphics Project, Department of Computer Science, University of Toronto, 1989.

[85] FOURNIER, A., FUSSELL, D., AND CARPENTER, L. Computer Rendering of Stochastic Models. *Communications of the ACM 25*, 6 (June 1982), 371–384.

[86] FOWLER, B. Geometric Manipulation of Tensor Product Surfaces. In *Proceedings, Symposium on Interactive 3D Graphics* (1992), pp. 101–108.

[87] GABOR, D. Theory of Communication. *J. of the IEEE 93* (1946), 429–457.

[88] GERSHBEIN, R. S., SCHRÖDER, P., AND HANRAHAN, P. Textures and Radiosity: Controlling Emission and Reflection with Texture Maps. In *Computer Graphics (Proc. SIGGRAPH)* (July 1994), ACM. To appear.

[89] GERSHO, A., AND GRAY, R. M. *Vector Quantizing and Signal Compression*. Kluwer Academic Publishers, 1992.

[90] GLOWINSKI, R., LAWTON, W. M., RAVECHOL, M., AND TENENBAUM, E. Wavelet Solution of Linear and Nonlinear Elliptic Parabolic and Hyperbolic Problems in One Space Dimension. In *Proceedings of the 9th International Conference on Numerical Methods in Applied Sciences and Engineering* (1990), SIAM, Philadelphia.

[91] GORAL, C. M., TORRANCE, K. E., GREENBERG, D. P., AND BATTAILE, B. Modelling the Interaction of Light between Diffuse Surfaces. *Computer Graphics (Proc. SIGGRAPH) 18*, 3 (July 1984), 213–222.

[92] GORTLER, S. personal communication, 1993.

[93] GORTLER, S., AND COHEN, M. F. Variational Modeling with Wavelets. Tech. Rep. Technical Report CS-TR-456-94, Departmentf of Computer Science, Princeton University, 1994.

[94] GORTLER, S., SCHRÖDER, P., COHEN, M., AND HANRAHAN, P. Wavelet Radiosity. In *Computer Graphics Annual Conference Series 1993* (August 1993), Siggraph, pp. 221–230.

[95] GORTLER, S. J. *Wavelet Methods for Computer Graphics*. PhD thesis, Princeton University, January 1995.

[96] GORTLER, S. J., COHEN, M. F., AND SLUSALLEK, P. Radiosity and Relaxation Methods; Progressive Refinement is Southwell Relaxation. Tech. Rep. CS-TR-408-93, Department of Computer Science, Princeton University, February 1993. To appear in IEEE Computer Graphics and Applications.

[97] GORTLER, S. J., SCHRÖDER, P., COHEN, M. F., AND HANRAHAN, P. Wavelet Radiosity. In *Computer Graphics (Proc. SIGGRAPH)* (August 1993), ACM, pp. 221–230.

[98] GREENGARD, L. *The Rapid Evaluation of Potential Fields in Particle Systems*. MIT Press, 1988.

[99] HAAR. Zur Theorie der Orthogonalen Funktionensysteme. *Math. Annal. 69* (1910), 331–371.

[100] HALSTEAD, M., KASS, M., AND DEROSE, T. Efficient, Fair Interpolation using Catmull-Clark Surfaces. In *Computer Graphics (Proc. SIGGRAPH)* (August 1993), ACM, pp. 35–44.

[101] HALSTEAD, M., KASS, M., AND DEROSE, T. Efficient, Fair Interpolation using Catmull-Clark Surfaces. In *Computer Graphics, Annual Conference Series, 1993* (1993), Siggraph, pp. 35–43.

[102] HANRAHAN, P., SALZMAN, D., AND AUPPERLE, L. A Rapid Hierarchical Radiosity Algorithm. *Computer Graphics (Proc. SIGGRAPH) 25*, 4 (July 1991), 197–206.

[103] HECKBERT, P. S. *Simulating Global Illumination Using Adaptive Meshing*. PhD thesis, University of California at Berkeley, January 1991.

[104] HECKBERT, P. S. Radiosity in Flatland. *Computer Graphics Forum 2*, 3 (1992), 181–192.

[105] HILTON, M. L., JAWERTH, B. D., AND SENGUPTA, A. N. Compressing Still and Moving Images with Wavelets. *Multimedia Systems 3* (1994).

[106] HOPPE, H., DEROSE, T., DUCHAMP, T., HALSTEAD, M., JIN, H., MCDONALD, J., SCHWEITZER, J., AND STUETZLE, W. Piecewise-Smooth Surface Reconstruction. In *Computer Graphics (Proc. SIGGRAPH)* (July 1994), ACM. To appear.

[107] JAFFARD, S. Exposants de Hölder en des Points Donnés et Coéfficients d'ondelettes. *Comptes Rendus de l'Acad. Sci. Paris 1*, 308 (1991), 79–81.

[108] JAFFARD, S. Wavelet Methods for Fast Resolution of Elliptic Problems. *SIAM J. Numer. Anal. 29*, 4 (1992), 965–986.

[109] JAFFARD, S., AND LAURENÇOT, P. Orthonormal Wavelets, Analysis of Operators, and Applications to Numerical Analysis. In *Wavelets: A Tutorial in Theory and Applications*, C. K. Chui, Ed. Academic Press, 1992, pp. 543–602.

[110] JAWERTH, B., HILTON, M. L., AND HUNSTBERGER, T. L. Local Enhancement of Compressed Images. *J. Math. Imag. Vision 3* (1993), 39–49.

[111] JAWERTH, B., LIU, Y., AND SWELDENS, W. Signal Compression with Smooth Local Trigonometric Bases. *Opt. Engineering* (To appear).

[112] JAWERTH, B., AND SWELDENS, W. Wavelet Multiresolution Analyses Adapted for the Fast Solution of Boundary Value Ordinary Differential Equations. In *Sixth Copper Mountain Conference on Multigrid Methods* (1993), N. D. Melson, T. A. Manteuffel, and S. F. McCormick, Eds., NASA Conference Publication 3224, pp. 259–273.

[113] JAWERTH, B., AND SWELDENS, W. An Overview of Wavelet Based Multiresolution Analyses. *SIAM Review* (To appear).

[114] JIA, R.-Q., AND MICCHELLI, C. A. Using the Refinement Equations for the Construction of Pre-Wavelets II: Powers of Two. In *Curves and Surfaces*, P. Laurent, A. L. Méhauté, and L. Schumaker, Eds. Academic Press, 1991, pp. 209–246.

[115] KAJIYA, J. T. The Rendering Equation. *Computer Graphics (Proc. SIGGRAPH) 20*, 4 (1986), 143–150.

[116] KONDO, J. *Integral Equations*. Oxford Applied Mathematics and Computing Science Series. Kodansha, 1991.

[117] LAWTON, W. M. Necessary and Sufficient Conditions for Constructing Orthonormal Wavelets Bases. *J. Math. Phys. 32*, 1 (1991), 57–61.

[118] LEMARIÉ, P. G. La Proprieté de Support Minimal dans les Analyses de Multirésolution. *Comptes Rendus de l'Acad. Sci. Paris 1*, 312 (1991), 773–776.

[119] LEWIS, A. S., AND KNOWLES, G. Video Compression using 3D Wavelet Transforms. *Electr. Letters 26*, 6 (1992), 396–397.

[120] LEWIS, J. Generalized stochastic subdivision. *ACM Transactions on Graphics 6*, 3 (July 1987), 167–190.

[121] LISCHINSKI, D., TAMPIERI, F., AND GREENBERG, D. P. Combining Hierarchical Radiosity and Discontinuity Meshing. In *Computer Graphics Annual Conference Series 1993* (August 1993), Siggraph, pp. 199–208.

[122] LIU, Z., GORTLER, S. J., AND COHEN, M. F. Hierarchical Spacetime Control. In *Computer Graphics, Annual Conference Series, 1994* (August 1994), pp. 35–42.

[123] LOOP, C. T. Smooth Subdivision Surfaces Based on Triangles. Master's thesis, Department of Mathematics, University of Utah, August 1987.

[124] LOUNSBERY, M., DEROSE, T., AND WARREN, J. Multiresolution Analysis for Surfaces of Arbitrary Topological Type. Tech. Rep. TR 93-10-05b, Department of Computer Science and Engineering, Princeton University, October 1993.

[125] LOUNSBERY, M., DEROSE, T., AND WARREN, J. Multiresolution Surfaces of Arbitrary Topological Type. Department of Computer Science and Engineering 93-10-05, University of Washington, October 1993. Updated version available as 93-10-05b, January, 1994.

[126] LOUNSBERY, M., DEROSE, T. D., AND WARREN, J. Multiresolution Surfaces of Arbitrary Topological Type. Department of Computer Science and Engineering 93-10-05, University of Washington, October 1993. Updated version available as 93-10-05b, January, 1994.

[127] LYCHE, T., AND MORKEN, K. Spline Wavelets of Minimal Support. *Numerical Methods of Approximation Theory 9* (1992), 177–194.

[128] LYCHE, T., AND MORKEN, K. Spline Wavelets of Minimal Support. In *Numerical Methods in Approximation Theory*, D.Braess and L. L. Schumaker, Eds., vol. 9. Birkhauser Verlag, Basel, 1992, pp. 177–194.

[129] MADAY, Y., PERRIER, V., AND RAVEL, J.-C. Adaptivité dynamique sur bases d'ondelettes pour l'approximation d'équations aux dérivées partielles. *Comptes Rendus de l'Acad. Sci. Paris I*, 312 (1991), 405–410.

[130] MALLAT, S. A Theory for Multiresolution Signal Decomposition: the Wavelet Representation. *IEEE Trans. Pattern Analysis and Machine Intelligence 11*, 7 (July 1989), 674–693.

[131] MALLAT, S., AND HWANG, W. L. Singularity Detection and Processing with Wavelets. *IEEE Trans. Information Theory*, 2 (1992), 617–643.

[132] MALLAT, S., AND ZHONG, S. Wavelet Transform Maxima and Multiscale Edges. In [164]. pp. 67–104.

[133] MALLAT, S., AND ZHONG, S. Characterization of Signals from Multiscale Edges. *IEEE Trans. Pattern Analysis and Machine Intelligence 14*, 7 (July 1992), 710–732.

[134] MALLAT, S. G. Multiresolution Approximations and Wavelet Orthonormal Bases of $L^2(\mathbf{RR})$. *Trans. Amer. Math. Soc. 315*, 1 (1989), 69–87.

[135] MALLAT, S. G. A Theory for Multiresolution Signal Decomposition: The Wavelet Representation. *IEEE Transactions on Pattern Analysis and Machine Intelligence 11* (July 1989), 674–693.

[136] MALVAR, H. S. Lapped Transforms for Efficient Transform/Subband Coding. *IEEE Trans. Acoust. Speech Signal Process. 38* (1990), 969–978.

[137] MANDELBROT, B. B., AND NESS, J. W. V. Fractional Brownian Motion, Fractional Noises and Applications. *SIAM Review 10*, 4 (October 1968), 422–437.

[138] MARR, D. *Vision*. W. H. Freeman Company, San Francisco, CA, 1982.

[139] MARR, D., AND HILDRETH, E. Theory of Edge Detection. *Proc. Royal Society of London B*, 207 (London, 1980), 187–217.

[140] MAX, J. Quantizing for Minimum Distortion. *IRE Trans. on Information Theory 6*, 1 (1960), 7–12.

[141] MEINGUET, J. Multivariate Interpolation at Arbitrary Points Made Simple. *Journal of Applied Mathematics and Physics (ZAMP) 30* (1979), 292–304.

[142] MEYER, Y. *Ondelettes et Opérateurs, I: Ondelettes, II: Opérateurs de Calderón-Zygmund, III:* (with R. Coifman), *Opérateurs multilinéaires*. Hermann, Paris, 1990. English translation of first volume is published by Cambridge University Press.

[143] MEYER, Y. Ondelettes sur l'intervalle. *Rev. Mat. Iberoamericana 7* (1992), 115–133.

[144] MILLER, G. The Definition and Rendering of Terrain Maps. D. C. Evans and R. J. Athay, Eds., vol. 20, pp. 39–48.

[145] MOKHTARIAN, F., AND MACKWORTH, A. Scale-based Description and Recognition of Planer Curves and Two-Dimensional Shapes. *IEEE Trans. Pattern Analysis and Machine Intelligence 8* (1986), 34–43.

[146] MOON, P. *The Scientific Basis for Illuminating Engineering*, Dover, 1961 ed. McGraw-Hill, 1936.

[147] MORETON, H., AND SEQUIN, C. Functional Optimization for Fair Surface Design. *Computer Graphics 26*, 4 (July 1992), 167–176.

[148] MUSGRAVE, F. K., KOLB, C. E., AND MACE, R. S. The Synthesis and Rendering of Eroded Fractal Terrains. J. Lane, Ed., vol. 23, pp. 41–50.

[149] NGO, J. T., AND MARKS, J. Spacetime Constraints Revisited. In *Computer Graphics (Proc. SIGGRAPH)* (August 1993), ACM, pp. 343–350.

[150] NISHITA, T., AND NAKAMAE, E. Continuous Tone Representation of Three-Dimensional Objects Taking Account of Shadows and Interreflection. *Computer Graphics (Proc. SIGGRAPH) 19*, 3 (July 1985), 23–30.

[151] PAI, D., AND REISSELL, L.-M. Multiresolution rough terrain motion planning. Tech. Rep. Technical Report TR 94–33, Department of Computer Science, UBC, Vancouver, May 1994.

[152] PATTANAIK, S. N., AND BOUATOUCH, K. Fast Wavelet Radiosity Method. *Computer Graphics Forum 13*, 3 (September 1994), C407–C420. Proceedings of Eurographics Conference.

[153] PEITGEN, H. O., AND SAUPE, D. *The Science of Fractal Images*. Springer Verlag, 1988.

[154] PENTLAND, A. Fast Solutions to Physical Equilibrium and Interpolation Problems. *The Visual Computer 8*, 5 (1992), 303–314.

[155] PRATT, W. K. *Digital Image Processing*. Wiley, New York, 1978.

[156] PRESS, W. H., FLANNERY, B. P., TEUKOLSKY, S. A., AND VETTERLING, W. T. *Numerical Recipies*. Cambridge University Press, 1986.

[157] PRESS, W. H., TEUKOLSKY, S. A., VETTERLING, W. T., AND FLANNERY, B. P. *Numerical Recipes in C: The Art of Scientific Computing*, Second ed. Cambridge University Press, 1992.

[158] QIAN, S., AND WEISS, J. Wavelets and the Numerical Solution of Partial Differential Equations. *Journal of Computational Physics 106*, 1 (May 1993), 155–175.

[159] QUAK, E., AND WEYRICH, N. Decomposition and Reconstruction Algorithms for Spline Wavelets on a Bounded Interval. Tech. Rep. 294, Department of Mathematics, Texas A&M University, April 1993.

[160] RANDO, T., AND ROULIER, J. Designing Faired Parametric Surfaces. *Computer Aided Design 23*, 7 (September 1991), 492–497.

[161] REISSELL, L. M. Multiresolution Geometric Algorithms Using Wavelets I: Representations for Parametric Curves and Surfaces. Tech. Rep. Technical Report 93-17, Department of Computer Science, UBC, Vancouver, May 1993.

[162] RIOUL, O., AND VETTERLI, M. Wavelets and Signal Processing. *IEEE Signal Processing Magazine* (October 1991), 14–38.

[163] RUSHMEIER, H. E., PATTERSON, C., AND VEERASAMY, A. Geometric Simplification for Indirect Illumination Calculations. *Proceedings Graphics Interface* (May 1993), 227–236.

[164] RUSKAI, M. B., BEYLKIN, G., COIFMAN, R., DAUBECHIES, I., MALLAT, S., MEYER, Y., AND RAPHAEL, L., Eds. *Wavelets and their Applications*. Jones and Bartlett, 1992.

[165] SAITO, N., AND BEYLKIN, G. Multiresolution Representations Using the Autocorrelation Functions of Compactly Supported Wavelets. Preprint University of Colorado at Boulder.

[166] SCHRÖDER, P., GORTLER, S. J., COHEN, M. F., AND HANRAHAN, P. Wavelet Projections For Radiosity. In *Fourth Eurographics Workshop on Rendering* (June 1993), Eurographics, pp. 105–114.

[167] SCHRÖDER, P., AND HANRAHAN, P. Wavelet Methods for Radiance Computations. In *Proceedings 5th Eurographics Workshop on Rendering* (June 1994), Eurographics.

[168] SCHRÖDER, P., AND SWELDENS, W. Spherical wavelets: Efficiently Representing Functions on the Sphere. *Computer Graphics, (SIGGRAPH '95 Proceedings)* (1995).

[169] SCHUMAKER, L. L., AND WEBB, G., Eds. *Recent Advances in Wavelet Analysis*. Academic Press, 1993.

[170] SHAPIRO, J. M. Embedded Image Coding using Zerotrees of Wavelet Coefficients. *IEEE Trans. Signal Processing 41*, 12 (1993), 3445–3462.

[171] SIEGEL, R., AND HOWELL, J. R. *Thermal Radiation Heat Transfer*. Hemisphere Publishing Corp., 1978.

[172] SILLION, F. Clustering and Volume Scattering for Hierarchical Radiosity Calculations. In *Proceedings of the 5th Eurographics Workshop on Rendering* (Darmstadt, June 1994), pp. 105–117.

[173] SMITS, B., ARVO, J., AND GREENBERG, D. A Clustering Algorithm for Radiosity in Complex Environments. *Computer Graphics Annual Conference Series* (July 1994), 435–442.

[174] SMITS, B. E., ARVO, J. R., AND SALESIN, D. H. An Importance Driven Radiosity Algorithm. *Computer Graphics (Proc. SIGGRAPH) 26*, 2 (August 1992), 273–282.

[175] STOER, J., AND BULIRSCH, R. *Introduction to Numerical Analysis*. Springer Verlag, New York, 1980.

[176] STOLLNITZ, E. J., DEROSE, T. D., AND SALESIN, D. H. Wavelets for Computer Graphics: A Primer, Part 1. *IEEE Computer Graphics and Applications 15*, 3 (May 1995), 76–84.

[177] STRANG, G. Wavelets and Dilation Equations: A Brief Introduction. *SIAM Review 31*, 4 (December 1989), 614–627.

[178] STRANG, G., AND FIX, G. A Fourier analysis of the finite element variational method.

[179] SWELDENS, W. The lifting scheme: A construction of second generation wavelets. Department of Mathematics, University of South Carolina.

[180] SWELDENS, W. *Construction and Applications of Wavelets in Numerical Analysis*. PhD thesis, Department of Computer Science, Katholieke Universiteit Leuven, Belgium, 1994. (`ftp://ftp.math.scarolina.edu/pub/wavelet/varia/thesis/*`).

[181] SWELDENS, W. The lifting scheme: A custom-design construction of biorthogonal wavelets. Tech. Rep. 1994:7, Industrial Mathematics Initiative, Department of Mathematics, University of South Carolina, 1994. (`ftp://ftp.math.scarolina.edu/pub/imi_94/imi94_7.ps`).

[182] SZELISKI, R. Fast Surface Interpolation Using Hierarchical Basis Functions. *IEEE Trans. PAMI 12*, 6 (June 1990), 413–439.

[183] SZELISKI, R., AND TERZOPOULOS, D. From Splines to Fractals. J. Lane, Ed., vol. 23, pp. 51–60.

[184] TELLER, S., FOWLER, C., FUNKHOUSER, T., AND HANRAHAN, P. Partitioning and Ordering Large Radiosity Computations. In *Computer Graphics (Proc. SIGGRAPH)* (July 1994), ACM. To appear.

[185] TERZOPOULOS, D. Image Analysis using Multigrid Relaxation Methods. *IEEE Trans. Pattern Analysis and Machine Intelligence 8*, 2 (March 1986), 129–139.

[186] TERZOPOULOS, D. Image Analysis Using Multigrid Relaxation Methods. *IEEE PAMI 8*, 2 (March 1986), 129–139.

[187] TERZOPOULOS, D. Regularization of Inverse Visual Problems Involving Discontinuities. *IEEE PAMI 8*, 4 (July 1986), 413–424.

[188] TROUTMAN, R., AND MAX, N. Radiosity Algorithms Using Higher-order Finite Elements. In *Computer Graphics (Proc. SIGGRAPH)* (August 1993), ACM, pp. 209–212.

[189] VAN DE PANNE, M., AND FIUME, E. Sensor-actuator Networks. In *Computer Graphics (Proc. SIGGRAPH)* (August 1993), ACM, pp. 335–342.

[190] VETTERLI, M., AND HERLEY, C. Wavelets and Filter Banks: Theory and Design. *IEEE Trans. Acoust. Speech Signal Process. 40*, 9 (1992), 2207.

[191] VOSS, R. P. Fractal Forgeries. In *Fundamental Algorithms for Computer Graphics*, R. A. Earnshaw, Ed. Springer-Verlag, 1985.

[192] WALLACE, G. K. The JPEG Still Picture Compression Standard. *Communications of the ACM 34*, 4 (1991), 30–44.

[193] WARE, C., ARTHUR, K., AND BOOTH, K. S. Fish Tank Virtual Reality. In *Proc. INTERCHI '93 Conference on Human Factors in Computing Systems* (April 1993), pp. 37–42.

[194] WELCH, W., AND WITKIN, A. Variational Surface Modeling. *Computer Graphics 26*, 2 (July 1992), 157–166.

[195] WITKIN, A., AND KASS, M. Spacetime Constraints. *Computer Graphics (Proc. SIGGRAPH) 22*, 4 (August 1988), 159–168.

[196] WORNELL, G. W. A Karhunen-Loève-like Expansion for $1/f$ Processes via Wavelets. *IEEE Trans. Information Theory 36*, 4 (July 1990), 859–861.

[197] WORNELL, G. W., AND OPPENHEIM, A. V. Estimation of Fractal Signals from Noisy Measurements Using Wavelets. *IEEE Trans. Signal Proc. 40*, 3 (March 1992), 611–623.

[198] YSERENTANT, H. On the Multi-level Splitting of Finite Element Spaces. *Numerische Mathematik 49* (1986), 379–412.

[199] ZATZ, H. R. Galerkin Radiosity: A Higher-order Solution Method for Global Illumination. In *Computer Graphics (Proc. SIGGRAPH)* (August 1993), ACM, pp. 213–220.

[200] ZHANG, Y., AND ZAFAR, S. Motion-compensated Wavelet Transform Coding for Video. *IEEE Trans. Circuits Systems Video Tech. 3*, 2 (1992), 285–296.

Index